VOLUME 24 ISSUE 6 2014 MENCEX (6) 319–388 (2014)

Mendeleev Communications

CONTENTS

AUTHOR INDEX

Abstracted/indexed in: Analytical Abstracts, Beilstein, CAB Abstracts, Chemical Abstracts, CASREACT, Chemical Engineering and Biotechnology Abstracts, Current Contents: Physical, Chemical and Earth Sciences, PASCAL, Science Citation Index, SciSearch, NAPRALERT, RAPRA. Also covered in the abstract and citation database SciVerse Scopus®. Full text available on SciVerse ScienceDirect®.

Funding body agreements and policies
Elsevier has established agreements and developed policies to allow authors whose articles appear in journals published by Elsevier, to comply with potential manuscript archiving requirements as specified as conditions of their grant awards. To learn more about existing agreements and policies please visit http://www.elsevier.com/fundingbodies

Available online at www.sciencedirect.com
ScienceDirect
Focus Article, *Mendeleev Commun.*, 2014, **24**, 319–326
Mendeleev Communications

Hybrid membranes containing inorganic nanoparticles

Andrei B. Yaroslavtsev[a,b] and Yuri P. Yampolskii[a]

[a] *A. V. Topchiev Institute of Petrochemical Synthesis, Russian Academy of Sciences, 119991 Moscow, Russian Federation*
[b] *N. S. Kurnakov Institute of General and Inorganic Chemistry, Russian Academy of Sciences, 119991 Moscow, Russian Federation. Fax: +7 495 954 1279; e-mail: yaroslav@igic.ras.ru*

DOI: 10.1016/j.mencom.2014.11.001

Hybrid ion-exchange and gas-diffusion membranes containing the nanoparticles of inorganic components are considered. These materials, in which transfer and separation processes occur by different mechanisms, similarly changed their properties upon the introduction of dopants into them to increase the rate and selectivity of transfer processes (ionic conductivity or gas permeability).

Introduction

The development of nanotechnologies substantially affected many branches of science, in particular, membrane technologies. Membranes including a system of nanosized pores and channels belong to this class. In this case, the nanosized pores are responsible for the transport properties and practical applications of the membranes.[1,2] At the same time, the production of so-called hybrid membranes based on high-molecular-weight materials containing the nanoparticles of inorganic substances has been actively developed since the 1980s. The development of these membranes was due to the extensive prospects of their use in fuel cells[3–12] and in gas separation processes, where the systems of this type are frequently referred to as mixed matrix membranes.[13–17] These membranes have also been used in the processes of pervaporation.[18,19]

It is amazing that these completely different classes of materials, ion-exchange and gas-diffusion membranes, in which transfer and separation processes occur by completely different mechanisms, similarly change their properties upon the introduction of the nanoparticles of inorganic compounds. Correctly chosen dopants and doping methods can increase both the rate and the selectivity of transfer processes in the obtained materials.[14,20,21] For this reason, the attention of scientists in membrane technologies is focused on both ion-exchange and gas-separation membranes.

In this context, the aim of this small survey was to consider the structure and transport properties of hybrid membranes intended for ion transfer and gas fractionation.

Hybrid ion-exchange membranes

Methods of synthesis and morphology

In the first experiments on the synthesis of hybrid membranes, the simplest method of the introduction of nanodispersed particles into solution, from which a membrane was cast, was used.[4] Aggregation considerably decreases the effectiveness of modification with the use of this approach. The introduction of large particles and aggregates leads to the blocking of a part of the membrane matrix and to a dramatic worsening of its mechanical properties. Therefore, another approach related to the synthesis of nanoparticles directly in membrane pores when they serve as nanoreactors was found much more effective.[7] The pore walls restrict the reaction volume, and they can sorb initial reagents due to the presence of ion-exchange groups. The diameter of the formed nanoparticles is 2–5 nm because the characteristic nanopore size does not exceed 5 nm. Furthermore, the walls of the membranes isolate the formed particles from each other, and they can decrease surface tension forces due to additional binding. This ensures the thermodynamic stability of the formed nanoparticles.

The majority of precursors used for the synthesis of inorganic nanoparticles contain hydrophilic fragments, and they are capable of forming coordinate bonds with the functional groups of ion-exchange membranes. After the introduction of the second reagent, the formation of nanoparticles also occurs in the pores of membranes. The diffusion-limited processes of agglomeration and nucleation proceed very rapidly because of the thermodynamic

Yuri Yampolskii, Professor, Doctor of Science (Chemistry) is the head of the Laboratory of Membrane Gas Separation, A. V. Topchiev Institute of Petrochemical Synthesis, Russian Academy of Sciences. His field of expertise and scientific activity includes membrane science and technology, materials science, the physical chemistry of polymers and thermodynamics. He is an author of about 300 peer-reviewed publications including 7 books. Much of his attention was devoted to the structure–properties relationships of membrane materials and investigation of their free volume. Recently, his activity was focused on mixed matrix membranes containing metal organic frameworks, zeolites *etc*.

Andrei Yaroslavtsev, Corresponding Member of the Russian Academy of Sciences is the head of the Laboratory of Membrane Catalysis, A. V. Topchiev Institute of Petrochemical Synthesis, Russian Academy of Sciences, and head the of Ion Transport Sector, N. S. Kurnakov Institute of General and Inorganic Chemistry, Russian Academy of Sciences. His fields of scientific activity are materials science, membrane science and technology, solid-state chemistry and solid-state ionics. He is an author of about 300 peer-reviewed publications including 12 books. The main areas of his research activities are related to the investigation of ionic mobility in solids, including solid electrolytes and membrane materials. In recent years, much attention was paid to the synthesis of new materials for alternative energy, such as hybrid membranes including inorganic nanoparticles and electrode nanomaterials for lithium-ion batteries.

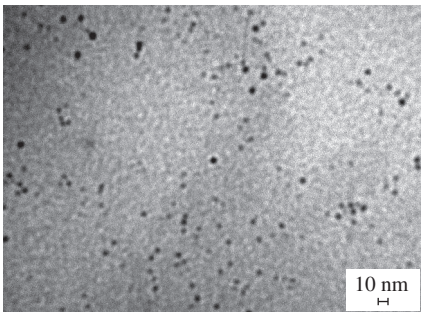

Figure 1 TEM image of SiO_2 particles in a Nafion membrane. Figure from ref. 21(*a*). ©2008 Pleiades Publishing, Ltd. Reproduced with permission.

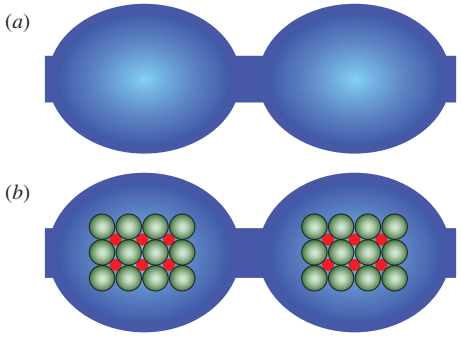

Figure 2 Schematic diagram of an increase in the size of channels connecting membrane pores upon the introduction of nanoparticles into the membranes. (*a*) Pores of initial membrane; (*b*) pores of hybrid membrane containing nanoparticles.

instability of small nanoparticles, the high rate of reagent transfer inside a pore and the small length of a diffusion zone (3–4 nm). So more than one nanoparticle cannot be formed in a pore (Figure 1). This was confirmed by transmission electron microscopy data.[21(*b*)] Therefore, an increase in the number of cycles of nanoparticles synthesis and the concentration of a precursor in a membrane first leads to an increase in the size rather than the amount of nanoparticles. However, it is impossible to increase the dopant concentration above several volume percents. For this purpose, a precursor is introduced into a membrane solution followed by casting and chemical treatment. The size of the particles obtained with the aid of this approach is greater and the formation of agglomerates becomes possible.[22]

Ionic conductivity of hybrid membranes

The introduction of nanoparticles can considerably change the proton conductivity, gas permeability, strength, thermal stability and some other parameters of the membranes. These changes depend on the synergism of the properties of individual components.[4,23,24] Therefore, the properties of a material depend on the properties of a dopant. Thus, the hydrophilic nature of the surface of nanoparticles introduced into the membrane ensures the absorption of additional water molecules and an increase in conductivity.[4] However, this cannot explain the possibility of membranes conductivity increase upon the introduction of finely dispersed hydrophobic additives and an increase in the conductivity observed in a number of cases upon decreasing the mobility of interstitial solution containing water molecules and protons formed by the dissociation of functional groups.[25] For explaining these phenomena, a model was proposed, according to which the introduction of a dopant into membrane pores leads to their expansion simultaneously with the expansion of channels, which limit the conductivity of membranes.[26] Indeed, the moisture content of the membranes is determined by the binding of water by the protons of functional groups, whose concentration insignificantly changes as a result of modification. Therefore, the water uptake of the membranes will remain almost constant or even somewhat increase due to the additional sorption of water on the surface of hydrophilic particles. The size of connecting channels also grows due to an increase in the total pore size (Figure 2). As a result, the acceleration of proton transfer through narrow channels and the conductivity of membranes as a whole was observed.

The dependence of conductivity on dopant concentration passed through a maximum at a dopant content of about 2 vol%. A further increase led to a decrease in the water uptake and the conductivity of membranes. Pressure (elastic force) proportional to the deformation of material acts on pore walls; it can be characterized by an increase in the pore radius. According to Hooke's law, the force required for pore expansion increases with the pore size. After equilibration, the pressure of elastic forces and the osmotic pressure on the pore walls become equal. Thus, an increase in the elastic forces prevents the further widening of pores and facilitates a decrease in the moisture content and conductivity at a high dopant content (with a rise of the particle size).[27] The model proposed was confirmed by a comparison between NMR-spectroscopic data and the conductivity of hybrid membranes.[25]

An important advantage of hybrid membranes is the possibility of maintaining high proton conductivity at a low humidity when the conductivity of ordinary membranes is reduced by several orders of magnitude due to dehydration and a decrease in the volume of pores and channels.[28] This is especially important for fuel cells.[12] The introduction of either individual heteropoly acids[29] or their mixtures with silica or other oxides[30,31] can increase the conductivity at a low humidity. Note that the power of fuel cells at a low humidity raised by 50% due to the use of the membranes containing mesoporous zirconium phosphate.[32]

Within the scope of the above model, the reason for an increase in the conductivity of membranes with low water uptake is that a part of the membranes pore volume is occupied by dopant particles. This prevents the contraction of pores at a lowered water uptake and, as a result, increases the size of channels that join pores.[27] Furthermore, proton transfer occurs between water molecules at a high humidity, whereas the SO_3^- functional groups, which are characterized by a much lower proton affinity, do almost not participate in the transfer. In the dehydrated MF-4SK membranes, protons are contained in the form of $H_5O_2^+$ ions,[33] in which direct proton transfer is hindered at a low temperature because of the high enthalpy of the proton transfer reaction[21]

$$2\,H_5O_2^+ \rightarrow 2\,H_2O + 2\,H_3O^+. \qquad (1)$$

Note that an increase in the distance between these groups upon dehydration results in the participation of functional groups in transfer processes. This leads to the advantage of hybrid membranes, which contain a significant number of additional oxygen-containing groups capable of participating in proton transfer in pores.

Transfer process selectivity

Selectivity is one of the important features of membranes; in the case of cation-exchange membranes, it depends on their ability to transfer cations much faster in comparison with anions or neutral molecules.[1] The selectivity of ion transfer in these membranes is determined by transfer numbers (charge fractions transferred by ions of a given charge). An increase in the transfer numbers of cations was detected for MF-4SK perfluorinated membranes modified by the nanoparticles of silica and zirconia,[34] acid zirconium phosphate,[35] silver,[36] carbon nanotubes[37] and polyaniline.[38]

The diffusion of gas and alcohol molecules in the hybrid membranes is of special interest. This is due to the fact that the

power of fuel cells and the fuel efficiency depend on a ratio between the rates of proton diffusion and the crossover of fuel (hydrogen, alcohols) and oxidant (oxygen) molecules. The possibility of crossover decrease is one of the most important advantages of hybrid membranes. Thus, for instance, the hybrid perfluorinated membranes containing silica are characterized by reduced permeability to gases and methanol.[39–43] The combination of high conductivity and low permeability to methanol makes these membranes highly applicable to direct methanol fuel cells. According to published data,[44] the specific power of this fuel cell on their basis is as high as 350 mA cm^{-2}. The surface of silica nanoparticles can be additionally modified to improve the properties of hybrid membranes. The Nafion membranes containing silica nanoparticles with grafted sulfo groups[45–47] or different sulfonic acid fragments[45,47,48] exhibited increased proton conductivity and low methanol permeability. The doping of Nafion membranes with silica and phosphotungstic acid diminished the permeability to methanol to 2×10^{-7} cm^2 s^{-1},[49] and the permeability of membranes from sulfonated polyether (ether) ketone (SPEEK) doped with a heteropoly acid to methanol was found lower than that of Nafion 117 by a factor of 20.[50] The membranes modification with sulfonated zeolites makes it possible to decrease permeability to methanol with the retention of proton conductivity and a considerable increase in the power of methanol fuel cells.[51,52] Choi *et al.*[53] managed to decrease the permeability of sulfonated polyaryl ether sulfone to methanol by modification with zeolites by a factor of more than 20.

The transfer processes occur in aqueous solution localized in the system of pores and channels in cation-exchange membranes where the distribution of cations and anions is nonhomogeneous. This is determined by the negative charge of pore walls due to the presence of fixed SO_3^- ions on them; the charge of these ions is compensated by the adjacently located protons. The thickness of this Debye layer is small (about 1 nm). On the contrary, anions and nonpolar molecules are excluded from it. On the other hand, almost electrically neutral solution localized at the pore center contains cations and anions in equal amounts. It can also contain

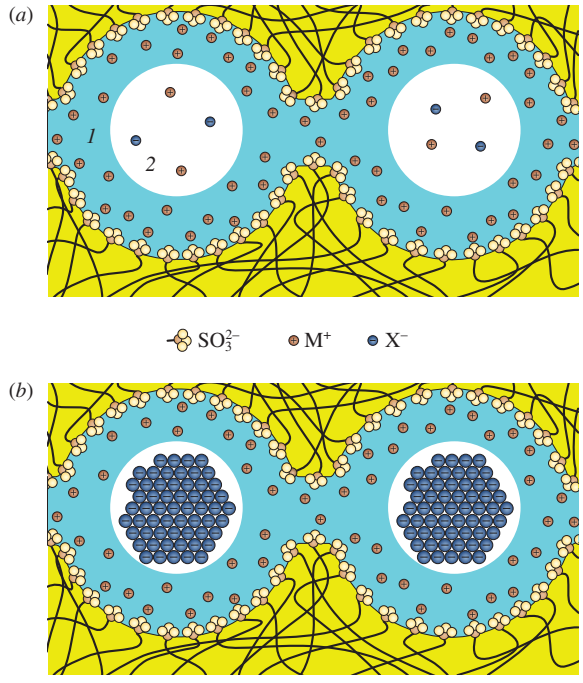

Figure 3 Diagram of the distribution of positively and negatively charged ions in the pores of (*a*) an ion-exchange membrane and (*b*) a membrane containing dopant nanoparticles: (*1*) Debye layer and (*2*) electrically neutral solution. Figure from ref. 21(*b*). ©2012 OOO 'Park-media'. Reproduced with permission.

nonpolar molecules.[54] Thus, a charge distribution in the pores and channels system of the membrane can be presented by the scheme [Figure 3(*a*)].[21]

The proton conductivity of the membranes is predominantly determined by transfer in the Debye layer along pore walls, but anions and nonpolar molecules mainly moved through free solution localized at the centers of pores. The formation of nanoparticles occurs directly in the membrane pores. Moreover, as follows from the above examples, their surface most frequently manifests acidic properties, and it will be charged negatively. Therefore, the localization of such particles near the walls of a channel is unfavorable in terms of electrostatics. Hence, such particles primarily displace free solution from the center of membrane pores without affecting the thin Debye layer localized near the walls [Figure 3(*b*)].[21,55] This leads to a decrease in the concentration of anions and neutral molecules like hydrogen or alcohols in the membrane (this is important in the use of the membranes in fuel cells). Therefore, their transfer becomes substantially slower, while the cation conductivity of hybrid membranes remains at the same level or increases.

Effect of the surface of dopant particles

It is obvious that the nature of a dopant can substantially affect the membranes water uptake (hydrophilicity or hydrophobicity) and the concentration of carriers (proton-acceptor ability). In turn, these parameters essentially influence the membrane conductivity.[56] The essential effect of the hydrophilicity of a dopant on the properties of membranes was noted.[4,57] Thus, for instance, the influence of the surface hydrophilicity of silica,[58,59] zirconium oxide[60–63] and zirconium phosphate[35,41,57,64–67] was considered.

Upon the introduction of hydrophobic particles (carbon, silicon carbide and fullerenes) into a membrane, its water uptake decreases, but the conductivity can also somewhat increase at a low dopant content or weakly change with decelerating of anions and neutral molecules transfer and raising the selectivity. A small improvement in the transport properties of Nafion membranes was noted only upon the membranes modification with C_{60} fullerene and fullerenol,[68] whereas modification with carbon nanotubes did not improve the conductivity of the membranes as well as the power of fuel cells.[69]

The influence of carrier concentrations can be even more important. The transfer of protons in the membranes is carried along the system of hydrogen bonds between water molecules and oxonium ions by the Grotthus mechanism.[28] The protons of acidic groups, whose concentration is proportional to the conductivity, are the current carrier. For increasing their number, it is reasonable to increase the acidity of a dopant by its acidic functionalization.

Indeed, the Nafion membranes doped with silica nanoparticles with a sulfonated surface were found very effective for fuel cells due to their higher proton conductivity and low methanol permeability.[45–47,70] Similar results were obtained upon the modification of membranes with the silica particles modified by different sulfonic acid fragments[45,48] or by metal oxides with sorbed heteropoly acids[49,71–76] or their salts[72,77–79] on their surface. The proton conductivity of the Nafion membranes with the additives of silicotungstic, phosphotungstic and phosphomolybdic heteropoly acids increased to 1.5×10^{-2}–9.5×10^{-2} Ω^{-1} cm^{-1}.[29,30] Good results were also obtained for other membranes doped by heteropoly acids.[80–83] Their conductivity at room temperature reached 9×10^{-2} Ω^{-1} cm^{-1}, and the permeability of membranes from sulfonated polyether (ether) ketone doped with a heteropoly acid was lower than that of Nafion 117 by a factor of more than 20.[50] The surface functionalization of single-wall carbon nanotubes (0.05 wt%) with sulfo groups made it possible to noticeably increase the proton conductivity of the Nafion membranes.[84]

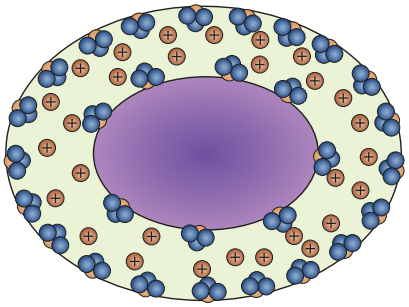

Figure 4 Distribution of ions in the pores of an ion-exchange membrane containing dopant nanoparticles whose surface contains groups with acidic properties.

Note that the membranes water uptake is assigned by osmotic pressure, which is determined by the number of acidic groups in its matrix. Therefore, the acidic modification of a dopant unavoidably leads to an increase in the water uptake of hybrid membranes.[21] At a low humidity, dopant particles actively participate in proton transfer, and nanoparticles whose surface has a clearly pronounced acid function also become most preferred.[31]

Surface modification also leads to a change in the selectivity of transport processes, as confirmed by a decrease in the permeability of neutral molecules and anions in the hybrid cation-exchange membranes with dopants whose surface is characterized by acidic properties.[45–52,84,85] It was noted above that an increase in the selectivity of hybrid membranes depends on the displacement of free solution, in which neutral molecules and anions are predominantly localized, from the pore center by dopant particles. Simultaneously, the negative charge of fixed ions localized on the pores walls prevents transfer of neutral molecules and anions in the thin Debye layer. The introduction of dopant nanoparticles whose surface contains groups with acidic properties results in the formation of an additional Debye layer (Figure 4), which decreases the concentration of anions and nonpolar molecules in the pore. This is responsible for a higher selectivity of transport processes in the membrane.

The nitrogen-containing groups of such species as amines and polyaniline are capable of binding the protons of SO_3H groups by strong hydrogen bonds.[86] This reduces the concentration of current carriers, the hydrophilicity and water uptake of the membranes.[38] Meantime, the conductivity of the membranes can be somewhat increased at a low polyaniline content[86] due to a change in the size of the pores and channels system. The modification of silica with hydrocarbon fragments containing the basic nitrogen atoms leads to the same effect.[87] Upon the introduction of these particles, their surface can be positively charged to form a Debye layer with an increased anions concentration. At the same time, their surface is bound to the walls of pores to decrease the volume of interstitial solution and to make it close to the Debye layer volume. This, on the contrary, provides a higher selectivity of transport processes.[87]

Hybrid materials for membrane gas separation

The development of hybrid membrane materials for gas separation was preceded by long-term works on filled polymers (*e.g.,* see ref. 88). The introduction of impenetrable inorganic particles (for example, SiO_2, Al_2O_3 and salts) into polymeric matrices increased the tortuosity of diffusion paths and, therefore, reduced the coefficients of diffusion and gas permeability without a gain in the selectivity of gas permeability. However, principally different results were obtained more recently with the use of much smaller particles (10–100 nm). This effect was convincingly demonstrated in a study of gas transport in polymethylpentyne with the additives of fumed silica (SiO_2) and other particles.[89] It was found that the permeability coefficients did not decrease upon the introduction of nanoadditives in accordance with the Maxwell model[90] for filled polymers; on the contrary, they noticeably raised. Moreover, this increase was more significant for particles with minimal sizes of introduced particles (SiO_2, soot and Al_2O_3):

Particle size, nm	500	30	15	12
Relative increase in permeability, P/P_0	1.05	1.25	1.6	1.9

These results were confirmed in numerous subsequent works. The permeability coefficients grew due to an increase in the free volume near phase boundaries and, consequently, by an increase in the diffusion coefficients.[91,92] An increase in the free volume was demonstrated by the positron annihilation method.[93,94] Meanwhile, in some cases, the introduction of nanoparticles is accompanied by a reduction of the coefficients of permeability and diffusion, and this behavior was explained by the densification of macrochains near the phase boundary.[95]

Two principally distinguished types of nanoparticles introduced into polymeric matrices were used. The nonporous nanoparticles include different oxides; the additives of SiO_2, TiO_2 and MgO were studied in most detail. The additives of porous nanoparticles are more diverse: interesting results were obtained for hybrid membrane materials containing carbon nanotubes, organometallic skeleton structures and zeolites.

The dependence of the permeability coefficients on additive concentration is important. In the overwhelming majority of cases, this dependence is nonlinear: at small additive concentrations, the permeability to different gases weakly depends on the amount of introduced nanoparticles; then, a sharp increase in the permeability is observed starting from concentrations of 30–35%.[96,97] This behaviour can be accounted for in terms the Takahashi–Paul model,[98] according to which a sharp increase in the diffusion and permeability coefficients begins after the formation of large clusters with an enhanced free volume at the interfaces. In some cases, the permeability passes through a minimum at the small concentrations of additives (*e.g.*, in the polytrimethylsilylpropyne–TiO_2 system[99]).

Hybrid systems with SiO_2 additives

Different behaviour in terms of the transport properties was observed upon the introduction of SiO_2 additives into glassy polymers and highly elastic polymers. Thus, for matrices based on the polymer with intrinsic microporosity (PIM-1)[96] or polysulfone,[97] an increase in the permeability with reducing different separation factors, for example, $\alpha(O_2/N_2)$, was observed (Figure 5).[97,100]

At the same time, the permeability decreased as a result of the introduction of a SiO_2 additive into highly elastic matrices (polyurethane, polydimethylsiloxane).[101,102] In terms of the Moore–Koros model,[95] this can be indicative of phase densification at the interfaces.

The introduction of SiO_2 additives makes the glassy matrix more loosely packed; this manifests itself in the transport properties of hydrocarbons with different molecular weights in polyacetylenes. It is well known that these highly permeable polyacetylenes exhibit so-called thermodynamic (solubility controlled) selectivity: an increase in the permeability coefficients with the molecular weight of a C_1–C_4 penetrant due to an increase in their solubility.[103] The introduction of SiO_2 nanoparticles into polytrimethylsilylpropyne and polymethylpentyne[104] increases the permeability coefficients of all of the hydrocarbons with the retention of thermodynamic selectivity. This is caused by raising diffusion coefficients since the sorption isotherms of gases and vapors in the hybrid systems do not depend on the concentration of SiO_2 added. An interesting result was obtained for other highly

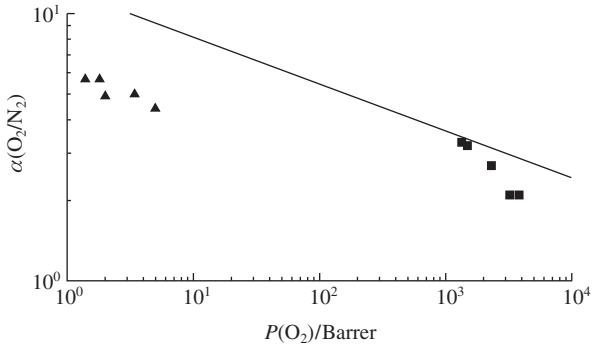

Figure 5 Permeability–selectivity relationship for the (squares) PIM-1–SiO_2 and (triangles) polysulfone–SiO_2 systems.The left and right points of the arrays correspond to pure polymers and maximum additive contents, respectively. The straight line corresponds to the upper boundary of the Robeson diagram (2008), which characterizes a maximum gas separation selectivity [$\alpha(O_2/N_2)$] at a given permeability [$P(O_2)$].

permeable polymer, amorphous Teflon AF2400, which has diffusion (size sieving) selectivity for the transport of the hydrocarbons: $P(CH_4) > P(C_4H_{10})$. The introduction of SiO_2 additives into this glass matrix made its structure much looser; as a result of this, the thermodynamic selectivity was observed: $P(CH_4) < P(C_4H_{10})$.[93] Thus, the introduction of nanoparticles can qualitatively change the regularities and mechanism of gas transport.

Hybrid membranes with carbon nanotube additives

Carbon nanotubes (CNTs) differ significantly from other nanoparticles introduced into the hybrid gas-separating membranes. First, they have large shape anisotropy (length-to-diameter ratio). Furthermore, there are both multiwall and single-wall CNTs. Unlike other nanoadditives, they were successfully used as membrane construction elements. In membranes of this kind, the CNT arrays are oriented perpendicularly to the base layer.[105] In this case, the Knudsen mechanism of transport occurred with very high parameters caused by the smooth walls of CNTs.[106] However, these systems with a very high throughput are low selective, and the mouths of CNTs should be functionalized for their use as membranes; in turn, this functionalization will affect the permeability. An additional special feature of CNTs is related to the fact that transport in the systems containing CNTs can occur not only through a matrix with changed properties but also through the channels of CNTs. Therefore, different properties are observed in CNTs with open and closed mouths. The role of transport through the channels of CNTs can be revealed by comparing experiments performed with compositions containing CNTs with closed and open ends. Thus, the introduction of CNTs with closed ends into a polyimide matrix led to a significant decrease in permeability.[107] This can be interpreted as an indication of the lengthening of diffusion paths in the membrane and the appearance of a closer packing at the interface. At the same time, the introduction of CNTs with open channels led to an increase in the permeability due to rapid transport inside the channels. It was found that, in the presence of functionalized CNTs, the permeability coefficients of gases in the systems based on PIM-1 polymer with intrinsic microporosity increased even at the small concentrations of an additive.[108]

CNT concentration (wt%)	0	1	2	3
Permeability to CO_2/Barrer	6210	7810	12270	4820

Studies on the transport of gases (N_2, O_2, CH_4 and C_3H_8) in the hybrid membranes based on glassy polyvinyltrimethylsilane with the small (0.3–3 wt%) additives of multiwall CNTs showed that, starting at a concentration of 0.4 wt%, the system passed through a threshold of percolation; thereafter, transport through the channels of CNTs, which is characterized by large flows and low selectivity, was predominant; that is, the Knudsen diffusion occurred.[109]

Hybrid systems with zeolite additives

Zeolites were the first to attract the attention of researchers as nanoadditives. Thus, Paul and Kemp[110] proposed an idea related to the more recent studies of hybrid membranes: zeolite introduced into siloxane simulated free volume elements in the glassy polymers. Zeolites are available and cheap feedstock, and this makes them useful additives in combination with different polymers. The geometric parameters of the porous crystal structure of zeolites are well known; thus, it seems possible to match specific zeolites for the selective sorption of particular components from a separated gas mixture. Figure 6 compares the pore sizes of some zeolites with the gas-kinetic sizes of some molecules.[111] This offers the possibility of the size sieving separation of specific gas mixtures. Note that numerous experimental data did not completely confirm expectations of this kind.

Various zeolites were considered as additives to different gas-separating membranes: SAPO-34, zeolites 3A and 4A, ZSM-5 (MFI), *etc*. They were introduced into polyvinyl acetate, Ultem polyesterimide, polycarbonate, polyethersulfone and other polymers. Zeolite additives do not principally differ from metal-organic frameworks (MOF) structures or nonporous nanoparticles (for example, SiO_2) by the type of their action.

On the one hand, as expected in accordance with the relative molecular dimensions of gases and pores in zeolites, the introduction of zeolite additives in a number of cases led to an increase in selectivity for pairs such as H_2/CH_4 and H_2/CO_2. For example, this occurred in the polyethersulfone–SAPO-34[112] and polycarbonate–zeolite 4A[113] systems. In some cases, both selectivity and permeability increased.[112] At the same time, in certain examples, the introduction of zeolite nanoadditives into polymers led to a decrease in selectivity: this was observed in the polyethersulfone–zeolite 4A[114] (for the pair CO_2/CH_4), polyether ether ketone–zeolite NaA[115] and polymethylmethacrylate–zeolite 4A (for the pair O_2/N_2).[116]

Defects appear at the interfaces between inorganic zeolite particles and an organic polymer matrix, and they can be responsible for a dramatic decrease in selectivity. To overcome these problems, third components, namely, organic molecules capable of improving the compatibility of zeolite nanoparticles and the matrix, are frequently introduced into the hybrid membranes containing zeolites. 2-Hydroxy-5-aniline, aminopropyltriethoxysilane and other substances were used as such additives.[117,118] Indeed, a simultaneous growth of permeability and selectivity is sometimes observed in ternary systems,[112] but this effect is absent from classical binary systems. Meantime, the introduced organic additives can partially block the pores of zeolites to decrease the permeability.[117]

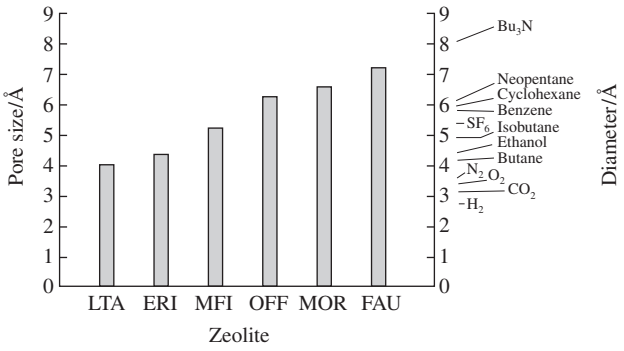

Figure 6 Correlation between the zeolite pore size and the molecular dimensions of gases and vapors.

In spite of the expected advantages of hybrid membranes containing zeolites, in the majority of studies of this type, even an increase in the permeability and selectivity does not provide a considerable improvement in the separating properties. As a result, in the Robeson diagrams,[100] which characterize maximum gas separation selectivity at a given permeability, the majority of the obtained systems lies considerably lower than the record values from Upper Bound. The reason for this is related to insufficiently high level of permeability and selectivity of the used polymer matrices.[112,113,115–117,119] Gorgojo *et al.*,[120] who introduced exfoliated zeolite Nu-6(2) into co-polyimide prepared based on 6FDA-containing dianhydrides, reported a rare example when the barrier of an upper boundary was overcome. The reason for this behavior of a system of this type is probably related to the fact that the representing points for the polymer matrix without additives are already located near upper boundaries of the Robeson diagram.

Mechanical properties of hybrid membranes

It is often assumed that the mechanical properties of high-molecular ion exchange membranes are among their prime advantages. A number of authors noted an improvement in the mechanical properties of hybrid membranes due to the synergism of their properties.[4] However, the modification of membranes with nanoparticles more frequently led to an inverse effect especially at high dopant contents.[21] This result is quite reasonable. It is well known that a decrease in the strength of solids is determined by the presence of extended defects (nanosized cracks) in their structures. The greater the size of a crack, the smaller the load at which its expansion occurs and the lower the mechanical strength of material as a whole.[121] The nanopores of membranes play the role of such cracks. From this point of view, it is possible to conclude that the higher the dopant concentration, the greater the pore size and the lower the membrane strength.

In the case of hybrid ion-exchange membranes, osmotic pressure inside pores becomes insufficient for compensating the elastic deformation forces of the walls at a large size of introduced particles; this diminishes the moisture content of the membranes. In this case, the concentration of protons in the interstitial solution and the osmotic pressure, which deforms the membrane from the inside, increase.[21]

Numerous studies of gas-separating membranes with the additives of nanoparticles also showed that the introduction of nanoparticles into different polymer matrices leads to a considerable worsening in the mechanical properties of composites. Some examples are represented in Table 1. As a result of the introduction of nanoadditives, polymer matrices become more brittle: both the tensile strength and ultimate elongation decrease. Note that low mechanical properties are a crucial factor that impedes the introduction of large dopant quantities. Analogous behavior was noted for both dense films and hollow-fiber membranes (*e.g.*, see refs. 126, 127).

On the other hand, based on the above theory of the solids destruction,[121] strengthening can be expected only upon the introduction of extensive one-dimensional nanoparticles, which are characterized by high strength, for example, CNTs, into the membranes. These dopants can be an analogue of nonwoven reinforcing material for the membrane to impart it a higher strength. Indeed, the introduction of a small quantity of single-wall CNTs into the membranes results in an essential improvement in their mechanical properties.[37,69,108] Thus, the doping of Nafion ion-exchange membranes with 1 wt% carbon nanotubes leads to an increase in their Young modulus by a factor of about 2 (from 50 to 110 N mm^{-2}) and the tensile stress from 8–10 to 13–15 MPa.[37] Analogously, a rise of the tensile strength and ultimate elongation was observed at small (up to 2%) concentrations of CNTs introduced into the PIM-1 polymer.[108] This fact can be considered as a confirmation of the formation of an additional extensive nanosized network from dopant particles, which increases the strength of the membrane. Note that a similar tendency is also observed upon the introduction of CNT additives into different polymers.[128] However, the mechanical properties of the membranes dramatically decrease with the concentration of CNTs.[37]

Table 1 Effect of the concentration of an introduced additive on the mechanical properties of the resulting hybrid membrane materials.

Polymer	Dopant	Dopant concentration (%)	Tensile strength/ MPa	Ultimate elongation (%)	Ref.
Polyimide Matrimid	MOF Cu-BPY-HFS	0	87	21.0	122
		10	75	6.6	
		20	69	4.6	
		30	53	3.0	
	MOF ZIF8	0	109		123
		20	98		
		30	93		
		60	47		
Polyimide 6FDA-ODA	MOF MIL53	0		12.0	124
		20		3.3	
		30		2.6	
		36		0.8	
Brominated poly(2,6-diphenyl-1,4-phenylene oxide)PPO	CNTs (single-wall)	0		4	125
		5		2	

Note that the problems of improving the mechanical properties of hybrid membranes have been inadequately considered in the literature. An obvious approach can assume crosslinking. However, this can be made only with the fabricated matrices; as a consequence, the technology of membrane preparation can become more expensive.

Conclusions

The above data show that, in a number of cases, the introduction of nanoparticles can lead to an essential improvement in the properties of the hybrid membranes, among which an increase in the proton conductivity of ion-exchange membranes and the permeability of gas-diffusion membranes can be noted. In addition, the selectivity of transport processes in many of them grows. Due to these facts, hybrid membranes can find a broad application in actual practice. Thus, the above data indicate that they are in wide current use for the construction of fuel cells with improved operational parameters and for gas separation processes. Furthermore, an increase in the selectivity of transport processes is responsible for their effective use in water purification processes,[129–131] for drug delivery[132] and as sensor materials.[133]

This work was supported by the Russian Foundation for Basic Research (project no. 14-29-04054).

References

1 A. B. Yaroslavtsev, V. V. Nikonenko and V. I. Zabolotsky, *Russ. Chem. Rev.*, 2003, **72**, 393 (*Usp. Khim.*, 2003, **72**, 438).
2 V. V. Volkov, B. V. Mchedlishvili, V. I. Roldugin, S. S. Ivanchev and A. B. Yaroslavtsev, *Nanotechnologies in Russia*, 2008, **3** (11–12), 656 [*Ross. Nanotekhnologii*, 2008, **3** (11–12), 67].
3 K. A. Mauritz and R. M. Warren, *Macromolecules*, 1989, **22**, 1730.
4 D. J. Jones and J. Roziere, *Handbook of Fuel Cells – Fundamentals, Technology and Applications*, eds. W. Vielstich, H. A. Gasteiger and A. Lamm, *Vol. 3, Fuel Cell Technology and Applications*, John Wiley & Sons, Ltd., 2003.
5 T. Xu, *J. Membr. Sci.*, 2005, **263**, 1.
6 A. B. Yaroslavtsev and V. V. Nikonenko, *Nanotechnologies in Russia*, 2009, **4** (3–4), 137 [*Ross. Nanotekhnologii*, 2009, **4** (3–4), 44].

7 A. B. Yaroslavtsev, *Russ. Chem. Rev*., 2009, **78**, 1013 (*Usp. Khim*., 2009, **78**, 1094).
8 H. Ahmad, S. K. Kamarudin, U. A. Hasran and W. R. W. Daud, *Int. J. Hydrogen Energy*, 2010, **35**, 2160.
9 S. J. Peighambardoust, S. Rowshanzamir and M. Amjadi, *Int. J. Hydrogen Energy*, 2010, **35**, 9349.
10 S. Bose, T. Kuila, T. X. Hien Nguyen, N. H. Kim, K.-t. Lau and J. H. Lee, *Prog. Polym. Sci.*, 2011, **36**, 813.
11 B. P. Tripathi and V. K. Shahi, *Prog. Polym. Sci*., 2011, **36**, 945.
12 A. B. Yaroslavtsev, Yu. A. Dobrovolsky, N. S. Shaglaeva, L. A. Frolova, E. V. Gerasimova and E. A. Sanginov, *Russ. Chem. Rev*., 2012, **81**, 191.
13 S. Kulprathipania, R. W. Neuzel and N. N. Li, *US Patent 5127925*, 1992.
14 T.-S. Chung, L. Y. Jiang, Y. Li and S. Kulprathipanja, *Prog. Polym. Sci.*, 2007, **32**, 483.
15 H. Vinh-Thang and S. Kaliaguine, *Chem. Rev.*, 2013, **113**, 4980.
16 M. A. Aroon, A. F. Ismail, T. Matsuura and M. M. Montazer-Rahmati, *Sep. Purif. Technol*., 2010, **75**, 229.
17 D. Bastani, N. Esmaeili and M. Asadollahi, *J. Ind. Eng. Chem*., 2013, **19**, 375.
18 J. C. Te Hennepe, D. Bargeman, M. H. V. Mulder and C. A. Smolders, *J. Membr. Sci*., 1987, **35**, 39.
19 P. Merten, K. Heinrich, M. Lazar and M. Priske, *J. Membr. Sci*., 2012, **222**, 401.
20 Y. Gu, R. M. Dorin and U. Wiesner, *Nano Lett*., 2013, **13**, 5323.
21 (*a*) E. Yu. Voropaeva, I. A. Stenina and A. B. Yaroslavtsev, *Russ. J. Inorg. Chem.*, 2008, **53**, 1531 (*Zh. Neorg. Khim.*, 2008, **53**, 1637); (*b*) A. B. Yaroslavtsev, *Nanotechnologies in Russia*, 2012, **7** (9–10), 437 [*Ross. Nanotekhnologii*, 2012, **7** (9–10), 8].
22 E. Yu. Safronova and A. B. Yaroslavtsev, *Solid State Ionics*, 2012, **221**, 6.
23 B. P. Tripathi and V. K. Shahi, *Prog. Polym. Sci.*, 2011, **36**, 945.
24 L. Y. Ng, A. W. Mohammad, C. P. Leo and N. Hilal, *Desalination*, 2013, **308**, 15.
25 E. Yu. Voropaeva, E. A. Sanginov, V. I. Volkov, A. A. Pavlov, A. S. Shalimov, I. A. Stenina and A. B. Yaroslavtsev, *Russ. J. Inorg. Chem.*, 2008, **53**, 1536 (*Zh. Neorg. Khim.*, 2008, **53**, 1643).
26 S. A. Novikova, E. Yu. Safronova, A. A. Lysova and A. B. Yaroslavtsev, *Mendeleev Commun*., 2010, **20**, 156.
27 A. B. Yaroslavtsev, Yu. A. Karavanova and E. Yu. Safronova, *Petroleum Chem.*, 2011, **51**, 473 (*Membrany Membran. Tekhnol*., 2011, **1**, 3).
28 K. D. Kreuer, S. Paddison, E. Spohr and M. Schuster, *Chem. Rev*., 2004, **104**, 4637.
29 H. Xu, M. Wu, Y. Liu, V. Mittal, F. Kassim, B. Vieth, L. Bonville, H. R. Kunz and J. M. Fenton, *ECS Trans*., 2006, **3**, 561.
30 V. Ramani, H. R. Kunz and J. M. Fenton, *J. Membr. Sci*., 2004, **232**, 31.
31 E. Yu. Safronova, I. A. Stenina and A. B. Yaroslavtsev, *Russ. J. Inorg. Chem.*, 2010, **55**, 13 (*Zh. Neorg. Khim*., 2010, **55**, 16).
32 A. K. Sahu, S. Pitchumani, P. Sridhar and A. K. Shukla, *Fuel Cells*, 2009, **9**, 139.
33 V. I. Volkov and A. A. Marinin, *Russ. Chem. Rev.*, 2013, **82**, 248.
34 I. A. Stenina, E. Yu. Voropaeva, A. A. Ilyina and A. B. Yaroslavtsev, *Polym. Adv. Technol*., 2009, **20**, 566.
35 A. S. Shalimov, S. A. Novikova, I. A. Stenina and A. B. Yaroslavtsev, *Russ. J. Inorg. Chem*., 2006, **51**, 700 (*Zh. Neorg. Khim*., 2006, **51**, 767).
36 S. A. Novikova, G. Yu. Yurkov and A. B. Yaroslavtsev, *Mendeleev Commun*., 2010, **20**, 89.
37 A. I. Perepelkina, E. Yu. Safronova, A. S. Shalimov and A. B. Yaroslavtsev, *Petroleum Chem.*, 2012, **52**, 475 (*Membrany Membran. Tekhnol*., 2012, **2**, 27).
38 A. A. Lysova, I. A. Stenina, Yu. G. Gorbunova, N. A. Kononenko and A. B. Yaroslavtsev, *Russ. J. Electrochem*., 2011, **47**, 579 (*Elektrokhimiya*, 2011, **47**, 618).
39 S. Ren, G. Sun, C. Li, Z. Liang, Z. Wu, W. Jin, X. Qin and X. Yang, *J. Membr. Sci*., 2006, **282**, 450.
40 R. Jiang, H. R. Kunz and J. M. Fenton, *J. Membr. Sci*., 2006, **272**, 116.
41 H. Tang, Z. Wan, M. Pan and S. P. Jiang, *Electrochem. Commun*., 2007, **9**, 2003.
42 A. D'Epifanio, B. Mecher, E. Fabbri, A. Rainer, E. Traversa and S. Licoccia, *J. Electrochem. Soc*., 2007, **154**, B1148.
43 Y. Tominaga, I.-C. Hong, S. Asai and M. Sumita, *J. Power Sources*, 2007, **171**, 530.
44 K. T. Adjemian, S. J. Lee, S. Srinivasan, J. Benziger and A. B. J. Bocarsly, *J. Electrochem. Soc.*, 2002, **149**, A256.
45 B. P. Ladewig, R. B. Knott, A. J. Hill, J. D. Riches, J. W. White, D. J. Martin, J. C. D. da Costa and G. Q. Lu, *Chem. Mater*., 2007, **19**, 2372.
46 Y.-F. Lin, C.-Y. Yen, C.-C. M. Ma, S.-H. Liao, C.-H. Lee, Y.-H. Hsiao and H.-P. Lin, *J. Power Sources*, 2007, **171**, 388.
47 F. Pereira, K. Valle, P. Belleville, A. Morin, S. Lambert and C. Sanchez, *Chem. Mater*., 2008, **20**, 1710.
48 C. Li, G. Sun, S. Ren, J. Liu, Q. Wang, Z. Wu, H. Sun and W. Jin, *J. Membr. Sci*., 2006, **272**, 50.
49 W. Xu, T. Lu, C. Liu and W. Xing, *Electrochim. Acta*, 2005, **50**, 3280.
50 J. Shan, G. Vaivars, H. Luo, R. Mohamed and V. Linkov, *Pure Appl. Chem.*, 2006, **78**, 1781.
51 B. A. Holmberg, X. Wang and Y. S. Yan, *Microporous Mesoporous Mater*., 2004, **74**, 189.
52 Z. Chen, B. Holmberg, W. Li, X. Wang, W. Deng, R. Munoz and Y. Yan, *Chem. Mater*., 2006, **18**, 5669.
53 Y. S. Choi, T. K. Kim, E. A. Kim, S. H. Joo, C. Pak, Y. H. Lee, H. Chang and D. Seung, *Adv. Mater*., 2008, **20**, 2341.
54 V. V. Nikonenko, A. B. Yaroslavtsev and G. Pourcelly, in *Ionic Interactions in Natural and Synthetic Macromolecules*, eds. A. Ciferri and A. Perico, John Wiley & Sons Inc., 2012, p. 267.
55 E. Yu. Safronova and A. B. Yaroslavtsev, *Solid State Ionics*, 2013, **251**, 23.
56 *Perfluorinated Ionomer Membranes*, eds. A. Eisenberg and H. L. Yager, Am. Chem. Soc., Washington, 1982.
57 Y. Zhang, H. Zhang, C. Bi and X. Zhu, *Electrochim. Acta*, 2008, **53**, 4096.
58 F. Lufrano, V. Baglio, P. Staiti, A. Arico and V. Antonucci, *Desalination*, 2006, **199**, 283.
59 L. M. de Carvalho, A. R. Tan and G. A. de Souza, *J. Appl. Polym. Sci*., 2008, **110**, 1690.
60 N. H. Jalani, K. Dunn and R. Datta, *Electrochim. Acta*, 2005, **51**, 553.
61 V. S. Silva, B. Ruffmann, H. Silva, V. B. Silva, A. Mendes, L. M. Madeira and S. J. Nunes, *Membr. Sci*., 2006, **284**, 137.
62 W.-B. Yang, H. Zhu, M. Wang and S.-C. Zhang, *J. Funct. Mater*., 2007, **38**, 2077.
63 Z.-G. Shao, H. Xu, I.-M. Hsing and H. Zhang, *Chem. Eng. Commun.*, 2007, **194**, 667.
64 C. Yang, S. Srinivasan, A. B. Bocarsly, S. Tulyani and J. B. Benziger, *J. Membr. Sci*., 2004, **237**, 145.
65 G. Alberti, M. Casciola, D. Capitani, A. Donnadio, R. Narducci, M. Pica and M. Sganappa, *Electrochim. Acta*, 2007, **52**, 8125.
66 S. Sang, Q. Wu and K. Huang, *J. Membr. Sci*., 2007, **305**, 118.
67 A. I. Fomenkov, I. Yu. Pinus, A. S. Peregudov, Ya. V. Zubavichus, A. B. Yaroslavtsev and A. R. Khokhlov, *Polym. Sci., Ser. B*, 2007, **49**, 177 (*Vysokomol. Soedin., Ser. B*, 2007, **49**, 1299).
68 K. Tasaki, R. DeSousa, H. B. Wang, J. Gasa, V. A. Venkatesan, P. Pugazhendhi and R. O. Loutfy, *J. Membr. Sci.*, 2006, **281**, 570.
69 Y. H. Liu, B. L. Yi, Z. G. Shao, D. M. Xing and H. M. Zhang, *Electrochem. Solid State Lett.*, 2006, **9**, A356.
70 N. Miyake, J. S. Wainright and R. F. Savinell, *J. Electrochem. Soc.*, 2001, **148**, A905.
71 Z.-G. Shao, P. Joghee and I.-M. Hsing, *J. Membr. Sci*., 2004, **229**, 43.
72 V. Ramani, H. R. Kunz and J. M. Fenton, *J. Membr. Sci*., 2006, **279**, 506.
73 G. Ye, C. A. Hayden and G. R. Goward, *Macromolecules*, 2007, **40**, 1529.
74 M. Helen, B. Viswanathan and S. S. Murthy, *J. Membr. Sci*., 2007, **292**, 98.
75 A. Mahreni, A. B. Mohamad, A. A. H. Kadhum, W. R. W. Daud and S. E. Iyuke, *J. Membr. Sci*., 2009, **327**, 32.
76 E. Yu. Safronova, I. A. Stenina, A. A. Pavlov, V. I. Volkov, G. Yu. Yurkov and A. B. Yaroslavtsev, *Russ. J. Inorg. Chem*., 2011, **55**, 152 (*Zh. Neorg. Khim*., 2011, **55**, 187).
77 V. Ramani, H. R. Kunz and J. M. Fenton, *J. Power Sources*, 2005, **152**, 182.
78 M. Amirinejad, S. S. Madaeni, M. A. Navarra, E. Rafiee and B. Scrosati, *J. Power Sources*, 2011, **196**, 988.
79 Y. Xiang, M. Yang, J. Zhang, F. Lan and S. Lu, *J. Membr. Sci.*, 2011, **368**, 241.
80 P. Genova-Dimitrova, B. Baradie, D. Foscallo, C. Poinsignon and J. Y. Sanchez, *J. Membr. Sci*., 2001, **185**, 59.
81 L. Li and Y. Wang, *J. Power Sources*, 2006, **162**, 541.
82 M. Yamada and I. Honmia, *J. Phys. Chem. B*, 2006, **110**, 20486.
83 Z. Wang, H. Ni, C. Zhao, X. Li, T. Fu and H. Na, *J. Polym. Sci., Part B: Polym. Phys*., 2006, **44**, 1967.
84 R. Kannan, B. A. Kakade and V. K. Pillai, *Angew. Chem. Int. Ed*., 2008, **47**, 2653.
85 P. Staiti, A. S. Aricò, V. Baglio, F. Lufrano, E. Passalacqua and V. Antonucci, *Solid State Ionics*, 2001, **145**, 101.
86 I. A. Stenina, A. A. Il'ina, I. Yu. Pinus, V. G. Sergeev and A. B. Yaroslavtsev, *Russ. Chem. Bull., Int. Ed.*, 2008, **57**, 2261 (*Izv. Akad. Nauk, Ser. Khim.*, 2008, 2219).
87 A. G. Mikheev, E. Yu. Safronova, G. Yu. Yurkov and A. B. Yaroslavtsev, *Mendeleev Commun*., 2013, **23**, 172.
88 S. A. Reitlinger, *Pronitsayemost polimernykh materialov (Permeability of Polymeric Materials)*, Khimiya, Moscow, 1974 (in Russian).

89 T. C. Merkel, B. D. Freeman, R. J. Spontak, Z. He, I. Pinnau, P. Meakin and A. J. Hill, *Science*, 2002, **296**, 519.
90 J. C. Maxwell, *A Treatise on Electricity and Magnetism*, Oxford University Press, London, 1873, vol. 1.
91 T. C. Merkel, Z. He, I. Pinnau, B. D. Freeman, P. Meakin and A. J. Hill, *Macromolecules*, 2003, **36**, 6844.
92 J. Zhong, W.-Y. Wen and A. A. Jones, *Macromolecules*, 2003, **36**, 6430.
93 T. C. Merkel, Z. He, I. Pinnau, B. D. Freeman, P. Meakin and A. J. Hill, *Macromolecules*, 2003, **36**, 8406.
94 A. F. Bushell, M. P. Attfield, C. R Mason, P. M. Budd, Yu. Yampolskii, L. Starannikova, A. Rebrov, F. Bazzarelli, P. Bernardo, J. C. Jansen, M. Lanc, K. Friess, V. Shantarovich, V. Gustov and V. Isaeva, *J. Membr. Sci*., 2013, **427**, 48.
95 T. T. Moore and W. J. Koros, *J. Mol. Struct*., 2005, **739**, 87.
96 J. Ahn, W.-J. Chung, I. Pinnau, J. Song, N. Du, G. P. Robertson and M. D. Guiver, *J. Membr. Sci*., 2010, **346**, 280.
97 J. Ahn, W.-J. Chung, I. Pinnau and M. D. Guiver, *J. Membr. Sci*., 2008, **314**, 123.
98 S. Takahashi and D. R. Paul, *Polymer*, 2006, **47**, 7519.
99 S. Matteucci, V. A. Kusuma, D. Sanders, S. Swinnea and B. D. Freeman, *J. Membr. Sci.*, 2008, **307**, 196.
100 L. M. Robeson, *J. Membr. Sci.*, 2008, **320**, 390.
101 J. M. A. Semsarzadeh and B. Ghalei, *J. Membr. Sci*., 2013, **432**, 115.
102 E. Farno, A. Ghadimi, N. Kasiri and T. Mohammadi, *Sep. Purif. Technol*., 2011, **81**, 400.
103 K. Nagai, T. Masuda, T. Nakagawa, B. D. Freeman and I. Pinnau, *Prog. Polym. Sci*., 2001, **26**, 721.
104 I. Pinnau and Z. He, *US Patent 6316684*, 2001.
105 B. J. Hinds, N. Chopra, T. Rantell, R. Andrews, V. Gavalas and L. Bachas, *Science*, 2004, **303**, 62.
106 J. K. Holt, H. G. Park, Y. Wang, M. Stadermnn, A. B. Artyukhin, C. P. Grigoropoulos, A. Noy and O. Bakajin, *Science*, 2006, **312**, 1034.
107 M. A. Aroon, A. F. Ismail, M. M. Montazer-Rahmati and T. Matsuura, *J. Membr. Sci*., 2010, **364**, 309.
108 M. M. Khan, V. Filiz, G. Bengtson, S. Shishatskiy, M. M. Rahman, J. Lillepaerg and V. Abetz, *J. Membr. Sci*., 2013, **436**, 109.
109 A. M. Grekhov, Yu. S. Eremin, G. A. Dibrov and V. V. Volkov, *Petroleum Chem.*, 2013, **53**, 549 (*Membrany Membran. Tekhnol.*, 2013, **3**, 168).
110 D. R. Paul and D. R. Kemp, *J. Polym. Sci.: Polym. Phys. Ed.*, 1973, **41**, 79.
111 H. Kita, in *Material Science of Membranes for Gas and Vapor Separation*, eds. Yu. Yampolskii, I. Pinnau and B. D. Freeman, Wiley, Chichester, 2006, p. 373.
112 E. Karatay, H. Kalipcilar and L. Yilmaz, *J. Membr. Sci.*, 2010, **364**, 75.
113 D. Sen, H. Kalipcilar and L. Yilmaz, *J. Membr. Sci*., 2007, **303**, 194.
114 Y. Li, F. Liang, H. Bux, W. Yang and J. Caro, *J. Membr. Sci*., 2010, **354**, 48.
115 G. Clarizia, C. Algieri, A. Regina and E. Drioli, *Microporous Mesoporous Mater*., 2008, **115**, 67.
116 C.-C. Hu, T.-C. Liu, K.-R. Lee, R.-C. Ruan and J.-Y. Lai, *Desalination*, 2006, **193**, 14.
117 P. S. Goh, A. F. Ismail, S. M. Sanip, B. C. Ng and M. Aziz, *Sep. Purif. Technol*., 2011, **81**, 243.
118 M. G. Buonomenna, W. Yave and G. Golemme, *RSC Adv.*, 2012, **2**, 10745.
119 J. Ahmad and M.-B. Hagg, *J. Membr. Sci*., 2013, **427**, 73.
120 P. Gorgojo, D. Sieffert, C. Staudt, C. Tellez and J. Coronas, *J. Membr. Sci.*, 2012, **411**–**412**, 146.
121 C. Kittel, *Introduction to Solid State Physics*, 7th edn., Wiley, New York, 1996.
122 Y. Zhang, I. H. Musselman, J. P. Ferraris and K. J. Balkus, *J. Membr. Sci*., 2008, **313**, 170.
123 M. J. C. Ordonez, K. J. Balkus, J. P. Ferraris and I. M. Musselman, *J. Membr. Sci*., 2010, **361**, 28.
124 X. Y. Chen, H. Vinh-Thang, D. Rodrigue and S. Kaliaguine, *Ind. Eng. Chem. Res*., 2012, **51**, 6895.
125 H. Cong, J. Zhang, M. Radosz and Y. Shen, *J. Membr. Sci*., 2007, **294**, 178.
126 S. Basu, A. Cano-Odena and I. F. J. Vankelecom, *J. Membr. Sci*., 2010, **362**, 478.
127 J. Hu, H. Cai, H. Ren, Y. Wei, Z. Xu, H. Liu and Y. Hu, *Ind. Eng. Chem. Res*., 2010, **49**, 12605.
128 M. Moniruzzaman and K. I. Winey, *Macromolecules*, 2006, **39**, 5194.
129 V. I. Zabolotskii, K. V. Protasov, M. V. Sharafan and A. B. Yaroslavtsev, *RF Patent 2451540*, 2012.
130 A. K. Singh, P. Singh, S. Mishra and V. K. Shahi, *J. Mater. Chem*., 2012, **22**, 1834.
131 H. Dong, K.-j. Xiao, X.-l. Li, Y. Ren and S.-y. Guo, *Desalination and Water Treatment*, 2013, **51**, 3685.
132 N. Wang, C. Wu, Y. Cheng and T. Xu, *Int. J. Pharm*., 2011, **408**, 39.
133 O. V. Bobreshova, A. V. Parshina, K. A. Polumestnaya, E. Yu. Safronova, K. Yu. Yankina and A. B. Yaroslavtsev, *Mendeleev Commun*., 2012, **22**, 83.

Received: 7th May 2014; Com. 14/4368

Available online at www.sciencedirect.com
ScienceDirect
Mendeleev Commun., 2014, **24**, 327–328
Mendeleev Communications

Modulation of chemical interactions across graphene layers and metastable domains in carbon materials

Evgeniy O. Pentsak and Valentine P. Ananikov*

N. D. Zelinsky Institute of Organic Chemistry, Russian Academy of Sciences, 119991 Moscow, Russian Federation. Fax: + 7 499 135 5328; e-mail: val@ioc.ac.ru

DOI: 10.1016/j.mencom.2014.11.002

Attachment of palladium clusters to carbon surface was investigated by SEM and STEM methods that have suggested plausible modification of chemical interactions across graphene layers; the fact can explain mismatches between domain structures and alignment patterns of palladium nanoparticles observed experimentally by the electron microscopy.

Carbon materials have been used in chemistry and catalysis for more than a century and made substantial impact on various fields of science. At the present time, a huge number of catalysts and reagents based on carbon materials was developed for research and industry.[1,2] However, only in the recent years, after tremendous interest in graphene, detailed investigations of carbon materials at molecular level and estimations of effect of carbon structure on metal-containing catalysts were emerged to a new level.[3]

Recently we have shown that Pd_2dba_3 complex possesses intrinsic dynamics and easily decomposes with formation of Pd nanoparticles even under ambient conditions.[4] In the present study we have utilized this fascinating feature of Pd_2dba_3 for covering carbon surface with Pd nanoparticles. We have prepared Pd nanoparticles supported on graphite and investigated the morphology of Pd/C system using field-emission scanning electron microscopy (SEM) and scanning transmission electron microscopy (STEM).† We have found that Pd nanoparticles did not settle on the graphite surface uniformly (neither chaotically), but formed certain patterns on carbon surface. At the first sight we concluded that nanoparticles lined up along visible graphite edges and grain boundaries, which is expected and was discussed in the literature.[5,6] However, the further analysis evidenced more complex patterns with non-obvious surface distribution of attached particles.

Figure 1(*a*) shows studied graphite surface coated with palladium nanoparticles. We used a low accelerating voltage of 30 kV for the microscopy observation, which allowed us to study the morphology of a thin layer of graphite on the edge of the carbon particle without a damage of the sample by electron beam. Carbon material, metal nanoparticles and several sets of dark/grey lines were clearly seen in the studied Pd/graphite sample.

Important to note that dark/grey lines, visible in the image, had different widths and directions. Variation of image recording parameters (such as angle of sample tilt, focal length, and accelerating voltage) did not affect detected patterns. It appears the observed combination of dark/grey lines originates from the moiré effect.[7] This effect is known to appear when one or few graphene layers in a stack of graphite rotate on a small angle around the axis perpendicular to the basal plane of graphite. Such arrangement results in overlapping of periodic lattice and, consequently, leads to interference of electron beam of the microscope. Observation of moiré effect in graphite by TEM was reported by Gillin *et al.* in 1968.[8] The moiré pattern in graphene was observed by Kuwabara *et al.* in 1990 by scanning tunnel microscope upon characterization of a freshly cleaved sample of highly oriented pyrolytic graphite.[9] Afterwards, numerous publications have focused on the moiré effect in graphene and graphite studied by STM methods.[10] From simple geometric considerations the constant of the superlattice can be calculated by the formula $d = p/[2\sin(\alpha/2)]$, where α is the angle of rotational misorientation, d is the distance between two pale lines (*i.e.* constant of superlattice), and p is the lattice constant.[7] With this simple relationship, the angle of shift of the two planes can be calculated according to the formula: $\alpha = 2\arcsin(p/2d)$. From the structural point of view, the wider the observed lines, the smaller the angle of graphene layer rotation.

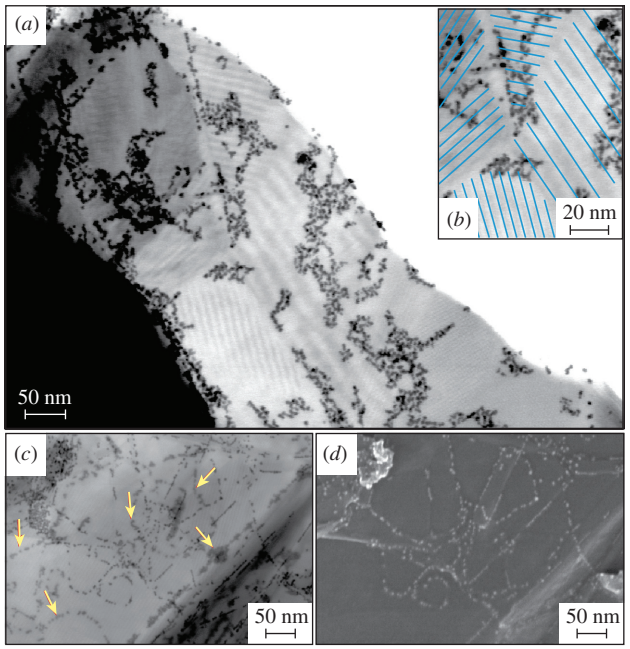

Figure 1 Pd nanoparticles supported on graphite studied by (*a*)–(*c*) STEM and (*d*) SEM methods. Directions of the dark/grey lines on graphite surface are highlighted by straight lines in the insert (*b*). Arrows on the STEM image (*c*) indicate Pd nanoparticles, which were not visible in the SEM image of the same region of the sample (*d*).

† *Experimental details.* STEM: powdered sample was attached on copper grid and fixed in aluminum specimen holder with copper cap. Images were acquired by transmitted electron detector (scintillator + photomultiplier system) in bright field image mode at 30 kV accelerating voltage and at working distance of 8 mm. SEM: the same sample was used and the image was recorded at the same region. Images were acquired in secondary electron mode at 30 kV accelerating voltage and at working distance of 8 mm. The observations were carried out using Hitachi SU8000 field-emission scanning electron microscope (FE-SEM).

For the studied sample, the longest distance between the white lines on graphite surface was around 100 Å, and the smallest distance was around 35 Å. According to the above formula and considering that the lattice constant of graphene is 2.46 Å, the angle of graphene sheets rotation was estimated as 1°24′ for the lines with 100 Å step and 4°1′ for the lines with 35 Å step.

As shown in Figure 1(*a*), the areas with bounded Pd nanoparticles and chains do not always match those areas, where one type of direction and geometry of moiré patterns was observed. The finding suggests that domain structure does not always affect the interaction of metals with the surface of the carbon material.

Microscopy images of the same region of surface characterized by both SEM and STEM methods have further highlighted the observation [Figure 1(*c*),(*d*)]. Note that many additional Pd nanoparticles and nanoparticle chains became visible in the STEM mode. The nanoparticles and chains were only partially seen in the secondary electrons mode of SEM, which reflects morphology from the surface of the sample.

Presumably, additional particles, appeared in the STEM image, may be bound between the graphene layers, penetrated into the inner part of the carbon sample or located on the other side of the sheets. It is important to note that the distribution pattern in the curvature of lines and chains also retained for these palladium particles.

To summarize, two experimental findings deserve a special note: (i) binding of metal nanoparticles does not always correlate with simple domain structure of the carbon material, where defective and most reactive carbon centers are expected; (ii) appearance of more complex 3D carbon structures (metastable 3D carbon domains) could be proposed by joint analysis of SEM and STEM images.

These experimental observations gave us an idea that graphene layers modulate chemical interactions across their surface. This modulation (modification) of chemical reactivity can be sensed by reactive particles and active species. Such domains and patterns of carbon materials were not obviously visible upon surface characterization of native carbon material with standard analytic tools (prior to Pd nanoparticles attachment).

We anticipate more detailed studies in the nearest future dealing with the origins of chemical reactivity across graphene layers and the nature of carbon domains.

The study was supported by the Russian Science Foundation (grant no. 14-13-01030). The authors are grateful to Dr. E. G. Gordeev for helpful discussion.

References

1 (*a*) F. Rodríguez-reinoso, *Carbon*, 1998, **36**, 159; (*b*) P. Serp, M. Corrias and P. Kalck, *Appl. Catal., A*, 2003, **253**, 337; (*c*) P. Serp and E. Castillejos, *ChemCatChem*, 2010, **2**, 41; (*d*) P. M. Ajayan, *Chem. Rev*., 1999, **99**, 1787; (*e*) D. Tasis, N. Tagmatarchis, A. Bianco and M. Prato, *Chem. Rev.*, 2006, **106**, 1105; (*f*) M. J. Allen, V. C. Tung and R. B. Kaner, *Chem. Rev*., 2010, **110**, 132; (*g*) D. S. Su, S. Perathoner and G. Centi, *Chem. Rev*., 2013, **113**, 5782.

2 V. P. Ananikov, L. L. Khemchyan, Yu. V. Ivanova, V. I. Bukhtiyarov, A. M. Sorokin, I. P. Prosvirin, S. Z. Vatsadze, A. V. Medved'ko, V. N. Nuriev, A. D. Dilman, V. V. Levin, I. V. Koptyug, K. V. Kovtunov, V. V. Zhivonitko, V. A. Likholobov, A. V. Romanenko, P. A. Simonov, V. G. Nenajdenko, O. I. Shmatova, V. M. Muzalevskiy, M. S. Nechaev, A. F. Asachenko, O. S. Morozov, P. B. Dzhevakov, S. N. Osipov, D. V. Vorobyeva, M. A. Topchiy, M. A. Zotova, S. A. Ponomarenko, O. V. Borshchev, Yu. N. Luponosov, A. A. Rempel, A. A. Valeeva, A. Yu. Stakheev, O. V. Turova, I. S. Mashkovsky, S. V. Sysolyatin, V. V. Malykhin, G. A. Bukhtiyarova, A. O. Terent'ev and I. B. Krylov, *Russ. Chem. Rev*., 2014, **83**, 885.

3 (*a*) J. C. Meyer, A. K. Geim, M. I. Katsnelson, K. S. Novoselov, T. J. Booth and S. Roth, *Nature*, 2007, **446**, 60; (*b*) J. Granatier, P. Lazar, R. Prucek, K. Šafářová, R. Zbořil, M. Otyepka and P. Hobza, *J. Phys. Chem. C,* 2012, **116**, 14151; (*c*) Z. Zhang and C. H. Turner, *J. Phys. Chem. C*, 2013, **117**, 8758; (*d*) T.-T. Jia, C.-H. Lu, Y.-F. Zhang and W.-k. Chen, *J. Nanopart. Res*., 2014, **16**, 2206; (*e*) E. O. Pentsak, E. G. Gordeev and V. P. Ananikov, *ACS Catal.*, 2014, **4**, 3806.

4 S. S. Zalesskiy and V. P. Ananikov, *Organometallics*, 2012, **31**, 2302.

5 A. N. Khlobystov and A. Hirsch, *Dalton Trans*., 2014, **43**, 7345.

6 (*a*) E. L. Evans, R. J. M. Griffiths and J. M. Thomas, *Science*, 1971, **15**, 174; (*b*) R. T. Yang and C. Wong, *Science*, 1981, **214**, 437; (*c*) Y. Fan, M. Burghard and K. Kern, *Adv. Mater.*, 2002, **14**, 130; (*d*) T. J. Davies, M. E. Hyde and R. G. Compton, *Angew. Chem. Int. Ed*., 2005, **44**, 5121; (*e*) V. C. Diculescu, A.-M. Chiorcea-Paquim, O. Corduneanu and A. M. Oliveira-Brett, *J. Solid State Electrochem*., 2007, **11**, 887; (*f*) J. Taing, M. H. Cheng and J. C. Hemminger, *ACS Nano*, 2011, **5**, 6325; (*g*) Z. Liang, H. Khosravian, A. Uhl, R. J. Meyer and M. Trenary, *Surf. Sci.*, 2012, **606**, 1643.

7 I. Amidror, *The Theory of the Moiré Phenomenon, Vol. I. Periodic Layer*, 2nd edn., Springer, 2009.

8 L. M. Gillin and A. Kelly, *J. Mater. Sci.*, 1968, **3**, 408.

9 M. Kuwabara, D. R. Clarke and D. A. Smith, *Appl. Phys. Lett*., 1990, **56**, 2396.

10 (*a*) A. H. MacDonald and R. Bistritzer, *Nature*, 2011, **474**, 453; (*b*) A. Luican, G. Li, A. Reina, J. Kong, R. R. Nair, K. S. Novoselov, A. K. Geim and E. Y. Andrei, *Phys. Rev. Lett*., 2011, **106**, 126802; (*c*) R. Bistritzer and A. H. MacDonald, *Proc. Natl. Acad. Sci. U.S.A.*, 2011, **108**, 12233; (*d*) M. K. Singh, E. Titus, G. Gonçalves, P. A. A. P. Marques, I. Bdikin, A. L. Kholkin and J. J. A. Gracio, *Nanoscale*, 2010, **2**, 700; (*e*) K. Kobayashi, *Phys. Rev. B*, 1996, **53**, 11091.

Received: 29th September 2014; Com. 14/4475

Available online at www.sciencedirect.com
ScienceDirect
Mendeleev Commun., 2014, **24**, 329–331
Mendeleev Communications

Cobalt diketonate adducts with redox-active diiminosuccinonitriles

Alyona A. Starikova,[a] Vladimir I. Minkin[a,b] and Andrey G. Starikov*[b]

[a] *Institute of Physical and Organic Chemistry, Southern Federal University, 344090 Rostov-on-Don, Russian Federation. Fax: +7 863 243 4667; e-mail: andr@ipoc.sfedu.ru*
[b] *Southern Scientific Center of the Russian Academy of Sciences, 344006 Rostov-on-Don, Russian Federation*

DOI: 10.1016/j.mencom.2014.11.003

The DFT calculations predict that adducts of cobalt diketonates with diiminosuccinonitriles can exhibit a valence tautomeric behavior.

Transition metal complexes with redox-active (noninnocent) ligands, in which interconversion between high-spin and low-spin states is caused by the intramolecular electron transfer between the metal and the ligand externally tuned by temperature, light, or applied pressure, have significant promise for the design of magnetically responsive molecular switches and sensors.[1,2] The reversible rearrangements of these coordination compounds, termed as valence tautomerism (VT), have now been extensively studied and amply reviewed.[2–4] Since the first report on a VT transition,[5] attention has been focused on studying octahedral mononuclear Co and Mn 1 : 2 complexes with benzoquinone ligands.[6,7] We have recently noted that the area of prospective VT coordination compounds can be substantially extended by turning attention to the adducts of tetracoordinate transition metal complexes with redox-active ligands in the case when the energy barrier to the VT rearrangement of the adduct is less than the energy required for its thermal dissociation. The density functional theory (DFT) calculations performed on the adducts of Co diketonates with *o*-benzoquinone and its imines[8] and diimines of glyoxal[9] have shown that these adducts meet the necessary requirements. The recently synthesized mixed-ligand adducts of redox-active 2,4,6,8-tetra-*tert*-butylphenoxazin-1-one with cobalt bis(salicylaldiminates) demonstrate temperature-dependent magnetic properties related to the Co^{II}/Co^{III} transitions.[10]

Here, we report a computational study of the molecular and electronic structures of adducts **1** of Co^{II} acetylacetonate (acac) and hexafluoroacetylacetonate (hfacac) with redox-active diimines of glyoxal containing electron-withdrawing cyano groups – diiminosuccinonitriles,[11] aimed at the search for new coordination compounds capable of VT rearrangements. Bis-chelate Ni^{II} and Pt^{II} complexes with semidiiminosuccinonitrile anions (R = H) were previously synthesized.[12]

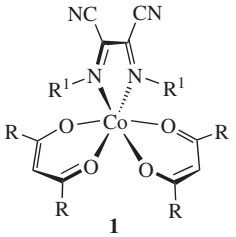

1

R = Me, CF_3
R^1 = H, Me

The unrestricted DFT (B3LYP*) calculations were performed using the Gaussian 03 program package[13] with the 6-311++G(d,p) basis set. As has been previously shown,[14,15] the modified B3LYP* functional[16] and the employed basis set generally well reproduce the energy parameters of VT rearrangements in transition metal complexes. For all the geometry-optimized structures, force constants were calculated and the stability of wave functions was checked.

Table 1 Stabilization energies (E_{stab}), relative energies without (E_{rel}) and with (E_{rel}^{ZPE}) the energies of the zero harmonic vibrations taken into account, spin densities at the metal centers (q_{sM}) and spin state (S) of adducts **1** (R = Me, CF_3; R^1 = H, Me), calculated by the DFT B3LYP*/6-311++G(d,p) method.

Structure	E_{stab}^{a}/ kcal mol^{-1}	E_{rel}/ kcal mol^{-1}	E_{rel}^{ZPE}/ kcal mol^{-1}	q_{sM} (a.u.)	S
$\mathbf{2}_{HS}$	6.8	12.9	10.8	2.75	3/2
$\mathbf{2}_{LS}$	19.7	0.0	0.0	0.01	1/2
$\mathbf{3}_{HS}$	8.1	6.7	4.4	2.67	3/2
$\mathbf{3}_{LS}$	14.8	0.0	0.0	0.03	1/2
$\mathbf{3}_{MECP}$	4.0	10.8	–		–
$\mathbf{4}_{HS}$	14.9	2.0	0.2	2.69	3/2
$\mathbf{4}_{LS}$	16.9	0.0	0.0	0.07	1/2
$\mathbf{5}_{HS}$	19.3	–5.7	–7.8	2.65	3/2
$\mathbf{5}_{LS}$	13.6	0.0	0.0	0.00	1/2

[a]As calculated relative to the isolated molecules of diketonate and α-diimine (see Online Supplementary Materials, Table S1).

Figure 1 illustrates the results of the calculations of electrically neutral α-diimine ligands **L** in the most energetically preferred *trans*-form. The calculated geometry of parent ligand **L** (R^1 = H) is consistent with the experimental data.[11] The replacement of hydrogen atoms by methyl groups negligibly affects the ligand geometry. According to the calculations of the complexes of diiminosuccinonitriles (Table 1), the ground states of the adducts of $Co^{II}(acac)_2$ are represented by low-spin structures $\mathbf{2}_{LS}$ and $\mathbf{3}_{LS}$, in which spin density is mainly localized at the ligands. This finding points to the occurrence of electron transfer from the metal to the redox-active ligand as a result of complexation. Small energy difference between low-spin isomer $\mathbf{3}_{LS}$ and compound $\mathbf{3}_{HS}$ with its Co^{II} centre in a high-spin state makes it possible to expect the VT behavior of adduct **1** (R = R^1 = Me).

In order to evaluate the energy barrier to the expected VT rearrangement, the minimal energy crossing point (MECP) on the seam of the intersecting doublet and quartet potential energy surfaces has been located. Corresponding compound $\mathbf{3}_{MECP}$ is energetically disfavored, as compared with low-spin isomer $\mathbf{3}_{LS}$, by 10.8 kcal mol^{-1}. This result is consistent with the experimental energy barriers of valence tautomeric rearrangements.[17,18]

As follows from Table 1, $\mathbf{3}_{MECP}$ is stabilized with respect to the isolated molecules of $Co^{II}(acac)_2$ and the diimine (R^1 = Me), which indicates that the intramolecular spin-forbidden VT rearrangement reaction can proceed without interference with a competitive process, the dissociation of the complex into the initial components.

The results of the calculations on the adducts containing electron-withdrawing substituents in both the redox-active ligand and the diketonate (hfacac) (Figure 2) showed that the low-spin

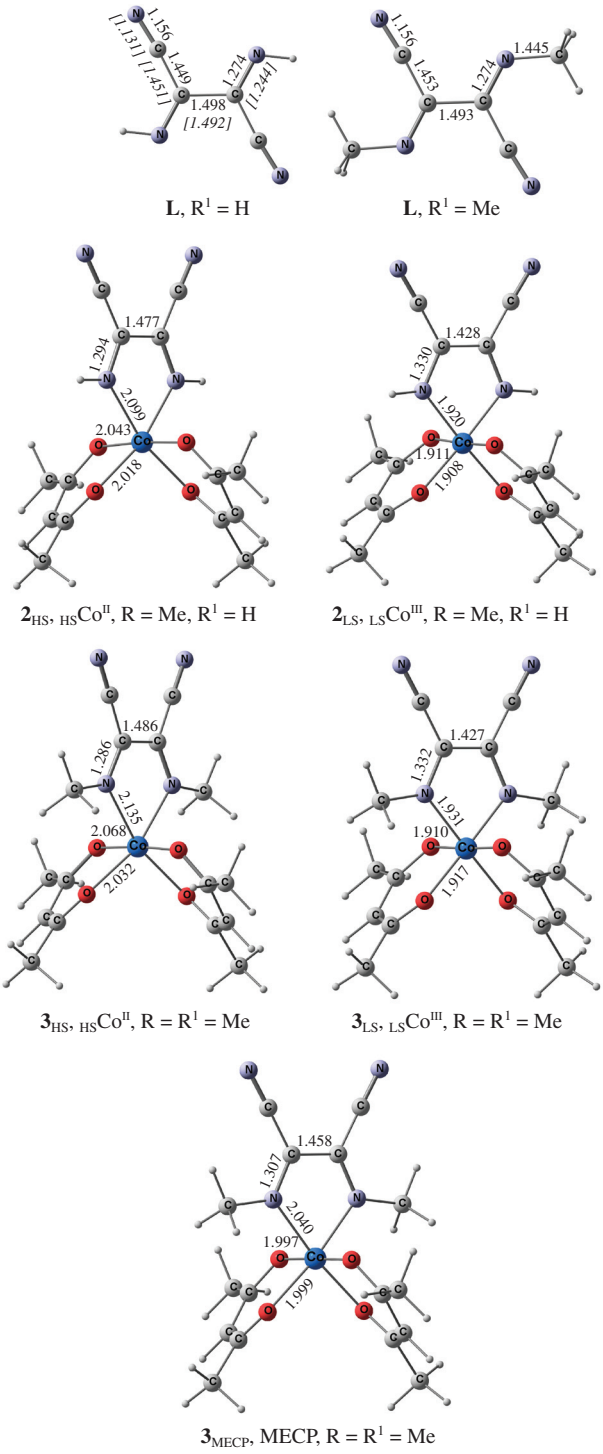

Figure 1 Optimized geometries of ligands **L** (R^1 = H, Me) and adducts **1** (R = Me; R^1 = H, Me), calculated by the DFT B3LYP*/6-311++G(d,p) method. Italicized figures given in brackets refer to X-ray determined parameters.[11] Hereinafter, the bond lengths are given in Å.

structure of $\mathbf{4}_{LS}$ (R = CF_3, R^1 = H) is by only 2 kcal mol^{-1} energy preferred compared with the high-spin electromeric form. Such a low energy difference between the two electronic isomers allows one to expect that, in a solution, these complex species occur in equilibrium, which would complicate the detection of valence tautomerism. The replacement of NH hydrogens in diimine **L** by methyl groups (R = CF_3, R^1 = Me) leads to a 5.7 kcal mol^{-1} energy preference of high-spin form $\mathbf{5}_{HS}$ over the low-spin one. Therefore, we concluded that the steric hindrances induced by the alkyl groups destabilize the low-spin state forms and obstruct VT processes in the test adducts.

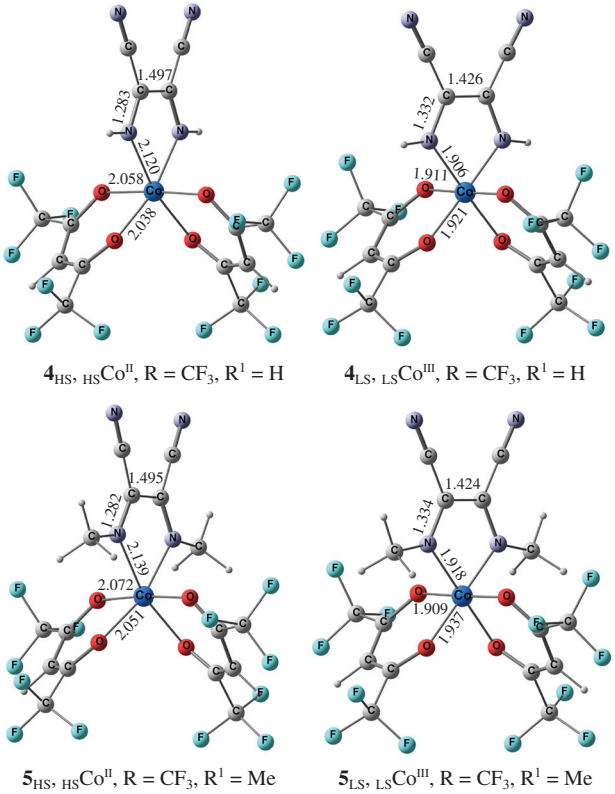

Figure 2 Optimized geometries of adducts **1** (R = CF_3; R^1 = H, Me), calculated by the DFT B3LYP*/6-311++G(d,p) method.

The DFT UB3LYP*/6-311++G(d,p) calculations showed that the interaction of Co^{II} diketonates with diiminosuccinonitriles leads to the formation of thermodynamically stable adducts due to intramolecular metal to ligand electron transfer. The pseudo-octahedral structure of the coordination site of all the adducts has been predicted. Changeable magnetic properties, manifested as a result of intramolecular redox processes, are expected in the adduct of $Co^{II}(acac)_2$ with methyl-substituted diiminosuccinonitrile. The insertion of electron-withdrawing CF_3 groups into the diketonate increases the stability of the high-spin forms and inhibits valence tautomeric rearrangements.

This work was supported by the Russian Science Foundation (grant no. 14-13-00573).

Online Supplementary Materials

Supplementary data associated with this article can be found in the online version at doi:10.1016/j.mencom.2014.11.003.

References

1 *Spin-Crossover Materials: Properties and Applications*, ed. M. A. Halcrow, Wiley & Sons, 2013, p. 546.
2 T. Tezgerevska, K. G. Alley and C. Boskovic, *Coord. Chem. Rev.*, 2014, **268**, 23.
3 *Spin Crossover in Transition Metal Compounds. II, Topics in Current Chemistry*, eds. P. Gütlich and H. A. Goodwin, Springer-Verlag, Berlin, 2004, vol. 234, p. 294.
4 E. Evangelio and D. Ruiz-Molina, *C. R. Chim.*, 2008, **11**, 1137.
5 R. M. Buchanan and C. G. Pierpont, *J. Am. Chem. Soc.*, 1980, **102**, 4951.
6 O.-S. Jung and C. G. Pierpont, *Inorg. Chem.*, 1994, **33**, 2227.
7 A. S. Attia and C. G. Pierpont, *Inorg. Chem.*, 1995, **34**, 1172.
8 V. I. Minkin, A. A. Starikova and R. M. Minyaev, *Dalton Trans.*, 2013, **42**, 1726.
9 A. G. Starikov, R. M. Minyaev, A. A. Starikova and V. I. Minkin, *Dokl. Chem.*, 2011, **440**, 289 (*Dokl. Akad. Nauk*, 2011, **440**, 646).
10 M. Yu. Antipin, E. P. Ivakhnenko, Yu. V. Koshchienko, P. A. Knyazev, M. S. Korobov, A. V. Chernyshev, K. A. Lyssenko, A. G. Starikov and

V. I. Minkin, *Russ. Chem. Bull., Int. Ed*., 2013, **62**, 1744 (*Izv. Akad. Nauk, Ser. Khim*., 2013, 1744).
11 C.-T. Chen, D.-S. Law, G.-H. Lee and S.-M. Peng, *Transition Met. Chem.*, 1989, **14**, 76.
12 A. A. Sidorov, I. G. Fomina, V. V. Nesterov, S. E. Nefedov, I. L. Eremenko and I. I. Moiseev, *Russ. Chem. Bull*., 1999, **48**, 573 (*Izv. Akad. Nauk, Ser. Khim*., 1999, 578).
13 M. J. Frisch, G. W. Trucks, H. B. Schlegel, G. E. Scuseria, M. A. Robb, J. R. Cheeseman, J. A. Montgomery Jr., T. Vreven, K. N. Kudin, J. C. Burant, J. M. Millam, S. S. Iyengar, J. Tomasi, V. Barone, B. Mennucci, M. Cossi, G. Scalmani, N. Rega, G.A. Petersson, H. Nakatsuji, M. Hada, M. Ehara, K. Toyota, R. Fukuda, J. Hasegawa, M. Ishida, T. Nakajima, Y. Honda, O. Kitao, H. Nakai, M. Klene, X. Li, J. E. Knox, H. P. Hratchian, J. B. Cross, V. Bakken, C. Adamo, J. Jaramillo, R. Gomperts, R. E. Stratmann, O. Yazyev, A. J. Austin, R. Cammi, C. Pomelli, J. W. Ochterski, P. Y. Ayala, K. Morokuma, G. A. Voth, P. Salvador, J. J. Dannenberg, V. G. Zakrzewski, S. Dapprich, A.D. Daniels, M. C. Strain, O. Farkas, D.K. Malick, A. D. Rabuck, K. Raghavachari, J. B. Foresman, J. V. Ortiz, Q. Cui, A. G. Baboul, S. Clifford, J. Cioslowski, B. B. Stefanov, G. Liu, A. Liashenko, P. Piskorz, I. Komaromi, R.L. Martin, D.J. Fox, T. Keith, M. A. Al-Laham, C. Y. Peng, A. Nanayakkara, M. Challacombe, P. M. W. Gill, B. Johnson, W. Chen, M. W. Wong, C. Gonzalez and J. A. Pople, *GAUSSIAN 03. Revision E.01*, Gaussian, Inc., Wallingford CT, 2004.
14 V. V. Koval, A. G. Starikov, R. M. Minyaev and V. I. Minkin, *Dokl. Chem*., 2010, **435**, 319 (*Dokl. Akad. Nauk*, 2010, **435**, 624).
15 A. G. Starikov, V. V. Koval, R. M. Minyaev and V. I. Minkin, *Dokl. Chem*., 2011, **441**, 365 (*Dokl. Akad. Nauk*, 2011, **441**, 629).
16 M. Reiher, O. Salomon and B. A. Hess, *Theor. Chem. Acc*., 2001, **107**, 48.
17 A. Caneschi, A. Cornia and A. Dei, *Inorg. Chem*., 1998, **37**, 3419.
18 A. Dei, A. Feis, G. Poneti and L. Sorace, *Inorg. Chim. Acta*, 2008, **361**, 3842.

Received: 20th May 2014; Com. 14/4379

Available online at www.sciencedirect.com
ScienceDirect
Mendeleev Commun., 2014, **24**, 332–333
Mendeleev Communications

Simple and efficient Au^{I}-based catalyst for hydroamination of alkynes

Maksim V. Anokhin, Arina V. Murashkina, Alexei D. Averin and Irina P. Beletskaya*

Department of Chemistry, M. V. Lomonosov Moscow State University, 119991 Moscow, Russian Federation. Fax: +7 495 939 1139; e-mail: beletska@org.chem.msu.ru

DOI: 10.1016/j.mencom.2014.11.004

Hydroamination of terminal alkynes with anilines in the presence of $(C_6F_5)_3PAuNTf_2$ catalyst affords 2-aryliminoalkanes whose reduction *in situ* with sodium borohydride gives the corresponding secondary amines in high yields.

The establishment of an important fact that gold nanoparticles (AuNPs) possess unique properties which are quite different from those of bulk gold encouraged many researchers to investigate catalytic properties of nano-gold. The majority of works dealing with AuNPs study oxidation[1] and reduction processes,[2] making an emphasis on the molecular structure of the gold clusters.[3,4] There are some publications considering other reactions, usually catalyzed by the complexes of Pd, Pt, *etc*. Among such works a special place is occupied by the investigations dedicated to the C–N bond formation in the course of hydroamination of alkynes.[5] Other Au-catalyzed processes include the addition of HX to carbon–carbon multiple bonds,[6–8] however, hydroamination was found to be most problematic[9] but simultaneously one of the most important in the atom-economy synthesis. Such processes are attractive when the catalyst can be recycled, what depends not only on the size and structure of AuNPs but also on the support nature. The drawbacks of this approach include the unclear reaction mechanism and the possibility of its different interpretation when changing the reaction conditions and support nature.[10]

The attractiveness of gold as a catalyst evoked serious interest in Au^{I} and Au^{III} salts as Lewis acids. The first homogeneous intermolecular hydroamination of alkynes was carried out by Tanaka *et al*.[11] who used aromatic amines in the presence of $(Ph_3P)AuMe$ complex and acidic promoter like $H_3PW_{12}O_{40}$. High efficiency was manifested by Au complexes with N-heterocyclic carbenes[12–14] as well as $AuNTf_2$ complexes with triphenylphosphine and 2-(dicyclohexylphosphino)-2′,6′-dimethoxybiphenyl ligands.[15] In that study, 1-octyne was coupled with aliphatic amines and chiral α-phenylethylamine which are usually less active than aromatic ones. Supposing that the reaction proceeds due to the activation of the triple bond with $LAuNTf_2$, we have chosen the complex of Au^{I} with a weak donor ligand $(C_6F_5)_3P$. The complex was obtained from $HAuCl_4$ and $(C_6F_5)_3P$ *via* intermediate $(C_6F_5)_3PAuCl$ which was then subjected to the anion exchange with $AgNTf_2$.[16,17] The reaction conditions were optimized on coupling of phenylacetylene **1** with *p*-toluidine **2a** and 4-methoxyaniline **2b** (Scheme 1, Table 1).

Reactions were run at ambient temperature using 20% excess of alkyne. The reaction with **2a** in the presence of 2.5 mol% catalyst in CH_2Cl_2 provided 84% yield of the corresponding

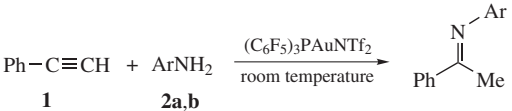

1 **2a**,**b** **3a**,**b**

a Ar = 4-MeC$_6$H$_4$
b Ar = 4-MeOC$_6$H$_4$

Scheme 1

Table 1 Optimization of the Au^{I}-catalyzed hydroamination conditions.

Entry	Amine	Catalyst (mol%)	Solvent	Imine	Yield[a] (%)
1	**2a**	2.5	CH_2Cl_2	**3a**	84
2	**2a**	1	neat	**3a**	88
3	**2b**	1	neat	**3b**	80

[a]Yields after chromatographic isolation.

ketimine **3a** (entry 1), while on application of 1 mol% catalyst under neat conditions this product was obtained in 88% yield (entry 2). The reaction of a more donor *p*-methoxyaniline **2b** resulted in 80% yield of **3b** (entry 3). Note that we succeeded to use fivefold lower quantity of catalyst at room temperature than described in literature.[15]

As ketimines may always contain admixtures of the relative ketones due to easy hydrolysis, further we reduced them *in situ* with $NaBH_4$ (Scheme 2, Table 2).† Intermediate imines were synthesized under the optimized conditions, and the yields of the secondary amines **4a**,**b** were high enough (entries 1, 2). The highest yield (98%) was achieved with the simplest aniline **3c**

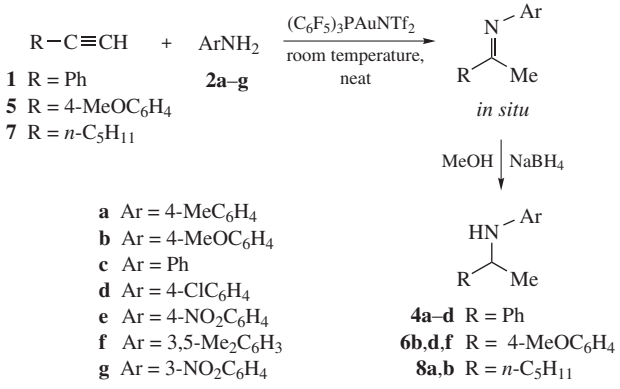

1 R = Ph
5 R = 4-MeOC$_6$H$_4$
7 R = *n*-C$_5$H$_{11}$

a Ar = 4-MeC$_6$H$_4$
b Ar = 4-MeOC$_6$H$_4$
c Ar = Ph
d Ar = 4-ClC$_6$H$_4$
e Ar = 4-NO$_2$C$_6$H$_4$
f Ar = 3,5-Me$_2$C$_6$H$_3$
g Ar = 3-NO$_2$C$_6$H$_4$

4a–d R = Ph
6b,**d**,**f** R = 4-MeOC$_6$H$_4$
8a,**b** R = *n*-C$_5$H$_{11}$

Scheme 2

† *Catalytic hydroamination of alkynes (general procedure)*. Alkyne **1**, **5** or **7** (1.2 mmol), aniline derivative **2a–g** (1 mmol) and $(C_6F_5)_3PAuNTf_2$ catalyst (10 mg, 1 mol%) were placed into a vial and stirred at ambient temperature for *ca.* 24 h until the reaction was complete (TLC control). The mixture was diluted with 3 ml MeOH, followed by addition of $NaBH_4$ (2 mmol, 76 mg) and stirring for 3 h (TLC control). The mixture was diluted with CH_2Cl_2 (15 ml), washed with water (15 ml) and saturated NaCl aqueous solution (15 ml). The organic layer was separated, dried over anhydrous Na_2SO_4, evaporated *in vacuo* and the residue was chromatographed on silica gel using 3–5% EtOAc in light petroleum. ^{1}H and ^{13}C NMR spectroscopic data of compounds **3a**,[15] **3b**,[18] **4a–c**,[19] **4d**,[20] **6b**,[21] **6d**,[22] **6f**,[23] **8a**,[24] **8b**[25] are consistent with those described in the literature.

Table 2 Synthesis of secondary amines *via* Au^{I}-catalyzed hydroamination.

Entry	Alkyne	Amine	Product	Yield[a] (%)
1	**1**	**2a**	**4a**	78
2	**1**	**2b**	**4b**	81
3	**1**	**2c**	**4c**	98
4	**1**	**2d**	**4d**	88
5	**1**	**2e**	No reaction	—
6	**5**	**2b**	**6b**	82
7	**5**	**2d**	**6d**	70
8	**5**	**2f**	**6f**	75
9	**5**	**2g**	No reaction	—
10	**7**	**2a**	**8a**	61
11	**7**	**2b**	**8b**	56

[a]Yields after chromatographic isolation.

(entry 3), the use of a weak electron-withdrawing *p*-chloroaniline **2d** also resulted in a high yield of product **4d** (88%, entry 4). However, in the case of stronger electron-withdrawing nitro-substituted reactant the reaction was completely cancelled (entry 5). The presence of electron-donating methoxy group in alkyne **5** did not decrease its reactivity and amines **6b**,**d**,**f** were isolated in 70–82% yields (entries 6–8). 3-Nitroaniline was essentially unreactive (entry 9). Aliphatic 1-heptyne **7** gave amines **8a**,**b** in lower yields, what is in good agreement with published data.[15]

The catalyst can be easily separated from product **4c** by adding hexane and can be used at least three times without substantial loss in activity.

This work was supported by the Russian Science Foundation (grant no. 14-23-00186).

References

1 C. Della Pina, E. Faletta, L. Prati and M. Rossi, *Chem. Soc. Rev*., 2008, **37**, 2077.
2 A. Corma and P. Serna, *Nature*, 2006, **313**, 332.
3 A. A. Herzing, C. J. Kiely, A. F. Carley, P. Landon and G. J. Hutchings, *Science*, 2008, **321**, 1331.
4 M. Boronat and A. Corma, *J. Catal*., 2011, **284**, 138.
5 A. Corma, P. Concepcion, I. Dominguez, V. Fornes and M. J. Sabater, *J. Catal*., 2007, **251**, 39.
6 X. Giner, C. Najera, G. Kovacs, A. Lledos and G. Ujaque, *Adv. Synth. Catal*., 2011, **353**, 3451.
7 T. E. Muller, K. C. Hultzsch, M. Yus, F. Foubelo and M. Tada, *Chem. Rev*., 2008, **108**, 3795.
8 F. Alonso, I. P. Beletskaya and M. Yus, *Chem. Rev.*, 2004, **104**, 3079.
9 J. Seayad, A. Tillack, C. G. Hartung and M. Beller, *Adv. Synth. Catal*., 2002, **344**, 795.
10 J. Zhao, Z. Zheng, S. Bottle, A. Chou, S. Sarina and H. Zhu, *Chem. Commun*., 2013, **49**, 2676.
11 E. Mizushima, T. Hayashi and M. Tanaka, *Org. Lett.*, 2003, **5**, 3349.
12 V. Lavallo, G. D. Frey, B. Donnadieu, M. Soleilhavoup and G. Bertrand, *Angew. Chem. Int. Ed*., 2008, **47**, 5224.
13 X. Zeng, G. D. Frey, S. Kousar and G. Bertrand, *Chem. Eur. J.*, 2009, **15**, 3056.
14 X. Zeng, G. D. Frey, R. Kinjo, B. Donnadieu and G. Bertrand, *J. Am. Chem. Soc.*, 2009, **131**, 8690.
15 A. Leyva and A. Corma, *Adv. Synth. Catal*., 2009, **351**, 2876.
16 C. Shu, L. Li, C.-B. Chen, H.-C. Shen and L.-W. Ye, *Chem. Asian J*., 2014, **9**, 1525.
17 J.-E. Kang and S. Shin, *Synlett*, 2006, **5**, 717.
18 N. Senthilkumar, P. Gandeepan, J. Jayakumar and C.-H. Cheng, *Chem. Commun*., 2014, 3106.
19 Q. Sun, Y. Wang, D. Yuan, Y. Yao and Q. Shen, *Organometallics*, 2014, **33**, 994.
20 Q. Lei, Y. Wei, D. Talwar, C. Wang, D. Xue and J. Xiao, *Chem. Eur. J*., 2013, **19**, 4021.
21 W. Tang, C. Lau, X. Wu and J. Xiao, *Synlett*, 2014, **25**, 81.
22 G. Ghattas, D. Chen, F. Pan and J. Klankermayer, *Dalton Trans*., 2012, **41**, 9026.
23 N. Mrsic, L. Panella, E. G. IJpeij, A. J. Minnaard, B. L. Feringa and J. G. de Vries, *ChemCatChem*, 2011, **3**, 1139.
24 L. Rubio-Perez, F. J. Perez-Florez, P. Sharma, L. Velasco and A. Cabrera, *Org. Lett*., 2009, **11**, 265.
25 C. Wang, A. Pettman, J. Bacsa and J. Xiao, *Angew. Chem. Int. Ed*., 2010, **49**, 7548.

Received: 13th October 2014; Com. 14/4483

Available online at www.sciencedirect.com
ScienceDirect
Mendeleev Commun., 2014, **24**, 334–335
Mendeleev Communications

Effect of a sacrificial anode material on the electrochemical generation of phosphane oxide (H_3PO)

Elena V. Gorbachuk,[a,b] Khasan R. Khayarov,[a] Oleg G. Sinyashin[b] and Dmitry G. Yakhvarov*[a,b]

[a] *A. M. Butlerov Institute of Chemistry, Kazan Federal University, 420008 Kazan, Russian Federation*
[b] *A. E. Arbuzov Institute of Organic and Physical Chemistry, Kazan Scientific Center of the Russian Academy of Sciences, 420088 Kazan, Russian Federation. Fax: +7 843 273 2253; e-mail: yakhvar@iopc.ru*

DOI: 10.1016/j.mencom.2014.11.005

The highest yields of phosphane oxide in the title process were obtained in electrochemical cells supplied with aluminium (49%), tin (36%) or zinc (67%) anodes.

The phosphorous oxyacids are an important source for the production of pharmaceuticals, fertilizers, pesticides, herbicides, flame retardants, lubricants, *etc*.[1] Thus, new methods for the selective preparation of phosphorous compounds starting from elemental (white) phosphorus are of high practical interest. From synthetic viewpoint, reagents like phosphane (PH_3) and hypophosphorous (hypo) acid (H_3PO_2) are of considerable importance. The phosphane oxide H_3PO is a highly reactive intermediate between a reduced form of phosphorus hydride and hypo acid. According to the electronic structure of H_3PO, the oxygen atom carries a partial negative charge and phosphorus has a partial positive charge.[2] The high reactivity of this molecule is most likely due to its polarity, which converts phosphorus into an electrophile. The charge imbalance between the P and O atoms is considerable to make it unstable.[3] Note that this molecule can occur in its tautomeric form as phosphinous acid $H_2P(OH)$.[4]

Previously, it was considered that the phosphane oxide molecule H_3PO does not exist at room temperature. Some experimental observations of this molecule include the application of molecular beam sampling mass spectrometry[5] for monitoring the reaction of atomic oxygen with PH_3 in a discharge-flow system, IR spectroscopy of the photolysis products of the phosphane-ozone complex in a solid state,[6] the product of PH_3 oxidation by atomic oxygen in an argon matrix[7] and the microwave spectrum detection of the radical H_2PO[8] and the molecule H_3PO.[9] The matrix isolation and theoretical study of the photochemical reaction of PH_3 with $OVCl_3$ and $CrCl_2O_2$ were also described.[10]

Recently, we found that this compound can be easily generated in solution by the mild electrochemical oxidation of phosphane PH_3 generated *in situ* from white phosphorus (P_4).[11] Phosphane oxide was characterized by NMR spectroscopy as free species in solution and in a coordinated form as a ligand in water-soluble ruthenium complexes. The phosphane oxide molecule in our former experiments was generated in a single electrochemical cell supplied with a sacrificial zinc anode.

Here, we describe the effects of sacrificial anodes made from Al, Cd, Co, Mg, Ni, Nb, Sn and Zn on the electrochemical reduction of white phosphorus and generation of phosphane oxide.[†]

The reduction of white phosphorus is irreversible and proceeds through radical anion formation:[12] $P_4 + e \rightarrow P_4^{\bullet-}$.

The formed $P_4^{\bullet-}$ radical anion initiates the polymerization of white phosphorus leading to polyphosphorus compounds. The derivatives containing the P–H bond are formed in the presence of active proton donors which can protonate phosphide anions initially produced in the electrochemical process. Thus, in protic media, all P–P bonds in white phosphorus tetrahedrons and formed polyphosphorus intermediates are sequentially opened and phosphane PH_3 is formed as the main product of the electrochemical process: $P_4 + 12e + 12H^+ \rightarrow 4PH_3$.[13] From the viewpoint of electrochemical process efficiency, cathodes with high hydrogen overvoltage, like lead and mercury, have been used.[14,15]

According to the cyclic voltammetry data, the electrochemically produced phosphane PH_3 displays one irreversible peak of oxidation.[16,17] We were interested in the study of the products formed in the oxidation process and performed the electrochemical oxidation of PH_3 on different metal anodes in order to generate phosphane oxide H_3PO.

Thus, we carried out the *in situ* generation of PH_3 in acidic ethanol–water mixtures in a single electrochemical cell supplied with sacrificial anodes of Al, Cd, Co, Mg, Ni, Nb, Sn or Zn at a constant current density of 5 mA cm^{-2} (10–20 V cell voltage). In case of niobium and tin electrodes displaying relatively high electric resistivity,[18] the current density was limited by 1–2 mA cm^{-2} at a cell voltage increased up to 40 V.

The electrochemical reactions in the systems are shown in Scheme 1.

Cathode: $P_4 + 12H^+ + 12e \longrightarrow 4PH_3$

Anode: $M^0 \longrightarrow M^{n+} + ne$

$4PH_3 + 4H_2O \longrightarrow 4H_3PO + 8H^+ + 8e$

Summary: $P_4 + 4H_2O + M^0 + 4H^+ + 4e \longrightarrow 4H_3PO + M^{n+} + ne$

M = Sn, Zn (n = 2), Al (n = 3)

Scheme 1

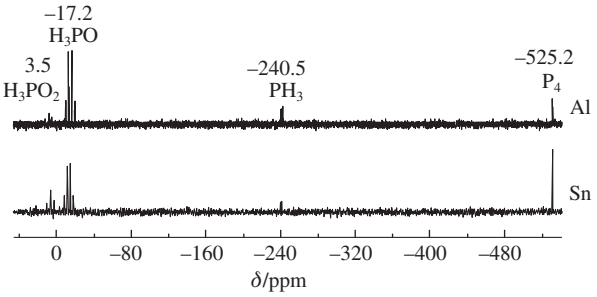

Figure 1 ^{31}P NMR spectra of an acidic EtOH–H_2O solution of P_4 after electrolysis (30 min) in an undivided electrochemical cell supplied with Al (top) and Sn (bottom) anodes.

[†] For experimental details, see Online Supplementary Materials.

Table 1 Distribution (%)[a] of phosphorous products in the reaction mixture after the electrolysis of the solution containing white phosphorus and standard electrode potentials (E^0) for the M^{n+}_{aq}/M^0 systems, where M = Cd, Co, Mg, Ni or Zn (n = 2) and Al or Nb (n = 3).

Entry	Anode	E^0/ (M^{n+}_{aq}/M^0)	P_4	PH_3	H_3PO	H_3PO_2
1	Al	–1.66	17	7	49	27
2	Cd	–0.40	traces	traces	traces	traces
3	Co	–0.28	traces	–	traces	–
4	Mg	–2.37	40	10	–	50
5	Nb	–1.10	8	–	–	–
6	Ni[b]	–0.25	–	–	–	–
7	Sn	–0.13	21	2	36	32
8	Zn[11]	–0.76	7	15	67	11

[a] Determined by the integral intensity of signals in the ^{31}P NMR spectra. [b] The ^{31}P NMR signals are not determined due to the presence of paramagnetic Ni^{2+} ions.

The highest yields of phosphane oxide were obtained with Al, Sn and Zn[11] anodes (Table 1). The reaction mixture after 30 min of electrolysis contained only the phosphorous products formed in the electrochemical process (Figure 1).

The lowest conversion of white phosphorus was observed with a Mg anode due to the low cell voltage that limited the cathodic process of P_4 electroreduction. However, at the same time, the formation of hypophosphorous acid H_3PO_2 proceeded with the highest yield. In principle, the potential of the system is sufficient for the oxidation of electrochemically generated phosphane PH_3 to phosphane oxide H_3PO, while a strong increase of the anodic potential can result in the formation of H_3PO_2 as the final product (Figure 2, Table 1).

The experimental data allow us to conclude that the nature of the metal anode has a crucial influence on the electrochemical generation of phosphane oxide. Nevertheless, although we did not observe the coordination of phosphane oxide to anodically generated Al^{3+}, Sn^{2+} and Zn^{2+} cations in our experiments, we cannot exclude the stabilization of H_3PO through coordination to these metals *via* the oxygen atom of phosphane oxide. Taking into account the standard electrode potentials determined in aqueous solutions, we believe that the formation of H_3PO is a more complicated process than a simple function of the standard electrode potentials of the metals used.

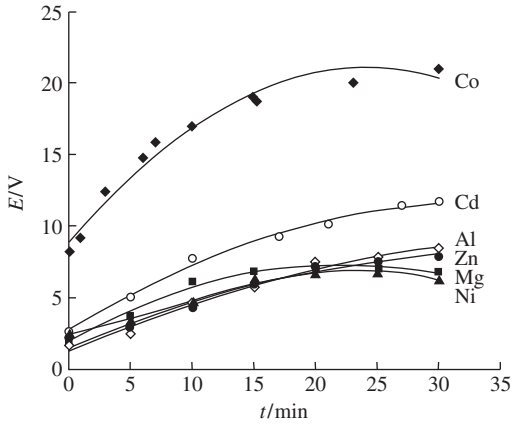

Figure 2 Cell voltage of the electroreduction of white phosphorus in acidic ethanol–water (1:2) solution with different sacrificial anodes: Zn, Mg, Al, Ni, Cd and Co.

Thus, we found that the illusive phosphane oxide molecule H_3PO can also be easily generated in an undivided electrochemical cell supplied with sacrificial aluminium and tin anodes. These results nicely supplement the data obtained using a sacrificial zinc anode.[11]

This work was supported by the Russian Science Foundation (project no. 14-13-01122).

Online Supplementary Materials

Supplementary data associated with this article can be found in the online version at doi:10.1016/j.mencom.2014.11.005.

References

1 D. E. C. Corbridge, *Studies in Inorganic Chemistry 20. Phosphorus. An Outline of its Chemistry, Biochemistry and Technology*, Elsevier, Amsterdam, 1995, p. 1208.
2 W. Kutzelnigg, *Angew. Chem., Int. Ed. Engl.*, 1984, **23**, 272.
3 N. S. Nath, I. Bhattacharya, A. G. Tuck, D. I. Schlipalius and P. R. Ebert, *J. Toxicol*., 2011, **2011**, 1.
4 G. Manca, M. Caporali, A. Ienco, M. Peruzzini and C. Mealli, *J. Organomet. Chem*., 2014, **760**, 177.
5 P. A. Hamilton and T. P. Murrells, *J. Chem. Soc., Faraday Trans. 2*, 1985, **81**, 1531.
6 R. Withnall and L. Andrews, *J. Phys. Chem.*, 1987, **91**, 784.
7 R. Withnall and L. Andrews, *J. Phys. Chem*., 1988, **92**, 4610.
8 T. Hirao, S. Saito and H. Ozeki, *J. Chem. Phys*., 1996, **105**, 3450.
9 K. A. Imtiaz, H. Ozeki and S. Saito, *J. Chem. Phys*., 1999, **110**, 912.
10 D. A. Kayser and B. S. Ault, *J. Phys. Chem. A*, 2003, **107**, 6500.
11 D. Yakhvarov, M. Caporali, L. Gonsalvi, Sh. Latypov, V. Mirabello, I. Rizvanov, O. Sinyashin, P. Stoppioni, M. Peruzzini and W. Schipper, *Angew. Chem. Int. Ed*., 2011, **50**, 5370.
12 I. N. Brago and A. P. Tomilov, *Elektrokhimiya*, 1968, **4**, 697 (in Russian).
13 I. M. Osadchenko and A. P. Tomilov, *Zh. Prikl. Khim*., 1970, **43**, 1255 (in Russian).
14 N. Ya. Shandrinov and A. P. Tomilov, *Elektrokhimiya*, 1968, **4**, 237 (in Russian).
15 V. V. Turygin, M. K. Smirnov, A. V. Khudenko, S. V. Nikolashin, V. A. Fedorov and A. P. Tomilov, *Inorg. Mater*., 2009, **45**, 1388 (*Neorg. Mater.*, 2009, **45**, 1484).
16 D. G. Yakhvarov, E. V. Gorbachuk and O. G. Sinyashin, *Eur. J. Inorg. Chem*., 2013, 4709.
17 D. G. Yakhvarov, E. V. Gorbachuk, R. M. Kagirov and O. G. Sinyashin, *Russ. Chem. Bull., Int. Ed.*, 2012, **61**, 1300 (*Izv. Akad. Nauk, Ser. Khim*., 2012, 1285).
18 http://www.webelements.com.

Received: 9th July 2014; Com. 14/4421

Available online at www.sciencedirect.com
ScienceDirect
Mendeleev Commun., 2014, **24**, 336–337
Mendeleev Communications

Preparative synthesis of selectively substituted 1,6-anhydro-α-D-galactofuranose derivatives

Vadim B. Krylov, Dmitry A. Argunov and Nikolay E. Nifantiev*

N. D. Zelinsky Institute of Organic Chemistry, Russian Academy of Sciences, 119991 Moscow, Russian Federation. Fax: +7 499 135 8784; e-mail: nen@ioc.ac.ru

DOI: 10.1016/j.mencom.2014.11.006

Heating of trisodium salt of allyl 3-*O*-benzyl-2,5,6-tri-*O*-sulfonato-β-D-galactofuranoside with pyridinium chloride in dioxane affords 1,6-anhydro-3-*O*-benzyl-α-D-galactofuranose which was regioselectively acylated to give useful precursors for oligosaccharide synthesis.

Growing biological interest to furanoside-containing natural carbohydrates of plant, bacterial and fungal origin challenges the development of new synthetic approaches to their chemical preparation. One of the convenient type of building blocks for assembling of a variety of galactofuranoside-containing oligosaccharides includes 1,6-anhydro-α-D-galactofuranose derivatives.[1,2] Recently, a simple three-step procedure for the synthesis of unprotected 1,6-anhydro-α-D-galactofuranose was reported.[3] However, this compound appeared to be inconvenient for the use in the assembling of oligosaccharides because of difficulties for further regioselective reactions through hydroxy groups at C^2, C^3 and C^5.

Here (Scheme 1) we describe a simple and convenient preparation of selectively protected 1,6-anhydro-3-*O*-benzyl-α-D-galactofuranose **4** and its derivatives **5**, **6**. Compound **4** was unexpectedly obtained during the study of solvolytic O-desulfation of trisulfate **2** – the product of the pyronaside-*into*-furanoside rearrangement[4] of allyl galactopyranoside **1**[5] under the conditions of acid promoted per-O-sulfation.[6] Particularly, O-desulfation of compound **2** upon heating in a dioxane–pyridine (10:1) mixture in the presence of Py·HCl[7,8] gave the expected triol **3**,† while the same treatment but in dioxane afforded only unexpected 1,6-anhydro product **4**.‡ The same compound was formed upon heating of triol **3** in dioxane in the presence of pyridine·HCl (Scheme 1). Evidently, compound **4** is produced in the course of acid-catalyzed transacetalyzation.

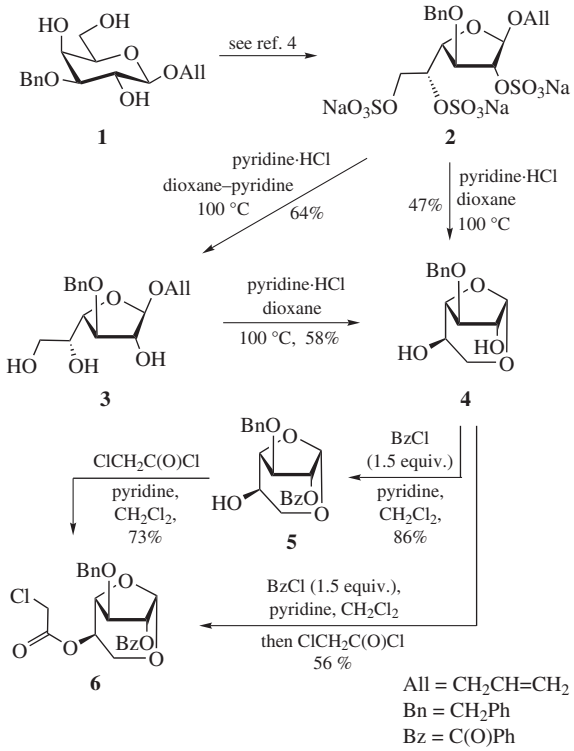

Scheme 1

The structure of product **4** was undoubtedly proved by NMR spectroscopy and mass spectrometry. In particular, the cross-peak H^1/C^6 in the HMBC spectrum (Figure 1) of **4** confirmed the presence of H^1–C^1–O^6–C^6 structural fragment in **4**, while the correlation peak between H^1 and C^4 and the absence of the cross-peak H^1/C^5 clearly indicated the presence of the five-membered

† *Allyl 3-O-benzyl-β-D-galactofuranoside* **3**. Dioxane (2.7 ml) was added to an intensively stirred suspension of trisodium salt of allyl 3-*O*-benzyl-2,5,6-tri-*O*-sulfonato-β-D-galactofuranoside **2**[4] (108 mg, 0.175 mmol) and Py·HCl (50 mg, 0.433 mmol) in pyridine (0.3 ml). The mixture was heated at 100 °C for 90 min and then cooled to room temperature. The mixture was dissolved in $CHCl_3$ (15 ml) and washed with saturated aqueous NaCl (15 ml). The organic layer was concentrated, and the residue was purified by column chromatography on silica gel in ethyl acetate–toluene (2:1) to give the furanoside derivative **3** (35 mg, 64%) identical to the previously described product.[4]

‡ *1,6-Anhydro-3-O-benzyl-α-D-galactofuranose* **4**.

Procedure 1. A suspension of **2**[4] (98 mg, 0.159 mmol) and Py·HCl (50 mg, 0.433 mmol) in dioxane (3.0 ml) was stirred at 100 °C for 30 min and then cooled to room temperature. The reaction mixture was dissolved in $CHCl_3$ (15 ml) and washed with saturated aqueous NaCl (15 ml). The organic layer was concentrated and the residue was purified by column chromatography on silica gel in ethyl acetate–toluene (2:1) to give product **4** (19 mg, 47%) as white solid, R_f = 0.69 (EtOAc), $[\alpha]_D$ = 62° (*c* = 1.0, MeOH). ^{1}H NMR (400 MHz, $CDCl_3$) δ: 7.44–7.30 (m, 5H, H_{Ph}), 5.24 (d, 1H, H^1, $J_{1,2}$ 4.6 Hz), 4.68 (d, 1H, $PhCH_aH_b$, *J* 11.8 Hz), 4.64 (d, 1H, $PhCH_aH_b$, *J* 11.8 Hz), 4.37–4.33 (m, 1H, H^2), 4.28 (d, 1H, H^4, *J* 4.3 Hz), 4.13–3.99 (m, 3H, H^5, H^3, H^{6a}), 3.57 (t, 1H, $J_{6b,6a} = J_{6b,5}$ = 10.5 Hz), 2.39 (br. s, 1H, OH), 2.20 (br. s, 1H, OH). ^{13}C NMR (100 MHz, $CDCl_3$) δ: 137.59 (q, Ph), 128.50 (Ph), 127.91 (Ph), 98.07 (C^1), 82.66 (C^3), 82.35 (C^4), 79.53 (C^2), 71.50 ($PhCH_2$), 65.39 (C^6), 62.53 (C^5). HRMS (ESI), *m/z*: 275.0882 $[M+Na]^+$ (calc. for $C_{13}H_{16}O_5$, *m/z*: 275.0890).

Procedure 2. A solution of triol **3**[4] (30 mg, 0.0967 mmol) and Py·HCl (31 mg, 0.268 mmol) in dioxane (1.5 ml) was stirred at 100 °C for 45 min and then cooled to room temperature. The mixture was dissolved in $CHCl_3$ (10 ml) and washed with saturated aqueous NaCl (10 ml). The organic layer was concentrated and the residue was purified by column chromatography on silica gel in ethyl acetate–toluene (2:1) to give product **4** (14 mg, 58%).

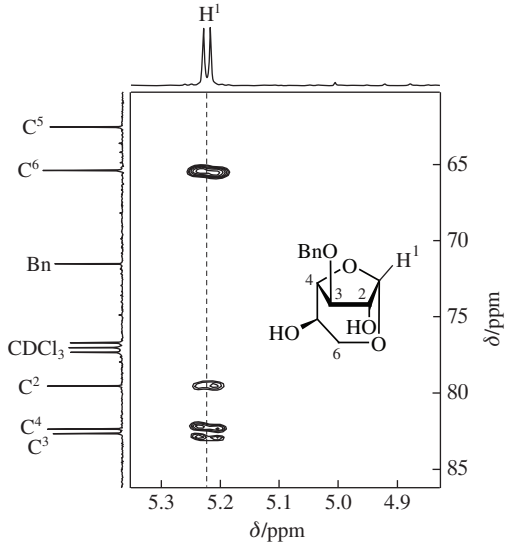

Figure 1 Part of the HMBC spectrum of 1,6-anhydrogalactofuranose **4**.

furanoside ring. Low-field resonance of C^6 in the ^{13}C NMR spectrum of **4** also confirmed the formation of the 1,6-anhydro cycle.

Compound **4** contains two OH groups of different reactivity. Thus, the treatment of diol **4** with 1.5 equiv. of BzCl in the presence of pyridine regioselectively led to 2-O-benzoylated product **5**[§] along with traces of the corresponding dibenzoate (detected by TLC). The structure of benzoate **5** was confirmed by characteristic downfield resonance of H^2 in the ^1H NMR spectrum as a result of 2-O-benzoylation (4.35 → 5.34 ppm). Further 5-O-chloroacetylation of compound **5** with 2 equiv. of $ClCH_2C(O)Cl$ gave totally protected derivative **6**.[¶] Remarkable difference in reactivity of the OH groups in diol **4** permits an easy transformation of this compound into **6** within a one-pot process by successive treatment first with BzCl and then by $ClCH_2C(O)Cl$.[††]

In conclusion, we developed the regioselective synthesis of galactofuranose derivative, which seems promising for the preparation of a variety of furanoside-containing oligosaccharides. Particularly, the galactofuranoside **6** related compounds were applied by us as key synthetic blocks for the assembling of large oligosaccharide chains related to *Aspergillus* galactomannan. These results will be published elsewhere.

This work was supported by the Russian Science Foundation grant 14-23-00199 (NEN).

Online Supplementary Materials

Supplementary data associated with this article can be found in the online version at doi:10.1016/j.mencom.2014.11.006.

References

1 M. Černý, *Adv. Carbohydr. Chem. Biochem.*, 2003, **58**, 121.
2 S. S. Kulkarni, J.-C. Lee and S.-C. Hung, *Curr. Org. Chem*., 2004, **8**, 475.
3 L. Baldoni and C. Marino, *Beilstein J. Org. Chem.*, 2014, **10**, 1651.
4 V. B. Krylov, D. A. Argunov, D. Z. Vinnitskiy, S. A. Verkhnyatskaya, A. G. Gerbst, N. E. Ustyuzhanina, A. S. Dmitrenok, J. Huebner, O. Holst, H.-C. Siebert and N. E. Nifantiev, *Chem. Eur. J*., DOI: 10.1002/chem.201405083.
5 Y. Zhou, J. Li, Y. Zhan, Z. Pei and H. Dong, *Tetrahedron*, 2013, **69**, 2693.
6 V. B. Krylov, N. E. Ustyuzhanina, A. A. Grachev and N. E. Nifantiev, *Tetrahedron Lett*., 2008, **49**, 5877.
7 A. I. Usov, K. S. Adamyants, L. I. Miroshnikova, A. A. Shaposhnikova and N. K. Kochetkov, *Carbohydr. Res*., 1971, **18**, 336.
8 I. J. Miller and J. W. Blunt, *Carbohydr. Res*., 1998, **309**, 39.

Received: 5th September 2014; Com. 14/4456

[§] *1,6-Anhydro-2*-O-*benzoyl-3*-O-*benzyl-α-D-galactofuranose* **5**. Benzoyl chloride (26 μl, 0.22 mmol) was added dropwise to a stirred solution of galactoside **4** (37 mg, 0.147 mmol) and pyridine (60 μl, 0.735 mmol) in CH_2Cl_2 (2 ml) at 0 °C. After disappearance of the starting compound (TLC control), MeOH (1 ml) was added and the mixture was co-evaporated with toluene (2×10 ml) *in vacuo*. Purification of the crude product by column chromatography on silica gel (hexane–ethyl acetate, 1.5:1) gave the 2-O-benzoylated derivative **5** (45 mg, 86%) as colorless oil. ^1H NMR (600 MHz, $CDCl_3$) δ: 8.06 (d, 2H, *o*-H_{Bz}, *J* 7.6 Hz), 7.61 (t, 1H, *p*-H_{Bz}, *J* = 7.6 Hz), 7.48 (t, 2H, *m*-H_{Bz}, *J* 7.6 Hz), 7.41–7.28 (m, 5H, H_{Ph}), 5.66 (d, 1H, H^1, $J_{1,2}$ 4.4 Hz), 5.34 (br. s, 1H, H^2), 4.70 (d, 1H, PhC$H_a$$H_b$, *J* 11.8 Hz), 4.63 (d, 1H, PhC$H_a$$H_b$, *J* 11.8 Hz), 4.47 (s, 1H, H^3), 4.36 (d, 1H, H^4, $J_{4,5}$ 4.2 Hz), 4.17–4.11 (m, 1H, H^5), 4.01 (dd, 1H, H^{6a}, $J_{6a,6b}$ 11.2 Hz, $J_{6a,5}$ 6.6 Hz), 3.60 (t, 1H, H^{6b}, $J_{6b,6a} = J_{6b,5}$ = 10.8 Hz), 2.24 (br. s, 1H, OH). ^{13}C NMR (150 MHz, $CDCl_3$) δ: 165.54 [Ph*C*(O)], 137.21 (q, $PhCH_2$), 133.47 (*p*-C_{Bz}), 129.76 (*o*-C_{Bz}), 129.19 [q, PhC(O)], 128.51 (Ph), 128.44 (Ph), 127.89 (Ph), 96.65 (C^1), 81.92 (C^4), 80.38 (C^2), 79.65 (C^3), 71.64 (Ph*C*H_2), 65.32 (C^6), 62.37 (C^5).

[¶] *1,6-Anhydro-2*-O-*benzoyl-3*-O-*benzyl-5*-O-*chloroacetyl-α-D-galactofuranose* **6**. Chloroacetyl chloride (28 μl, 0.25 mmol) was added to a stirred solution of galactoside **5** (45 mg, 0.126 mmol) and pyridine (40 μl, 0.5 mmol) in CH_2Cl_2 (2 ml). After 20 min, the mixture was diluted with $CHCl_3$ (15 ml) and washed with saturated $NaHCO_3$ (15 ml). The organic layer was concentrated, pyridine was co-evaporated with toluene (15 ml), and the residue was purified by column chromatography [silica gel, hexane–ethyl acetate (5:1)] to give product **6** (40 mg, 73%) as colorless syrup. ^1H NMR (600 MHz, $CDCl_3$) δ: 8.05 (d, 2H, *o*-H_{Bz}, *J* 7.6 Hz), 7.63 (t, 1H, *p*-H_{Bz}, *J* 7.6 Hz), 7.50 (t, 2H, *m*-H_{Bz}, *J* 7.6 Hz), 7.38–7.28 (m, 5H, Ph), 5.69 (d, 1H, H^1, $J_{1,2}$ 4.5 Hz), 5.38 (dd, 1H, H^2, $J_{2,1}$ 4.5 Hz, $J_{2,3}$ 2.3 Hz), 5.17 (ddd, 1H, H^5, *J* 10.9, 6.6 and 4.4 Hz), 4.72 (d, 1H, PhC$H_a$$H_b$, *J* 12.2 Hz), 4.62 (d, 1H, PhC$H_a$$H_b$, *J* 12.2 Hz), 4.52 (d, 1H, H^4, $J_{4,5}$ 4.4 Hz), 4.35 (d, 1H, H^3, $J_{3,2}$ 2.3 Hz), 4.17–4.12 (m, 1H, H^{6a}), 4.02 [d, 1H, C(O)C$H_a$$H_b$Cl, *J* 14.9 Hz], 3.99 [d, 1H, C(O)C$H_a$$H_b$Cl, *J* 14.8 Hz], 3.68 (t, 1H, H^{6b}, $J_{6b,6a} = J_{6b,5}$ = 10.9 Hz). ^{13}C NMR (150 MHz, $CDCl_3$) δ: 165.88 [*C*(O)CH_2Cl], 165.35 [Ph*C*(O)], 136.94 (q, $PhCH_2$), 133.59 (*p*-C_{Bz}), 129.77 (*o*-C_{Bz}), 129.07 [q, PhC(O)], 128.57 (Ph), 128.52 (Ph), 128.06 (Ph), 127.85 (Ph), 97.15 (C^1), 80.20 (C^2), 79.60 (C^3), 78.88 (C^4), 71.57 (Ph*C*H_2), 65.41 (C^5), 62.21 (C^6), 40.33 [C(O)*C*H_2Cl]. HRMS (ESI), *m/z*: 455.0859 $[M+Na]^+$ (calc. for $C_{13}H_{16}O_5$, *m/z*: 455.0868).

[††] *1,6-Anhydro-2*-O-*benzoyl-3*-O-*benzyl-5*-O-*chloroacetyl-α-D-galactofuranose* **6** *(one-pot method)*. Benzoyl chloride (12 μl, 0.100 mmol) was added to a stirred solution of galactoside **4** (17 mg, 0.067 mmol) and pyridine (22 μl, 0.27 mmol) in CH_2Cl_2 (2 ml) at 0 °C. Immediately after the disappearance of the starting compound (TLC control), chloroacetyl chloride (11 μl, 0.134 mmol) was added. After 20 min, the reaction was quenched with MeOH (0.5 ml) and co-evaporated with toluene. Purification of the crude product by column chromatography on silica gel (hexane–ethyl acetate, 7:1) gave desired product **6** (16 mg, 56%).

Available online at www.sciencedirect.com
ScienceDirect
Mendeleev Commun., 2014, **24**, 338–339
Mendeleev Communications

Preparation and structural characterization of nanocrystalline vanadium carbide VC_y powder on the upper boundary of its homogeneity interval

Alexey S. Kurlov,[a] Aleksandr I. Gusev[a] and Andrey A. Rempel*[a,b]

[a] *Institute of Solid State Chemistry, Ural Branch of the Russian Academy of Sciences, 620990 Ekaterinburg, Russian Federation. Fax: +7 343 374 4495; e-mail: rempel@ihim.uran.ru*
[b] *B. N. Yeltsin Ural Federal University, 620002 Ekaterinburg, Russian Federation*

DOI: 10.1016/j.mencom.2014.11.007

A nanocrystalline powder of nonstoichiometric vanadium carbide $VC_{0.875}$ with a coherent scattering region of 20±5 nm has been prepared by high-energy ball milling. The crystal structure, microstructure and particle size of the initial and milled powders have been investigated using X-ray diffraction analysis and scanning electron microscopy.

Vanadium carbide is a widely used cubic transition metal carbide. The disordered cubic (space group $Fm\bar{3}m$) vanadium carbide VC_y belongs to strongly nonstoichiometric compounds and has a wide homogeneity interval from $VC_{0.65}$ to $VC_{0.875}$. It forms a V_8C_7 cubic (space group $P4_332$) superstructure and a V_6C_5 superstructure with monoclinic (space groups $C2/c$ or $C2/m$) or trigonal (space group $P3_112$) symmetry.[1–4] The nanocrystalline powders of vanadium carbide including V_8C_7 have been actively studied.[5–10]

The initial coarse-grained vanadium carbide $VC_{0.875}$ powder was produced by the carbothermal reduction of V_2O_5 and then subjected to long-term aging at room temperature. According to the chemical analysis data, the aged vanadium carbide contains 18.5±0.1 wt% carbon, including 1.8±0.1 wt% free carbon, and 0.1 wt% oxygen impurity dissolved in the lattice of vanadium carbide. The composition $VC_{0.875}$ corresponds to the upper boundary of the homogeneity interval of the cubic phase with the $B1$ structure.

The initial powder of nonstoichiometric vanadium carbide was ground in a PM-200 Retsch planetary ball mill in an automatic regime at 8.33 rps. The charge M was 10 g, the weight of milling balls was ~100 g, and the number of milling balls was ~450. The bowl capacity for milling was 50 ml. The duration t of milling was 15 h. The milling was performed with the addition of isopropanol (5 ml).[11,12]

The microscopic examination of the initial vanadium carbide powder at a magnification factor of 100 has shown that it contains large agglomerates of irregular shape with an average size of 6–10 μm. However, at a magnification factor of 2000, it is seen that large agglomerates have a complex structure and are a set of a large number of very small particles with a size of ~2–3 μm, which looks like an open flower (Figure 1).† The observed crystallites have the shape of curved leaves or petals. As a first approximation, the crystallites can be simulated by a disk with a diameter of 600–800 nm and a thickness of 20–40 nm. Such a microstructure of nonstoichiometric vanadium carbide was experimentally observed and explained by Rempel and Gusev.[14] They showed that the coral-like microstructure of the $V_{C0.875}$ carbide is caused by the disorder-order structural phase transition $VC_{0.875} \rightarrow V_8C_7$, which occurs during the aging of nonstoichiometric carbide and is accompanied by an abrupt change in the lattice constant a_{B1} of the basic phase of the disordered carbide.

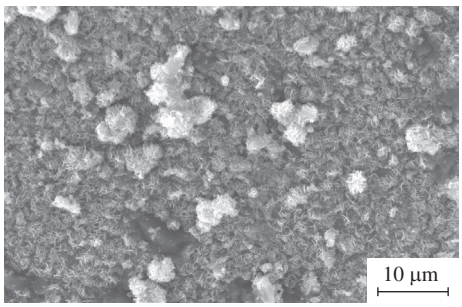

Figure 1 SEM image of the initial coarse-grained powder of $VC_{0.875}$.

The XRD pattern of the initial powder of $VC_{0.875}$ is shown in Figure 2.† Along with the structural reflections of the basic cubic phase with the $B1$ structure and the lattice constant a_{B1} = 416.5 pm, the XRD pattern exhibits additional weak reflections. The structure refinement of the initial powder of the $VC_{0.875}$ carbide revealed that all the additional reflections are superstructure reflections, which, in their position and intensity, correspond to the cubic ordered phase V_8C_7 with space group $P4_332$. The lattice constant of the ordered phase is 833.2±0.1 pm. The ideal cubic superstructure of the M_8C_7 type with space group $P4_332$ (see lower inset in Figure 2) has a doubled (compared to the disordered basic phase $B1$) lattice constant.[1–3] Therefore, for the studied vanadium carbide, the lattice constant of the basic phase is a_{B1} = 416.6 pm. This value is ~0.1 pm larger than the lattice constant of the disordered carbide $VC_{0.875}$. According to published data,[1,2,4] such a significant difference in the lattice constants of the ordered and disordered $VC_{0.875}$ carbides can be observed when the degree of ordering is close to a maximum value.

Figure 2 shows that all the diffraction reflections of the milled vanadium carbide powder are strongly broadened, as compared to those of the initial coarse-grained powder $VC_{0.875}$. During the milling, a decrease in the particle size, *i.e.*, grinding, is accompanied by the generation of microstrains in the particles. The

† The morphology and particle size of the initial and milled powders of $VC_{0.875}$ were examined by scanning electron microscopy (SEM) with a JEOL JSM 6390 LA scanning electron microscope.

The crystal structure and phase composition of $VC_{0.875}$ were determined using X-ray diffraction (XRD) analysis on a Shimadzu XRD-7000 diffractometer in the Bragg–Brentano geometry within a range of 2θ angles from 10° to 140° with a scan step $\Delta(2\theta)$ = 0.03°, and high statistics in $CuK\alpha_{1,2}$ radiation. The XRD patterns were analyzed numerically using the X'Pert Plus software package.[13] The average size $\langle D \rangle$ of the particles [more precisely, the average size of coherent scattering regions (CSR)] in the milled vanadium carbide powder was determined from the broadening of diffraction reflections. The diffraction reflections were described by the pseudo-Voigt function.

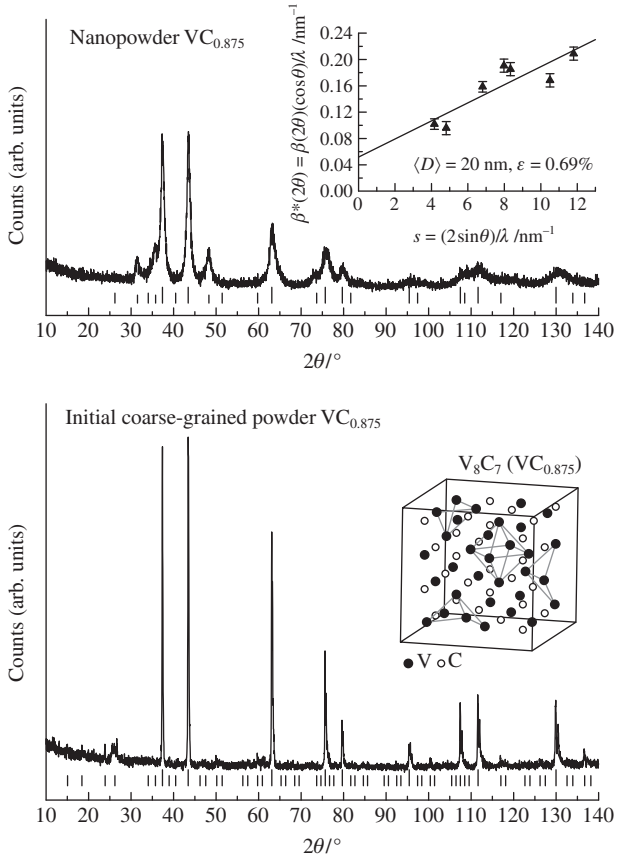

Figure 2 XRD patterns of the initial coarse-grained and milled nanocrystalline powders of $VC_{0.875}$ vanadium carbide. The XRD pattern of the initial vanadium carbide powder, in addition to the structural reflections, contains the superstructure reflections of the ordered cubic (space group $P4_332$) phase V_8C_7. The XRD pattern of the milled $VC_{0.875}$ powder contains also three reflections from the impurity phase WC. The long and middle ticks correspond to reflections of the disordered cubic (space group $Fm\bar{3}m$) phase $VC_{0.875}$ with the $B1$ structure and the ordered cubic (space group $P4_332$) phase V_8C_7, short ticks correspond to reflections of the impurity phase WC, respectively. The upper inset presents the estimate of the average particle size $\langle D\rangle$ and microstrains ε in nanocrystalline $VC_{0.875}$ powder prepared by 15 h high-energy milling: (▲) $\langle D\rangle$ = 20±5 nm, ε = 0.69±0.05%. The lower inset presents the unit cell of the ordered cubic phase V_8C_7: vacant (non-filled by carbon atoms) octahedral interstitials of the metallic sublattice are shown.

small (<200 nm) particle size and microstrains are responsible for the broadening of diffraction reflections. The average particle size $\langle D\rangle$ and the values of microstrains ε in the milled vanadium carbide powders were determined using XRD analysis.

The broadening $\beta(2\theta)$ of the diffraction reflection was determined as $\beta(2\theta) = [(\mathrm{FWHM}_{exp})^2 - (\mathrm{FWHM}_R)^2]^{1/2}$, where FWHM_{exp} is the full width of the experimental diffraction reflection at half-maximum and FWHM_R is the instrumental function of the angular resolution of the diffractometer. The resolution function $\mathrm{FWHM}_R(2\theta) = (u\tanh^2\theta + v\tanh\theta + w)^{1/2}$ of the Shimadzu XRD-7000 diffractometer was determined in a special experiment using cubic lanthanum hexaboride LaB_6 (NIST Standart Reference Powder 660a) with the lattice constant a = 415.692 pm; the parameters of this function u = 0.00616, v = –0.00457 and w = 0.00778.

The size and strain broadenings were separated, and the average size $\langle D\rangle$ of the coherent scattering regions and the value of the microstrains ε were found by the Williamson–Hall method[15–17] using the dependence of the reduced broadening $\beta^*(2\theta) = [\beta(2\theta)\cos\theta]/\lambda$ of the (hkl) reflections on the scattering vector $s = (2\sin\theta)/\lambda$.

The upper inset in Figure 2 presents the dependences of the reduced broadening $\beta^*(2\theta)$ of the reflections on the scattering vector s and illustrates the estimation of the average size $\langle D\rangle$ of the coherent scattering regions after the milling of 10 g of $VC_{0.875}$ for 15 h. The analysis of the broadening of diffraction reflections showed that the average size of the coherent scattering regions in the milled vanadium carbide powder is 20±5 nm, and the microstrain ε is 0.0069±0.0005 (0.69±0.05%).

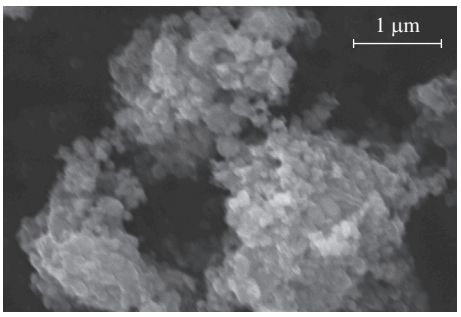

Figure 3 SEM image of nanocrystalline $VC_{0.875}$ powders produced by ball milling within 15 h.

The results of the electron microscopy investigation of the nanocrystalline vanadium carbide powder obtained by the ball milling are presented in Figure 3. At a magnification factor of 25 000, in the milled vanadium carbide powder, the particle size does not exceed 100–150 nm, but the nanoparticles are joined together into large loose agglomerates with a size of 2 μm or greater.

This study was supported by the Russian Science Foundation (grant no. 14-23-00025) through the Institute of Solid State Chemistry of the Ural Branch of the RAS.

References

1 A. I. Gusev, A. A. Rempel and A. J. Magerl, *Disorder and Order in Strongly Non-stoichiometric Compounds. Transition Metal Carbides, Nitrides and Oxides*, Springer, Berlin–Heidelberg–New York–London, 2001.
2 V. N. Lipatnikov, *Russ. Chem. Rev*., 2005, **74**, 697 (*Usp. Khim*., 2005, **74**, 768).
3 D. Rafaja, W. Lengauer, P. Ettmayer and V. N. Lipatnikov, *J. Alloys Compd*., 1998, **269**, 60.
4 A. I. Gusev, *Usp. Fiz. Nauk*, 2014, **189**, 905 (in Russian).
5 Z. Zhao, H. Zheng, W. Song, S. Mao and Y. Li, *Adv. Mater. Res.*, 2012, **476–478**, 480.
6 L. Wu, T. Yao, Y. Wang, J. Zhang, F. Xiao and B. Liao, *J. Alloys Compd*., 2013, **548**, 60.
7 A. S. Kurlov and A. I. Gusev, *Phys. Solid State*, 2013, **55**, 430 (*Fiz. Tverdogo Tela*, 2013, **55**, 385).
8 M. Mahajan, K. Singh and O. P. Pandey, *Int. J. Refract. Met. Hard Mater*., 2013, **36**, 110.
9 M. Hossein-Zadeh and O. Mirzaee, *Adv. Powder Technol*., 2014, **25**, 978.
10 A. S. Kurlov and A. I. Gusev, *J. Alloys Compd*., 2014, **582**, 108.
11 A. I. Gusev and A. S. Kurlov, *Nanotechnology*, 2008, **19**, paper 265302.
12 A. S. Kurlov and A. I. Gusev, *Zh. Techn. Fiz*., 2011, **81**, 76 (in Russian).
13 *X'Pert Plus Version 1.0. Program for Crystallography and Rietveld Analysis*, Philips Analytical B. V., Koninklijke Philips Electronics N. V.
14 A. A. Rempel and A. I. Gusev, *JETP Lett*., 1999, **69**, 472 (*Pis'ma Zh. Eksp. Teor. Fiz*., 1999, **69**, 436).
15 B. E. Warren, B. L. Averbach and B. W. Roberts, *J. Appl. Phys.*, 1951, **22**, 1493.
16 G. K. Williamson and W. H. Hall, *Acta Metall.*, 1954, **1**, 22.
17 B. E. Warren, *X-Ray Diffraction*, Dower Publications, New York, 1990.

Received: 8th September 2014; Com. 14/4460

Available online at www.sciencedirect.com
ScienceDirect
Mendeleev Commun., 2014, **24**, 340–341
Mendeleev Communications

Computational study of the catalytic olefination reaction

Ilya D. Gridnev,*[a] Aleksey V. Shastin,[b] Vasiliy M. Muzalevskiy,[c] Elizabeth S. Balenkova[c] and Valentine G. Nenajdenko*[c,d]

[a] *Department of Chemistry, Graduate School of Science, Tohoku University, Sendai 980-8578, Japan. Fax: +81 22 795 6581; e-mail: igridnev@m.tohoku.ac.jp*
[b] *Institute of Problems of Chemical Physics, Russian Academy of Sciences, 142432 Chernogolovka, Moscow Region, Russian Federation*
[c] *Department of Chemistry, M. V. Lomonosov Moscow State University, 119991 Moscow, Russian Federaton. Fax: +7 495 932 8846; e-mail: nen@acylium.chem.msu.ru*
[d] *A. N. Nesmeyanov Institute of Organoelement Compounds, Russian Academy of Sciences, 119991 Moscow, Russian Federation. Fax: +7 499 135 5085*

DOI: 10.1016/j.mencom.2014.11.008

Catalytic olefination of hydrazones was computed to proceed with effective activation barrier of 19.9 kcal mol^{-1}. Initially the catalyst-assisted abstraction of Cl^- anion from CCl_4 occurs that is accompanied by simultaneous C–C bond formation; then proton is eliminated by ammonia present in the reaction mixture yielding a neutral intermediate; the second CuCl-assisted abstraction of Cl^- anion from CCl_3 group is followed by synchronous reaction that affords the olefination product and releases N_2 together with CuCl·HCl.

Creation of new carbon–carbon bonds is a key problem of organic chemistry. Olefination of carbonyl compounds is one of the most versatile approaches for preparation of alkenes from aldehydes or ketones. Development of this area in past decades provided a variety of reliable synthetic protocols.[1] Nevertheless, taking into account the synthetic potential of these methods, the search for new carbonyl olefination reactions is steadily continued.

In 1999 some of us reported, that N-unsubstituted hydrazones of aldehydes and ketones could be transformed into alkenes by treatment with polyhalogenated alkanes in the presence of a base and catalytic amounts of copper salts (Scheme 1).[2] Symmetrical azines were the only side products of the reaction. The reaction revealed a wide synthetic scope allowing one to prepare various alkenes including fluorinated and functionalized ones.[3] Simple experimental procedure depriving of organometallic or toxic organophosphorous compounds, affordable price and availability of starting materials, high yields and stereoselectivity were the distinct advantages of this reaction.

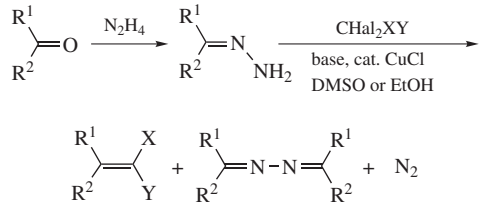

Scheme 1

Two mechanistic schemes were proposed previously for catalytic olefination reaction[4] involving the intermediate formation of either carbene or radical species. Here we report a simple mechanism found by state-of-art DFT calculations† that involves neither carbene nor radical intermediates, which may have important implications for the further synthetic improvements.

We reckoned that the simplest pathway for the formation of olefin from hydrazone **1** would be an electrophilic attack of CCl_4 on the double C=N bond followed by abstraction of HCl from the resulting intermediate **2** and synchronous release of N_2 and HCl from the intermediate **3** (Scheme 2).

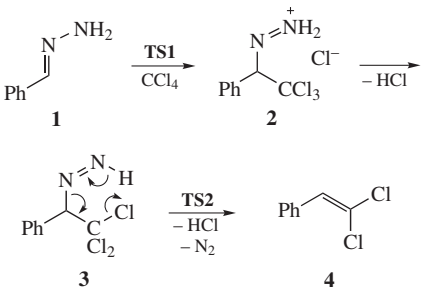

Scheme 2

A transition state for the rate-limiting stage of the non-catalyzed reaction (Figure 1) was found from a scan approaching CCl_4 molecule to the molecule of hydrazone **1**. The transition state **TS1** features a trigonal planar CCl_3 fragment and slightly

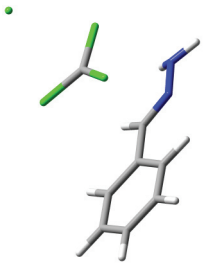

Figure 1 Transition state **TS1** for the first stage of the non-catalyzed reaction. The imaginary frequency ν = 89.5i.

† Computations were carried out using the latest long-range corrected hybrid functional with damped atom-atom dispersion (WB97XD)[5] as implemented in the GAUSSIAN 09 software package.[6] All atoms were modelled at the 6-31G(d) level of theory. The solvent influence has been accounted for by performing optimizations in the CPCM force field (DMSO).

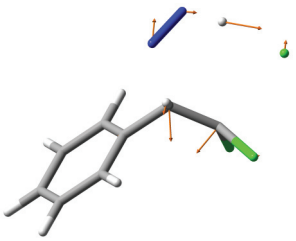

Figure 2 Transition state **TS2** for the second stage of the non-catalyzed reaction showing the displacement vectors. The imaginary frequency $\nu = 416.8$i.

non-planar terminal nitrogen atom. The activation barrier is high enough (51.0 kcal mol^{-1}) that is in accord with the practical impossibility of the non-catalyzed reaction. On the other hand, after the abstraction of HCl from initially formed salt **2**, the reaction becomes exogonic for 7.1 kcal mol^{-1} that indicates the possibility of this pathway in a catalytic reaction.

Scanning the distance between the NH proton and one of the chlorine atoms in **3** afforded the transition state for the second stage of the non-catalyzed reaction (Figure 2), which is a synchronous process involving simultaneous movement of six reaction centers. Hydrogen chloride released after this stage is quenched with ammonia present in the reaction mixture.‡

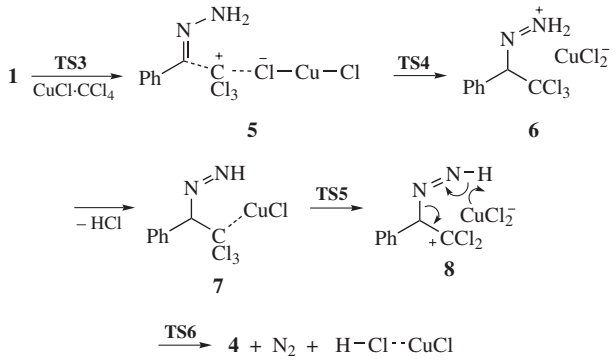

Scheme 3

The catalytic pathway for the olefination reaction is shown in Scheme 3. Under catalytic conditions, each of the two stages becomes stepwise that leads to the significant decrease of the effective activation barrier (Figure 3). Further formation of C–C bond requires relatively low activation barrier and yields the iminium salt **6**. Elimination of HCl with ammonia results in the metastable intermediate **7**. The next stage, the abstraction of Cl^- from the CCl_3 group, is rate-limiting in the catalytic process with activation barrier of 19.9 kcal mol^{-1}. It is followed by the facile concerted formation of the product **4** and regenerating the catalyst in the form of the HCl adduct (see Figure 4).

Potential profiles for the catalytic and non-catalytic reactions are shown in Figure 3. The effective Gibbs energy of activation (19.9 kcal mol^{-1}) is in a reasonable agreement with the experimentally optimized reaction conditions (4 h at ambient temperature). Thus, the studies designated to use the acquired mechanistic insights for the optimization of the reaction conditions and extending the scope are underway.

This work was supported by the Russian Science Foundation (grant no. 14-13-00083).

‡ We also considered the non-catalytic reaction in the triplet state. The triplet intermediate **2** can be formed in two stages *via* an extremely unstable transition state (36.0 kcal mol^{-1} less stable than **TS1**). Moreover, the triplet transition state could not be found for the second stage of the reaction since the corresponding energy scan exhibited only the steady rise of the energy without achieving any maximum.

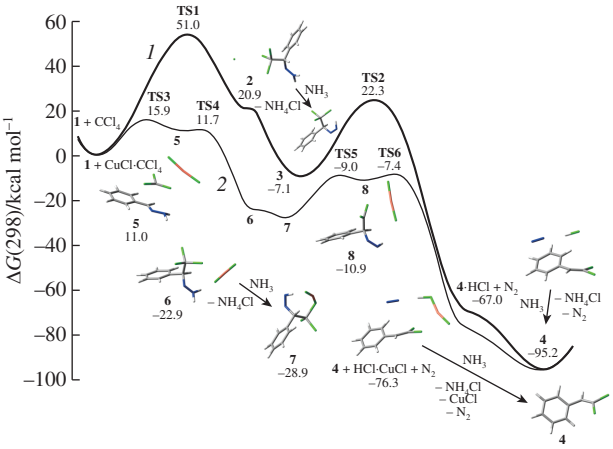

Figure 3 Potential Gibbs energy profiles for the (*1*) non-catalyzed and (*2*) catalyzed olefination reaction. The numbers indicate free energies at 298 K in kcal mol^{-1}. Computations were carried out at the WB97XD/6-31G*/CPCM(DMSO) level of theory.

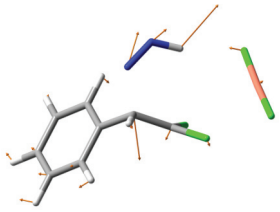

Figure 4 Transition state **TS6** for the olefination reaction catalyzed with CuCl, showing the displacement vectors. The imaginary frequency $\nu = 187.7$i.

Online Supplementary Materials

Supplementary data associated with this article (Cartesian coordinates of all computed compounds and transition states) can be found in the online version at doi:10.1016/j.mencom.2014.11.008.

References

1 *Modern Carbonyl Olefination: Methods and Applications*, ed. T. Takeda, Wiley-VCH, Weinheim, 2004.

2 (*a*) A. V. Shastin, V. N. Korotchenko, V. G. Nenaidenko and E. S. Balenkova, *Russ. Chem. Bull.*, 1999, **48**, 2184 (*Izv. Akad. Nauk, Ser. Khim.*, 1999, 2210); (*b*) A. V. Shastin, V. N. Korotchenko, V. G. Nenajdenko and E. S. Balenkova, *Tetrahedron*, 2000, **56**, 6557.

3 (*a*) V. N. Korotchenko, A. V. Shastin, V. G. Nenajdenko and E. S. Balenkova, *Synthesis*, 2001, 2081; (*b*) V. N. Korotchenko, A. V. Shastin, V. G. Nenajdenko and E. S. Balenkova, *J. Chem. Soc., Perkin Trans. 1*, 2002, 883; (*c*) V. N. Korotchenko, V. G. Nenajdenko, A. V. Shastin and E. S. Balenkova, *Org. Biomol. Chem.*, 2003, 1906; (*d*) V. G. Nenajdenko, A. V. Shastin, V. N. Korotchenko, G. N. Varseev and E. S. Balenkova, *Eur. J. Org. Chem.*, 2003, 302; (*e*) V. G. Nenajdenko, G. N. Varseev, V. N. Korotchenko, A. V. Shastin and E. S. Balenkova, *J. Fluorine Chem.*, 2003, **124**, 115; (*f*) V. G. Nenajdenko, A. V. Shastin, I. V. Golubinskii, O. N. Lenkova and E. S. Balenkova, *Russ. Chem. Bull., Int. Ed.*, 2004, **53**, 228 (*Izv. Akad. Nauk, Ser. Khim.*, 2004, 218); (*g*) V. G. Nenajdenko, A. L. Reznichenko, O. N. Lenkova, A. V. Shastin and E. S. Balenkova, *Synthesis*, 2005, 605; (*h*) V. G. Nenajdenko, O. N. Lenkova, A. V. Shastin and E. S. Balenkova, *Synthesis*, 2004, 573; (*i*) A. V. Shastin, V. M. Muzalevsky, E. S. Balenkova and V. G. Nenajdenko, *Mendeleev Commun.*, 2006, **16**, 179; (*j*) V. M. Muzalevskiy, N. G. Shikhaliev, A. M. Magerramov, N. V. Gurbanova, S. D. Geydarova, E. S. Balenkova, A. V. Shastin and V. G. Nenajdenko, *Russ. Chem. Bull., Int. Ed.*, 2013, **62**, 678 (*Izv. Akad. Nauk, Ser. Khim.*, 2013, 0677).

4 A. V. Shastin, V. M. Muzalevskii, V. N. Korotchenko, E. S. Balenkova and V. G. Nenajdenko, *Russ. J. Org. Chem.*, 2006, **42**, 183 (*Zh. Org. Khim.*, 2006, **42**, 200).

5 J.-D. Chai and M. Head-Gordon, *PhysChemPhys,* 2008, **10**, 6615.

6 M. J. Frisch, G. W. Trucks, H. B. Schlegel, *et al.*, *Gaussian 09, Revision C.01*, Gaussian, Inc., Wallingford CT, 2010.

Received: 21st May 2014; Com. 14/4382

Available online at www.sciencedirect.com
ScienceDirect
Mendeleev Commun., 2014, **24**, 342–344
Mendeleev Communications

Synthesis of 1,1,1-trifluorobut-3-yn-2-ones and their reactions with N-nucleophiles

Vasiliy M. Muzalevskiy,[a] Anton A. Iskandarov[a] and Valentine G. Nenajdenko*[a,b]

[a] *Department of Chemistry, M. V. Lomonosov Moscow State University, 119991 Moscow, Russian Federation. Fax: +7 495 932 8846; e-mail: nen@acylium.chem.msu.ru*
[b] *A. N. Nesmeyanov Institute of Organoelement Compounds, Russian Academy of Sciences, 119991 Moscow, Russian Federation. Fax: +7 499 135 5085; e-mail: nenajdenko@gmail.com*

DOI: 10.1016/j.mencom.2014.11.009

Bromination of 4-aryl-1,1,1-trifluorobut-3-yn-2-ones gives 4-aryl-3,4-dibromo-1,1,1-trifluorobut-3-en-2-ones whose reactivity towards N-nucleophiles (hydrazine and ethylenediamine) was investigated.

The importance of fluorinated compounds for medicinal chemistry can be hardly overestimated.[1] Among them, trifluoromethylated pyrazoles (*e.g.*, Celecoxib) are important type of pharmacologically relevant compounds.[2–5]

α,β-Unsaturated trifluoromethyl ketones are the versatile building blocks for the synthesis of various fluorinated molecules, especially heterocyclic ones.[6] Heterocyclization of trifluoromethyl-containing building blocks (for example, enones or 1,3-diketones) with hydrazines[7] is a common access to trifluoromethylated pyrazoles. Here, we report the synthesis of novel fluorinated building blocks, α,β-dibromo-CF_3-enones, and their reactions with hydrazine and ethylenediamine.

The presence of three electrophilic centers (trifluoroacetyl group, activated double bond and carbon adjacent with halogens) in the structure of α,β-dibromo-CF_3-enones led us to expect high activity of these compounds towards nucleophiles to open wide possibilities of incorporating a trifluoromethyl group into target compounds with the desired position of CF_3 group. Heterocycles of various sizes can be prepared using these building blocks depending on the nature of binucleophiles (1,2-, 1,3- and 1,4-binucleophiles).

CF_3-ynones **1** were prepared from lithiated terminal alkynes and ethyl trifluoroacetate.[8] Their bromination in CH_2Cl_2 afforded α,β-dibromo-CF_3-enones **2** in almost quantitative yields (Scheme 1).[†] The reaction was stereoselective and gave mixtures of *E*,*Z*-isomers in which content of a major isomer reached 80% (the ratio of the isomers was determined by ^{1}H NMR for **1b–e** or ^{19}F NMR for **1a**). The configuration of isomers was not assigned. Compounds **2** with both electron-donating and electron-withdrawing substituents in the phenyl ring were thus prepared.

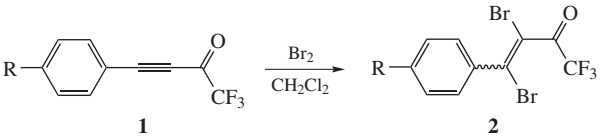

1 **2**

a R = H, 92%, 80:20
b R = Cl, 97%, 75:25
c R = MeO, 95%, 72:28
d R = Bu^t, 92%, 77:23
e R = Me, 93%, 79:21

Scheme 1

[†] ^{1}H (400.1 MHz), ^{13}C (100.6 MHz) and ^{19}F (376.3 MHz) NMR spectra in $CDCl_3$ were recorded on a Bruker AVANCE 400 MHz spectrometer. IR spectra were recorded on ThermoNicolet IR 200. The GC/MS analyses were performed with a Shimadzu GCMS-QP5050A instrument (EI, 70 eV). ESI-MS spectra were measured with a MicroTOF Bruker Daltonics instrument.

α,β-Dibromo-CF_3-enones **2** *(general procedure).* 1 M solution of Br_2 in CH_2Cl_2 (5.1 ml) was added dropwise to a solution of the corresponding CF_3-ynone **1** (0.005 mol) in CH_2Cl_2 (10 ml) on cooling with water bath. After stirring for 0.5 h, the volatiles were removed *in vacuo* and the residue was purified by column chromatography (silica gel, 230–400 Mesh, hexane–CH_2Cl_2, 3:1). All of products **2a–e** were obtained as yellowish viscous oils and as mixtures of isomers which were not resolved. Isomer ratios are specified in Scheme 1.

3,4-Dibromo-1,1,1-trifluoro-4-phenylbut-3-en-2-one **2a**. Yield 1.792 g (92%). For the mixture of isomers: IR (neat, ν/cm^{-1}): 1589 (C=C), 1745 (C=O). ^{1}H NMR, δ: 7.34–7.56 (m, 5H, Ph). ^{13}C NMR, δ: 105.0, 113.7, 114.8 (q, CF_3, *J* 291.9 Hz), 124.6, 128.6, 128.8, 130.5, 130.9, 136.5, 137.2, 138.0, 179.9 (q, C=O, *J* 38.7 Hz). ^{19}F NMR, δ: –74.0 (major), –73.8 (minor).

3,4-Dibromo-4-(4-chlorophenyl)-1,1,1-trifluorobut-3-en-2-one **2b**. Yield 1.905 g (97%). Major isomer: ^{1}H NMR, δ: 7.27 (d, 2H, Ar, *J* 8.6 Hz), 7.36 (d, 2H, Ar, *J* 8.6 Hz). ^{13}C NMR, δ: 114.4, 114.9 (q, CF_3, *J* 291.9 Hz), 129.2, 130.0, 135.6, 136.7, 137.2, 179.5 (q, C=O, *J* 38.3 Hz). ^{19}F NMR, δ: –73.9. Minor isomer: ^{1}H NMR, δ: 7.44 (d, 2H, Ar, *J* 8.7 Hz), 7.48 (d, 2H, Ar, *J* 8.7 Hz). ^{13}C NMR, δ: 105.7, 114.9 (q, CF_3, *J* 291.9 Hz), 123.3, 129.0, 130.3, 134.8, 179.4 (q, C=O, *J* 39.1 Hz). ^{19}F NMR, δ: –73.8.

3,4-Dibromo-1,1,1-trifluoro-4-(4-methoxyphenyl)but-3-en-2-one **2c**. Yield 1.840 g (95%). Major isomer: ^{1}H NMR, δ: 3.82 (s, 3H, MeO), 6.88 (d, 2H, Ar, *J* 8.8 Hz), 7.29 (d, 2H, Ar, *J* 8.8 Hz). ^{13}C NMR, δ: 55.3, 112.4, 114.8 (q, CF_3, *J* 292.3 Hz), 114.2, 129.6, 130.7, 138.6, 161.7, 180.4 (q, C=O, *J* 38.4 Hz). ^{19}F NMR, δ: –73.8. Minor isomer: ^{1}H NMR, δ: 3.86 (s, 3H, MeO), 6.96 (d, 2H, Ar, *J* 8.9 Hz), 7.53 (d, 2H, Ar, *J* 8.9 Hz). ^{13}C NMR, δ: 103.5, 113.8, 114.8 (q, CF_3, *J* 291.9 Hz), 124.9, 128.2, 130.8, 161.2, 179.8 (q, C=O, *J* 38.4 Hz). ^{19}F NMR, δ: –73.6.

*3,4-Dibromo-4-(4-*tert*-butylphenyl)-1,1,1-trifluorobut-3-en-2-one* **2d**. Yield 1.908 g (92%). Major isomer: ^{1}H NMR, δ: 1.33 (s, 9H, Bu^t), 7.28 (d, 2H, Ar, *J* 8.5 Hz), 7.40 (d, 2H, Ar, *J* 8.5 Hz). ^{13}C NMR, δ: 31.0, 34.9, 113.0, 114.8 (q, CF_3, *J* 292.3 Hz), 125.8, 128.7, 134.3, 138.5, 154.7, 180.2 (q, C=O, *J* 38.3 Hz). ^{19}F NMR, δ: –73.9. Minor isomer: ^{1}H NMR, δ: 1.37 (s, 9H, Bu^t), 7.47 (d, 2H, Ar, *J* 8.9 Hz), 7.51 (d, 2H, Ar, *J* 8.9 Hz). ^{13}C NMR, δ: 31.1, 35.0, 104.2, 114.8 (q, CF_3, *J* 291.1 Hz), 124.9, 125.5, 128.8, 133.3, 154.1, 179.8 (q, C=O, *J* 38.7 Hz). ^{19}F NMR, δ: –73.7.

*3,4-Dibromo-1,1,1-trifluoro-4-(*p*-tolyl)but-3-en-2-one* **2e**. Yield 1.736 g (93%). Major isomer: ^{1}H NMR, δ: 2.38 (s, 3H, Me), 7.19 (d, 2H, Ar, *J* 8.2 Hz), 7.25 (d, 2H, Ar, *J* 8.2 Hz). ^{13}C NMR, δ: 21.3, 113.0, 114.6 (q, CF_3, *J* 292.3 Hz), 128.8, 129.5, 134.5, 138.5, 141.6, 180.2 (q, C=O, *J* 38.7 Hz). ^{19}F NMR, δ: –73.9. Minor isomer: ^{1}H NMR, δ: 2.43 (s, 3H, Me), 7.27 (d, 2H, Ar, *J* 8.2 Hz), 7.46 (d, 2H, Ar, *J* 8.2 Hz). ^{13}C NMR, δ: 21.4, 104.3, 125.0, 128.8, 129.2, 133.5, 141.0. Other signals are identical to those of major isomer. ^{19}F NMR, δ: –73.7.

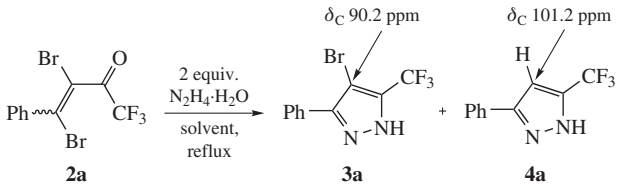

Scheme 2

Table 1 Reaction of **2a** with hydrazine hydrate in different solvents.

Solvent	Yield of **3a** + **4a** (%)	Yield of **3a** (%)	**3a**:**4a** ratio
THF	36	27	76:24
BuOH	68	58	86:14
EtOH	95	77	81:19
EtOH[a]	75	64	86:14
EtOH[b]	50	40	82:18
Toluene	97	85	87:13
MeOH	72	56	77:23
Pr^{i}OH	25	22	87:13
AcOH	20	16	80:20
CF_3CH_2OH	35	31	89:11
NEt_3	15	6	41:59
$CHCl_3$	61	46	75:25

[a] 1 equiv. of $N_2H_4·H_2O$ and 1 equiv. of AcONa. [b] 1 equiv. of $N_2H_4·H_2O$ and 1 equiv. of NEt_3.

We assumed that treatment of α,β-dibromo-CF_3-enones with hydrazine hydrate should afford the corresponding 3-bromo-2-trifluoromethylpyrazoles. Using compound **2a** as a model, we found that the highest yields (up to 85%, ^{19}F NMR monitoring) of the target bromopyrazole **3a** were achieved in boiling ethanol or toluene (Scheme 2, Table 1).‡ Surprisingly, in all cases a formation of pyrazole **4a** containing no bromine atom (up to 25%) also occurred. Structures of both products were confirmed by GC-MS (molecular ions with *m*/*z* 212 for H-pyrazole **4a** and doublet with *m*/*z* 290, 292 for bromopyrazole **3a**). Additionally ^{1}H, ^{13}C and ^{19}F NMR spectra of **3a** and **4a** are in total agreement with published ones. The most characteristic are signals of C^3 carbons in the pyrazole ring (C–Br of **3a**, 90.2 ppm and C–H of **4a**, 101.2 ppm).

We suppose that pyrazole **4a** is formed through the halophilic mechanism including an attack of a nucleophile to a bromine atom of reactant **2a**. Steric hindrance caused by bromine atoms in compound **2a** at the double bond creates difficulties for nucleophile attack at the double bond (Michael addition) as well as at the carbonyl group. To confirm this assumption, we performed DFT (B3LYP) quantum-chemical calculations and estimated charges on atoms in molecules of **2a**, which showed that the *Z* isomer was more stable by 0.23 kcal mol^{-1} but the difference was very small. The analysis of atomic charges (Mulliken and Levden) showed that both bromine atoms have a localized positive charge (Figure 1). Consequently, the calculations confirmed our assumption about the possibility of halophilic reaction for dibromoenones **2**.

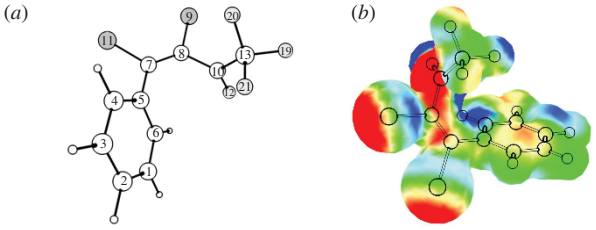

Figure 1 (*a*) The optimized geometry of enone **2a** and (*b*) the diagram of the electrostatic potential of the molecule.

Halophilic attack of hydrazine hydrate, which is also strong reducing agent, on bromine atom in **2a** gives intermediate anions **5** or **6**, which are transformed into acetylenic ketone **1a** by elimination of bromide. The subsequent reaction of **1a** with hydrazine hydrate affords pyrazole **4a**. This is confirmed by the presence of traces of acetylene **1a** in the reaction mixture (*m*/*z* 198, GC-MS, the signal at –77.8 ppm in ^{19}F NMR spectrum). Moreover, heterocyclization of similar ynones with hydrazine hydrate to pyrazoles is known.[9]

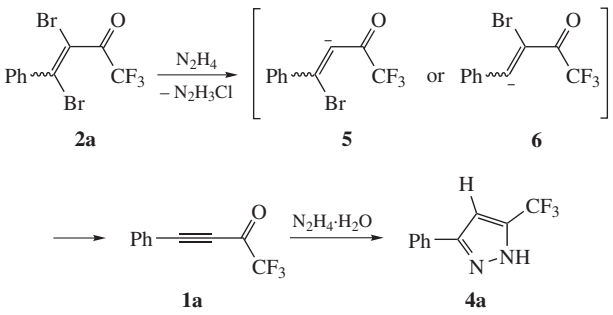

Scheme 3

Compound **2a** also reacted unusually with ethylenediamine§ to form *E*-α,β-dibromostyrene **7** and 2-trifluoromethylimidazoline **8** as a result of C–C bond cleavage. The possible mechanism includes an attack of ethylenediamine to the carbonyl group to produce trifluoromethylimine **9**, which cyclizes into trifluoro-

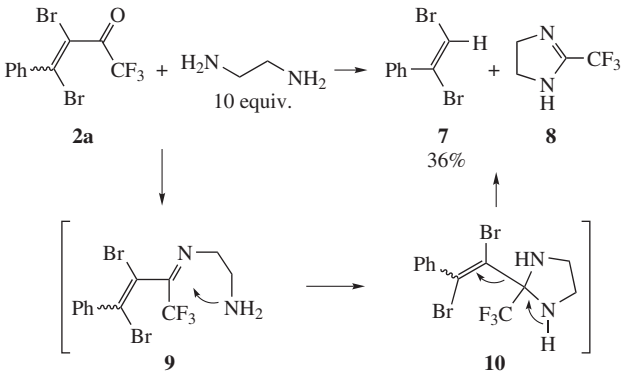

Scheme 4

‡ *Reaction of compound* **2a** *with hydrazine hydrate*. A mixture of compound **2a** (1.0 mmol) and hydrazine hydrate (2.0 mmol) in appropriate solvent (2 ml, see Table 1) was stirred at reflux for 10–12 h. The volatiles were evaporated *in vacuo*, the residue was purified by column chromatography on silica gel (eluent, hexane–CH_2Cl_2, 1:2). The pyrazoles **3a** and **4a** were not separated. NMR data of **3a**[11] and **4a**[12] are consistent with those in the literature.

*4-Bromo-5-(trifluoromethyl)-3-phenyl-1*H*-pyrazole* **3a**. ^{1}H NMR, δ: 7.48–7.83 (m, 5H, Ar), 14.39 (br. s, 1H, NH). ^{13}C NMR, δ: 88.8, 122.1 (q, CF_3, *J* 291.9 Hz), 126.8, 127.8, 129.0, 129.7, 139.9 (q, *C*CF_3, *J* 36.1 Hz), 142.5. ^{19}F NMR, δ: –61.9.

*5-(Trifluoromethyl)-3-phenyl-1*H*-pyrazole* **4a**: ^{1}H NMR, δ: 7.48–7.83 (m, 5H, Ar), 14.09 (br. s, 1H, NH). ^{13}C NMR, δ: 101.0, 117.0, 118.4 (q, CF_3, *J* 291.9 Hz), 125.6, 127.8, 129.1, 129.3, 135.8 (q, *C*CF_3, *J* 36.1 Hz), 144.0. ^{19}F NMR, δ: –61.3.

§ *Reaction of compound* **2a** *with ethylenediamine*. A mixture of compound **2a** (1.0 mmol) and ethylenediamine (1.0 ml) was kept at room temperature for 12 h. The volatiles were evaporated *in vacuo*, the residue was purified by column chromatography on silica gel (eluent, hexane–CH_2Cl_2, 1:1) to afford 0.094 g (36%) of *E*-α,β-dibromostyrene **7** as a colorless oil. ^{1}H NMR, δ: 6.81 (s, 1H, =CH), 7.36–7.54 (m, Ar) (*cf.* ref. 13).

methylimidazolidine **10**, followed by cleavage of the C–C bond to furnish compounds **7** and **8**. Similar examples of cleavage of C–C bonds were described for unsaturated compounds bearing electron-withdrawing substituents in reactions with ethylenediamine.[10] However, a significant difference with the published data should be noted. In the case of compound **2a** the cleavage of single C–C bond is observed, whereas previously formal cleavage of multiple C–C bonds proceeded.

In conclusion, synthesis of previously unknown α,β-dibromo-CF_3-enones by bromination of CF_3-ynones was elaborated. Their reactivity towards N-nucleophiles was examined, which opens prospects to new useful fluorinated compounds.

This work was supported by the Russian Science Foundation (grant no. 14-13-00083).

References

1 (*a*) P. Kirsch, *Modern Fluoroorganic Chemistry: Synthesis, Reactivity, Applications*, Wiley-VCH, Weinheim, 2004; (*b*) K. Uneyama, *Organofluorine Chemistry*, Blackwell Publishing, Oxford, 2006; (*c*) J. P. Bégué and D. Bonnet-Delpon, *Bioorganic and Medicinal Chemistry of Fluorine*, John Wiley & Sons, Hoboken, 2008; (*d*) *Fluorine and Health. Molecular Imaging, Biomedical Materials and Pharmaceuticals*, eds. A. Tressaud and G. Haufe, Elsevier, Amsterdam, 2008, pp. 553–778; (*e*) V. M. Muzalevskiy, V. G. Nenajdenko, A. V. Shastin, E. S. Balenkova and G. Haufe, *Synthesis*, 2009, 3905; (*f*) *Fluorinated Heterocyclic Compounds: Synthesis, Chemistry, and Applications*, ed. V. A. Petrov, Wiley, Hoboken, 2009; (*g*) O. V. Serdyuk, V. T. Abaev, A. V. Butin and V. G. Nenajdenko, *Synthesis*, 2011, 2505; (*h*) O. V. Serdyuk, V. M. Muzalevskiy and V. G. Nenajdenko, *Synthesis*, 2012, 2115; (*i*) T. Liang, C. N. Neumann and T. Ritter, *Angew. Chem. Int. Ed*., 2013, **52**, 8214; (*j*) J. Wang, M. Sanchez-Rosello, J. L. Acena, C. del Pozo, A. E. Sorochinsky, S. Fustero, V. A. Soloshonok and H. Liu, *Chem. Rev.*, 2014, **114**, 2432; (*k*) I. Ojima, *J. Org. Chem.*, 2013, **78**, 6358; (*l*) *Fluorine in Heterocyclic Chemistry*, ed. V. G. Nenajdenko, Springer, 2014.

2 T. D. Penning, J. J. Talley, S. R. Bertenshaw, J. S. Carter, P. W. Collins, S. Docter, M. J. Graneto, L. F. Lee, J. W. Malecha, J. M. Miyashiro, R. S. Rogers, D. J. Rogier, S. S. Yu, G. D. Anderson, E. G. Burton, J. N. Cogburn, S. A. Gregory, C. V. Koboldt, W. E. Perkins, K. Seibert, A. W. Veenhuizen, Y. Y. Zhang and P. C. Isakson, *J. Med. Chem*., 1997, **40**, 1347.

3 (*a*) A. G. Habeeb, P. N. P. Rao and E. E. Knaus, *J. Med. Chem.*, 2001, **44**, 3039; (*b*) S. K. Singh, S. Vobbalareddy, S. Shivaramakrishna, A. Krishnamraju, S. A. Rajjak, S. R. Casturi, V. Akhila and Y. K. Rao, *Bioorg. Med. Chem. Lett.*, 2004, **14**, 1683.

4 (*a*) S. K. Singh, P. G. Reddy, K. S. Rao, B. B. Lohray, P. Misra, S. A. Rajjak, Y. K. Rao and A. Venkateswarlu, *Bioorg. Med. Chem. Lett.*, 2004, **14**, 499; (*b*) S. K. Singh, S. Vobbalareddy, S. R. Kalleda, S. A. Rajjak, S. R. Casturi, S. R. Datla, R. N. V. S. Mamidi, R. Mullangi, R. Bhamidipati, R. Ramanujan, V. Akella and K. R. Yelewarapu, *Org. Biomol. Chem.*, 2004, **2**, 2442.

5 M. A. Chowdhury, K. R. A. Abdellatif, Y. Dong, D. Das, M. R. Suresh and E. E. Knaus, *J. Med. Chem*., 2009, **52**, 1525.

6 (*a*) V. G. Nenaidenko and E. S. Balenkova, *Zh. Org. Khim*., 1992, **28**, 600 (in Russian); (*b*) V. G. Nenajdenko, I. F. Leshcheva and E. S. Balenkova, *Tetrahedron*, 1994, **50**, 775; (*c*) V. G. Nenajdenko, A. L. Krasovsky, M. V. Lebedev and E. S. Balenkova, *Synlett*, 1997, 1349; (*d*) A. L. Krasovsky, V. G. Nenajdenko and E. S. Balenkova, *Tetrahedron*, 2001, **57**, 201; (*e*) V. G. Nenajdenko, A. L. Krasovsky and E. S. Balenkova, *Tetrahedron*, 2007, **63**, 12481; (*f*) A. Yu. Rulev, V. M. Muzalevskiy, E. V. Kondrashov, I. A. Ushakov, A. R. Romanov, V. N. Khrustalev and V. G. Nenajdenko, *Org. Lett*., 2013, **15**, 2726; (*g*) V. G. Nenajdenko, A. V. Sanin and E. S. Balenkova, *Molecules*, 1997, **2**, 186; (*h*) V. G. Nenajdenko, A. V. Sanin and E. S. Balenkova, *Russ. Chem. Rev*., 1999, **68**, 437 (*Usp. Khim.*, 1999, **68**, 483); (*i*) S. V. Druzhinin, E. S. Balenkova and V. G. Nenajdenko, *Tetrahedron*, 2007, **63**, 7753; (*j*) V. G. Nenajdenko and E. S. Balenkova, *ARKIVOC*, 2011, 246.

7 (*a*) S. Fustero, M. Sánchez-Roselló, P. Barrio and A. Simón, *Chem. Rev*., 2011, **111**, 6084; (*b*) S. Fustero, A. Simón-Fuentes and J. F. Sanz-Cervera, *Org. Prep. Proced. Int*., 2009, **41**, 253.

8 S. Sasaki, Y. Ikekame, M. Tanayama, T. Yamauchi and K. Higashiyama, *Synlett*, 2012, 2699.

9 (*a*) R. J. Linderman and S. Kirollos, *Tetrahedron Lett.*, 1989, **30**, 2049; (*b*) B. G. Jones, S. K. Branch, A. S. Thompson and M. D. Threadgill, *J. Chem. Soc., Perkin Trans. 1*, 1996, 2685.

10 (*a*) V. G. Nenajdenko, V. M. Muzalevskiy, A. V. Shastin, E. S. Balenkova, E. V. Kondrashov, I. A. Ushakov and A. Yu. Rulev, *J. Org. Chem*., 2010, **75**, 5679; (*b*) S. Roy, M. P. Davydova, R. Pal, K. Gilmore, G. A. Tolstikov, S. F. Vasilevsky and I. V Alabugin, *J. Org. Chem*., 2011, **76**, 7482.

11 S. L. Jeon, J. H. Choi, B. T. Kim and I. H. Jeong, *J. Fluorine Chem.*, 2007, **128**, 1191.

12 M. A. P. Martins, P. H. Beck, D. N. Moreira, L. Buriol, C. P. Frizzo, N. Zanatta and H. G. Bonacorso, *J. Heterocycl. Chem*., 2010, **47**, 301.

13 K. Schuh and F. Glorius, *Synthesis*, 2007, 2297.

Received: 15th September 2014; Com. 14/4465

Available online at www.sciencedirect.com
ScienceDirect
Mendeleev Commun., 2014, **24**, 345
Mendeleev Communications

A convenient synthesis of cyclopropane malonyl peroxide

Alexander O. Terent'ev,* Vera A. Vil', Olga M. Mulina, Kazimir K. Pivnitsky and Gennady I. Nikishin

N. D. Zelinsky Institute of Organic Chemistry, Russian Academy of Sciences, 119991 Moscow, Russian Federation. Fax: +7 499 135 8824; e-mail: alterex@yandex.ru

DOI: 10.1016/j.mencom.2014.11.010

Cyclopropane-1,1-dicarbonyl peroxide was prepared in 85% yield by the reaction of diethyl cyclopropane-1,1-dicarboxylate with the urea hydrogen peroxide clathrate in the presence of methanesulfonic acid.

Cyclic diacyl peroxide oxidation known since the 1950s[1] has recently undergone a renaissance.[2,3] Cyclopropane malonyl peroxide **1** is the most widely used and the most active oxidizing agent among malonyl peroxides.[2(*a*),(*b*),(*d*),(*f*),(*g*)]

The main preparative synthesis of compound **1** is based on the reaction of cyclopropane-1,1-dicarboxylic acid **2** with urea hydrogen peroxide clathrate in the presence of methanesulfonic acid (Scheme 1).[2(*a*),(*f*)]

Diacid **2** was prepared in moderate (52–72%) yields in one-pot by alkylation of diethyl malonate with 1,2-dibromoethane in the presence of alkali and a phase-transfer catalyst *via* the stages of formation and hydrolysis of cyclopropane diester **3**.[2(*f*),4] Higher yield of diacid **2** can be achieved by two-step procedure.[5,6] First, diester **3** was obtained in 92% yield by alkylation of diethyl malonate with 1,2-dibromoethane in the presence of K_2CO_3 and a phase-transfer catalyst. Second, diacid **2** was prepared in high yield by hydrolysis of ester **3**. However, this two-step procedure is more laborious.

Here, we demonstrated that peroxide **1** can be directly prepared in 85% yield by the reaction between diethyl cyclopropane-1,1-dicarboxylate **3** and urea hydrogen peroxide clathrate in the presence of methanesulfonic acid.† This reaction is a rare example of the synthesis of peroxides from esters,[7] since peroxides are generally synthesized from acids, anhydrides, or acid chlorides.[8] The method developed in the present study provides an essentially facile approach to the synthesis of peroxide **1**. The reaction can be scaled up to yield gram amounts providing total yield 78% based on diethyl malonate **3**, thus making cyclopropyl malonyl peroxide **1** readily available in laboratory practice.

This work was supported by the Russian Science Foundation (grant no. 14-23-00150).

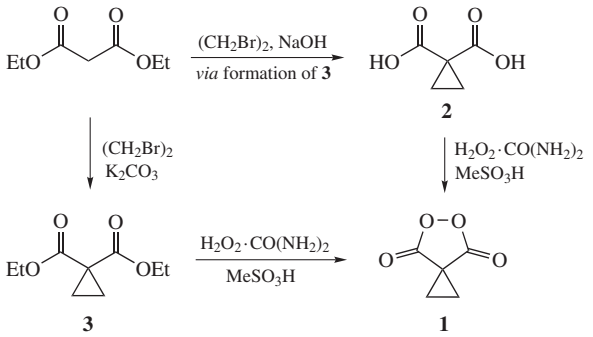

Scheme 1

† *Synthesis of cyclopropane-1,1-dicarbonyl peroxide* **1**. *Caution:* Although we have encountered no difficulties in working with peroxides, precautions, such as the use of shields, fume hoods, and the avoidance of transition metal salts, heating and shaking, should be taken whenever possible.

Urea hydrogen peroxide clathrate (50.80 g, 0.540 mol) was added with stirring to methanesulfonic acid (155.70 g, 105.13 ml), and the mixture was stirred for 2 min. Then diethyl cyclopropane-1,1-dicarboxylate **3** (10.00 g, 0.054 mol) was added, and the mixture was stirred for 24 h. Water (200 ml) and ethyl acetate (200 ml) were added, the organic layer was separated, and the aqueous layer was extracted with ethyl acetate (4×50 ml). The combined organic layers were washed with water (2×30 ml), a 5% aqueous $NaHCO_3$ solution (2×30 ml), and again with water (2×30 ml) and dried over $MgSO_4$. The solvent was removed under water jet vacuum. Product **1** was obtained as white crystals in 85% yield (5.88 g, 0.046 mol), mp 89–91 °C (lit.,[2(*a*)] mp 90 °C). ^{1}H NMR (300.13 MHz, $CDCl_3$) δ: 2.11 (s, 4H). ^{13}C NMR (75.48 MHz, $CDCl_3$) δ: 19.8, 23.6, 172.1.

References

1 (*a*) W. Adam and J. W. Diehl, *J. Chem. Soc., Chem. Commun*., 1972, **13**, 797; (*b*) C. L. Perrin and T. Arrhenius, *J. Am. Chem. Soc*., 1978, **100**, 5249; (*c*) F. D. Greene, *J. Am. Chem. Soc*., 1956, **78**, 2246; (*d*) F. D. Greene, *J. Am. Chem. Soc*., 1956, **78**, 2250; (*e*) F. D. Greene, *J. Am. Chem. Soc.*, 1959, **81**, 1503; (*f*) F. D. Greene and W. W. Rees, *J. Am. Chem. Soc*., 1960, **82**, 890; (*g*) F. D. Greene and W.W. Rees, *J. Am. Chem. Soc.*, 1960, **82**, 893.

2 (*a*) J. C. Griffith, K. M. Jones, S. Picon, M. J. Rawling, B. M. Kariuki, M. Campbell and N. C. O. Tomkinson, *J. Am. Chem. Soc*., 2010, **132**, 14409; (*b*) M. Schwarz and O. Reiser, *Angew. Chem. Int. Ed*., 2011, **50**, 10495; (*c*) C. Yuan, A. Axelrod, M. Varela, L. Danysh and D. Siegel, *Tetrahedron Lett*., 2011, **52**, 2540; (*d*) S. Picon, M. Rawling, M. Campbell and N. C. O. Tomkinson, *Org. Lett*., 2012, **14**, 6250; (*e*) K. M. Jones and N. C. O. Tomkinson, *J. Org. Chem.*, 2012, **77**, 921; (*f*) M. J. Rawling, J. H. Rowley, M. Campbell, A. R. Kennedy, J. A. Parkinson and N. C. O. Tomkinson, *Chem. Sci.*, 2014, **5**, 1777; (*g*) M. J. Rawling and N. C. O. Tomkinson, *Org. Biomol. Chem*., 2013, **11**, 1434.

3 C. Yuan, Y. Liang, T. Hernandez, A. Berriochoa, K. N Houk and D. Siegel, *Nature*, 2013, **499**, 192.

4 (*a*) R. K. Singh and S. Danishefsky, *J. Org. Chem.*, 1975, **40**, 2969; (*b*) R. K. Singh and S. Danishefsky, *Org. Synth. Coll. Vol*., 1981, **7**, 411.

5 (*a*) J. Heiszman, I. Bitter, K. Harsanyi and L. Toeke, *Synthesis*, 1987, **8**, 738; (*b*) K. M. Jones, *PhD Thesis*, Cardiff University, 2010.

6 W. Dmowski and A. Wolniewicz, *J. Fluorine Chem*., 2000, **102**, 141.

7 (*a*) W. Adam and L. Szendrey, *Tetrahedron Lett*., 1972, **26**, 2669; (*b*) C. Singh, N. C. Srivastav, N. Srivastava and S. K. Puri, *Tetrahedron Lett*., 2005, **46**, 2757; (*c*) E. H. White, D. F. Roswell, A. C. Dupont and A. A. Wilson, *J. Am. Chem. Soc*., 1987, **109**, 5189; (*d*) P. Dussault and I. Q. Lee, *J. Org. Chem.*, 1992, **57**, 1952; (*e*) D. L. Yin, P. Bernhardt, K. L. Morley, Y. Jiang, J. D. Cheeseman, V. Purpero, J. D. Schrag and R. J. Kazlauskas, *Biochemistry*, 2010, **49**, 1931; (*f*) L. Wiermans, S. Hofzumahaus, C. Schotten, L. Weigand, M. Schallmey, A. Schallmey and P. Domínguez de María, *ChemCatChem*, 2013, **5**, 3719.

8 (*a*) A. M. Eliasen, R. P. Thedford, K. R. Claussen, C. Yuan and D. Siegel, *Org. Lett*., 2014, **16**, 3628; (*b*) Z. Rappoport, *The Chemistry of Peroxides*, John Wiley & Sons, Hoboken, 2007.

Received: 20th August 2014; Com. 14/4449

Available online at www.sciencedirect.com
ScienceDirect
Mendeleev Commun., 2014, **24**, 346–348
Mendeleev Communications

Unexpected formation of substituted naphthalenes and phenanthrenes in a $GaCl_3$ mediated dimerization–fragmentation reaction of 2-arylcyclopropane-1,1-dicarboxylates

Roman A. Novikov,[a] Anna V. Tarasova,[a] Kyrill Yu. Suponitsky[b] and Yury V. Tomilov*[a]

[a] *N. D. Zelinsky Institute of Organic Chemistry, Russian Academy of Sciences, 119991 Moscow, Russian Federation. Fax: +7 499 135 6390; e-mail: tom@ioc.ac.ru*
[b] *A. N. Nesmeyanov Institute of Organoelement Compounds, Russian Academy of Sciences, 119991 Moscow, Russian Federation*

DOI: 10.1016/j.mencom.2014.11.011

Dimethyl 2-arylcyclopropane-1,1-dicarboxylates on heating with $GaCl_3$ undergo dimerization to afford arylnaphthalenes or phenanthrenes. A possible reaction mechanism including elimination of two dimethyl malonate molecules was proposed, dimethyl malonate gallium complex $Ga^{3+}[H_2C(CO_2Me)_2]_3(GaCl_4^-)_3$ was isolated and characterized by X-ray diffraction analysis.

Donor–acceptor cyclopropanes (DACs) containing donor and acceptor substituents in the vicinal position are widely used in present-day organic synthesis as the sources of 1,3-dipoles which are generated from them in the presence of Lewis acids.[1–5] Recently, it was shown that donor–acceptor cyclopropanes can undergo dimerization under the action of Lewis acids and organic catalysts in the absence of unsaturated substrates and other scavengers of generated 1,3-dipoles, the dimers having various origin such as arylidene malonates,[6] diarylhexenes,[6,7] cyclohexanes,[7] tetralins,[7–9] dihydroanthracenes,[7] pentaleno[1,6-*a*,*b*]-indoles,[10] polysubstituted cyclopentanes[6,8] and 2-oxabicyclo-[3.3.0]octanes.[11] Among the discovered DAC transformations, attention should be focused on the dimerization of 2-arylcyclopropane-1,1-dicarboxylates **1** to polysubstituted cyclopentanes and/or tetralins under the action of anhydrous $GaCl_3$,[8,9,12] the ratio of the products being dependent only on the reaction temperature and the amount of gallium trichloride used.

We studied the behaviour of phenylcyclopropane dicarboxylate **1a** with $GaCl_3$ under conditions different from those used previously:[8,9] the reaction temperature was raised to 80 °C and the amount of $GaCl_3$ was 1–2 equiv. Under these conditions, a new route of DAC transformation occurred with the unexpected formation of 2-phenylnaphthalene **2a**, whose molecule did not contain ester groups (Scheme 1, R = H).† Unlike the previously described products of donor–acceptor cyclopropanes dimerization,[6–11] compound **2a** is not a true dimer, although it is formed from two cyclopropane dicarboxylate molecules. In the course of this reaction, two malonic ester molecules are eliminated, and the formation of **2a** formally corresponds to the dimerization of phenylacetylene, which was not observed earlier. Other Lewis acids, *e.g.*, $EtAlCl_2$ or scandium and ytterbium triflates, do not provide compounds like **2a**. Thus, the application of anhydrous $GaCl_3$ is a unique procedure for performing fragmentation processes under the conditions of DAC dimerization.

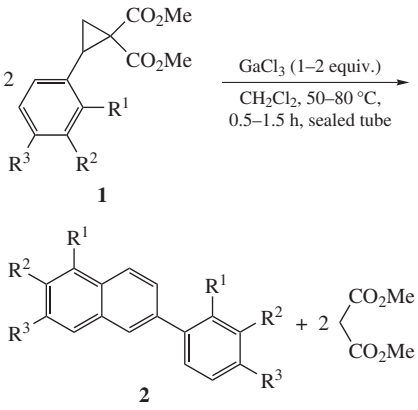

DAC	R^1	R^2	R^3	Product	Yield (%)
1a	H	H	H	**2a**	93
1b	H	H	Me	**2b**	80
1c	Cl	H	H	**2c**	22
1d	H	Cl	H	**2d**	65
1e	H	Br	H	**2e**	67

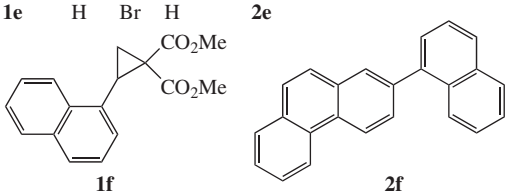

94

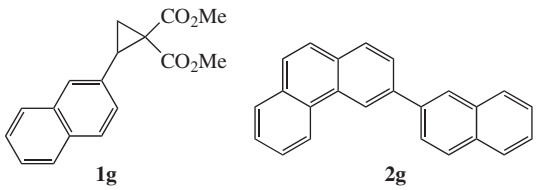

59

Scheme 1

† ^1H and ^{13}C NMR spectra were recorded on Bruker AMX-III 400 (400.1 and 100.6 MHz, respectively) and Bruker AVANCE II 300 (300 and 75 MHz, respectively) spectrometers in $CDCl_3$ containing 0.05% TMS as the internal standard. Assignments of ^1H and ^{13}C signals were made with the aid of 1D DEPT-135 and 2D COSY, NOESY, HSQC and HMBC spectra.

Compounds **2** (*general procedure).* Solid $GaCl_3$ (0.45–0.75 mmol, 150 mol%) was added in one portion to a solution of cyclopropane **1** (0.3–0.5 mmol) in 4 ml of dry CH_2Cl_2 in dry argon atmosphere at room temperature under vigorous stirring. The mixture was heated to 80 °C under slight pressure in sealed tube and was stirred for 1 h. Then aqueous 5% HCl solution was added at room temperature to reach pH 3, and the mixture was extracted with CH_2Cl_2 (3×10 ml). The organic layer was dried over $MgSO_4$ and the solvent was removed *in vacuo*. The residue was purified by column chromatography on silica gel (benzene–EtOAc, 20 : 1) to afford pure compounds **2** in yields specified in Scheme 1.

2-Phenylnaphthalene **2a**: yield 93%, colourless crystals, mp 97–98 °C. NMR spectra correspond to published data.[14]

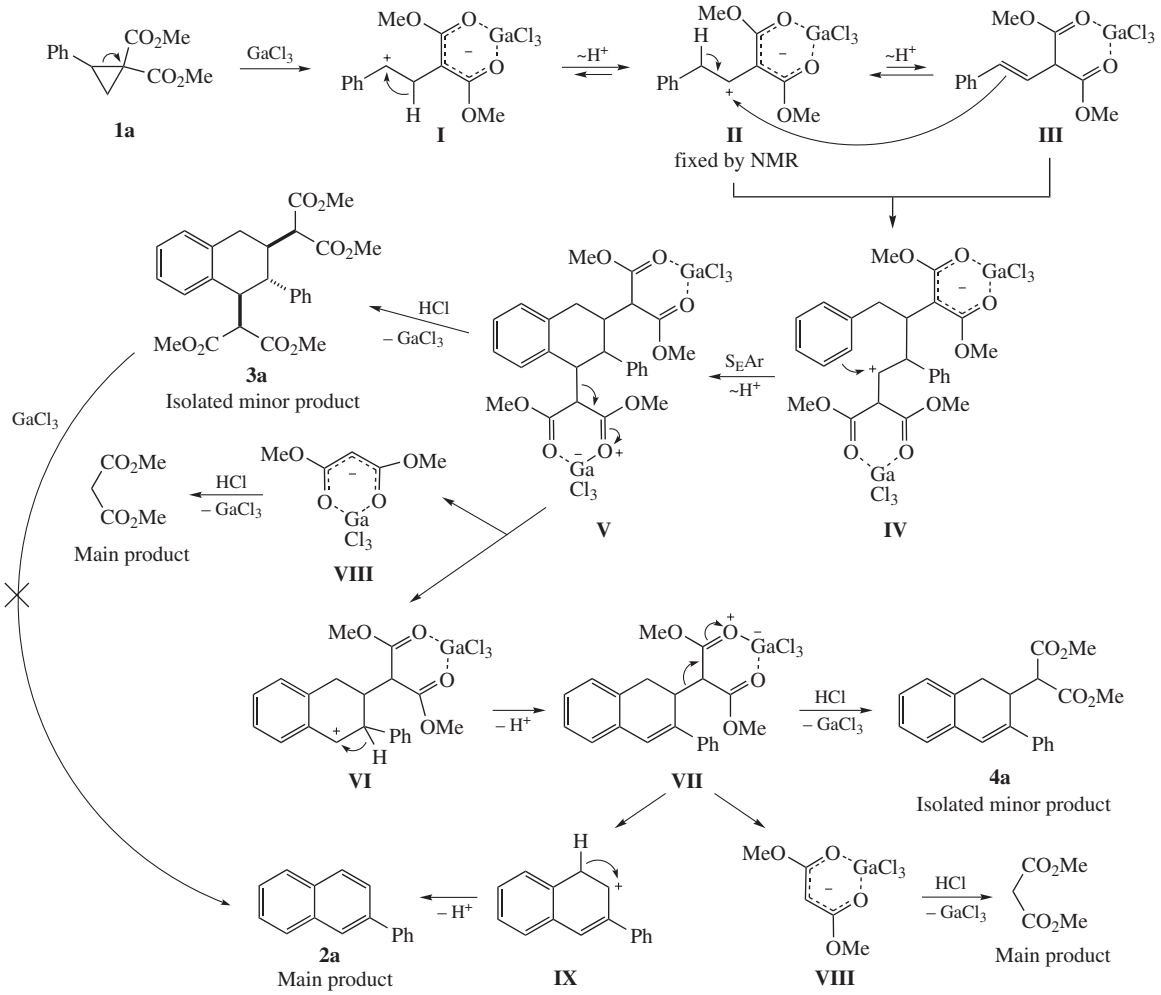

Scheme 2

The conditions found were successfully extended on other aryl-substituted cyclopropane dicarboxylates **1**. In this case, dimerization–fragmentation reactions effectively occurred with cyclopropanes containing phenyl, *p*-tolyl and 1-naphthyl substituents, whereas cyclopropanes **1c–e** with halogen atoms in the *ortho* and *meta* positions of the benzene ring, were found less reactive. Interestingly, cyclopropanes with halogen atoms in the *para* position of the benzene ring did not form similar products.

The possible mechanism of this process is outlined on Scheme 2. Under the action of $GaCl_3$, cyclopropane **1** undergoes ring opening to afford 1,2-dipolar intermediate **II** after a number of consecutive reactions.[13] This is a key intermediate in the dimerization of cyclopropanes **1** into tetralins **3**.[9] However, this reaction does not reach the formation of tetralins **3** as a result of an elevated reaction temperature and the use of a larger amount of $GaCl_3$. Under these conditions dimeric intermediate **V** undergoes the elimination of a malonyl fragment induced by the Ga atom, which possesses considerable Lewis acidity, like an acid-catalyzed retro-aldol reaction. As a result, intermediate **VI** is generated, which is converted into intermediate **VII** and the gallium enolate of malonic ester **VIII** after proton migration. Similarly to intermediate **V**, intermediate **VII** eliminates the second malonyl fragment and gives a naphthalene fragment as a result of aromatization.

To rationalize the stepwise mechanism of the elimination of malonyl fragments from the DAC dimerization products, one should note that tetralins **3** are formed as minor reaction products; in the case of cyclopropane **1a**, monoelimination product **4a** was isolated in a yield of ~1%.‡ It is likely that the energetically favourable aromatization of a six-membered ring is the driving force of the main process observed. However, it requires the rupture of two C–C bonds, which, in turn, requires the use of

7-Methyl-2-(4-methylphenyl)naphthalene **2b**: yield 80%, colourless crystals, mp 134–136 °C. ^{1}H NMR, δ: 2.41 (s, 3H, C$^{4'}$Me), 2.52 (s, 3H, C^{7}Me), 7.24–7.32 (m, 2H, *m*-H), 7.30 (dd, 1H, C^{6}H, ^3J 8.3 Hz, ^4J 1.6 Hz), 7.58–7.64 (m, 2H, *o*-H), 7.64 (br.s, 1H, C^{8}H), 7.66 (dd, 1H, C^{3}H, ^3J 8.4 Hz, ^4J 1.6 Hz), 7.74 (d, 1H, C^{5}H, ^3J 8.3 Hz), 7.84 (d, 1H, C^{4}H, ^3J 8.4 Hz), 7.92 (br.s, 1H, C^{1}H). ^{13}C NMR, δ: 21.2 and 21.8 (2Me), 124.8, 124.9, 127.2, 127.5, 128.12 and 128.16 (6CH), 127.3 and 129.6 (*o*-C, *m*-C), 130.9, 134.1, 135.9, 137.1, 138.5 and 138.6 (6C). Found (%): C, 92.85; H, 6.73. Calc. for $C_{18}H_{16}$ (%): C, 93.06; H, 6.94.

1-Chloro-6-(2-chlorophenyl)naphthalene **2c**: yield 22%, colourless crystals, mp 46–48 °C. IR ($CHCl_3$, ν/cm^{-1}): 3020, 2975, 2923, 1646, 1520, 1466, 1419. ^{1}H NMR, δ: 7.34 (ddd, 1H, C$^{4'}$H or C$^{5'}$H, ^3J 7.4 and 7.3 Hz, ^4J 2.0 Hz), 7.37 (ddd, 1H, C$^{4'}$H or C$^{5'}$H, ^3J 7.4 and 7.3 Hz, ^4J 2.0 Hz), 7.42 (dd, 1H, C^{3}H, ^3J 8.3 and 7.4 Hz), 7.44 (dd, 1H, C$^{3'}$H or C$^{6'}$H, ^3J 7.3 Hz, ^4J 2.0 Hz), 7.52 (dd, 1H, C$^{3'}$H or C$^{6'}$H, ^3J 7.3 Hz, ^4J 2.0 Hz), 7.60 (dd, 1H, C^{2}H, ^3J 7.4 Hz, ^4J 1.1 Hz), 7.71 (dd, 1H, C^{7}H, ^3J 8.7 Hz, ^4J 1.7 Hz), 7.81 (br.d, 1H, C^{4}H, ^3J 8.3 Hz), 7.91 (d, 1H, C^{5}H, ^4J 1.7 Hz), 8.33 (br.d, 1H, C^{8}H, ^3J 8.7 Hz). ^{13}C NMR, δ: 124.3 (C^8), 126.3 (C^3), 126.6 (C^2), 127.1 and 129.1 (C$^{4'}$ and C$^{5'}$), 127.5 (C^4), 128.8 (C^5), 129.0 (C^7), 130.2 and 131.7 (C$^{3'}$ and C$^{6'}$), 130.3 (C^{8a}), 132.0 (C$^{2'}$), 132.1 (C^1), 134.5 (C^{4a}), 138.1 (C^6), 140.2 (C$^{1'}$). MS, *m*/*z* (%): 272 (96) [M]$^+$ for ^{35}Cl, 232 (18), 202 (65), 149 (39), 100 (36), 83 (30), 59 (43), 57 (88), 43 (100). Found (%): C, 70.87; H, 3.80. Calc. for $C_{16}H_{10}Cl_2$ (%): C, 70.35; H, 3.69.

2-(1-Naphthyl)phenanthrene **2f**: yield 94%, thick colourless oil. NMR spectra correspond to published data.[15]

3-(2-Naphthyl)phenanthrene **2g**: yield 59%, colourless crystals, mp 122–123 °C. NMR spectra correspond to published data.[16]

For characteristics of compounds **2d**,**e**, see Online Supplementary Materials.

severe reaction conditions. It is obvious that the elimination of the second malonyl fragment proceeds much more rapidly than that of the first one because aromatization occurs at this step, as observed experimentally; that is, the reaction does almost not stop with the formation of monoelimination products **4**. Note that dimeric tetralins **3** do not give even the traces of compounds **2** on the interaction with $GaCl_3$ under the conditions of fragmentation. This is likely due to the fact that a complex with $GaCl_3$ (like compound **V**) should be formed for the elimination of a malonyl fragment; however, it was found previously[13] that substituted malonates do not produce stable complexes on the interaction with $GaCl_3$. This complex can be formed only indirectly through the dimerization of complex **II** and its fragmentation described above. In all cases, the above transformations occur with very high regioselectivity. Thus, cyclopropanes **1d**,**e**,**g**, which can react at both *ortho* positions of the aromatic ring, form only one regioisomer. However, the mechanism of this electrophilic substitution remains unclear.

Note that Ga enolate **VIII** converted into new complex **5**, whose structure was determined by X-ray diffraction analysis (Figure 1), in a matter of several days. This complex includes three fragments of malonic ester and four gallium atoms, three of which exist in the form of the $GaCl_4^-$ anions.§

Thus, we found a new uncommon reaction of 2-arylcyclopropane-1,1-dicarboxylates with anhydrous $GaCl_3$ on heating resulting in the regiospecific formation of substituted naphthalenes and phenanthrenes in good yields. In this case, the dimeric intermediate formed from two DAC molecules undergoes fragmentation with the elimination of two malonyl fragments as dimethyl malonate.

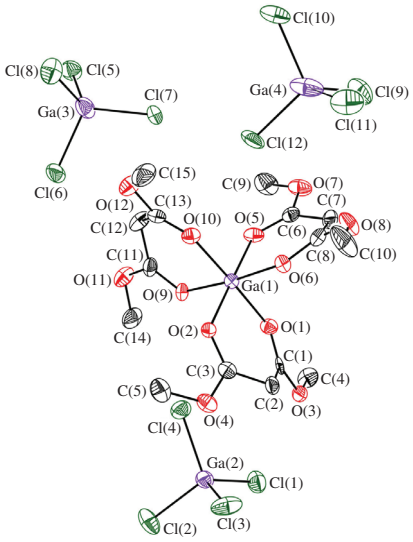

Figure 1 X-ray structure of a molecule of **5** in the representation of atoms as thermal ellipsoids (p = 50%).

This work was supported by the Russian Science Foundation (grant no. 14-13-01054).

Online Supplementary Materials

Supplementary data associated with this article can be found in the online version at doi:10.1016/j.mencom.2014.11.011.

References

1 H. U. Reissig and R. Zimmer, *Chem. Rev.*, 2003, **103**, 1151.
2 (*a*) M. Yu and B. L. Pagenkopf, *Tetrahedron*, 2006, **61**, 321; (*b*) F. de Simone and J. Waser, *Synthesis*, 2009, **20**, 3353; (*c*) M. J. Campbell, J. S. Johnson, A. T. Parsons, P. D. Pohlhaus and S. D. Sanders, *J. Org. Chem.*, 2010, **75**, 6317.
3 M. Ya. Mel'nikov, E. M. Budynina, O. A. Ivanova and I. V. Trushkov, *Mendeleev Commun.*, 2011, **21**, 293.
4 M. A. Cavitt, L. H. Phun and S. France, *Chem. Soc. Rev.*, 2014, **43**, 804.
5 (*a*) T. F. Schneider, J. Kaschel and D. B. Werz, *Angew. Chem. Int. Ed.*, 2014, **53**, 5504; (*b*) S. Chakrabarty, I. Chatterjee, B. Wibbeling, C. G. Daniliuc and A. Studer, *Angew. Chem. Int. Ed.*, 2014, **53**, 5964; (*c*) F. de Nanteuil, E. Serrano, D. Perrotta and J. Waser, *J. Am. Chem. Soc.*, 2014, **136**, 6239; (*d*) M. K. Ghorai, R. Talukdar and D. P. Tiwari, *Org. Lett.*, 2014, **16**, 2204; (*e*) M. Zhu, J. Liu, J. Yu, L. Chen, C. Zhang and L. Wang, *Org. Lett.*, 2014, **16**, 1856; (*f*) W. D. Mackay, M. Fistikci, R. M. Carris and J. S. Johnson, *Org. Lett.*, 2014, **16**, 1626.
6 A. O. Chagarovskiy, O. A. Ivanova, E. M. Budynina, I. V. Trushkov and M. Ya. Melnikov, *Tetrahedron Lett.*, 2011, **52**, 4421.
7 O. A. Ivanova, E. M. Budynina, A. O. Chagarovskiy, I. V. Trushkov and M. Ya. Melnikov, *J. Org. Chem.*, 2011, **76**, 8852.
8 R. A. Novikov, V. A. Korolev, V. P. Timofeev and Yu. V. Tomilov, *Tetrahedron Lett.*, 2011, **52**, 4996.
9 R. A. Novikov, A. V. Tarasova, V. A. Korolev, V. P. Timofeev and Yu. V. Tomilov, *Angew. Chem. Int. Ed.*, 2014, **53**, 3187.
10 O. A. Ivanova, E. M. Budynina, A. O. Chagarovskiy, E. R. Rakhmankulov, I. V. Trushkov, A. V. Semeykin, N. L. Shimanovskii and M. Ya. Melnikov, *Chem. Eur. J.*, 2011, **17**, 11738.
11 R. A. Novikov, V. P. Timofeev and Yu. V. Tomilov, *J. Org. Chem.*, 2012, **77**, 5993.
12 R. A. Novikov, Yu. V. Tomilov and O. M. Nefedov, *Mendeleev Commun.*, 2012, **22**, 181.
13 R. A. Novikov, D. O. Balakirev, V. P. Timofeev and Yu. V. Tomilov, *Organometallics*, 2012, **31**, 8627.
14 T. E. Storr and M. F. Greaney, *Org. Lett.*, 2013, **15**, 1410.
15 S. Y. Lee, H. N. Shin, Y. J. Cho, H. J. Kwon, B. O. Kim, S. M. Kim and S. S. Yoon, *US Patent 2009230852*, 2009.
16 C. W. Ong and C. Y. Yu, *Tetrahedron*, 2003, **59**, 9677.

Received: 16th June 2014; Com. 14/4395

‡ *Compounds* **3a** *and* **4a**. Solid $GaCl_3$ (113 mg, 0.64 mmol, 100 mol%) was added in one portion to a solution of cyclopropane **1a** (150 mg, 0.64 mmol) in dry CH_2Cl_2 (4 ml) under dry argon at 40 °C and the mixture was stirred at the same temperature for 30 min. Then an aqueous HCl solution (5%) was added at room temperature to reach pH 3 and the mixture was extracted with CH_2Cl_2 (3×10 ml). The organic layer was dried over $MgSO_4$ and the solvent was removed *in vacuo*. The residue was separated by column chromatography on silica gel (benzene–EtOAc, 50:1 to 10:1) to afford 118 mg (79%) of known[9] tetralin **3a** as a thick colourless oil and a small fraction containing compound **4a**. This fraction was additionally purified on a Silufol chromatographic plate (20×20 cm) to afford ~1.5 mg of 2-(1,3-dimethoxy-1,3-dioxopropan-2-yl)-3-phenyl-1,2-dihydronaphthalene-2 **4a**. IR ($CHCl_3$, ν/cm^{-1}): 3020, 2956, 2926, 2853, 1732 (O=C–O), 1659, 1519, 1468, 1423. ^{1}H NMR, δ: 2.71–2.87 (m, 2H, C^{1}H$_2$), 3.30–3.38 and 4.10–4.18 (2m, 2×1H, C^{2}H and C$^{2'}$H), 3.69 and 3.72 (2s, 2×3H, 2OMe), 7.04–8.00 (m, 10H, C^{4}H–C^{8}H, Ph). ^{13}C NMR, δ: 34.5 (C^{1}H$_2$), 48.9 and 52.7 (C^{2}H and C$^{2'}$H), 50.2 (2OMe), 125.7, 126.0, 126.9, 127.5, 128.2, 128.5, 128.8 and 129.0 (C^4–C^8, 5C$_{Ph}$), 132.7, 132.8, 141.1 and 143.3 (C^3, C^{4a}, C^{8a} and *i*-C), 169.9 (2COO). MS, *m*/*z* (%): 336 (6) [M]$^+$, 306 (100), 291 (13), 276 (12), 215 (22), 204 (33), 115 (23), 91 (32), 59 (46).

§ *Crystallographic data for* **5**. Crystals of $C_{16}H_{26}Cl_{14}Ga_4O_{12}$ (M = 1185.55) are orthorhombic, space group $P2_12_12_1$, at T = 100(2) K: a = 13.8249(10), b = 14.8020(11) and c = 20.4605(15) Å, V = 4187.0(5) Å^3, Z = 4, F(000) = = 2320, d_{calc} = 1.881 g cm^{-3}, μ = 3.485 mm^{-1}. Intensities of 38 393 reflections were measured on an automated SMART 1000 CCD diffractometer [λ(MoKα) radiation, graphite monochromator, φ and ω-scanning techniques, θ_{max} = 28°]. The structure was solved by direct methods and refined by a full-matrix least-squares method against F^2 in the anisotropic–isotropic approximation. The positions of the hydrogen atoms were calculated geometrically. The final R factors were as follows: R_1 = 0.0625 for 10 086 independent reflections with $I > 2\sigma(I)$ and wR_2 = 0.1334 for all 7723 independent reflections, GOF = 1.270. All calculations were carried out using the SHELXTL PLUS software (Version 5.0).

CCDC 1024005 contains the supplementary crystallographic data for this paper. These data can be obtained free of charge from The Cambridge Crystallographic Data Centre *via* http://www.ccdc.cam.ac.uk. For details, see 'Notice to Authors', *Mendeleev Commun.*, Issue 1, 2014.

Available online at www.sciencedirect.com
ScienceDirect
Mendeleev Commun., 2014, **24**, 349–350
Mendeleev Communications

Hydrogenation of carbon dioxide: a comparison of different types of active catalysts

Leonid M. Kustov*[a,b] and Andrei L. Tarasov[a]

[a] *N. D. Zelinsky Institute of Organic Chemistry, Russian Academy of Sciences, 119991 Moscow, Russian Federation. Fax: +7 499 135 5328; e-mail: lmk@ioc.ac.ru*
[b] *Department of Chemistry, M. V. Lomonosov Moscow State University, 119991 Moscow, Russian Federation*

DOI: 10.1016/j.mencom.2014.11.012

Comparison of the activity and CO selectivity of four principally different types of catalysts in CO_2 hydrogenation, namely, $LaNi_5$, Rh/ZnO–CuO, fumed Fe_2O_3–K_2O–Al_2O_3 and Au/SO_4–ZrO_2, in the entire temperature range at an atmospheric pressure was performed. The use of the intermetallide $LaNi_5$ catalyst provides an enhanced activity in CO_2 hydrogenation with prevailing methane formation, while other catalysts demonstrated predominant formation of CO.

Catalytic carbon dioxide transformations are of prime importance in view of the potential industrial applications for organic syntheses.[1] Carbon dioxide is the major green house gas and its emissions should be reduced to the sustainable minimum. The challenge is not just the capture and storage of CO_2 emissions, but also finding attractive utilization for CO_2.[2,3] The existing approaches to solve this problem in chemical processes with the goal of producing value-added products are in their infancy: only a few feasible approaches are known, such as the production of polycarbonates from epoxides and CO_2. The inventive use of catalysts can help the enterprises producing vast amounts of CO_2 to diversify the product portfolio by designing the modern and green technologies for the synthesis of high-value added fine chemical products in responding to the needs of the market.

One of the solutions to the problem of CO_2 sequestration is CO_2 hydrogenation yielding either methane (methanation) or CO (the reverse water–gas shift reaction):[4,5]

$$CO_2 + 4H_2 = CH_4 + 2H_2O, \quad (1)$$

$$CO_2 + H_2 = CO + H_2O. \quad (2)$$

Of particular interest is the conversion of CO_2 into a more reactive product, CO, which in turn can be further converted into methanol or diverse hydroformylation, carbonylation, alkoxycarbonylation products, in particular, to the marketable chemicals (linear aldehydes C_4–C_6, some esters).

The reactions of methane and carbon monoxide formation are reverse ones to the industrial process of methane water steam conversion ($CH_4 + 2H_2O = CO_2 + 4H_2$) and water–gas shift reaction ($CO + H_2O = CO_2 + H_2$). Therefore, one can anticipate that the catalysts that are active in the direct reactions are perspective for the application in the reverse reactions of hydrogenation of CO_2 with formation of methane and carbon monoxide.

Intermetallide $LaNi_5$ was reported[6–8] as a good catalyst for hydrogenation of carbon dioxide to produce methane at 250–350 °C and 5 MPa. The catalytic activity increased with the time on stream in the course of the reaction and X-ray diffraction analysis provided evidence for the decomposition of the intermetallide to $La(OH)_3$, $LaCO_3OH$, and metallic nickel.

The catalysis of the water–gas shift reaction by gold nanoparticles supported on metal oxides has recently been the subject of several studies.[9] Gold on zirconia and sulfated zirconia catalysts were tested in the water–gas shift reaction.[10] Sulfated catalysts showed higher activities than the samples prepared using unmodified zirconia, presumably, due to the stabilization of a higher specific surface area for the sulfated zirconia unlike the unsulfated carrier, which leads eventually to a better dispersion of gold nanoparticles on the surface.

The objective of this work was to examine and compare four principally different types of catalysts in hydrogenation of carbon dioxide at an atmospheric pressure.[†] Catalysts possessing high activity and selectivity in reactions with participation of CO, CO_2 and H_2, such as a Rh promoted ZnO–CuO catalyst for methanol synthesis from synthesis gas containing CO_2, an Au/SO_4–ZrO_2 catalyst for the water–gas shift reaction, a Fe_2O_3–K_2O catalyst for Fisher–Tropsh process and an intermetallide $LaNi_5$ catalyst for direct CO_2 methanization were chosen.

Figure 1 depicts the data on the performance of four catalysts in carbon dioxide hydrogenation. The data on the selectivity of catalysts studied towards CO formation are shown in Figure 2.

As it is seen in Figure 1, the catalytic activity of the $LaNi_5$ catalyst was significantly higher as compared with those of other

[†] A conventional intermetallide $LaNi_5$ was prepared as described.[11] The specific surface area of the sample was 4 m^2 g^{-1}.

5% Rh/ZnO–CuO is the Rhodium supported catalyst on the commercial 64% ZnO–36% CuO catalyst for methanol production from synthesis gas (CHM-1, Russia). The ZnO–CuO support (5 g) was loaded with 5 wt% Rh by incipient–wetness impregnation with a water solution of $RhCl_3$ (7 ml). The sample was dried overnight at room temperature in air. The resulting material was calcined at 500 °C (2 h) in flowing air (~300 ml min^{-1}). The specific surface area of the catalyst was 155 m^2 g^{-1}.

Fused Fe_2O_3–K_2O is a commercial catalyst (Sasol) for the Fischer–Tropsch process prepared by fusion of iron at 1600–2000 °C with the subsequent oxidation of the fusion while supplying oxygen and introducing K_2CO_3 and Al_2O_3 promoters. The specific surface area of the catalyst was 95 m^2 g^{-1}.

2% Au/SO_4–ZrO_2, the sample for the water–gas shift reaction, was prepared as described.[12] The sulfated zirconia support and the catalyst sample prepared after calcination contain 2 wt% of sulfates. The specific surface area of the catalyst was 140 m^2 g^{-1}.

The catalytic activity of the samples was tested using a conventional flow-type fixed-bed reactor made of a quartz tube with an inner diameter of 7 mm under an atmospheric pressure. In a typical experiment, 1.0 g of a catalyst was packed in the reactor tube and was pretreated in a hydrogen stream at VHSV = 1800 h^{-1} at 250 °C for 3 h. Then a reactant gas mixture (33% carbon dioxide in hydrogen) was introduced at VHSV = 1800 h^{-1} and the temperature was raised to 500 °C with a step of 50 °C. The effluent gas was analyzed by an on-line gas chromatograph with packed columns (Porapak-Q for carbon dioxide and molecular sieves 5A for methane and carbon monoxide).

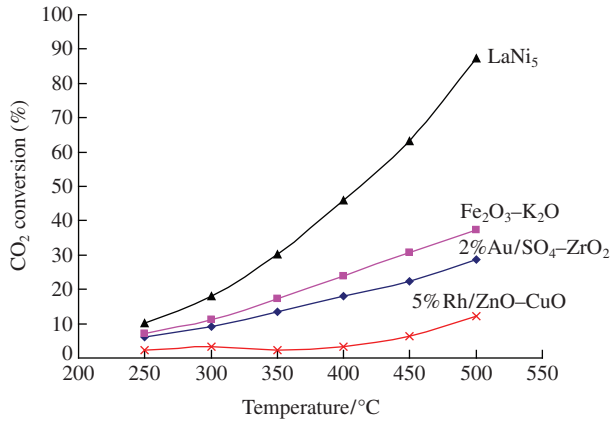

Figure 1 Dependence of the conversion of CO_2 in the reaction with hydrogen on the reaction temperature.

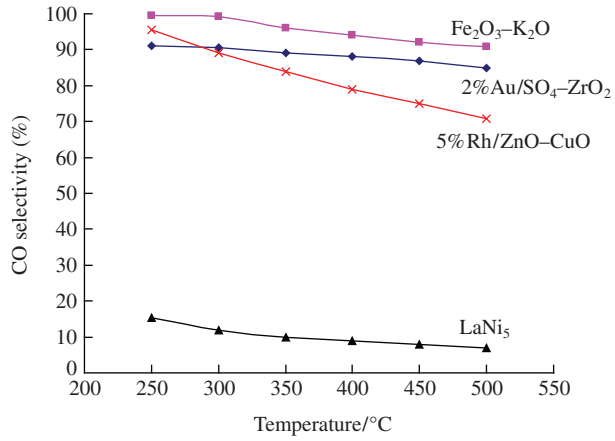

Figure 2 Dependence of the CO selectivity on the reaction temperature.

three catalysts. The conversion of CO_2 at 500 °C is near 90%. The main products of the hydrogenation of carbon dioxide over the $LaNi_5$ catalyst were methane and water. Small amounts of carbon monoxide were also formed with the selectivity below 15% in total. No coke formation occurs on this catalyst up to 500 °C.

The other studied catalysts perform the hydrogenation process mainly with CO formation, and the best catalyst both in terms of the activity and selectivity is the fused Fe_2O_3–K_2O (see Figures 1 and 2). The conversion of CO_2 on this sample at 500 °C is close to 40% and the selectivity towards CO in the entire temperature range does not fall below 90%. Note that the conversion of 40% is close to the thermodynamic equilibrium of the reaction (2).

In conclusion, the obtained results provide a rationale in choosing the best catalysts for the reduction of CO_2 into CO. This reaction is considered nowadays to be the most economically vaiable method of CO_2 utilization with downstream conversion of CO into other valuable chemicals *via* carbonylation, hydroformylation and other reactions.

This work was supported by the Russian Science Foundation (grant no. 14-33-00001).

References

1 T. Sakakura, J. C. Choi and H. Yasuda, *Chem. Rev.*, 2007, **107**, 2365.
2 K. S. Lackner, *Science*, 2003, **300**, 1677.
3 D. S. Golomb, *Science*, 2003, **301**, 1326.
4 T. Inui, *Catal. Today*, 1996, **29**, 329.
5 E. Vesselli, M. Rizzi, L. D. Rogatis, X. Ding, A. Baraldi, G. Comelli, L. Savio, L. Vattuone, M. Rocca, P. Fornasiero, A. Baldereschi and M. Peressi, *J. Phys. Chem. Lett*., 2010, **1**, 402.
6 H. Ando, M. Fujiwara, Y. Matsumura, M. Tanaka and Y. Souma, *J. Mol. Catal. A: Chem*., 1999, **144**, 117.
7 H. Ando, M. Fujiwara, Y. Matsumura, H. Miyamura, M. Tanaka and Y. Souma, *J. Alloys Compd.*, 1995, **223**, 139.
8 H. Ando, M. Fujiwara, Y. Matsumura, H. Miyamura and Y. Souma, *Energy Convers. Management*, 1995, **36**, 653.
9 D. Andreeva, I. Ivanov, L. Ilieva and M. V. Abrashev, *Appl. Catal., A*, 2006, **302**, 127.
10 F. Zane, V. Trevisan, F. Pinna, M. Signoretto and F. Menegazzo, *Appl. Catal., B*, 2009, **89**, 303.
11 B. P. Tarasov, M. V. Lototskii and V. A. Yartys, *Ross. Khim. Zh. (Zh. Ross. Khim. Ob-va im. D. I. Mendeleeva)*, 2007, **77**, 694 (in Russian).
12 A. Kuperman and M. E. Moir, *WO Patent 2005005032*, assigned to Chevron Inc., 2005.

Received: 13th October 2014; Com. 14/4485

Available online at www.sciencedirect.com
ScienceDirect
Mendeleev Commun., 2014, **24**, 351–352
Mendeleev Communications

Pt/SnO_x-C composite material for electrocatalysis

Alexandra B. Kuriganova* and Nina V. Smirnova

Department of Technology, M. I. Platov South-Russia State Polytechnic University, 346428 Novocherkassk, Russian Federation. Fax: +7 8635 255 974; e-mail: kuriganova_@mail.ru

DOI: 10.1016/j.mencom.2014.11.013

The Pt/SnO_x-C composite material was obtained by an electrochemical dispersion method, and a good catalytic activity of this material in the electrochemical oxidation of CO has been demonstrated.

Nanosized carbon-supported platinum (Pt/C) catalysts are good catalytic materials for proton exchange membrane fuel cells (PEMFCs). The efficiency of a PEMFC is determined by the system parameters: polymer membrane stability under fuel cell operation conditions, good water and heat management, high catalytic activity and stability of Pt/C catalysts. Meantime, these catalysts can be poisoned with CO, which always occurs in hydrogen generated by the steam reforming of light hydrocarbons. The presence of CO traces in hydrogen leads to an increase in the anode overvoltage and a decrease in the PEMFC power density. Thus, enhancing the resistance of platinum catalysts to carbon monoxide is a challenge of considerable current interest for PEMFC technology.

The chemisorption of carbon monoxide on platinum irreversibly occurs in a wide range of potentials, and CO can be removed from the platinum surface only by oxidation which proceeds *via* the Langmuir–Hinshelwood mechanism.[1] However, the adsorption of oxygen-containing species on platinum starts at relatively high potentials $E \geqslant 0.6$ V (RHE).[2] Therefore, if the adsorption potential of the oxygen-containing species is lower, the oxidation potential of adsorbed CO_{ad} can decrease. For this purpose, metals that adsorb oxygen better than platinum are introduced into the catalyst.[3–5]

Tin has a good oxygen adsorption capacity, and it can be introduced into the catalyst system as adatoms,[6] platinum–tin alloy[7] or tin oxide which serves as a support for platinum nanoparticles.[8] We used this approach for the preparation of a Pt/SnO_x-C catalyst.

Nanocrystalline tin oxides are currently produced by hydrothermal and sol-gel methods.[9] Then, tin oxide is introduced into a carbon support with the subsequent deposition of platinum nanoparticles onto the SnO_x-C support to obtain the Pt/SnO_x-C catalyst.

In this work, we used the electrochemical oxidation and dispersion of the metal.[10,11] Earlier, Pt/C catalysts with a Pt particle size of 6–8 nm and a uniform distribution of Pt particles over the carbon support surface were obtained.[11]

We found that, in neutral and alkaline solutions, tin electrodes are oxidized and dispersed under the action of an alternating current. The structure of the products depends on current density used in the synthesis, as found by XRD analysis [Figure 1(*a*)] and SEM [Figure 1(*b*),(*c*)]. At a low current density, agglomerates with a lamellar structure and a crystallite size of 15–120 nm were obtained [Figure 1(*b*)]. Tin oxide particles with a narrow size distribution of 15–20 nm were prepared at a current density higher by a factor of 10 [Figure 1(*c*)]. These particles consisted of SnO_2 doped with SnO and Sn.

The Pt/SnO_x-C catalysts were produced in two stages:[†] (i) the preparation of tin oxide nanoparticles and the simultaneous deposition of the particles on a carbon support and (ii) the deposition of platinum nanoparticles onto the SnO_x-C support in accordance with a previously published procedure.[11]

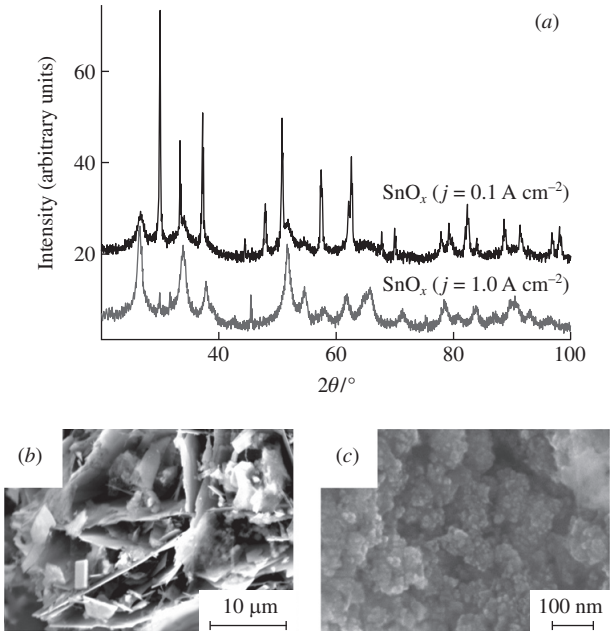

Figure 1 (*a*) X-ray diffraction patterns and (*b*), (*c*) SEM images of SnO_x powders prepared at current densities of (*b*) 0.1 and (*c*) 1.0 A cm^{-2}.

For the electrochemical studies of Pt/SnO_x-C catalysts, catalyst ink[‡] was prepared. The electrochemical oxidation of CO on Pt/C

[†] At the first stage of Pt/SnO_x-C catalyst preparation, two tin electrodes with the equal surface areas were immersed in a suspension of a Vulcan XC-72 carbon support (CabotCorp., 240 m^2 g^{-1}) in a 2 M aqueous solution of NaCl. In a non-diaphragm electrolytic cell, the electrodes were connected to an ac source operating at 50 Hz (pulse duration, 2.5 ms; current density, 1 A cm^{-2}) at 50–55 °C. After the synthesis, the suspension was filtered, and the SnO_x-C composite was washed with distilled water and dried at 80 °C to constant weight. At the second stage, platinum nanoparticles were deposited onto the SnO_x-C support. Two platinum electrodes with equal areas were immersed in the suspension of the SnO_x-C composite in a 2 M aqueous solution of NaOH. The electrodes were connected to the ac source operating as described above. Then, the suspension was filtered; the prepared catalyst was rinsed with H_2O to a neutral pH and dried at 80 °C to constant weight. Platinum loading for all catalysts was 25%.

[‡] Catalyst ink and working electrodes for electrochemical measurements were prepared by mixing 0.0140 g of the synthesized catalyst with 1 ml of isopropanol and a 10% aqueous solution of Nafion DE-1020 (25% on a catalyst weight basis). After stirring with a magnetic stirrer (30 min), the ink was dropped onto a glassy carbon electrode and dried at 80 °C in air for 40–50 min.

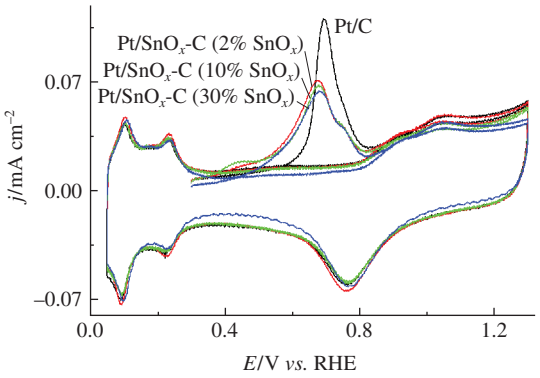

Figure 2 CV curves of the oxidation of CO_{ad} on Pt/C and Pt/SnO_x-C catalysts in 0.5 M H_2SO_4 at E = 0.3 V; scan rate, 20 mV s^{-1}.

and Pt/SnO_x-C catalysts was studied[§] after CO pre-adsorption. A small amount of tin oxide in the catalyst shifted the start of the CO oxidation potential by 200 mV and the CO stripping peak potential by 60 mV to the cathode side, as compared with the Pt/C catalyst obtained by the same method (Figure 2). Thus, the greatest effect was observed in a SnO_x concentration range of 2–10% in the Pt/SnO_x-C catalyst: the rate of CO oxidation at E = 0.6 V (RHE) increased by a factor of 2 (Figure 3). Moreover, in the course of the long-term investigations of Pt/SnO_x-C, the CO stripping peak potential remained almost unchanged (Figure 4).

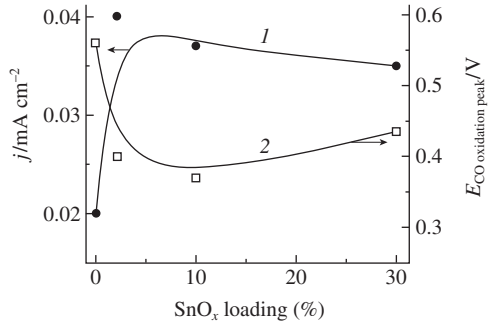

Figure 3 Effect of SnO_x loading on (*1*) the catalytic activity of Pt/SnO_x-C at 0.6 V and (*2*) the initial oxidation potential of CO.

§ All electrochemical measurements were performed in a three-electrode cell with separated compartments using a P-150 potentiostat/galvanostat (Elins). Platinum wire and saturated Ag/AgCl were used as counter and reference electrodes, respectively. All potentials are referred to a reversible hydrogen electrode (RHE). For the CO oxidation kinetics, at first Ar was bubbled into a 0.5 M H_2SO_4 electrolyte solution for 60 min. Then, CO was adsorbed on the surface of the working electrode by bubbling CO into a 0.5 M H_2SO_4 electrolyte solution for 15 min, while the electrode was kept at a constant potential of 0.3 V *vs.* RHE. After CO bubbling, the electrolyte was purged with Ar (30 min) to remove dissolved CO, and the CV curves were measured (potential was scanned from 0.05 to 1.3 V at a scan rate of 20 mV s^{-1}).

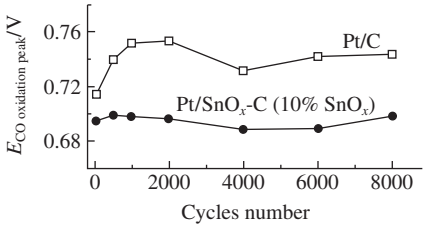

Figure 4 Changes of CO oxidation peak potentials during long-term studies.

Thus, the mechanism of electrocatalysis was implemented on the Pt/SnO_x-C bifunctional catalysts.[12] CO_{ad} species adsorbed on platinum nanoparticles were oxidized by oxygen-containing species (OH_{ad} or O_{ad}) adsorbed on tin oxide *via* the Langmuir–Hinshelwood mechanism at lower potentials than those of pure platinum.

In conclusion, the method proposed for obtaining Pt/SnO_x-C by electrochemical dispersion is technologically simple and environmentally safe. The presence of a small amount of tin oxide in platinum-based catalysts increases the stability of carbon-supported platinum catalysts.

This work was supported by the Russian Science Foundation (grant no. 14-23-00078). The experiments were performed using the equipment of the Center for Shared Scientific Equipment ‘Nanotechnology’ at the M. I. Platov South-Russia State Polytechnic University.

References

1 J. M. Thomas and W. J. Thomas, *Introduction to the Principles of Heterogeneous Catalysis*, Academic Press, London, 1967.
2 G. Jerkiewicz, *Interfacial Electrochemistry*, ed. A. Wieckowski, Marcel Dekker, New York, 1999, pp. 559–576.
3 J. H. Wee and K. Y. Lee, *J. Power Sources*, 2005, **157**, 128.
4 A. V. Ruban, H. L. Skriver and J. K. Norskov, *Phys. Rev. B*, 1999, **59**, 15990.
5 B. I. Podlovchenko, T. D. Gladysheva, V. A. Krivchenko, Yu. M. Maksimov, A. Yu. Filatov and L. V. Yashina, *Mendeleev Commun*., 2012, **22**, 203.
6 N. V. Smirnova, O. A. Petrii and A. Grzejdziak, *J. Electroanal. Chem*., 1988, **251**, 73.
7 B.-J. Su, K.-W. Wang, C.-J. Tseng, C.-H. Wang and Y.-J. Hsueh, *Int. J. Electrochem. Sci*., 2012, **7**, 5246.
8 L. A. Frolova, Yu. A. Dobrovolsky and N. G. Bukun, *Russ. J. Electrochem*., 2011, **47**, 697 (*Elektrokhimiya*, 2011, **47**, 745).
9 M. Yoshimura and J. Livage, *MRS Bulletin*, 2000, **25**, 12.
10 D. V. Leontieva and N. V. Smirnova, *Int. Sci. J. Alternative Energy Ecology*, 2012, **10**, 65.
11 I. Leontyev, A. Kuriganova, Y. Kudryavtsev, B. Dkhil and N. Smirnova, *Appl. Catal., A*, 2012, **431**–**432**, 120.
12 M. Watanabe, M. Uchida and S. Motoo, *J. Electroanal. Chem*., 1987, **229**, 395.

Received: 8th September 2014; Com. 14/4458

Available online at www.sciencedirect.com
ScienceDirect
Mendeleev Commun., 2014, **24**, 353–354
Mendeleev Communications

Transformations of Bjorkman lignin from European spruce (*Picea abies*) in superacidic media

Aleksandra V. Kalugina,[a] Dmitry S. Ryabukhin,[b] Tatyana O. Artamonova,[c] Mikhail A. Khodorkovsky,[c] Mikhail Ya. Zarubin[a] and Aleksander V. Vasilyev*[a,b]

[a] *Department of Organic Chemistry, St. Petersburg State Forest Technical University, 194021 St. Petersburg, Russian Federation. Fax: +7 812 670 9390; e-mail: aleksvasil@mail.ru*
[b] *Institute of Chemistry, St. Petersburg State University, 198504 Petrodvoretz, St. Petersburg, Russian Federation*
[c] *Institute of Nanobiotechnologies, St. Petersburg State Polytechnical University, 195251 St. Petersburg, Russian Federation*

DOI: 10.1016/j.mencom.2014.11.014

The Bjorkman lignin and products of its destruction under the action of Brønsted and Lewis superacids (CF_3SO_3H, $AlBr_3$ and zeolite CBV-720) were analyzed by MALDI mass spectrometry and their stabilities under superacidic conditions were compared.

Renewable lignocellulose materials are an alternative to coal, natural gas and oil.[1–3] A serious effort has been made to obtain fine chemicals[4–7] and fuels[8–12] based on the chemical transformations of lignin and lignocellulose. Matrix-assisted laser desorption ionization mass spectrometry (MALDI-MS) has been used for estimating the molecular weights of lignin oligomers.[13–17]

Based on our preliminary data,[18] we studied the transformation of lignin in Brønsted and Lewis superacids, which promote selective chemical reactions, such as bond cleavage, electrophilic addition, substitution and coupling.[19] The conversion of Bjorkman lignin from European spruce (*Picea abies*) was performed under the action of CF_3SO_3H (Brønsted superacid), $AlBr_3$ (Lewis superacid) and zeolite CBV-720 (solid Brønsted–Lewis superacid). Ion cyclotron resonance MALDI-MS was used for the analysis of lignin conversion products (Figures S13–S16, see Online Supplementary Materials).

First, we characterized the initial Bjorkman lignin by ^{13}C NMR spectroscopy (see Online Supplementary Materials), elemental analysis and MALDI-MS (Figure S13). The molecular weight of oligomeric lignin varies from 600 to 4500 Da. The main groups of oligomers are located at 1000–2000 and 2500–3500 Da. The spectrum contains clusters of peaks with mass differences Δm of 180–196 Da, which correspond to the so-called aryl propane lignin structural unit of guaicil type. This cluster structure is very clear for light part of the spectrum in the mass range 900–2400 Da. For masses of 2500–4500 Da, the separation into definite clusters of oligomers is not so strict due to the irregular lignin structure. The highest masses of ~4500 Da correspond to lignin oligomers consisting of about 25 aryl propane units.

After treatment in CF_3SO_3H, the molecular mass distribution occupied a range of 1500–3000 Da with a broad maximum at 2000–2500 Da (Figure S14). These data show that lignin underwent intra- and intermolecular condensation to form crosslinked oligomeric structures in addition to destruction.

According to MALDI-MS data, the treatment of lignin in the $AlBr_3$–benzene system gives oligomers with masses of 700–2000 Da (Figure S15). The MALDI-MS spectrum shows sharp clusters of peaks with the difference Δm ~ 180 Da in guaicil aryl propane unit. Thus, the destruction of lignin with $AlBr_3$ is more selective compared to that with CF_3SO_3H (Figure S14).

The conversion of lignin with zeolite CBV-720 containing Brønsted and Lewis acid sites at 130 °C for 24 h resulted in deep depolymerization and condensation of lignin oligomers with masses smaller than 1800 Da (Figure S16). The MALDI-MS spectrum contains several series of peaks with the mass differences Δm 178 Da: 843, 1021, 1199, 1377, 1555, 1733; and in the heavy part of the spectrum Δm 198 Da: 823, 1021, 1219; 1043, 1241; and Δm 196: 1223, 1419; 1401, 1597; 1419, 1615; 1555, 1751.

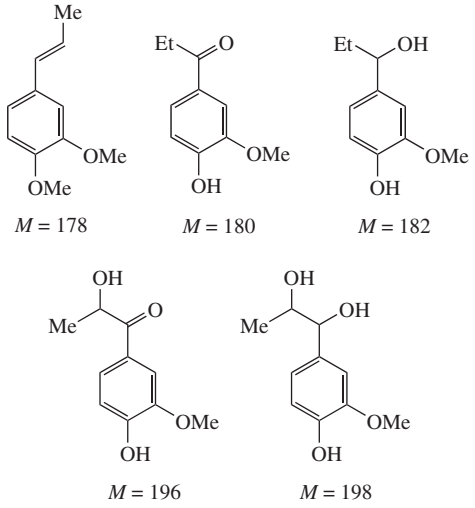

Figure 1 Aryl propane lignin units of guaicil type with masses of 178, 180, 182, 196 and 198 Da.

The possible structures of aryl propane lignin units of guaicil type with masses of 178, 180, 182, 196 and 198 Da are presented in Figure 1. The lignin oligomers detected by MALDI-MS (see Figures S13–S16) differ in these structural fragments.

The following lignin destruction products soluble in $CHCl_3$ (see Online Supplementary Materials) were detected by the gas chromatography–mass spectrometry (GC-MS) analysis of low-molecular-weight compounds formed after treatment with CF_3SO_3H, $AlBr_3$ and zeolite CBV-720 in yields of 6–10%: 4-hydroxy-3-methoxybenzaldehyde (vanillin), 4-hydroxy-3-methoxyacetophenone (acetovanillon), 4-hydroxy-3-methoxybenzoic acid (vanillic acid), 3-(4-hydroxy-3-metoxyphenyl)propenal (coniferaldehyde), 2-hydroxy-1-(4-hydroxy-3-methoxyphenyl)ethanone and 3-hydroxy-1-(4-hydroxy-3-metoxyphenyl)propan-1-one. These compounds were formed because of the destructive protosolvolysis of lignin macromolecules.

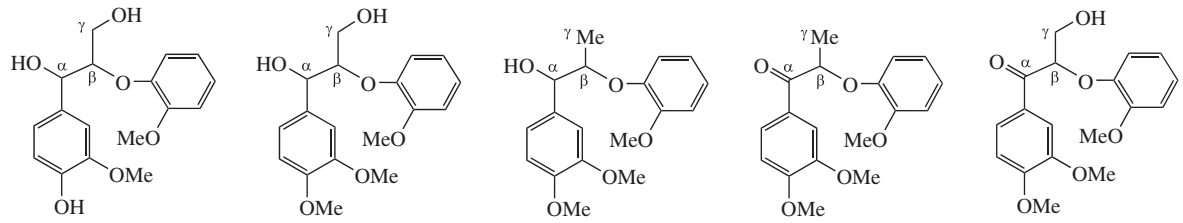

Figure 2 Lignin model compounds **1**–**5** containing β-O-4 linkage.

The initial Bjorkman lignin and products of its destruction in TfOH and $AlBr_3$ were characterized by elemental analysis. The starting lignin contained 60.16% C and 5.77% H. Lignin after treatment with TfOH or $AlBr_3$ contained 36.47% C and 2.67% H or 39.06% C and 2.20% H, respectively, due to the functionalization and condensation of lignin and the subsequent reactions of intermediate cation particles with water.

We studied the transformation of model lignin compounds **1**–**5** of guaicil type containing β-O-4 linkages[20] to elucidate the stability of this linkage under protosolvolysis in CF_3SO_3H (Figure 2). The β-O-4 bond is the most representative type of linkages between lignin structural subunits.[1] Compounds **1**–**5** have an *ortho*-methoxyphenyl group in the β-site of the propane chain and differ in substituents in the α- and γ-positions.

After the conversion of compounds **1**–**5** in CF_3SO_3H at 20 °C for 2 h, the reaction mixtures were analyzed by ^{1}H NMR spectroscopy and GC-MS. Compounds **4** and **5** bearing a carbonyl group in the α-position remained unreacted.

On the other hand, compounds **1**–**3** with α-OH group underwent complete conversion into complicated mixtures according to ^{1}H NMR data. The GC-MS analysis of these reaction residues showed the presence of no more than 20% *ortho*-methoxyphenol (guaiacol). In these cases, guaiacol was formed due to β-O-4 bond cleavage under the action of superacids. However, it is difficult to estimate quantitatively the degree of β-O-4 bond destruction for compounds **1**–**3** since guaiacol molecules as strong π-nucleophiles can participate in secondary reactions with cationic intermediate species under the reaction conditions.

We propose the following mechanism of the protosolvolytic cleavage of lignin β-O-4 bonds in superacids: the protonation of the $C^β$–O–Ar bond at the oxygen atom in lignin fragment **I** leads to oxonium cation **II** which eliminates the phenol molecule ArOH with $C^β$–O bond cleavage to give cation **III** (Scheme 1). This cation is hardly generated in the case when the α-position is occupied with the carbonyl group (like in compounds **4**, **5**) due to its electron-withdrawing character, which destabilizes the cationic center on the carbon $C^β$. α,γ-Hydroxy substituted lignin structures (like **1**–**3**) can also lose OH group from these positions under protonation in superacids, affording various reactive cationic species.

Cations **III** can undergo further inter- and intramolecular transformations, such as rearrangements, fragmentation and deprotonation. The released compound ArOH as a π-nucleophile can also participate in secondary processes, for instance, in electrophilic aromatic substitution. All these cationic reactions result in the destruction and condensation of lignin oligomers under the action of various superacids.

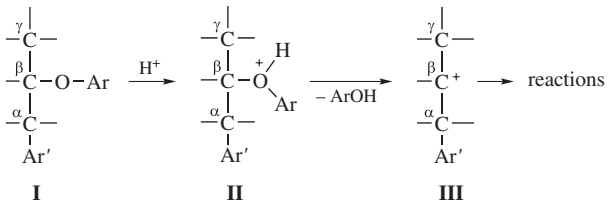

Scheme 1

Thus, the Bjorkman lignin from European spruce (*Picea abies*) undergoes destruction and condensation under the action of Brønsted and Lewis superacids, such as CF_3SO_3H, $AlBr_3$, and zeolite CBV-720. The superacidic destruction of lignin can be used for obtaining valuable organic compounds.

This study was supported by the Russian Science Foundation (grant no. 14-13-00448).

Online Supplementary Materials

Supplementary data associated with this article (experimental procedures, ^{1}H, ^{13}C NMR and mass spectral data) can be found in the online version at doi:10.1016/j.mencom.2014.11.014.

References

1 M. N. Belgacem and A. Gandini, *Monomers, Polymers and Composites from Renewable Resources*, Elsevier, Amsterdam, 2008.
2 G. W. Huber and A. Corma, *Angew. Chem. Int. Ed.*, 2007, **46**, 7184.
3 W. Reschetilowski, *Russ. Chem. Rev.*, 2013, **82**, 624.
4 R. Auvergne, S. Caillol, G. David, B. Boutevin and J.-P. Pascault, *Chem. Rev*., 2014, **114**, 1082.
5 P. Gallezot, *Chem. Soc. Rev*., 2012, **41**, 1538.
6 A. V. Ponomarev and B. G. Erschov, *Russ. Chem. Rev.*, 2012, **81**, 918.
7 J. Zakzeski, P. C. A. Bruijnincx, A. L. Jongerius and B. M. Weckhuysen, *Chem. Rev*., 2010, **106**, 4044.
8 N. Armaroli and V. Balzani, *Angew. Chem. Int. Ed.*, 2007, **46**, 52.
9 G. W. Huber, S. Iborra and A. Corma, *Chem. Rev*., 2006, **106**, 4044.
10 K. Kohse-Hoinghaus, P. Obwald, T. A. Cool, T. Kasper, N. Hansen, F. Qi, C. K. Westbrook and P. R. Westmoreland, *Angew. Chem. Int. Ed.*, 2010, **49**, 3572.
11 M. Stocker, *Angew. Chem. Int. Ed.*, 2008, **47**, 9200.
12 S. D. Varfolomeev, E. N. Efremenko and L. P. Krylova, *Russ. Chem. Rev*., 2010, **79**, 439 (*Usp. Khim*., 2010, **79**, 491).
13 R. Bayerbach, V. D. Nguyen, U. Schurr and D. Meier, *J. Anal. Appl. Pyrolysis*, 2006, **77**, 95.
14 P. Bocchini, G. C. Galetti, R. Seraglia, P. Traldi, S. Camarero and A.T. Martinez, *Rapid Commun. Mass. Spectrom.*, 1996, **10**, 1144.
15 A. Jacobs and O. Dahlman, *Nordic Pulp Paper Res. J*., 2000, **15**, 120.
16 S. Reale, A. Di Tullio, N. Spreti and F. De Angelis, *Mass Spectrom. Rev*., 2004, **23**, 87.
17 A. Richel, C. Vanderghem, M. Simon., B. Wathelet and M. Paquot, *Anal. Chem. Insight*, 2012, **7**, 79.
18 D. S. Ryabukhin, A. V. Vasilyev and M. Ya. Zarubin, *Russ. J. Bioorg. Chem*., 2012, **38**, 717 (*Khim. Rastit. Syr'ya*, 2011, 55).
19 G. A. Olah, G. K. S. Prakash, A. Molnar and J. Sommer, *Superacid Chemistry*, 2nd edn., Wiley, New York, 2009.
20 G. F. Zakis, *Sintez model'nykh soedinenii lignina (Synthesis of Lignin Model Compounds)*, Zinatne, Riga, 1980 (in Russian).

Received: 8th September 2014; Com. 14/4459

Available online at www.sciencedirect.com
ScienceDirect
Mendeleev Commun., 2014, **24**, 355–357
Mendeleev Communications

Novel Pd–Zn/C catalyst for selective alkyne hydrogenation: evidence for the formation of Pd–Zn bimetallic alloy particles

Igor S. Mashkovsky,[a] Galina N. Baeva,[a] Aleksandr Yu. Stakheev,*[a] Michael N. Vargaftik,[b] Natalia Yu. Kozitsyna[b] and Ilya I. Moiseev[b]

[a] *N. D. Zelinsky Institute of Organic Chemistry, Russian Academy of Sciences, 119991 Moscow, Russian Federation. Fax: +7 499 135 5328; e-mail: st@ioc.ac.ru*
[b] *N. S. Kurnakov Institute of General and Inorganic Chemistry, Russian Academy of Sciences, 119991 Moscow, Russian Federation*

DOI: 10.1016/j.mencom.2014.11.015

The formation of Pd–Zn alloy was revealed in a highly selective Pd–Zn/C catalyst for acetylene hydrogenation prepared *via* the heterobimetallic $PdZn(OAc)_4(OH_2)$ complex.

The selective hydrogenation of acetylene to ethylene is a commercially important process used to remove trace acetylene from ethylene feed for the production of polyethylene because acetylene is a poison for the polymerization catalyst.[1] High selectivity to ethylene is particularly desired for the process.[2] The liquid-phase hydrogenation of mono- or disubstituted acetylenes is widely used in the industrial synthesis of fine chemicals and pharmaceuticals.[3]

Pd-supported catalysts are routinely employed for this process due to their high activity.[4] However, they suffer from insufficient selectivity for ethylene at high acetylene conversions because of undesired ethylene hydrogenation. The addition of metal (M = Ag, Zn, Cu and Co) promoters improves the performance of a Pd catalyst due to Pd–M alloy formation.[5–7] However, the formation of homogeneous Pd–M alloy nanoparticles is difficult to achieve. Previously, the heterobimetallic lantern complex $PdZn(OAc)_4(OH_2)$ was found the most promising precursor for the preparation of a selective Pd–Zn supported catalyst for gas-phase and liquid-phase hydrogenation of alkynes.[8] The process of $PdZn(OAc)_4(OH_2)$ transformation was studied in detail by Murzin and co-authors by XANES and XRD methods.[9] In this study, we carried out a detailed investigation into Pd–Zn/C catalysts synthesized *via* the $PdZn(OAc)_4(OH_2)$ complex† by catalytic tests in selective acetylene hydrogenation and characterized it by transmission (TEM) and scanning (SEM) electron microscopy in combination with energy dispersive X-ray spectrometry (EDS)‡ analysis to reveal Pd–Zn alloy formation.

The catalytic performance in selective acetylene hydrogenation was studied in a temperature range of 30–120 °C at atmospheric pressure and a total gas flow rate of 150 ml min^{-1} ($H_2:C_2H_2 = 2:1$). The catalyst sample weight was 6 mg. The catalyst was thoroughly mixed with 1 g of SiC in order to minimize the reaction heat effect. The feedstock contained ~1.3% acetylene in ethylene. Note that the experimental conditions were similar for all catalysts. The reaction products were analyzed using on-line gas chromatography.

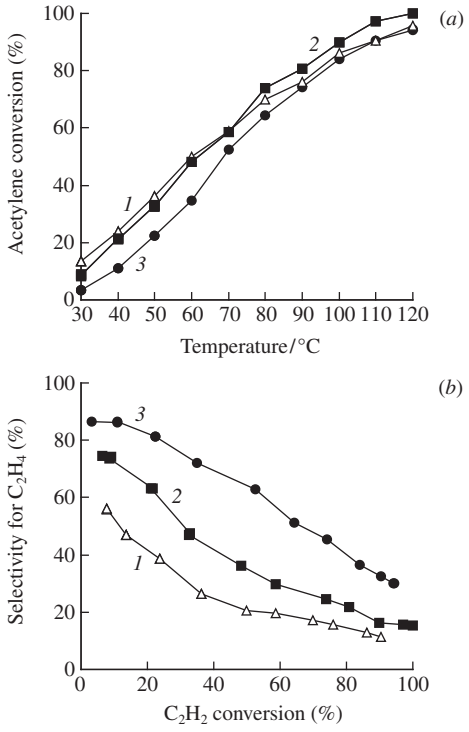

Figure 1 Dependence of (*a*) acetylene conversion on temperature and (*b*) selectivity for C_2H_4 on C_2H_2 conversion. Performance of (*1*) Pd/C, (*2*) Pd–Zn/C *via* $Pd(OAc)_2$ and $Zn(OAc)_2OH_2$ and (*3*) Pd–Zn/C *via* **1** in acetylene hydrogenation. T = 30–120 °C; P = 1 atm; $H_2:C_2H_2 = 2:1$.

† The catalysts were prepared using a Sibunit mesoporous carbon carrier (BET specific surface area, 332 $m^2\ g^{-1}$; total pore volume, 0.45 $cm^3\ g^{-1}$). The reference monometallic Pd catalysts [0.9 wt% Pd in accordance with inductively coupled plasma (ICP) analysis] was prepared by the incipient-wetness impregnation of the carrier with a methanol solution of $Pd(OAc)_2$. Bimetallic catalysts (0.9 wt% Pd and 0.59 wt% Zn in accordance with ICP analysis) were prepared by (1) incipient-wetness impregnation using complex $PdZn(OAc)_4(OH_2)$ **1** and (2) co-impregnation with aqueous solutions of individual $Pd(OAc)_2$ and $Zn(OAc)_2{\cdot}2H_2O$. The synthesis of complex **1** was described elsewhere.[10] The catalysts were dried in an Ar flow (80 °C, 2 h) and reduced in H_2 (250 °C, 1 h) before experiments. The ICP-OES analysis was performed on a Perkin Elmer Optima 3000 instrument.

‡ Reduced samples were analyzed by TEM on a Philips CEM200 instrument operated at 200 kV. The samples were crushed, ultrasonically dispersed in ethanol, and dropped on a 200 mesh copper grid for TEM analysis. SEM images were acquired using a Philips XL30 ESEM-FEG microscope operating at 10 keV, spot size 3 and using the backscattered electron signal. The samples were crushed, and fixed on a sample holder using carbon tape. Qualitative chemical analyses of the samples were made by EDS. For the analysis of nanoparticle size, the Digital Micrograph software[11] was used.

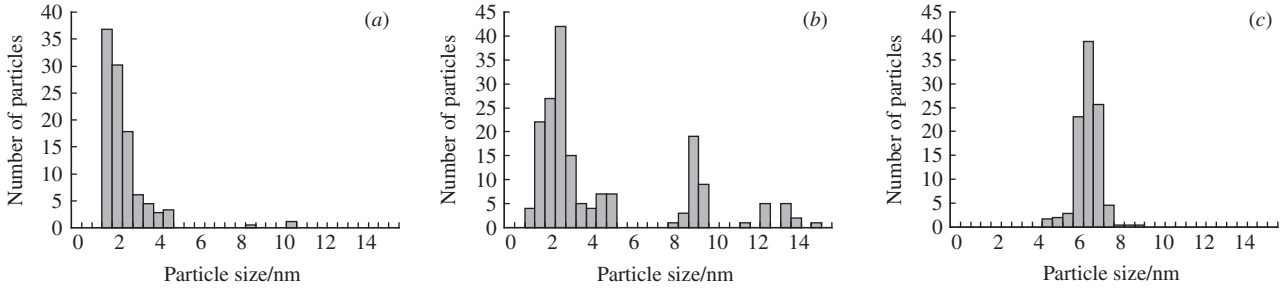

Figure 2 Pd particle size distribution determined from the microscopic images of (*a*) Pd/C, (*b*) Pd–Zn/C prepared using $Pd(OAc)_2$ and $Zn(OAc)_2OH_2$ complexes and (*c*) Pd–Zn/C prepared using complex **1**.

Figure 1 compares the activity and selectivity of the Pd–Zn/C catalysts in acetylene hydrogenation. Activities of all samples are comparable, though one can observe an activity decrease in the sequence [Figure 1(*a*)], as evidenced by this shift of the acetylene conversion profile toward higher temperature for Pd–Zn/C *via* **1**: Pd/C ~ Pd–Zn/$C_{coimpregnated}$ > Pd–Zn/C *via* **1**.

The selectivity trend is opposite. The ethylene selectivity is low for the 0.9% Pd/C sample prepared *via* a $Pd(AcO)_2$ precursor (Figure 1, curve *1*). The introduction of Zn to the Pd/C significantly improved the selectivity. Note that the Pd–Zn/C catalyst prepared using complex **1** showed notably higher selectivity compared to the catalyst prepared by co-impregnation *via* individual $Pd(OAc)_2$ and $Zn(OAc)_2·2H_2O$ complexes (Figure 1, curves *2* and *3*).

We performed a comparative microscopic study of the catalysts in order to characterize the selectivity of the catalyst prepared *via* the heterobimetallic lantern complex $PdZn(OAc)_4(OH_2)$. Figure 2 displays the particle size distribution (PSD) determined from corresponding TEM images. For the monometallic 0.9% Pd/C catalyst, the majority of Pd particles fell within a range of 1–2 nm [Figure 2(*a*)]. For the bimetallic Pd–Zn/C sample prepared by co-impregnation from $Pd(OAc)_2$ and $Zn(OAc)_2·2H_2O$ complexes, TEM revealed a bimodal PSD with Pd metal particle size varying from 2 to 15 nm [Figure 2(*b*)]. The bimetallic Pd–Zn/C prepared using the bimetallic complex $PdZn(OAc)_4(OH_2)$ has a relatively narrow PSD centered at 6–7 nm [Figure 2(*c*)].

Figure 3(*a*) shows a representative SEM image of 0.9% Pd–0.59% Zn/C catalyst prepared by co-impregnation. In accordance with EDS analysis, the Pd and Zn co-impregnation procedure results in a catalyst with both bimetallic [Figure 3(*b*)] and monometallic Pd [Figure 3(*c*)] or Zn [Figure 3(*d*)] particles and agglomerates with prevalence of the monometallic particles.

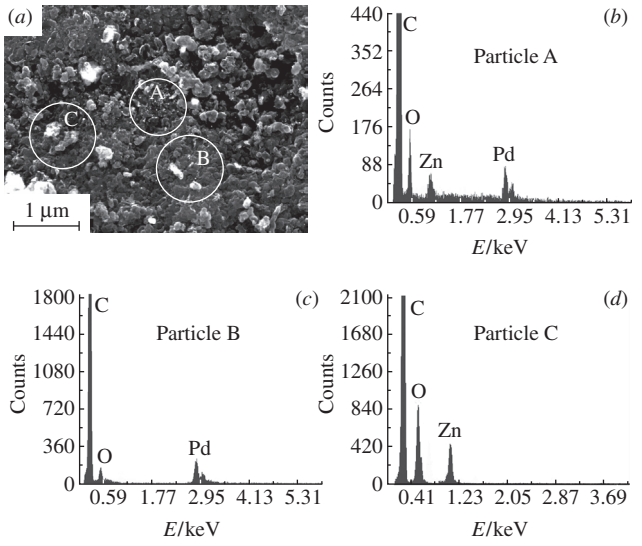

Figure 3 (*a*) SEM image of the Pd–Zn/C catalyst [from $Pd(OAc)_2$ and $Zn(OAc)_2OH_2$ complexes] and (*b*), (*c*), (*d*) the corresponding EDS spectra.

Figure 4(*a*) exhibits typical SEM image of the 0.9% Pd–0.59% Zn/C sample prepared *via* bimetallic complex **1**. EDS analysis detected only Pd–Zn bimetallic particles [Figure 4(*b*)] Calculations of the EDS spectra gives a 4:1 Pd:Zn atomic ratio in average for the metallic particles. Note that according to ICP elemental analysis, the catalyst has a Pd:Zn atomic ratio of 1:1 [calc. (%): Pd, 0.93; Zn, 0.593]. A possible explanation of the higher Pd:Zn elemental ratio could be the fact that the Zn sublimates under exposure to an electron beam during EDS analysis.[12] This suggestion is supported by the fact that we observed a continuous decrease in the Zn intensity upon electron beam irradiation. The bimetallic particles changed their shape after exposure to the electron beam. The second EDS analysis of the same particles led to their noticeable agglomeration because of the beam damage of the catalyst.

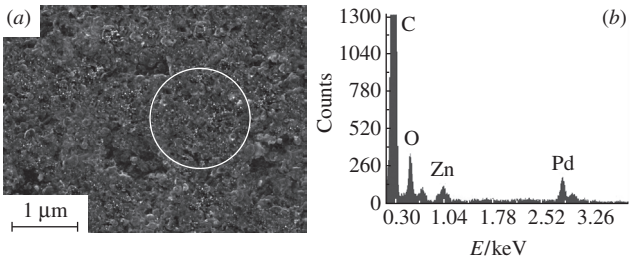

Figure 4 (*a*) SEM image of the Pd–Zn/C catalyst (from complex **1**) and (*b*) the corresponding EDS spectrum.

To further examine Pd–Zn particles in the catalyst prepared *via* bimetallic complex **1**, we calculated the lattice fringers using HRTEM images and the Digital Micrograph software.[11] The particles with a 2.06 Å lattice spacing were identified (Figure 5), which suggests that a Pd:Zn atomic ratio of 1:1 in complex **1** provides the formation of a β_1-tetragonal Pd–Zn phase[9(a),13] with contracted lattice spacing, as compared to monometallic Pd (2.25 Å). Note that, for PdO, Zn or ZnO particles, the next

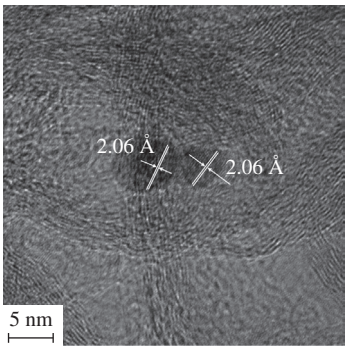

Figure 5 TEM image of the Pd–Zn/C catalyst prepared *via* complex **1**.

nearest d-lines of the sample would be 2.82, 1.33 or 2.53 Å, respectively.[14–16] These data are in a good agreement with our previous findings obtained by EXAFS and XRD.[8(*a*)]

The characterization data provide the following explanation of the favorable selectivity of the Pd–Zn/C sample prepared using complex **1**. In accordance with published data, selectivity changes can be attributed to either the particle size effect or Pd–Zn alloy formation. The particle size effect is related to the formation of a β-PdH hydride phase.[1,17] The probability of palladium β-hydride formation decreases with decreasing Pd particle size. Therefore, highly dispersed Pd catalysts show better selectivity in alkene formation in the course of triple C–C bond hydrogenation.[18,19] However, this explanation should be omitted since TEM and SEM analysis revealed a lower dispersion of metallic particles in the Pd–Zn/C sample prepared using complex **1**, as compared to the monometallic Pd/C.

Thus, the most plausible explanation for the favorable selectivity of the catalyst prepared *via* complex **1** is the formation of homogeneous bimetallic Pd–Zn alloy nanoparticles revealed by TEM and SEM. This explanation is in line with the results of density functional calculations of acetylene hydrogenation pathway reported by Studt *et al*. for various Pd alloys.[20] The addition of metals such as Ag, Zn, Ga or Pb primarily changes the stability of adsorbed acetylene and ethylene rather than the activation energies. The addition of these metals affects the electronic structure of Pd and decreases the heat of adsorption of acetylene and ethylene. However, acetylene adsorption remains sufficiently exothermic, and its hydrogenation is facile, though some decrease in the activity can be expected, as it was observed for Pd–Zn/C prepared *via* **1** [Figure 1(*a*)]. On the other hand, the decrease in ethylene adsorption heat facilitates its desorption since the activation barrier for ethylene desorption becomes lower than the activation barrier for its hydrogenation. As a result, the selectivity of Pd–Zn catalyst in ethylene formation is significantly enhanced, as compared to monometallic, though at the expense of some activity loss.

We acknowledge the support of Haldor Topsøe A/S (Denmark) for performing TEM and SEM studies. We are grateful to Dr. P. L. Hansen, Dr. Ch. C. Appel, Dr. F. M. Cano and Dr. A. Molenbroek for their asistance and fruitful discussions. This work was supported by the Russian Foundation for Basic Research (grant nos. 12-03-31487, 13-03-00408 and 13-03-12176).

References

1 (*a*) A. Borodziński and G. C. Bond, *Catal. Rev.*, 2006, **48**, 91; (*b*) A. Borodziński and G. C. Bond, *Catal. Rev*., 2008, **50**, 379.
2 J. H. Kang, E. W. Shin, W. J. Kim, J. D. Park and S. H. Moon, *Catal. Today*, 2000, **63**, 183.
3 V. P. Ananikov, L. L. Khemchyan, Yu. V. Ivanova, V. I. Bukhtiyarov, A. M. Sorokin, I. P. Prosvirin, S. Z. Vatsadze, A. V. Medved'ko, V. N. Nuriev, A. D. Dilman, V. V. Levin, I. V. Koptyug, K. V. Kovtunov, V. V. Zhivonitko, V. A. Likholobov, A. V. Romanenko, P. A. Simonov, V. G. Nenajdenko, O. I. Shmatova, V. M. Muzalevskiy, M. S. Nechaev, A. F. Asachenko, O. S. Morozov, P. B. Dzhevakov, S. N. Osipov, D. V. Vorobyeva, M. A. Topchiy, M. A. Zotova, S. A. Ponomarenko, O. V. Borshchev, Yu. N. Luponosov, A. A. Rempel, A. A. Valeeva, A. Yu. Stakheev, O. V. Turova, I. S. Mashkovsky, S. V. Sysolyatin, V. V. Malykhin, G. A. Bukhtiyarova, A. O. Terent'ev and I. B. Krylov, *Russ. Chem. Rev.*, 2014, **83**, 885.
4 G. C. Bond, *Metal-Catalysed Reactions of Hydrocarbons*, Springer, New York, 2005.
5 S. A. Nikolaev, L. N. Zanaveskin, V. V. Smirnov, V. A. Averyanov and K. L. Zanaveskin, *Russ. Chem. Rev*., 2009, **78**, 231 (*Usp. Khim.*, 2009, **78**, 248).
6 S. Chinayon, O. Mekasuwandumrong, P. Praserthdam and J. Panpranot, *Catal. Commun.*, 2008, **9**, 2297.
7 A. A. Lamberov, S. R. Egorova, I. R. Il'yasov, Kh. Kh. Gil'manov, S. V. Trifonov, V. M. Shatilov and A. Sh. Ziyatdinov, *Kinet. Catal*., 2007, **48**, 136 (*Kinet. Katal*., 2007, **48**, 143).
8 (*a*) O. P. Tkachenko, A. Yu. Stakheev, L. M. Kustov, I. S. Mashkovsky, M. van den Berg, W. Grünert, N. Yu. Kozitsyna, S. E. Nefedov, Zh. V. Dobrokhotova, V. I. Zhilov, M. N. Vargaftik and I. I. Moiseev, *Catal. Lett*., 2006, **112**, 155; (*b*) I. S. Mashkovsky, O. P. Tkachenko, G. N. Baeva and A. Yu. Stakheev, *Kinet. Catal*., 2009, **50**, 768 (*Kinet. Katal*., 2009, **50**, 798).
9 (*a*) A. A. Veligzhanin, Ya. V. Zubavichus, N. Yu. Kozitsyna, V. Yu. Murzin, E. V. Khramov and A. A. Chernyshov, *J. Surf. Invest. X-Ray, Synchrotron Neutron Tech.*, 2013, **7**, 422 (*Poverkhnost'. Rentgenovskie, Sinkhrotronnye i Neitronnye Issledovaniya*, 2013, **5**, 26); (*b*) V. Yu. Murzin, A. A. Veligzhanin, Ya. V. Zubavichus, M. N. Vargaftik, N. Yu. Kozitsyna, M. V. Tsodikov and I. I. Moiseev, *Abstracts of I Russian Congress on Catalysis*, Moscow, 2011, vol. 1, p. 60.
10 N. Yu. Kozitsyna, S. E. Nefedov, F. M. Dolgushin, N. V. Cherkashina, M. N. Vargaftik and I. I. Moiseev, *Inorg. Chim. Acta*, 2006, **359**, 2072.
11 *Digital Micrograph™ Software (ver. 3.5.2)*, Gatan Inc., Pleasanton, CA, USA, 1999.
12 Z.-X. Chen, K. M. Neyman and N. Rösch, *Surf. Sci*., 2004, **548**, 291.
13 T. B. Massalski and H. Okamoto, *Binary Alloy Phase Diagrams*, 2nd edn., ASM International, USA, 1990.
14 *PDF-4+ Database*, The International Centre for Diffraction Data, Newton Square, PA, USA, 2006.
15 S. Giorgio, H. Graoui, C. Chapon and C. R. Henry, *Mater. Sci. Eng. A*, 1997, **229**, 169.
16 Y.-H. Chin, R. Dagle, J. Hu, A. C. Dohnalkova and Y. Wang, *Catal. Today*, 2002, **77**, 79.
17 I. T. Caga, E. Shutt and J. M. Winterbottom, *J. Catal*., 1976, **44**, 271.
18 A. Borodziński and A. Cybulski, *Appl. Catal., A*, 2000, **198**, 51.
19 W. Palczewska, in *Hydrogen Effects in Catalysis*, eds. Z. Paal and P. G. Menon, Marcel Dekker, New York, 1988, p. 381.
20 F. Studt, F. Abild-Pedersen, Th. Bligaard, R. Z. Sørensen, C. H. Christensen and J. K. Nørskov, *Science*, 2008, **320**, 1320.

Received: 30th May 2014; Com. 14/4385

Available online at www.sciencedirect.com
ScienceDirect
Mendeleev Commun., 2014, **24**, 358–359
Mendeleev Communications

Protonation of Cp*Fe(η^5-C_6H_7) as a convenient procedure for the preparation of the valuable synthon [Cp*Fe$(MeCN)_3$]$^+$

Alexander S. Romanov, Mikhail M. Vinogradov, Dmitry V. Muratov and Alexander R. Kudinov*

A. N. Nesmeyanov Institute of Organoelement Compounds, Russian Academy of Sciences, 119991 Moscow, Russian Federation. Fax: +7 499 135 5085; e-mail: arkudinov@ineos.ac.ru

DOI: 10.1016/j.mencom.2014.11.016

The (cyclohexadienyl)iron complex Cp*Fe(η^5-C_6H_7) obtained by a reaction of the cation [Cp*Fe(η^6-C_6H_6)]$^+$ with $LiAlH_4$ reacts with HBF_4·Et_2O or TfOH in MeCN to afford the acetonitrile cation [Cp*Fe$(MeCN)_3$]$^+$ in a high yield. The structure of complex Cp*Fe(η^5-C_6H_7) was determined by X-ray diffraction analysis.

The acetonitrile complex [Cp*Fe$(MeCN)_3$]$^+$ is a milestone in the organometallic chemistry of pentamethylcyclopentadienyl iron compounds. Its reactivity was thoroughly investigated for obtaining various novel complexes[1] and catalysis (*e.g.*, for the cycloaromatization of acyclic and alicyclic enediynes or alkyne [2+2+2] cycloaddition reactions).[2] The cation [Cp*Fe$(MeCN)_3$]$^+$ was previously obtained by the exhaustive photochemical decarbonylation of [Cp*Fe$(CO)_2(MeCN)$]$^+$ or [Cp*Fe$(CO)_3$]$^+$ using an immersion UV lamp.[1(a),3] On the other hand, Kuhn *et al.* found that the cyclohexadienyl complex $CpFeC_6H_7$ is protonated by HBF_4·OEt_2 giving the very reactive diene tetrafluoroborate complex CpFe(η^4-C_6H_8)(FBF_3), which opens an access to a variety of half-sandwich complexes [$CpFeL_3$]$^+$ (L = SMe_2, $SeMe_2$, *etc.*).[4] However, examples of the reactivity of related Cp* derivatives are unknown. Here, we report a straightforward procedure for the preparation of the acetonitrile cation [Cp*Fe$(MeCN)_3$]$^+$ by protonation of the cyclohexadienyl complex Cp*Fe(η^5-C_6H_7) with different acids.

For the synthesis of the neutral cyclohexadienyl complex Cp*Fe(η^5-C_6H_7) **1**, we used a reaction of the cation [Cp*Fe(η^6-C_6H_6)]$^+$ **3** with $NaBH_4$, similar to the preparation of the parent compound CpFe(η^5-C_6H_7).[5] We found that the treatment of complex **1** with either TfOH or HBF_4·Et_2O in MeCN leads to the tris(acetonitrile) derivative [Cp*Fe$(MeCN)_3$]$^+$ **2** in a high yield (Scheme 1).† In both cases, the complex is formed reproducibly in a yield of 80–85%. Unfortunately, the product is contaminated with benzene cation **3** owing to competitive oxidation.[6] Carrying out the reaction at a low temperature (–30 °C) minimizes the formation of **3** to 4% (according to ^{1}H NMR data). Note that a further decrease in the temperature (using solvent mixtures) also slows down the formation of the target product. Fortunately, the undesirable admixture is easily removed by reprecipitation.

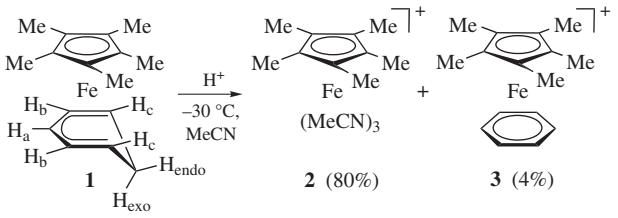

Scheme 1

The reaction of HCl·Et_2O with Cp*Fe(η^5-C_6H_7) led only to the benzene complex [Cp*Fe(η^6-C_6H_6)]Cl. Recently, we described a similar reaction for (cyclohexadienyl)ferracarborane analogues (η-9-L-7,8-$C_2B_9H_{10}$)Fe(η-C_6H_7) (L = SMe_2, NMe_3).[7]

The structure of complex **1** was determined by X-ray diffraction analysis (Figure 1).‡ In spite of the accurate reflection data, the disorder of the cyclohexadienyl ligand in **1** precludes a detailed comparison of the molecular geometry with that of relative compounds. Nevertheless, the bond lengths and angles are comparable with those of the previously reported structures. For example, the mean bond lengths Fe–C(Cp*) of 2.057(2) Å and Fe–C(C_6H_7) 2.060(7) Å are identical to those of the known sandwich cyclohexadienyl complexes, *e.g.*, 2.059(3) and 2.06(3) Å for CpFe(η^5-$C_6H_3Me_3C_6H_5$).[8] Two η^5-coordinated ligands are almost parallel with a dihedral angle of only 1.43(9)°. The methylene carbon atom C(11A) lies out of the C_5 plane of the cyclohexadienyl ligand by 0.649(7) Å, and the tilt angle between the C_5 and C_3 planes [C(12A)–C(11A)–C(16A)] is 43.7(3)°.

We conclude that the protonation of Cp*Fe(η^5-C_6H_7) by strong acids can be used as a simple procedure to prepare the valuable synthon [Cp*Fe$(MeCN)_3$]$^+$, which does not require the use of expensive immersion equipment for UV irradiation.

† All reactions were carried out in an argon atmosphere.

*Synthesis of Cp*Fe(η^5-C_6H_7)* **1**. THF (15 ml) was added to the mixture of benzene complex **3** (0.66 g, 1.6 mmol)[9] and $NaBH_4$ (0.3 g, 8.0 mmol). The yellowish-orange mixture was stirred overnight. Water (1.5 ml) was added and the mixture was stirred for 20 min. Hexane (30 ml) was added to the mixture; the precipitated solid was filtered off, and the filtrate was evaporated under a reduced pressure. The residue was dissolved in 10 ml of Et_2O; the solution was filtered and evaporated to dryness giving an orange solid. Yield 0.318 g (74%). The product should be stored in an argon atmosphere. ^{1}H NMR ($CDCl_3$) δ: 5.39 (br. t, 1H, H_a, $J_{H_aH_b}$ 4.8 Hz), 3.73 (br. t, 2H, H_b, $J_{H_bH_c}$ 5.4 Hz), 2.41 (dt, 1H, H_{exo}, $J_{H_{exo}H_{endo}}$ 12.3 Hz, $J_{H_{exo}H_c}$ 6.3 Hz), 1.86 (s, 15H, C_5Me_5), 1.53 (br. d, 1H, H_{endo}, $J_{H_{endo}H_{exo}}$ 12.3 Hz) overlapping with 1.48 (br. t, 2H, H_c, $J_{H_cH_b}$ 5.4 Hz). ^{13}C{^{1}H} NMR (CD_2Cl_2) δ: 83.97, 83.75, 81.46, 25.87, 25.27, 10.20. Found (%): C, 70.98; H, 8.16. Calc. for $C_{16}H_{22}Fe$ (%): C, 71.12; H, 8.21.

*Synthesis of [Cp*Fe$(MeCN)_3$](OTf)* **2**·OTf. Complex **1** (270 mg, 1.0 mmol) was suspended in 5 ml of MeCN and chilled to –30 °C. Triflic acid solution in Et_2O (1.4 ml, 1.13 M) was added through the septum cap. The mixture quickly turns into a clear purple solution. The stirring was continued for 30 min at –30 °C, and the product was precipitated with 40 ml of Et_2O chilled to –30 °C to give a purple precipitate. The crude product was repeatedly reprecipitated with Et_2O from MeCN to remove impurity compound **3**.The precipitate was filtered off, washed with 10 ml of Et_2O and dried *in vacuo*. Yield, 80–85%. ^{1}H NMR (CD_3CN) δ: 1.93 (s, 9H, MeCN), 1.48 (s, 15H, C_5Me_5). ^{1}H NMR (acetone-d_6) δ: 2.40 (s, 9H, MeCN), 1.65 (s, 15H, C_5Me_5). *Cf.* ref. 1.

Complex **2**·BF_4 was prepared similarly to **2**·OTf from compound **1** (270 mg, 1.0 mmol) and HBF_4·Et_2O (0.22 ml, 1.5 mmol). Purple powder. Yield, 80–85%.

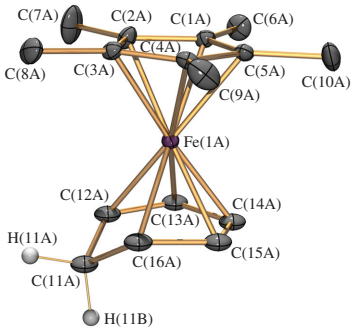

Figure 1 Molecular structure of compound **1** (independent molecule A). Ellipsoids are shown at a 50% probability level. Hydrogen atoms [except for the methylene carbon C(11A)] and a second part of the disordered cyclohexadienyl ligand are omitted for clarity. Selected bond lengths (Å) and angles (°): Fe(1A)–C(1A) 2.077(3), Fe(1A)–C(2A) 2.059(3), Fe(1A)–C(3A) 2.048(3), Fe(1A)–C(4A) 2.044(2), Fe(1A)–C(5A) 2.058(2), Fe(1A)–C(12A) 2.095(5), Fe(1A)–C(13A) 2.032(7), Fe(1A)–C(14A) 2.015(6), Fe(1A)–C(15A) 2.034(7), Fe(1A)–C(16A) 2.127(4), Fe(1A)···centroid(Cp) 1.661(1), Fe(1A)···centroid[C(12A) to C(16A)] 1.543(2); ∠(Cp/η^5-C_6H_7) 1.43(9).

‡ Crystals were grown by the slow evaporation of a hexane solution of **1**.

Crystal data for **1**: $C_{16}H_{22}Fe$, triclinic, space group $P\bar{1}$, a = 8.5507(4), b = 11.9706(6) and c = 13.9200(7) Å, α = 105.492(1)°, β = 94.310(1)°, γ = = 93.586(1)°, V = 1364.09(12) Å^3, Z = 4, d_{calc} = 1.316 g cm^{-3}, μ = 1.081 mm^{-1}, orange/plate, crystal size 0.31 × 0.26 × 0.14 mm, $F(000)$ = 576, T_{min}/T_{max} 0.7304/0.8633, R_1 = 0.0385 [from 4779 unique reflections with $I > 2\sigma(I)$] and wR_2 = 0.1056 (from all 5363 unique reflections), GOF = 0.991, $\Delta\rho_{min}/\Delta\rho_{max}$ = 1.239/–0.609. X-ray diffraction analysis was carried out on a Bruker SMART APEX2 diffractometer equipped with a CCD area detector at 100 K, using graphite monochromated MoKα radiation (λ = = 0.71073 Å). An absorption correction was applied semiempirically using the APEX2 program. The structure was solved by a direct method and refined by the full-matrix least-squares technique against F^2 in an anisotropic approximation for non-hydrogen atoms. The cyclohexadienyl ligand in complex **1** was disordered over two positions with equal occupancies for both independent molecules. All hydrogen atom positions were refined in an isotropic approximation in a 'riding' model with the U_{iso}(H) parameters of 1.2 $U_{eq}(C_i)$, for methyl groups equal to 1.5 $U_{eq}(C_{ii})$, where $U(C_i)$ and $U(C_{ii})$ are the equivalent thermal parameters of the carbon atoms to which the corresponding H atoms are bonded. All calculations were performed using the SHELXTL software.

CCDC 985004 contains the supplementary crystallographic data for this paper. These data can be obtained free of charge from The Cambridge Crystallographic Data Centre *via* http://www.ccdc.cam.ac.uk. For details, see 'Notice to Authors', *Mendeleev Commun.*, Issue 1, 2014.

This work was supported by the Russian Foundation for Basic Research (grant no. 14-03-31970).

References

1 (*a*) D. Catheline and D. Astruc, *Organometallics*, 1984, **3**, 1094; (*b*) G. E. Herberich, A. Gaffke and H. J. Eckenrath, *Organometallics*, 1998, **17**, 5931; (*c*) G. E. Herberich, U. Englert, B. Ganter and C. Lamertz, *Organometallics*, 1996, **15**, 5236; (*d*) X. Zheng and G. E. Herberich, *Organometallics*, 2001, **20**, 3097; (*e*) G. E. Herberich and B. Ganter, *Organometallics*, 1997, **16**, 522; (*f*) D. V. Muratov, P. V. Petrovskii, Z. A. Starikova, G. E. Herberich and A. R. Kudinov, *J. Organomet. Chem.*, 2006, **691**, 3251; (*g*) T. J. Brunker, A. R. Cowley and D. O'Hare, *Organometallics*, 2002, **21**, 3123; (*h*) D. Catheline and D. Astruc, *J. Organomet. Chem.*, 1984, **269**, C33; (*i*) D. J. Harrison, A. G. De Crisci, A. J. Lough, M. J. Kerr and U. Fekl, *Inorg. Chem.*, 2008, **47**, 10199; (*j*) A. R. Kudinov, R. H. Herber, P. Zanello, D. S. Perekalin, I. V. Glukhov, I. Nowik, M. Corsini, S. Fedi and F. Laschi, *Eur. J. Inorg. Chem.*, 2007, **26**, 4190.

2 (*a*) J. M. O'Connor, S. J. Friese and B. L. Rodgers, *J. Am. Chem. Soc.*, 2005, **127**, 16342; (*b*) K. Ferre, L. Toupet and V. Guerchais, *Organometallics*, 2002, **21**, 2578.

3 J. L. Schrenk, A. M. McNair, F. B. McCormick and K. R. Mann, *Inorg. Chem.*, 1986, **25**, 3501.

4 N. Kuhn, H. Schumann, M. Winter and E. Zauder, *Chem. Ber.*, 1988, **121**, 111.

5 (*a*) M. L. H. Green, L. Pratt and G. Wilkinson, *J. Chem. Soc.*, 1960, 989; (*b*) R. A. Brown, A. Houlton, R. M. G. Roberts, J. Silver and E. Slade, *J. Chem. Soc., Dalton Trans.*, 1993, 1519.

6 R. M. Chin, A. Simonson, J. Mauldin, J. Criswell and W. Brennessel, *Organometallics*, 2010, **29**, 3868.

7 A. R. Kudinov, P. Zanello, R. H. Herber, D. A. Loginov, M. M. Vinogradov, A. V. Vologzhanina, Z. A. Starikova, M. Corsini, G. Giorgi and I. Nowik, *Organometallics*, 2010, **29**, 2260.

8 (*a*) M. J. Zaworotko, K. C. Sturge and P. S. White, *J. Organomet. Chem.*, 1990, **389**, 333 and references therein; (*b*) V. G. Andrianov, Yu. T. Struchkov, V. A. Petrakova and N. A. Vol'kenau, *Koord. Khim.*, 1986, 978 (in Russian).

9 J. R. Hamon, D. Astruc and P. Michaud, *J. Am. Chem. Soc.*, 1981, **103**, 758.

Received: 24th February 2014; Com. 14/4314

Available online at www.sciencedirect.com
ScienceDirect
Mendeleev Commun., 2014, **24**, 360–362
Mendeleev Communications

Synthesis of SrF_2–YF_3 nanopowders by co-precipitation from aqueous solutions

Maria N. Mayakova,[a] Anna A. Luginina,[a] Sergey V. Kuznetsov,[a] Valerii V. Voronov,[a] Roman P. Ermakov,[a] Alexander E. Baranchikov,[b] Vladimir K. Ivanov,[b,c] Oksana V. Karban[d] and Pavel P. Fedorov*[a]

[a] *A. M. Prokhorov General Physics Institute, Russian Academy of Sciences, 119991 Moscow, Russian Federation. Fax: +7 499 135 7744; e-mail: ppfedorov@yandex.ru*
[b] *N. S. Kurnakov Institute of General and Inorganic Chemistry, Russian Academy of Sciences, 119991 Moscow, Russian Federation*
[c] *Department of Materials Science, M. V. Lomonosov Moscow State University, 119991 Moscow, Russian Federation*
[d] *Physical-Technical Institute, Ural Branch of the Russian Academy of Sciences, 426000 Izhevsk, Russian Federation*

DOI: 10.1016/j.mencom.2014.11.017

The $Sr_{1-x}Y_xF_{2+x}$ ($x \leqslant 0.6$) nanocrystalline solid solutions precipitated at an ambient temperature from the aqueous solutions of metal nitrates crystallized in a cubic system with $a = 5.800 - 0.230x$ [Å]; their composition range of homogeneity is wider than that for samples prepared at a higher temperature (from 850 °C to melt).

Nanocrystalline fluorides have been intensively studied[1–4] because of their applications as scintillators, acidic catalysts, cathode materials for alkaline batteries, thin antireflective coatings, drug components, precursors for laser and scintillation optical ceramics, *etc*. Strontium nanofluorides doped with rare earth ions can be used as promising luminophores.[5,6] They have been prepared by the thermolysis of metal trifluoroacetates, the microwaving of metal nitrates in 1-butyl-3-methylimidazolium tetrafluoroborate and hydrothermal techniques or obtained as nanocrystalline components of glass ceramics.[4,7–9] However, modern literature lacks information on the preparation of strontium rare-earth nanofluorides by co-precipitation from aqueous solutions. Recently, we found[4,6,7,10] that the latter approach is a very productive method for the preparation of equilibrium and non-equilibrium nanophases of variable composition formed under ambient conditions *via* a non-classical crystal growth mechanism (*i.e.*, by the oriented attachment of nanoparticles). Therefore, the goal of this study was to characterize nanopowders formed in the SrF_2–YF_3 model system during the precipitation of nanophases in aqueous solutions with hydrofluoric acid (HF).[†] The yttrium system was used as a model because it has similar physical and chemical properties to those of rare earth elements from Gd to Lu.

Chemical analysis and X-ray diffraction data for SrF_2–YF_3 samples, including pure SrF_2, are presented in Table 1 and Figure 1, respectively. They confirm a good agreement between the experimental and initial yttrium concentrations in the specimens.

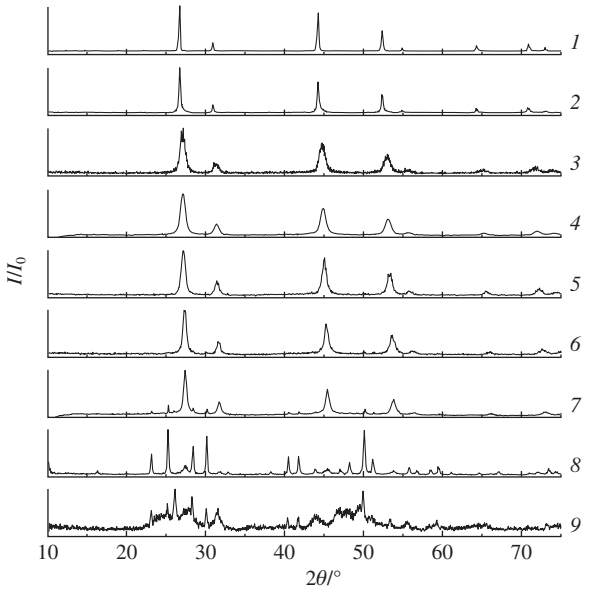

Figure 1 X-ray diffraction patterns of SrF_2–YF_3 samples precipitated from aqueous solutions, containing (*1*) 0, (*2*) 10, (*3*) 20, (*4*) 30, (*5*) 40, (*6*) 60, (*7*) 70, (*8*) 90 and (*9*) 100 mol% YF_3.

Samples with up to 60 mol% YF_3 displayed a single fluorite-type cubic phase (phase F). They also contained 2.5–4 wt% adsorbed water, which was removed after heating to 300 °C. This thermal treatment did not affect the unit cell parameters. Phase

[†] High-purity $Sr(NO_3)_2$ and $Y(NO_3)_3 \cdot 6H_2O$ (99.99%), HF (99.9%) and twice distilled water were used as starting materials. The precipitation experiments were carried out in polypropylene vessels at room temperature. The starting 0.17–0.20 M metal nitrate solutions were mixed in order to achieve Y/(Y + Sr) molar ratios from 10 to 90% and treated dropwise with aqueous HF (6 vol%) with vigorous stirring. The formed precipitates were decanted, thoroughly washed with twice distilled water and dried under air at 40 °C. In some experiments, pH of the mother solution was adjusted to 5–6.

The phase composition of the synthesized samples was controlled by X-ray diffraction analysis (DRON-4M diffractometer; CuKα radiation). The sizes of the domains of coherent scattering (DCS) and microdeformations were determined by a fundamental parameters technique[11] with the use of full profile analysis by the TOPAS software.[12]

Scanning electron microscopy (SEM) studies were carried out using a Carl Zeiss NVision 40 microscope, and atomic force microscopy (AFM) was performed with a Ntegra Prima scanning AFM probe.

The yttrium content in the prepared samples was determined by wet chemical analysis. A fluoride sample (~1 g) was placed in a glass-carbon dish and treated three times with sulfuric acid with complete evaporation after each treatment. Then, the residue was dissolved in 250 ml of water to completely transfer yttrium to the aqueous solution, whereas strontium remained in the undissolved precipitate. The resulting solution was titrated with a 0.1 M ethylenediaminetetraacetic acid (EDTA) solution at pH 5–6 and 50 °C. The equivalency point was determined by a change in the color of a xylenol orange indicator from red to yellow.

Table 1 Composition, crystal lattice parameters, values of the calculated sizes of the domains of coherent scattering D, and values of microdeformation e of the samples in SrF_2–YF_3 system.

Designated YF_3 content (mol%)	Experimental YF_3 content (wet chemical analysis data) (mol%)	Cubic crystal lattice parameter a/Å	D/nm	e
0	—	5.799±0.008	37±3	0.05±0.01
20	19±0.6	5.750±0.001	11±1	0.13±0.02
30	29±1.0	5.740±0.007	15±1	0.18±0.03
40	38±1.3	5.710±0.001	13±1	0.09±0.01
60	57±1.9	5.676±0.001	30±6	0.28±0.03

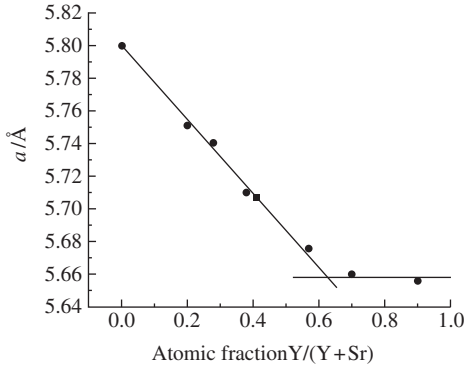

Figure 2 Parameters of the cubic crystal lattices of fluorite-type phases in the SrF_2–YF_3 system *vs.* the composition of samples prepared by high temperature synthesis[13] and precipitation from aqueous solutions.

F lattice parameter a varies from 5.799(8) Å for intrinsic SrF_2 (5.800 Å according to PCPDFWIN No. 060262) to 5.676(1) Å for $Sr_{1-x}Y_xF_{2+x}$ with x = 0.60, and it can be described with the following linear correlation: $a = 5.800 - 0.230x$ [Å], where x is the molar yttrium content in $Sr_{1-x}Y_xF_{2+x}$. This is consistent with data[13] for $Sr_{1-x}Y_xF_{2+x}$ ($x \leqslant 0.41$) (Figure 2). The latter fact is very important for practical purposes since it allows one to use known quantitative correlations for numerous SrF_2-based solid solutions of rare-earth fluorides[14] for the evaluation of the compositions of nanoparticles precipitated from aqueous solutions.

The scanning electron (SEM) and atomic force (AFM) microscopy images confirmed the hierarchic mechanisms of nanoparticle agglomeration. Thus, the SEM images of $Sr_{1-x}Y_xF_{2+x}$ specimens with x = 0.20 and 0.40 indicated the presence of ~20 nm nanoparticles [Figure 3(*a*),(*b*)]. This is in agreement with calculated D values (Table 1). The AFM data for the sample with x = 0.40 (Figure 4) show the formation of ~100 nm agglomerates.

Increasing the yttrium content of the specimens up to 70–90 mol% resulted in the formation of a second phase in the precipitates; in addition to the phase F with average a = 5.658(2) Å, one can observe another cubic phase, $(H_3O)Y_3F_{10}\cdot H_2O$,[10(*c*)] with the crystal lattice parameter a = 15.480(1) Å [*Fd*3*m* space group; $(H_3O)Yb_3F_{10}\cdot H_2O$ structure type[15]]. This phase contained hydroxonium ions; therefore, it can be represented as $(H_3O^+)Y_3F_{10}^-\cdot H_2O$. The two-phase composition of 90 mol% Y samples has also been confirmed by electron-microscopic data [Figure 3(*c*)]: the SEM images exhibit small 20 nm nanoparticles along with faceted octahedral ~200 nm $(H_3O)Y_3F_{10}\cdot H_2O$ nanocrystals, which are very similar to those observed earlier in the BaF_2–YF_3 system.[10(*c*)]

A comparison of the above results with known SrF_2–YF_3 phase diagram[16] (see Figure S1, Online Supplementary Materials) demonstrates that the composition area of the homogeneous fluorite-like cubic solid solution $Sr_{1-x}Y_xF_{2+x}$ (phase F) is wider for the precipitated samples (x = 0–0.60) than for the specimens prepared by high-temperature synthesis (x = 0–0.41). Additionally,

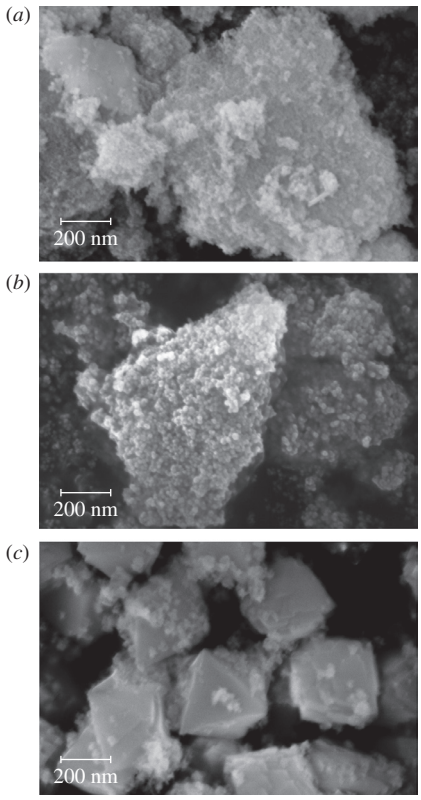

Figure 3 SEM images of (*a*) $0.8\,SrF_2$–$0.2\,YF_3$, (*b*) $0.6\,SrF_2$–$0.4\,YF_3$ and (*c*) $0.1\,SrF_2$–$0.9\,YF_3$ samples.

we did not observe the formation of a series of ordered fluorite-like phases at 33–44 mol% Y, which are thermodynamically stable at lower temperatures, as well as the formation of the high-temperature variable composition tysonite-type phase T.[16,17] One can assume that the boundary of the area of the phase F homogeneity is close to the spinodal border of the SrF_2–YF_3 system.[4,18]

The expansion of the area of homogeneity of the fluorite-type phase products prepared at an ambient temperature is very important for the synthesis of the new generation of solid electrolytes. The $Sr_{1-x}R_xF_{2+x}$ (R is a rare earth element) solid solutions possess high fluoride ionic conductivity which grows with the rare earth element (R) concentration.[19] Moreover, the nanoparticle character of such materials can seriously enhance the latter effect.[1,4]

Note that our experiments confirmed that the Sr:Y ratio in the starting solutions did not change during the precipitation of $Sr_{1-x}Y_xF_{2+x}$ nanopowders. This fact points to the congruent character of solid solution crystallization from aqueous solutions. This was also observed in CaF_2–RF_3 and BaF_2–RF_3 systems

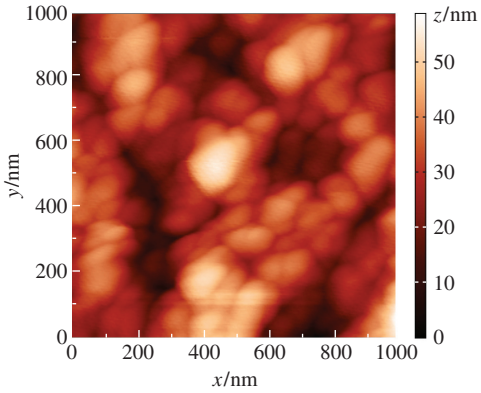

Figure 4 AFM image of the $0.6\,SrF_2$–$0.4\,YF_3$ sample.

convenient for the synthesis of optical material precursors.[6,7,10] Unfortunately, fluorite-type phases in $NaF–RF_3$ systems crystallize only incongruently from aqueous solutions.[10(*b*),(*d*)]

In conclusion, our experiments demonstrated that the treatment of $Sr(NO_3)_2$ and $Y(NO_3)_3$ with aqueous HF resulted in the precipitation of $Sr_{1-x}Y_xF_{2+x}$ nanopowder solid solutions. For $x \leqslant 0.6$, $Sr_{1-x}Y_xF_{2+x}$ specimens contained only one cubic phase with $a = 5.800 - 0.230x$ [Å]. If $x > 0.6$, the precipitates contained an additional cubic phase of $(H_3O)Y_3F_{10}·H_2O$.[15] In the precipitates, the Sr:Y molar ratio coincided with that for starting metal nitrate solutions. This fact confirmed the congruent character of $Sr_{1-x}Y_xF_{2+x}$ crystallization from aqueous media. The scanning electron and atomic force microscopy images of the synthesized nanoparticles justified the hierarchic mechanisms of their agglomeration.

We are grateful to R. Simoneaux, A. I. Popov and E. V. Chernova for their assistance in the preparation of this manuscript. This work was supported by the Russian Foundation for Basic Research (project no. 13-02-12162 ofi-m).

Online Supplementary Materials

Supplementary data associated with this article can be found in the online version at doi:10.1016/j.mencom.2014.11.017.

References

1 S. V. Kuznetzov, V. V. Osiko, E. A. Tkatchenko and P. P. Fedorov, *Russ. Chem. Rev*., 2006, **75**, 1065 (*Usp. Khim*., 2006, **75**, 1193).
2 *Fuctionalized Inorganic Fluorides: Synthesis, Characterization and Properties of Nanostructured Solids*, ed. A. Tressaud, John Wiley & Sons, Chichester, 2010.
3 M. Haase and H. Schafer, *Angew. Chem. Int. Ed.*, 2011, **50**, 5808.
4 P. P. Fedorov, A. A. Luginina, S. V. Kuznetsov and V. V. Osiko, *J. Fluorine Chem.*, 2011, **132**, 1012.
5 C. Cao, W. Qin, J. Zhang, Y. Wang, G. Wang, G. Wei, P. Zhu, L. Wang and L. Jin, *Opt. Commun.*, 2008, **281**, 1716.
6 Yu. A. Rozhnova, A. A. Luginina, V. V. Voronov, R. P. Ermakov, S. V. Kuznetsov, A. V. Ryabova, D. V. Pominova, V. V. Arbenina, V. V. Osiko and P. P. Fedorov, *Mat. Chem. Phys*., 2014, **148**, 201.
7 A. A. Luginina, P. P. Fedorov, S. V. Kuznetsov, M. N. Mayakova, V. V. Osiko, V. K. Ivanov and A. E. Baranchikov, *Inorg. Mater.*, 2012, **48**, 531 (*Neorg. Mater.*, 2012, **48**, 617).
8 J. Peng, S. Hou, X. Liu, J. Feng, X. Yu, Y. Xing and Z. Su, *Mater. Res. Bull*., 2012, **47**, 328.
9 X. S. Qiao, X. P. Fan, Z. Xue, X. H. Xu and O. Q. Lu, *J. Alloys Compd*., 2011, **509**, 4714.
10 (*a*) S. V. Kuznetsov, P. P. Fedorov, V. V. Voronov, K. S. Samarina, R. P. Ermakov and V. V. Osiko, *Russ. J. Inorg. Chem*., 2010, **55**, 484 (*Zh. Neorg. Khim*., 2010, **55**, 536); (*b*) P. P. Fedorov, S. V. Kuznetsov, M. N. Mayakova, V. V. Voronov, R. P. Ermakov, A. E. Baranchikov and V. V. Osiko, *Russ. J. Inorg. Chem*., 2011, **56**, 1525 (*Zh. Neorg. Khim*., 2011, **56**, 1604); (*c*) P. P. Fedorov, M. N. Mayakova, S. V. Kuznetsov, V. V. Voronov, R. P. Ermakov, K. S. Samarina, A. I. Popov and V. V. Osiko, *Mater. Res. Bull.*, 2012, **47**, 1794; (*d*) S. V. Kuznetsov, A. A. Ovsyannikova, E. A. Tupitsyna, D. S. Yasyrkina, V. V. Voronov, P. P. Fedorov, N. I. Batyrev, L. D. Iskhakova and V. V. Osiko, *J. Fluorine Chem*., 2014, **161**, 95; (*e*) P. P. Fedorov, V. V. Osiko, S. V. Kuznetsov, O. V. Uvarov, M. N. Mayakova, D. S. Yasirkina, A. A. Ovsyannikova, V. V. Voronov and V. K. Ivanov, *J. Cryst. Growth*, 2014, **401**, 63.
11 J. Bergmann, R. Kleeberg, A. Haase and B. Breidenstein, *Mater. Sci. Forum*, 2000, **347–349**, 303.
12 A. A. Coelho, J. S. O. Evans, I. R. Evans, A. Kern and S. Parsons, *Powder Diffr.*, 2011, **26**, 22.
13 B. P. Sobolev, K. B. Seiranian, L. S. Garashina and P. P. Fedorov, *J. Solid State Chem.*, 1979, **28**, 51.
14 P. P. Fedorov and B. P. Sobolev, *Sov. Phys. Crystallogr*., 1992, **37**, 651 (*Kristallografiya*, 1992, **37**, 1210).
15 F. Le Berre, E. Boucher, M. Allain and G. Courbion, *J. Mater. Chem*., 2000, **10**, 2578.
16 B. P. Sobolev and K. B. Seiranian, *J. Solid State Chem.*, 1981, **39**, 17.
17 B. P. Sobolev, V. B. Aleksandrov, P. P. Fedorov, K. B. Seiranyan and N. L. Tkachenko, *Sov. Phys. Crystallogr*., 1976, **21**, 49 (*Kristallografiya*, 1976, **21**, 96).
18 P. P. Fedorov, *Russ. J. Inorg. Chem.*, 2000, **45**, Suppl. 3, 268.
19 A. K. Ivanov-Shits, N. I. Sorokin, P. P. Fedorov and B. P. Sobolev, *Solid State Ionics*, 1989, **31**, 253.

Received: 24th March 2014; Com. 14/4330

Available online at www.sciencedirect.com
ScienceDirect
Mendeleev Commun., 2014, **24**, 363–364
Mendeleev Communications

Electrooxidation of potassium hepta(methoxycarbonyl)-cycloheptatrienide in acetonitrile

Vladimir A. Kokorekin,[a] Vitaliy V. Yanilkin,[b] Vladimir I. Morozov,[b] Yury V. Tomilov,[a] Dmitry N. Platonov[a] and Vladimir A. Petrosyan*[a]

[a] *N. D. Zelinsky Institute of Organic Chemistry, Russian Academy of Sciences, 119991 Moscow, Russian Federation. Fax: +7 499 135 5328; e-mail: petros@ioc.ac.ru*
[b] *A. E. Arbuzov Institute of Organic and Physical Chemistry, Kazan Scientific Center of the Russian Academy of Sciences, 420088 Kazan, Russian Federation. Fax: +7 843 275 2253; e-mail: yanilkin@iopc.ru*

DOI: 10.1016/j.mencom.2014.11.018

The quasi-reversible one-electron electrooxidation of the 1,2,3,4,5,6,7-hepta(methoxycarbonyl)cycloheptatrienide anion in MeCN at 22 °C gives a radical whose ESR spectrum consists of seven lines with splittings from six protons with an intensity ratio of 1 : 6 : 15 : 20 : 15 : 6 : 1, which likely corresponds to a substituted bicyclo[3.2.0]heptadienyl structure.

Previously, we synthesized hitherto unknown 1,2,3,4,5,6,7-hepta-(methoxycarbonyl)cycloheptatriene (HMCH) and demonstrated the high stability of the $HMCH^-$ anion.[1] Studies on the reactivity of this anion and the use of polyfunctional aromatic, heterocyclic and cage structures in directed synthesis are of interest.[1–4] According to X-ray diffraction analysis, the $HMCH^-$ anion features some flattening of the seven-membered ring with elongated double bonds and shortened single bonds closest to the anionic center, which indicates a partial conjugation of five carbon atoms of the carbocycle with negative charge delocalization on the oxygen atoms of the ester groups.[1] In this case, one of the double bonds is markedly out of the plane of the five-carbon ring part, and it is not involved in the conjugated system. Owing to the presence of such a double bond, the $HMCH^-$ anion displays dual reactivity: on the one hand, being an anion, it can react as a C- or O-nucleophile with electrophiles,[1,2] and, on the other hand, having an electron-deficient double bond, it can act as a Michael acceptor and react with primary amines.[3,4]

In the light of this concept, it is of considerable interest to study the redox properties of the $HMCH^-$ anion that provides a possibility of generating and characterizing the cycloheptatrienyl radical totally substituted with ester groups. Here, we report the electrooxidation of the $HMCH^-$ anion in acetonitrile based on the data of cyclic voltammetry and microelectrolysis in the resonator of an ESR spectrometer. Previously,[5] a similar unsaturated seven-membered comparatively stable system with an unpaired electron (heptaphenyltropylium radical) was generated by the reduction of heptaphenyltropylium bromide with zinc dust in dimethoxyethane or by mixing heptaphenyltropylium bromide and potassium heptaphenylcycloheptatrienide solutions.

The starting potassium hepta(methoxycarbonyl)cycloheptatrienide (HMCH-K)[1] is well dissociated in a MeCN solution. The CV curves of this salt (C = 0.002 mol dm^{-3}, MeCN, Pt electrode and 0.1 M Bu_4NClO_4 supporting electrolyte) recorded at 22 °C contain two oxidation peaks of the anion (Figure 1).[†]

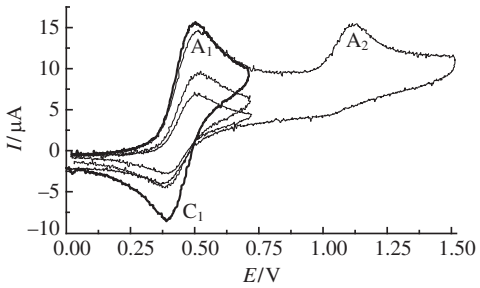

Figure 1 CV curves of HMCH-K (C = 0.002 mol dm^{-3}, v = 50, 100 and 200 mV s^{-1}) on a Pt electrode in MeCN/0.1 M Bu_4NClO_4.

Judging by the linear i_p^{1ox}–$v^{1/2}$ plot, the current of the first peak A_1 (E_p^{1ox} = 0.50 V) is diffusion-controlled and is approximately two times smaller than the one-electron level, as follows from a comparison with the one-electron diffusion peak of ferrocene oxidation. The rather steep shape of the A_1 peak is typical of reversible electron transfer, and the reverse potential scan displays a reduction peak C_1 (E_p^{1red} = 0.40 V) coupled with the A_1 peak. However, the potential difference (ΔE_p) of the A_1 and C_1 peaks at all potential scan rates was somewhat larger than the theoretical value for reversible one-electron processes. The ΔE_p value was usually 80–100 mV. A special comparison with CV of ferrocene has shown that the too high values of ΔE_p are not related to potential drop iR. Thus, it is believed that the first step of $HMCH^-$

[†] Electrooxidation of the $HMCH^-$ anion was studied by cyclic voltammetry (CV) and ESR spectroscopy combined with *in situ* electrolysis using an electrochemical cell placed in the resonator of an ESR spectrometer.[7] CV curves were recorded in an atmosphere of N_2 using a PI-50-1.1 potentiostat controlled by the LabView software. A platinum disc electrode (2.0 mm in diameter) sealed into glass was used as a working electrode. The electrodes were mechanically polished before measurements. A platinum wire served as an auxiliary electrode. The potentials were measured at 22 °C relative to a saturated calomel electrode (SCE). The diffusion nature of peak currents (i_p) was determined from a linear i_p–$v^{1/2}$ relationship[8] by varying the potential scan rate (v) in a range of 10–200 mV s^{-1}.

In ESR studies combined with *in situ* electrolysis (PI-50-1 potentiostat), a platinum plate served as a working electrode, a platinum wire was used as an auxiliary electrode, and a silver wire served as a reference electrode. The solutions were deaerated by repeating freezing–evacuation–thawing cycles in triplicate. The ESR spectra were recorded on an SE/X 2544 Radiopan spectrometer with an operating frequency of 9020 MHz using a quartz Dewar flask. The probe was calibrated relative to the impurity signal of the SiO_2 radical in quartz whose most intense component corresponds to g = 2.0002. The ESR spectra were simulated using the PEST WinSim standard program:[9] a Lorentz line shape with a width of 0.017 mT was chosen. Data were processed using Microcal Origin 6.1.

Potassium hepta(methoxycarbonyl)cycloheptatrienide (HMCH-K) was synthesized in accordance with a published procedure.[1] Commercial Bu_4NClO_4 (Acros) and acetonitrile for HPLC (Merck) were used without additional purification.

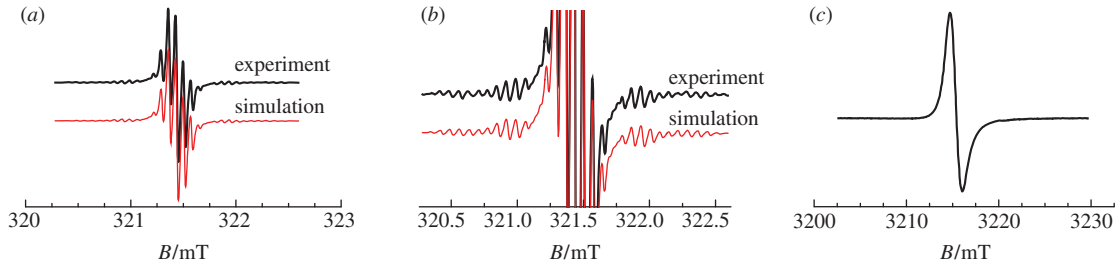

Figure 2 (*a*),(*b*) Experimental and simulated ESR spectra of HMCH$^{\bullet}$ radical generated by the electrochemical oxidation of HMCH-K (C = 0.002 mol dm^{-3}) at potentials of the A_1 peak on a Pt electrode in MeCN/0.1 M Bu_4NClO_4 at 22 °C and (*c*) the experimental spectrum measured at –40 °C.

anion oxidation corresponds to quasi-reversible electron transfer to give the HMCH$^{\bullet}$ [$C_7(CO_2Me)_7^{\bullet}$] radical.

On the other hand, the height of the A_1 peak, which is smaller than the one-electron level, is inconsistent with the concept of the stability of the HMCH$^{\bullet}$ radical on the time scale of CV curve recording. Therefore, its formation should be confirmed by an independent experiment.

This was performed by an ESR-spectroscopic study of the microelectrolysis products (Pt anode, MeCN, 0.1 M Bu_4NClO_4) of HMCH-K. Microelectrolysis at A_1 peak potentials was carried out in an electrochemical cell placed directly in the resonator of an ESR spectrometer.

The split spectrum of a paramagnetic species with g = 2.0034 (Figure 2) was recorded at the A_1 oxidation peak potentials of the HMCH$^-$ anion. The intensity of this signal increased during electrolysis. The spectrum consists of seven main lines with splittings from six protons with an intensity ratio of 1 : 6 : 15 : 20 : 15 : 6 : 1. Furthermore, splittings from at least twelve ^{13}C nuclei are observed at the periphery of the spectrum [Figure 2(*b*)]. A simulation of the spectrum gives the following hyperfine coupling constants: a_{6H} = 0.07, a_{1C} = 1.88, a_{1C} = 1.30, a_{2C} = 1.02, a_{2C} = 0.73, a_{2C} = 0.51, a_{2C} = 0.37 and a_{2C} = 0.26 mT. Judging by the ESR signal intensity after electrolysis, the radical species is stable and its concentration halved at room temperature in about 4 min. At –40 °C, one broad line of another stable radical species with g = 2.0035 was recorded [Figure 2(*c*)], which transformed to the above split spectrum upon warming to room temperature.

It is well known[6] that, in the series of isomeric C_7H_7 radicals, such as bicyclo[3.2.0]heptadienyl **1**, 3-quadricyclanyl **2**, 7-norbornadienyl **3**, homobenzvalenyl **4** and tropyl **5**, the latter radical **5** is the most stable and the other isomeric radicals are rearranged into it. Tropyl radical $C_7(CO_2Me)_7^{\bullet}$ **5′** is the primary oxidation product of the HMCH anion detected at –40 °C. Theoretically, by analogy with radical **5** [see refs. 6(*b*),(*c*)], 22 lines with splittings from 21 equivalent protons of methyl groups can be observed for this radical. Actually, a non-split spectrum is observed in the form of a broad band, which allows the possible hyperfine coupling constant with protons to be limited to $a_{21H} \leqslant 0.008$ mT.

With increasing temperature, primary tropylium radical **5′** is converted into another radical whose spectrum consists of seven main lines, indicating that the unpaired electron in this radical is delocalized to a greater extent on two equivalent methoxycarbonyl groups and to a smaller extent on the others, which is typical of allylic systems.[6] We believe that the well split signal corresponds to bicyclic allylic-type radical **1′**. At 22 °C, both radicals (**5′** and **1′**) are in an equilibrium, while the broad line of tropylium radical **5′** is hidden under the split spectrum of **1′**. Accounting for the broad line considerably improves the agreement between the simulated and experimental spectra.

1 **2** **3** **4** **5**

No examples of the transitions of tropylium radicals like **5** into isomeric radicals like **1**–**4** have been reported in the literature. This is apparently due to the very fast diffusion-controlled dimerization of radicals, whereas the isomerization of radicals occurs slowly and with a high activation energy. The presence of seven electron-withdrawing methoxycarbonyl groups in HMCH radicals hinders and slows down σ-dimerization so strongly that isomerization predominates over dimerization even at room temperature, and the formation of radicals **5′** and **1′** can be observed.

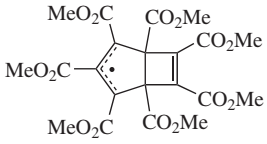

1′

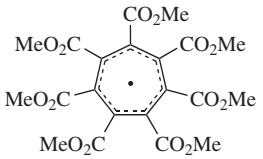

5′

The next peak A_2 (E_p^{2ox} = 1.10 V) also has diffusion nature, but it is totally irreversible and its current is markedly lower than that of the A_1 peak (Figure 1). The ratio of A_1 and A_2 peak currents is nearly independent of the potential scan rate. If the potential scan direction is reversed from peak A_2, only cathodic peak C_1 is recorded. Its height is smaller than the height of this peak recorded upon reversing the potential scan direction from peak A_1. It probably means that the HMCH$^-$ oxidation product at peak A_1 potentials can be irreversibly oxidized at peak A_2 potentials.

This work was supported by the Russian Foundation for Basic Research (project nos. 12-03-00517a and 12-03-00703a).

References

1 Yu. V. Tomilov, D. N. Platonov, R. F. Salikov and G. P. Okonnishnikova, *Tetrahedron*, 2008, **64**, 10201.
2 Yu. V. Tomilov, D. N. Platonov, E. V. Shulishov and G. P. Okonnishnikova, *Tetrahedron*, 2013, **69**, 6855.
3 Yu. V. Tomilov, D. N. Platonov and G. P. Okonnishnikova, *Tetrahedron Lett.*, 2009, **50**, 5605.
4 D. N. Platonov, G. P. Okonnishnikova and Yu. V. Tomilov, *Mendeleev Commun.*, 2010, **20**, 83.
5 (*a*) M. A. Battiste, *J. Am. Chem. Soc.*, 1962, **84**, 3780; (*b*) R. Breslow and H. W. Chang, *J. Am. Chem. Soc.*, 1965, **87**, 2200.
6 (*a*) F. Gerson and W. Huber, *Electron Spin Resonance Spectroscopy for Organic Radicals*, Wiley-VCH, Weinheim, 2003; (*b*) R. Sustmann, D. Brandes, F. Lanye and U. Nuchter, *Chem. Ber.*, 1985, **118**, 3500; (*c*) H.-G. Korth, W. Müller, R. Sustmann and M. Christi, *Chem. Ber.*, 1987, **120**, 1257; (*d*) R. Sustmann, D. Brandes, F. Lange and H. I. Tashtoush, *Magn. Reson. Chem.*, 1989, **27**, 340.
7 A. V. Il'yasov, Yu. M. Kargin and I. D. Morozova, *Spektry EPR organicheskikh ion-radikalov (ESR Spectra of Organic Radical Ions)*, Nauka, Moscow, 1980 (in Russian).
8 Z. Galus, *Teoreticheskie osnovy elektrokhimicheskogo analiza (Theoretical Bases of Electrochemical Analysis)*, Mir, Moscow, 1974 (in Russian).
9 D. R. Duling, *J. Magn. Reson., Ser. B*, 1994, **104**, 105.

Received: 1st April 2014; Com. 14/4338

Available online at www.sciencedirect.com
ScienceDirect
Mendeleev Commun., 2014, **24**, 365–367
Mendeleev Communications

Electrochemical behaviour of manganese and molybdenum mixed-oxide anodes in chloride- and sulfate-containing solutions

Vitaly V. Kuznetsov,* Sofia Yu. Kladiti, Elena A. Filatova and Artem V. Kolesnikov

Department of General and Inorganic Chemistry, D. I. Mendeleev University of Chemical Technology of Russia, 125047 Moscow, Russian Federation. Fax: +7 499 978 8660; e-mail: vitkuzn1@mail.ru

DOI: 10.1016/j.mencom.2014.11.019

The interaction between adsorbed chloride ions and the surface of $Mn_{1-x}Mo_xO_{2+x}\cdot nH_2O$ anodes at pH < 6.0 (in the vicinity of the anode during the electrolysis of neutral chloride solutions) leads to electrode material degradation.

Mixed-oxide $Mn_{1-x}Mo_xO_{2+x}\cdot nH_2O$ anodes have been used for the electrodialysis of seawater to prevent chlorine evolution at the anode.[1–3] The selective evolution of oxygen was observed at these electrodes[1–3] during the anode polarization in chloride-containing solutions, whereas chlorine evolution was almost completely inhibited. However, the use of $Mn_{1-x}Mo_xO_{2+x}\cdot nH_2O$ is limited to alkaline solutions with pH ⩾ 8.0. The degradation of a $Mn_{1-x}Mo_xO_{2+x}\cdot nH_2O$ active layer occurs even under these conditions.[2] No information concerning the origin of selectivity of the $Mn_{1-x}Mo_xO_{2+x}\cdot nH_2O$ anodes in chloride-containing solutions was reported previously.[1–3]

$Mn_{1-x}Mo_xO_{2+x}\cdot nH_2O$ can also be applied to the electrolysis of SO_4^{2-} and SO_4^{2-} + Cl^- containing solutions for electrosynthesis.[4] Note that the electrochemical evolution of oxygen results in significant acidification of the solution at the anode surface. The aim of this work was to estimate the selectivity and durability of $Mn_{1-x}Mo_xO_{2+x}\cdot nH_2O$ anodes in chloride and sulfate solutions.

The $Mn_{1-x}Mo_xO_{2+x}\cdot nH_2O$ anodes were prepared electrochemically as described elsewhere.[1] The oxide materials were deposited on the Ti/IrO_2 electrode surface. The MnO_2 anodes were prepared under the same conditions.†

Polarization measurements were carried out in a three-electrode cell. The cathode and anode compartments were separated by a ceramic Al_2O_3 diaphragm. A platinized titanium mesh was used as a cathode. The electrode potentials were measured against an AgCl/Ag electrode (in chloride-containing solutions) and Hg_2SO_4/Hg electrode (in solutions containing no Cl^- ions) and converted to a standard hydrogen electrode (s.h.e.). The ohmic potential drop between the Luggin–Gaber capillary and the working electrode was calculated from *E*–*t* relationships after polarization switching. The polarization measurements were performed in the presence of buffer solutions based on NaH_2PO_4–Na_2HPO_4 and H_3PO_4–NaH_2PO_4 mixtures.

The chlorine concentration in anode gases was determined by iodometric titration; both the gas mixture and the anolyte were analyzed. A Pt/Pt electrode was used to determine the redox potential of synthesized anolytes.

The mixed oxide material including 15–20 at% Mo was formed at the anode in the course of electrolysis (i = 0.01–0.10 A cm^{-2}, 90 °C) in a solution containing Mn^{II} and Mo^{VI} compounds. Stepwise deposition with gradually increasing current density (0.01, 0.03, 0.06 A cm^{-2}) prevented the formation of through-thickness cracks and made the distribution of elements over the sample surface uniform. The durability of anodes prepared in this manner was improved significantly.[4]

The obtained deposits were X-ray amorphous: γ-MnO_2[1] reflections detected for deposits with a zero content of molybdenum almost disappeared when the concentration of Mo in the deposits exceeded 15 at%. The molybdenum oxides act as amorphization agents. The BET specific surface area of $Mn_{1-x}Mo_xO_{2+x}\cdot nH_2O$ was significantly higher than that of $MnO_2\cdot nH_2O$ prepared under the same conditions (120.3 and 270.5 m^2 g^{-1}, respectively). On the other hand, the introduction of molybdenum oxides into the anode deposits had hardly any effect on the isoelectric point in solutions of sodium sulfate (~5.6 at $c_{Na_2SO_4}$ = 0.01–0.50 mol dm^{-3}, which is in good agreement with published data[5]).

The presence of molybdenum oxides in the anode material leads to a significant rise in its durability at anodic potentials in non-buffered Na_2SO_4 solutions. For $Ti/IrO_2/MnO_2$ electrodes, anodic currents over a potential range of 1.15–1.30 V were detected. These currents reached 4×10^{-3} A cm^{-2} and corresponded to the reaction $MnO_2 + 2H_2O \rightarrow MnO_4^- + 4H^+ + 3e$.[2,4,6] The formation of permanganate ions was confirmed by the colour of solution during anode polarization (1.25 V); the spectra of the anolyte indicated the presence of MnO_4^- ions. For $Ti/IrO_2/Mn_{1-x}Mo_xO_{2+x}$ electrodes, currents over the given potential range were much lower and did not exceed 5×10^{-4} A cm^{-2}. Apparently, the formation of an amorphous structure in the course of anodic deposition increased the durability of the oxide material.

In contrast, in non-buffered 0.5 M NaCl solution, the colouration due to MnO_2 colloid formation occurred during electrolysis. Hence, $Mn_{1-x}Mo_xO_{2+x}\cdot nH_2O$ anodes are unstable in chloride-containing solutions without buffer additives.

Anolytes prepared by electrolysis (in Na_2SO_4 solutions) with the use of $Ti/IrO_2/Mn_{1-x}Mo_xO_{2+x}$ anodes were characterized by a lower redox potential ($E_{red\text{-}ox}$ = 0.58 V) than that of anolytes obtained at Pt anodes (0.65 V) at pH 2.8. This fact agrees with the previous results[4] for $Mn_{1-x}Mo_xO_{2+x}$ and IrO_2 anodes. Lower redox potentials of the anolyte prepared with the use of $Mn_{1-x}Mo_xO_{2+x}$ anodes can be caused by a lower concentration of active oxygen species,[7] such as H_2O_2, $HO_2^{\bullet}$, HO_2^- and singlet oxygen. Oxygen in gases evolved at the anode at E > 1.4 V is formed from the oxide layer at the anode surface.[8,9] The metal–oxygen bond enthalpies for Pt, Ir, Mn and Mo oxides are different and this leads to dissimilar content of various oxygen forms in the anolyte prepared by electrolysis.

In the course of electrolysis in Cl^--containing buffer solutions (c_{Cl^-} ⩽ 0.6 mol dm^{-3}), no chlorine evolution was observed at pH 8.0–3.0. In spite of this fact, the cause of the anode material selectivity towards oxygen evolution can be different at various

† Deionized water purified in a Milli-Q system (Aldrich) and extra pure grade reagents were used.

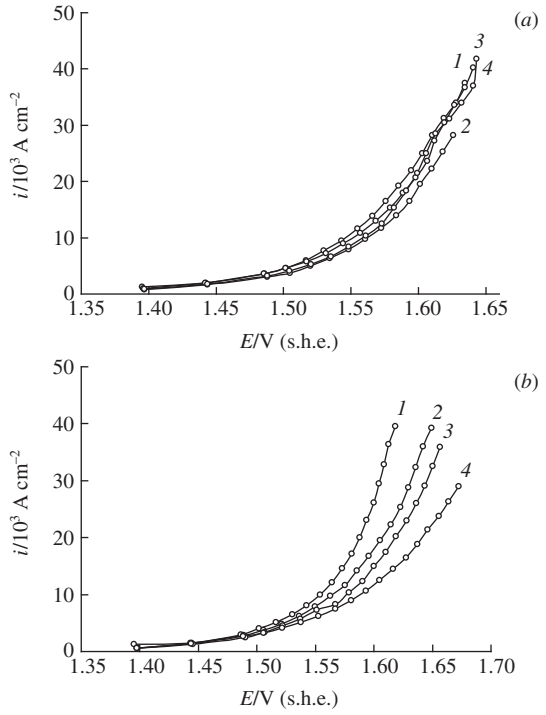

Figure 1 Stationary polarization curves at $Mn_{1-x}Mo_xO_{2+x}$ electrodes in the presence of buffer systems at constant ionic strength. pH (*a*) 8.0 and (*b*) 4.0. Concentration of Cl^- ions (mol dm^{-3}): (*1*) 0, (*2*) 0.05, (*3*) 0.10 and (*4*) 0.5.

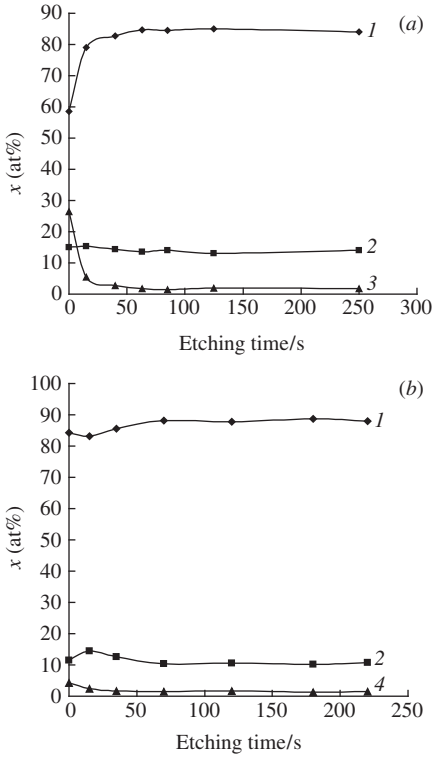

Figure 2 Element concentrations in the surface layers of $Mn_{1-x}Mo_xO_{2+x}$ after long-time electrolysis in (*a*) 0.5 M NaCl and (*b*) 0.5 M Na_2SO_4 solutions *vs.* etching time (by Ar^+ ions). The electrolysis conditions: 10 h, 0.10 A cm^{-2}. (*1*) Mn, (*2*) Mo, (*3*) Cl and (*4*) S.

pH. At pH > 6.0, the replacement of chloride by sulfate (in buffer solutions) exerts no effect on polarization curves [Figure 1(*a*)]. On the other hand, in acid buffer solutions (pH < 6.0), the introduction of Cl^- ions shifts the polarization curves to more positive potentials [Figure 1(*b*)]. Since chlorine does not evolve at the anode, the polarization curves correspond to oxygen evolution. At pH > 6.5, the surface of $Mn_{1-x}Mo_xO_{2+x}$ has a negative charge, and Cl^- ions are not adsorbed at the anode. For this reason, they do not affect the kinetics of O_2 evolution. At pH < 6.0, chloride ions are adsorbed at the active centers of the anode surface to inhibit oxygen evolution. Thus, one can assume interaction between Cl^- ions and oxide material at pH < 6.0. The next step of chlorine evolution (*e.g.*, the discharge of adsorbed chloride ions[10]) is strongly inhibited, and Cl_2 does not evolve at the anode. Note that pH 6.0 is close to an isoelectric point of $Mn_{1-x}Mo_xO_{2+x}$, which was evaluated from potentiometric titration.

The adsorption of chloride ions at the $Mn_{1-x}Mo_xO_{2+x}$-anode surface in the course of electrolysis in non-buffered solutions was confirmed by X-ray photoelectron spectroscopy (XPS)‡ [Figure 2(*a*)]. After the long-time electrolysis of non-buffered NaCl solutions (0.5 mol dm^{-3}, 10 h, 0.10 A cm^{-2}), a significant amount of chlorine was detected in the electrode surface layers. (Taking into account the fact that a great quantity of carbon is usually detected at the surface of electrode deposits,[11] we normalized XPS data to the sum of manganese, molybdenum and chlorine contents as 100%). High-resolution spectra [Figure 3(*a*)] suggest that all the detected Cl is in the form of chloride ions, which means that no ion discharge to Cl^0 (or Cl^+) occurs during the electrolysis. On the other hand, no significant accumulation of sulfur (from sulfate ions) was observed in the electrode surface layers as a result of long-term electrolysis in Na_2SO_4 solutions [Figure 2(*b*)]. The establishment of a low pH value for the anode region during the electrolysis of a 0.5 M NaCl solution was confirmed by high-resolution spectra for O 1*s* XPS [Figure 3(*b*)], which show a peak at 534 eV corresponding to the protonated form of OH groups at the oxide material surface ($M–OH_2^+$).

On the other hand, no adsorption of Cl^- ions at the $Mn_{1-x}Mo_xO_{2+x}$ electrode surface was detected by XPS at pH 8.0 in a sodium chloride solution (in the presence of a buffer system, Figure 4). The XPS data confirm the adsorption of Cl^- ions in weakly acidic media (or in non-buffered solutions, Figure 2) and no adsorption in a weakly alkaline solution (pH 8.0, Figure 4). It should be taken into account that experiments at pH 8.0

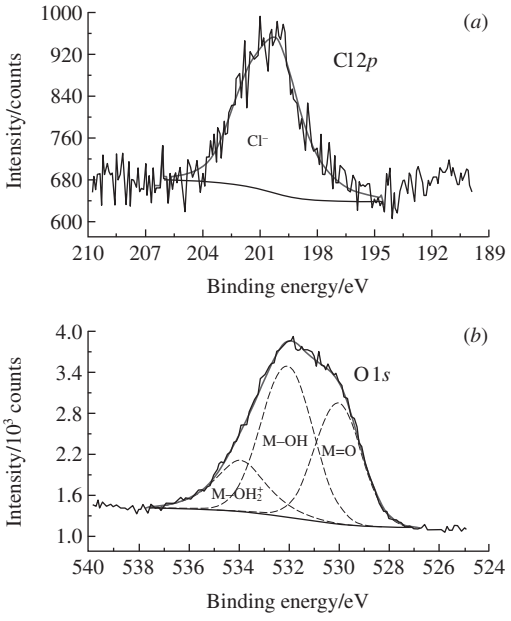

Figure 3 (*a*) Cl 2*p* and (*b*) O 1*s* XPS spectra obtained at the electrode surface after long-time electrolysis (10 h, 0.10 A cm^{-2}) in 0.5 M NaCl solution.

‡ The XPS studies were performed using a PHI 5500 ESCA X-ray photoelectron spectrometer (Physical Electronics) with monochromatic AlKα radiation ($h\nu$ = 1486.6 eV). The phase composition of oxide materials was determined by X-ray phase analysis (CuKα radiation).

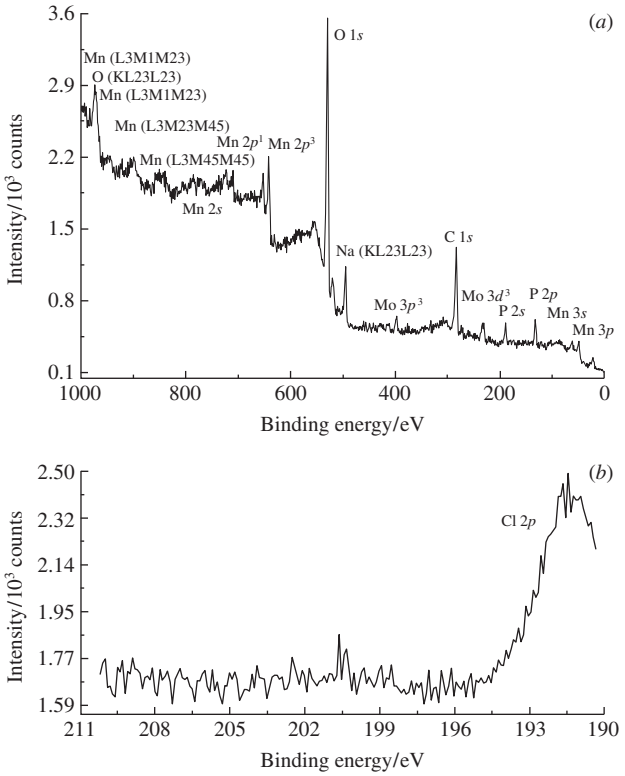

Figure 4 XPS spectra obtained at the $Mn_{1-x}Mo_xO_{2+x}$ electrode surface. Long-time electrolysis (10 h, 0.10 A cm^{-2}) was carried out in buffer solution (pH 8.0): (*a*) overall spectrum and (*b*) Cl 2*p* XPS spectrum.

were carried out in phosphate buffer solutions. Phosphate anions can displace Cl^- ions at the electrode surface. A very small amount of phosphorus can be found in the surface layer of $Mn_{1-x}Mo_xO_{2+x}$ (0–1 nm, Figure 4). Nevertheless, the displacement of Cl^- ions by PO_4^{3-} seems unlikely because phosphate ions are only slightly adsorbed at MnO_2 at pH > 7.0.[12]

The manganese content of the surface layer of $Mn_{1-x}Mo_xO_{2+x}$ anodes decreased in the course of prolonged electrolysis in non-buffered NaCl solutions [Figure 2(*a*)]. Such a decrease is caused by the formation of the soluble complexes $Mn(H_2O)_x(OH)_yCl_z^{(4-y-z)}$ and their subsequent removal from the electrode surface. This process leads to progressive anode degradation and sludge formation (MnO_2 as a result of hydrolysis in the bulk of solution). At the same time, these phenomena do not occur in sulfate solutions [Figure 2(*b*)].

No degradation of anodes occurs in buffered solutions at pH 8.0 because Cl^- ions are not adsorbed at the electrode under these conditions (Figure 4). Thus, in the long-time electrolysis of chloride-containing solutions, it is necessary to use buffer solutions to prevent the interaction of Cl^- ions with manganese oxides at electrode surface.

References

1 K. Izumiya, E. Akiyama, H. Habazaki, N. Kumagai, A. Kawashima and K. Hashimoto, *Electrochim. Acta*, 1998, **43**, 3303.
2 K. Fujimura, T. Matsui, H. Habazaki, A. Kawashima, N. Kumagai and K. Hashimoto, *Electrochim. Acta*, 2000, **45**, 2297.
3 N. A. Abdel Ghany, S. Meguro, N. Kumagai, K. Asami and K. Hashimoto, *Mater. Trans., JIM*, 2003, **44**, 2114.
4 V. V. Kuznetsov, O. A. Smakova, V. A. Kolesnikov, A. K. Evseev, A. G. Volkov and M. M. Goldin, *J. Electrochem. Soc.*, 2008, **155** (10), D671.
5 M. J. Gray, M. A. Malati and M. W. Rophael, *J. Electroanal. Chem.*, 1978, **89**, 135.
6 S. G. Bratsch, *J. Phys. Chem. Ref. Data*, 1989, **18**, 1.
7 M. R. Tarasevich, A. Sadkowski and E. Yeager, in *Comprehensive Treatise of Electrochemistry*, eds. B. E. Conway, J. O'M. Bockris, E. Yeager, S. U. M. Khan and R. E. White, Plenum Press, New York, 1983, vol. 7, p. 301.
8 L. A. Khanova, E. V. Kasatkin and V. I. Veselovskii, *Elektrokhimiya*, 1974, **10**, 800 (in Russian).
9 K. Macounova, M. Makarova and P. Krtil, *Electrochem. Commun.*, 2009, **11**, 1865.
10 L. I. Kristalik, *Electrochim. Acta*, 1981, **26**, 329.
11 V. V. Kuznetsov, K. E. Golyanin, T. V. Pshenichkina, B. F. Lyakhov and S. E. Lyashenko, *Mendeleev Commun.*, 2013, **23**, 331.
12 S. Mustafa, M. I. Zaman and S. Khan, *J. Collod Interface Sci.*, 2006, **301**, 370.

Received: 14th April 2014; Com. 14/4348

Available online at www.sciencedirect.com
ScienceDirect
Mendeleev Commun., 2014, **24**, 368–369
Mendeleev Communications

2-(2-Ethynyl-1-aziranyl)-3,4-dihydro-2*H*-pyrrole: a one-pot assembly from isopropyl phenyl ketoxime and acetylene during the synthesis of 3*H*-pyrrole

Dmitrii A. Shabalin, Tatyana E. Glotova, Igor A. Ushakov, Marina Yu. Dvorko, Alexander V. Vashchenko, Vladimir I. Smirnov, Elena Yu. Schmidt, Al'bina I. Mikhaleva and Boris A. Trofimov*

A. E. Favorsky Irkutsk Institute of Chemistry, Siberian Branch of the Russian Academy of Sciences, 664033 Irkutsk, Russian Federation. Fax: +7 3952 419 346; e-mail: boris_trofimov@irioch.irk.ru

DOI: 10.1016/j.mencom.2014.11.020

Reaction between isopropyl phenyl ketoxime and acetylene in the KOH–DMSO–*n*-hexane system (70 °C, ~5 min), along with known 3,3-dimethyl-2-phenyl-3*H*-pyrrole (51% yield) and 4,4-dimethyl-5-phenyl-1-vinyl-2-pyrrolidinone (7% yield), affords also unexpected 2-(2-ethynyl-3,3-dimethyl-2-phenyl-1-aziranyl)-4,4-dimethyl-5-phenyl-3,4-dihydro-2*H*-pyrrole (4% yield).

The most straightforward route to 3*H*-pyrroles by reaction between acetylene and ketoximes having just one α-hydrogen atom[1,2] still remains unoptimized. One means to improve moderate yields (~50%) of the target products seems in studying the intermediates and minor products of the reaction, which can shed light on the mechanism and hence provide better control of the process. The following intermediates and minor products have been isolated and identified: *O*-vinyloximes,[3] 2-hydroxypyrrolines,[4] pyrrolines,[5] and 4,4-dimethyl-5-phenyl-1-vinyl-2-pyrrolidinone,[6] most of them supporting the common mechanism[7] of the reaction course.

Here we report that during the further scrutinized work-up of the reaction mixture obtained from isopropyl phenyl ketoxime **1** and acetylene in the KOH–DMSO–*n*-hexane system (70 °C) we isolated and characterized (X-ray, ^{1}H, ^{13}C, ^{15}N NMR, IR, MS) the absolutely unexpected minor product, 2-(2-ethynyl-3,3-dimethyl-2-phenyl-1-aziranyl)-4,4-dimethyl-5-phenyl-3,4-dihydro-2*H*-pyrrole **2** apart from the regular 3,3-dimethyl-2-phenyl-3*H*-pyrrole **3**[1] and the aforementioned 4,4-dimethyl-5-phenyl-1-vinyl-2-pyrrolidinone **4**[6] (Scheme 1).†

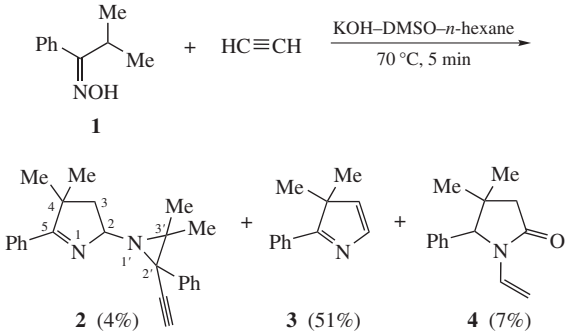

Scheme 1

† The IR spectra were recorded on a Bruker IFS25 spectrophotometer as KBr pellets or thin films. Mass spectra were measured on an Agilent 5975C spectrometer. Sample introduction was carried out through an Agilent 6890N gas chromatograph: the column was an HP-5MS (0.25 mm × 30 m × × 0.25 μm); carrier gas – helium, constant flow. NMR spectra were recorded on Bruker DPX-400 and AV-400 spectrometers (400.1 MHz for ^{1}H, 100.6 MHz for ^{13}C, and 40.5 MHz for ^{15}N) in $CDCl_3$ using HMDSO as internal standard. Basic aluminum oxide was used for column chromatography, and Silufol plates for TLC (eluent, hexane–diethyl ether, 1:1). Visualization was made with iodine vapor.

Although molecule **2** contains two asymmetric carbon atoms, only one diastereomer is formed: the NMR spectra manifest only one set of signals.

The structure of compound **2** unambiguously follows from single-crystal X-ray diffraction analysis (Figure 1)‡ and ^{1}H, ^{13}C

The reaction between isopropyl phenyl ketoxime **1** *and acetylene in the KOH–DMSO*–n-*hexane system*. A 0.3 dm^3 Parr reactor equipped with a magnetic stirrer (250 rpm) was charged with hexane (40 ml) and a potassium oximate solution in DMSO prepared by heating of a mixture of isopropyl phenyl ketoxime **1** (2.04 g, 12.5 mmol) and KOH·0.5H_2O (0.81 g, 12.5 mmol) in DMSO (50 ml) at 110–115 °C for 1 h. The reactor was fed with acetylene and then decompressed to atmospheric pressure to remove air. The reactor was fed again with acetylene (initial pressure was 10 atm) and heated up to 70 °C and then heating was immediately ceased that took overall 20 min (about 5 min at 70 °C). After cooling, the reaction mixture was discharged and the hexane layer was separated. The DMSO solution was poured into ice water (250 ml), neutralized with NH_4Cl, and extracted with diethyl ether (5×50 ml). The organic layers were combined, washed with H_2O (3×50 ml) and dried over $MgSO_4$ overnight. After distilling off the solvents, the residue (2.14 g, brown oil) was chromatographed on the column (1.9×30 cm, CH_2Cl_2 as eluent) to afford the fractions with R_f = 0.45–0.70 and 0.20–0.45.

By the repeated chromatography (1.8×20 cm, hexane–diethyl ether, 9:1) of the first fraction, 2-(2-ethynyl-3,3-dimethyl-2-phenyl-1-aziranyl)-4,4-dimethyl-5-phenyl-3,4-dihydro-2*H*-pyrrole **2** (0.09 g, 4%, R_f = 0.62) and 3,3-dimethyl-2-phenyl-3*H*-pyrrole **3** (1.09 g, 51%, R_f = 0.49) were isolated.

From the second fraction, 0.19 g (7%, R_f = 0.42) of 4,4-dimethyl-5-phenyl-1-vinyl-2-pyrrolidinone **4** was isolated by the repeated column chromatography (1.2×20 cm, hexane–diethyl ether, 3:1).

Physical-chemical characteristics of the isolated compounds corresponded to the literature data: compound **3**,[1] compound **4**.[6]

*2-(2-Ethynyl-3,3-dimethyl-2-phenyl-1-aziranyl)-4,4-dimethyl-5-phenyl-3,4-dihydro-2*H*-pyrrole* **2**: colourless crystals, mp 118–120 °C (hexane). IR (KBr, ν/cm^{-1}): 3229, 2962, 2929, 2106, 1628, 1601, 1492, 1449, 1339, 1147, 765, 697. ^{1}H NMR ($CDCl_3$) δ: 1.00 (s, 3H, C$^{3'}$Me), 1.42 (s, 3H, C^{4}Me), 1.50 (s, 3H, C^{4}Me), 1.75 (s, 3H, C$^{3'}$Me), 2.09 (dd, 1H, CH_2, ^3J 7.1 Hz, ^2J 12.5 Hz), 2.31 (dd, 1H, CH_2, ^3J 6.4 Hz, ^2J 12.5 Hz), 2.47 (s, 1H, ≡CH), 4.84 (dd, 1H, CH, ^3J 6.4 Hz, ^3J 7.1 Hz), 7.26 (m, 1H, *p*-H, C$^{2'}$Ph), 7.34 (m, 2H, *m*-H, C$^{2'}$Ph), 7.40 (m, 3H, *p*-H, *m*-H, C^{5}Ph), 7.58 (m, 2H, *o*-H, C$^{2'}$Ph), 7.80 (m, 2H, *o*-H, C^{5}Ph). ^{13}C NMR ($CDCl_3$) δ: 16.6 (C$^{3'}$*Me*), 23.4 (C$^{3'}$*Me*), 26.8 (C^4*Me*), 27.6 (C^4*Me*), 45.8 (C$^{2'}$), 48.7 (C^3), 49.6 (C$^{3'}$), 50.5 (C^4), 73.2 (C≡*C*H), 82.6 (C^2), 82.7 (*C*≡CH), 127.2 (*p*-C, C$^{2'}$Ph), 128.0 (*o*-C, *m*-C, C$^{2'}$Ph), 128.2 (*m*-C, C^{5}Ph), 128.3 (*o*-C, C^{5}Ph), 129.6 (*p*-C, C^{5}Ph), 134.9 (*i*-C, C^{5}Ph), 139.5 (*i*-C, C$^{2'}$Ph), 181.2 (C=N). ^{15}N NMR ($CDCl_3$) δ: –309.2 (N$^{1'}$), –50.0 (N^1). MS (EI), *m*/*z*: 342 [M]$^+$.

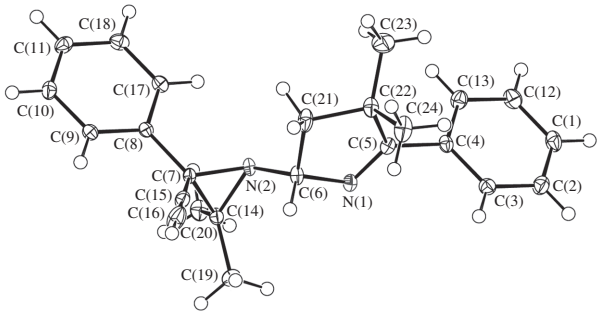

Figure 1 X-ray structure of 2-(2-ethynyl-3,3-dimethyl-2-phenyl-1-aziranyl)-4,4-dimethyl-5-phenyl-3,4-dihydro-2*H*-pyrrole. Thermal ellipsoids set at 50% probability.

and ^{15}N NMR spectra. The signals in the ^{1}H and ^{13}C NMR spectra have been assigned using 2D NMR technique (COSY, NOESY, HSQC and HMBC). So, the resonance lines at 1.42 and 1.50 ppm are attributed to the methyl groups in the 4-position of the pyrroline cycle according to correlations (2D NOESY) with 3-CH_2 and *o*-H protons of the phenyl cycle in the 5-position. The signals of the methyl groups in the 3′-position (1.00 and 1.75 ppm) show NOE only with *o*-H protons of the phenyl substituent in the 2′-position. In the 2D ^{1}H-^{13}C HMBC spectrum, long-range spin–spin interactions are observed that allows the resonance lines of quaternary carbon atoms to assign unambiguously in the ^{13}C NMR spectra. The values of chemical shifts of nitrogen atoms in the ^{15}N NMR spectrum, obtained from 2D heteronuclear spectra ^{1}H-^{15}N HMBC, confirm the presence of two different nitrogen atoms (sp^3-N$^{1'}$ and sp^2-N^1) in compound **2**.

The assembly of aziranylpyrroline **2** likely involves Hoch–Campbell-like[8] dehydration of the starting oxime **1** or elimination of vinyl alcohol from the intermediate *O*-vinylketoxime **A**[9] to afford azirine **B** which undergoes the Favorsky-type ethynylation involving C=N bond to give ethynylaziridine **C** (Scheme 2). The latter couples with hydroxypyrroline **D**, an isolable intermediate of the pyrrole synthesis from ketoximes and acetylene,[4] to eliminate the molecule of water finalizing the assembly of compound **2**.

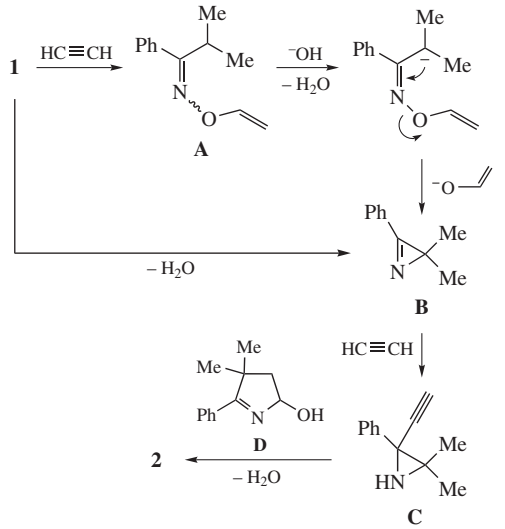

Scheme 2

The replacement of the hydroxyl group in hydroxypyrroline **D** by the aziranyl moiety closely relates to the Mannich type processes. Hydroxypyrroline **D** is the product of subsequent *O*-vinylketoxime **A** rearrangements (1,3-prototropic and 3,3-sigmatropic shifts) followed by cyclization of the formed imino aldehyde (Scheme 3).[4]

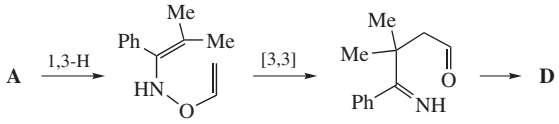

Scheme 3

The diastereoselectivity of the reaction implies the stereoselective ethynylation of the intermediate azirine **B** which should be of *trans*-mode judging from the mutual disposition of the substituents in the aziridine ring.

Despite the low (though non-optimized) yield of the acetylenic aziranylpyrroline, its simple one-pot preparation from inexpensive widespread basic chemicals deserves attention from both pharmaceutical and synthetic points of view. Pharmaceutically, the rare combination of pharmacophoric fragments in one molecule may result in novel useful properties. Synthetically, the alternative approach to such complex multi-functional molecules should inevitably be multi-step and laborious and consequently far from good total yields. We intend to further develop this conceptually new synthesis.

This work was supported by the Russian Foundation for Basic Research (grant no. 14-03-00426).

References

1 B. A. Trofimov, S. G. Shevchenko, S. E. Korostova, A. I. Mikhaleva and V. V. Shcherbakov, *Chem. Heterocycl. Compd*., 1985, **21**, 1299 (*Khim. Geterotsikl. Soedin*., 1985, 1573).
2 S. E. Korostova, S. G. Shevchenko and M. V. Sigalov, *Chem. Heterocycl. Compd*., 1991, **27**, 1101 (*Khim. Geterotsikl. Soedin*., 1991, 1371).
3 B. A. Trofimov, A. I. Mikhaleva, A. M. Vasil'tsov, E. Yu. Schmidt, O. A. Tarasova, L. V. Morozova, L. N. Sobenina, T. Preiss and J. Henkelmann, *Synthesis*, 2000, 1125.
4 B. A. Trofimov, S. E. Korostova, A. I. Mikhaleva, L. N. Sobenina, V. V. Shcherbakov and M. V. Sigalov, *Chem. Heterocycl. Compd.*, 1983, **19**, 231 (*Khim. Geterotsikl. Soedin*., 1983, 276).
5 S. E. Korostova, S. G. Shevchenko and V. V. Shcherbakov, *Zh. Org. Khim*., 1993, **29**, 1639 (in Russian).
6 D. A. Shabalin, T. E. Glotova, E. Yu. Schmidt, I. A. Ushakov, A. I. Mikhaleva and B. A. Trofimov, *Mendeleev Commun*., 2014, **24**, 100.
7 (*a*) B. A. Trofimov, A. I. Mikhaleva, E. Yu. Schmidt and L. N. Sobenina, in *Advances in Heterocyclic Chemistry*, ed. A. R. Katritzky, Academic Press, Oxford, 2010, vol. 99, p. 209; (*b*) B. A. Trofimov, A. I. Mikhaleva, E. Yu. Schmidt and L. N. Sobenina, *Khimiya pirrola. Novye stranitsy (Chemistry of Pyrrole. New Pages)*, Nauka, Novosibirsk, 2012 (in Russian).
8 (*a*) J. Hoch, *Compt. Rend*., 1934, **198**, 1865; (*b*) K. N. Campbell and J. F. McKenna, *J. Org. Chem*., 1939, **4**, 198.
9 (*a*) B. A. Trofimov, E. Yu. Schmidt, A. I. Mikhaleva, N. V. Zorina, I. A. Ushakov, A. V. Afonin and A. M. Vasil'tsov, *Mendeleev Commun*., 2007, **17**, 40; (*b*) B. A. Trofimov, E. Yu. Schmidt, A. I. Mikhaleva, I. A. Ushakov, N. I. Protsuk, E. Yu. Senotrusova, O. N. Kazheva, G. G. Aleksandrov and O. A. Dyachenko, *Tetrahedron Lett*., 2009, **50**, 3314.
10 G. M. Sheldrick, *Acta Crystallogr*., 2008, **D64**, 112.

Received: 2nd April 2014; Com. 14/4340

‡ *Crystal data for* **2**. Single crystals of **2** were grown from acetonitrile. The determination of the unit cell and the data collection was performed on a Bruker D8 VENTURE PHOTON 100 CMOS diffractometer with MoKα radiation (λ = 0.71073 Å) at 100(2) K using the ω–2θ scan technique. The final cell constants of a = 6.8105(5), b = 24.082(2) and c = 11.8292(10) Å, β = 94.450(3)°, V = 1934.3(3) Å^3, are based upon the refinement of the *XYZ*-centroids of 9914 reflections above 20σ(I) with 4.834° < 2θ < 59.69°. The structure was solved and refined using the Bruker SHELXTL Software Package, using the space group $P2_1/n$, with Z = 4 for the formula unit, $C_{24}H_{26}N_2$. The dihedral angle between the averaged planes of the benzene and pyrrole rings is 104.0°.

CCDC 992245 contains the supplementary crystallographic data for this paper. These data can be obtained free of charge from The Cambridge Crystallographic Data Centre *via* http://www.ccdc.cam.ac.uk. For details, see 'Notice to Authors', *Mendeleev Commun.*, Issue 1, 2014.

Available online at www.sciencedirect.com
ScienceDirect
Mendeleev Commun., 2014, **24**, 370–371
Mendeleev Communications

Synthesis of 5-hydroxy-4-methoxytricyclo[7.3.1.0^{2,7}]trideca-2,4,6-trien-8-one – precursor of putative bioisosteric colchicine analogues

Dmitrii V. Shishov,[a] Evgeniya V. Nurieva,[a] Nikolay A. Zefirov,[a] Alexandra V. Mamaeva[a] and Olga N. Zefirova*[a,b]

[a] *Department of Chemistry, M. V. Lomonosov Moscow State University, 119991 Moscow, Russian Federation. Fax: +7 495 939 0290; e-mail: olgaz@org.chem.msu.ru*
[b] *Institute of Physiologically Active Compounds, Russian Academy of Sciences, 142432 Chernogolovka, Moscow Region, Russian Federation*

DOI: 10.1016/j.mencom.2014.11.021

5-Hydroxy-4-methoxytricyclo[7.3.1.0^{2,7}]trideca-2,4,6-trien-8-one was synthesized from 1-benzyloxy-4-bromo-2-methoxybenzene in six steps comprising Corey–Chaykovsky epoxidation and Friedel–Crafts intramolecular cyclization. The crystal structure of the benzyl-protected derivative of the target compound was determined by X-ray analysis.

Last decade we were involved in the design and synthesis of physiologically active compounds with bridged and caged fragments (see, *e.g.*, refs. 1–8). We studied, in particular, the application of bridged groups for bioisosteric replacement of polycyclic cores of antitumour compounds taxol[9] and colchicine.[10] Based on the molecular modeling data, bicyclo[3.3.1]nonane derivatives **1** and **2** (R is ester, alkyl or alcohol moieties) were suggested as putative ligands of colchicine binding site in cell protein tubulin. However, the access to structural template **1** by the Diels–Alder strategy was not successful.[10] Herein, we report the synthesis of close in structure representative template **2** with R = H.

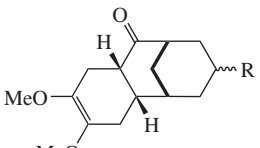

1

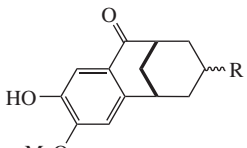

2

The target compound was synthesized in six steps (Scheme 1) from 1-benzyloxy-4-bromo-2-methoxybenzene **3** (obtained in two steps from guaiacol[11,12]). Copper-catalyzed conjugate addition[13] of arylmagnesium bromide obtained from **3** to 2-cyclohexenone gave product **4**. In the ^{1}H NMR spectrum of compound **4**, the axial proton at the C^3 atom of the cyclohexane ring resonates as triplet of triplets at 2.97 ppm (1H) with H–H coupling constant ^3J 11.6 Hz. Ketone **4** was subjected to the Corey–Chaykovsky epoxidation with dimethylsulfoxonium methylide generated *in situ* from trimethylsulfoxonium iodide in the presence of sodium hydride[14] to afford oxirane **5** as individual diastereomer in a high yield. The appearance of the signals of two additional (in comparison with **4**) aliphatic protons in the area of 2.60–2.80 ppm in ^{1}H NMR spectrum of **5** and the additional resonance of the carbon atom at 53.98 ppm in ^{13}C NMR spectrum proves the formation of the oxirane fragment. The product was assigned *trans*-configuration in compliance with the previous studies.[15]

The BF_3-assisted opening of epoxide in **5** gave aldehyde **6** as *cis*-isomer (the signal of the aldehyde proton in ^{1}H NMR spectrum is observed at 9.67 ppm, ^3J of the multiplets of H^1 and H^3 cyclohexyl protons are 11.9 and 13.4 Hz, respectively). Low isolated yield of compound **6** was due to the numerous reaction by-products one of which was separated and characterized as compound **6′** (two singlets of annelated aryl protons are observed at 6.62 and 6.72 ppm in ^{1}H NMR spectrum, whereas ^{13}C NMR spectrum comprises seven signals of alicyclic carbon atoms).

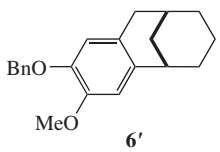

6′

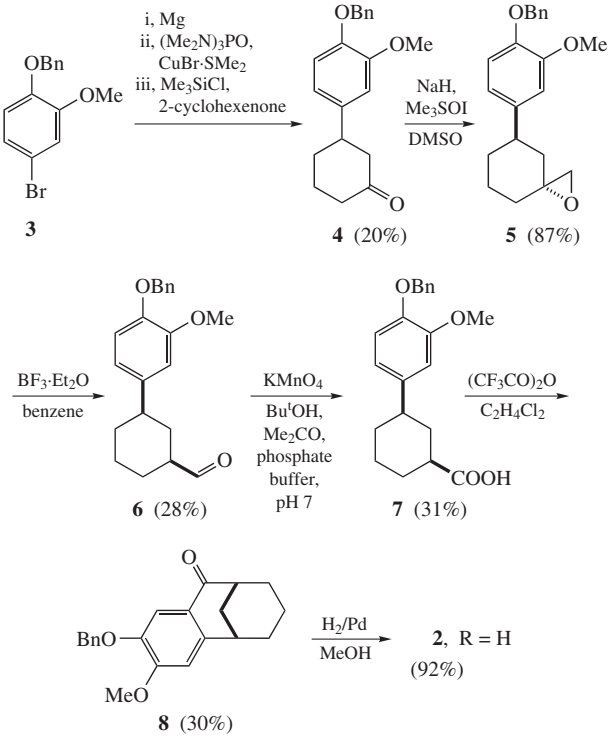

3 **4** (20%) **5** (87%) **6** (28%) **7** (31%) **8** (30%) **2**, R = H (92%)

Scheme 1

Literature survey gave no examples of similar intramolecular cyclization joint with auto reduction for aryl-substituted epoxides, so this reaction is the subject of our further detailed studies.

The following oxidation of compound **6** to a corresponding acid met some difficulties. An attempt to apply Oxone oxidizing agent was not successful, while the use of freshly prepared Ag_2O afforded acid **7** in a very low yield (11%). Only the treatment of aldehyde **6** with $KMnO_4$ at neutral pH gave carboxylic acid **7** in acceptable yield of 31% (the carboxylic group is displayed as a resonance at 181.82 ppm in ^{13}C NMR spectrum of **7**).

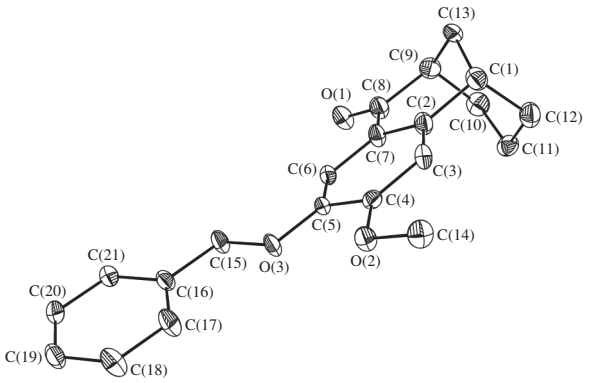

Figure 1 The general view of 5-benzyloxy-4-methoxytricyclo[7.3.1.0^{2,7}]-trideca-2,4,6-trien-8-one **8** in representation of atoms by thermal ellipsoids (p = 50%).

The Friedel–Crafts intramolecular cyclization[16] was performed for compound **7** to afford bicyclo[3.3.1]nonanone, annelated with the aromatic core, **8**. The structure of compound **8** was unambiguously proved by X-ray diffraction analysis.† According to these data (Figure 1), the six-membered ring C(1)–C(13)–C(9)–C(10)–C(11)–C(12) of the bicyclic fragment has Zefirov–Palyulin (ZP) and Cremer–Pople (CP) puckering parameters (calculated by RICON program[17]) S_2 = 0.085, θ = 4.2°, ψ_2 = = 22.0°, σ = 0.33 (ZP) and Q = 0.587, θ = 8.6°, φ_2 = 21.4° (CP), which correspond to the slightly distorted chair conformation. The ring C(1)–C(2)–C(7)–C(8)–C(9)–C(13) is strongly flattened (ZP: S_2 = 0.501, θ = 38.8°, ψ_2 = 3.7°, σ = 0.79; CP: Q = 0.534, θ = 54.1°, φ_2 = 3.3°) and adopts a conformation of slightly distorted envelope.

Deprotection of compound **8** led to the target compound **2** in a 92% yield. The spectral and elemental analysis data prove the structure of ketone **2** (R = H).

In summary, a six-step scheme for constructing 5-hydroxy-4-methoxytricyclo[7.3.1.0^{2,7}]trideca-2,4,6-trien-8-one skeleton using Corey–Chaykovsky epoxidation and Friedel–Crafts intramolecular cyclization was elaborated. The scheme is useful for the further synthesis of putative ligands of colchicine binding site in β-tubulin, which is now in progress and will be published in due course.

This work was supported by the Russian Foundation for Basic Research (project no. 12-03-00720) and Russian Academy of Sciences (OHNM-9). Part of the equipment was purchased at the expense of M. V. Lomonosov Moscow State University Program of Development. Authors are grateful to Dr. K. A. Lyssenko for his kind help with the X-ray crystallography experiment.

Online Supplementary Materials

Supplementary data associated with this article can be found in the online version at doi:10.1016/j.mencom.2014.11.021.

† *Crystallographic data.* Crystals of **8** ($C_{21}H_{22}O_3$, M = 322.39, from CH_2Cl_2) are tetragonal, space group $I4_1/a$, at 100(2) K: a = 18.6581(16), b = 18.6581(16) and c = 19.0674(17) Å, V = 6637.8(10) Å^3, Z = 16, d_{calc} = = 1.290 g cm^{-3}, μ(MoKα) = 0.085 cm^{-1}. Intensities of 35 250 reflections were measured with Bruker APEX-II CCD [λ(MoKα) = 0.71073 Å, 2θ < 58°] and 3820 independent reflections were used in the further refinement. The structure was solved by direct method and refined by the full-matrix least-squares technique against F^2 in the anisotropic–isotropic approximation. The refinement converged to wR_2 = 0.1567 and GOF = 1.042 for all independent reflections [R_1 = 0.0561 was calculated against F for 3114 observed reflections with $I > 2\sigma(I)$]. All calculations were performed using SHELXTL PLUS 5.1.

CCDC 992187 contains the supplementary crystallographic data for this paper. These data can be obtained free of charge from The Cambridge Crystallographic Data Centre *via* http://www.ccdc.cam.ac.uk. For details, see 'Notice to Authors', *Mendeleev Commun.*, Issue 1, 2014.

References

1 O. N. Zefirova, E. D. Plotnikova, E. V. Nurieva, D. I. Peregud, M. V. Onufriev and N. V. Gulyaeva, *Mendeleev Commun*., 2013, **23**, 76.
2 O. N. Zefirova, H. Lemcke, M. Lantow, E. V. Nurieva, B. Wobith, G. E. Onishchenko, A. Hoenen, G. Griffiths, N. S. Zefirov and S. A. Kuznetsov, *ChemBioChem*, 2013, **14**, 1444.
3 O. N. Zefirova, T. Yu. Baranova, K. A. Lyssenko, N. A. Zefirov, N. V. Zyk, P. M. Vassiliev, D. S. Yakovlev and A. A. Spasov, *Mendeleev Commun*., 2012, **22**, 75.
4 O. N. Zefirova, I. S. Raguzin, V. V. Gogol, E. V. Nurieva and M. S. Belenikin, *Mendeleev Commun*., 2011, **21**, 242.
5 O. N. Zefirova, T. Yu. Baranova, A. A. Ivanova, A. A. Ivanov and N. S. Zefirov, *Bioorg. Chem*., 2011, **39**, 67.
6 O. N. Zefirova, E. V. Nurieva, V. I. Chupakhin, I. S. Semenova, D. I. Peregud, M. V. Onufriev and N. V. Gulyaeva, *Mendeleev Commun.*, 2010, **20**, 323.
7 T. Yu. Baranova, N. V. Averina, N. V. Zyk, N. S. Zefirov, K. A. Lyssenko, M. Yu. Antipin and O. N. Zefirova, *Mendeleev Commun*., 2009, **19**, 10.
8 O. N. Zefirova and N. S. Zefirov, *Russ. Chem. Bull., Int. Ed*., 2013, **62**, 325 (*Izv. Akad. Nauk, Ser. Khim.*, 2013, 329).
9 O. N. Zefirova, E. V. Nurieva, H. Lemcke, A. A. Ivanov, N. V. Zyk, D. G. Weiss, S. A. Kuznetsov and N. S. Zefirov, *Mendeleev Commun*., 2008, **18**, 183.
10 E. V. Nurieva, I. S. Semenova, V. N. Nuriev, D. V. Shishov, I. I. Baskin, O. N. Zefirova and N. S. Zefirov, *Russ. J. Org. Chem*., 2010, **46**, 1892 (*Zh. Org. Khim*., 2010, **46**, 1877).
11 N. Fujikawa, T. Ohta, T. Yamaguchi, T. Fukuda, F. Ishibashi and M. Iwao, *Tetrahedron*, 2006, **62**, 594.
12 S. Cardinal and N. Voyer, *Tetrahedron Lett*., 2013, **54**, 5178.
13 G. Varchi, A. Ricci, G. Cahiez and P. Knochel, *Tetrahedron*, 2000, **56**, 2727.
14 E. J. Corey and M. Chaykovsky, *J. Am. Chem. Soc.*, 1965, **87**, 1353.
15 F. Toda and N. Imai, *J. Chem. Soc., Perkin Trans. 1*, 1994, 2673.
16 Y. Ohtsuka and A. Tahara, *Chem. Pharm. Bull*., 1973, **21**, 643.
17 A. Yu. Zotov, V. A. Palyulin and N. S. Zefirov, *J. Chem. Inf. Comput. Sci.*, 1997, **37**, 766.

Received: 17th March 2014; Com. 14/4325

Available online at www.sciencedirect.com
ScienceDirect
Mendeleev Commun., 2014, **24**, 372–373
Mendeleev Communications

Synthesis of the C^6–C^{21} fragment of epothilone analogues

Ruslan F. Valeev,* Radmir F. Bikzhanov and Mansur S. Miftakhov

Institute of Organic Chemistry, Ufa Scientific Centre of the Russian Academy of Sciences, 450054 Ufa, Russian Federation. Fax: +7 347 235 6066; e-mail: rusl0@yandex.ru

DOI: 10.1016/j.mencom.2014.11.022

(2*S*,4*E*,6*Z*,9*S*,10*E*)-9-[*tert*-Butyl(diphenyl)silyloxymethyl]-2,6,10-trimethyl-11-(2-methylthiazol-4-yl)undeca-4,6,10-trien-1-ol, a key precursor for epothilone analogues, was prepared by multi-step synthesis using the Julia–Kocienski olefination at the key step.

Among microtubule stabilizing natural products (taxol, discodermolide, dictyostatin),[1–4] the sixteen-membered epothilones (Epo)[5] are one of the most prospective candidates for drug development (Scheme 1).[6,†] Many different epothilone analogues have been synthesized and studied,[6–9] thus providing a rather comprehensive understanding of the structure–activity relationship for epothilone class of compounds. We concentrated on the synthesis of a novel type epothilone structure **3** in which the methylene unit is isosterically displaced in the C^{15}–C^3 fragment.[10] Once we obtained the northern C^{10}–C^{21} fragment of an Epo analogue **6**,[10] we planned to synthesize the C^6–C^9 chiral block, which seemed promising to be coupled with C^{10}–C^{21} carbon chain. The Julia–Kocienski olefination[11] as the coupling strategy was chosen, therefore sulfone **5** was required. The chiral building block **4** can be used in the total synthesis of an Epo D analogue **1** since the selective C^9–C^{10} double bond reduction in unsaturated analogue Epo 490 **2**[12] is possible.[12]

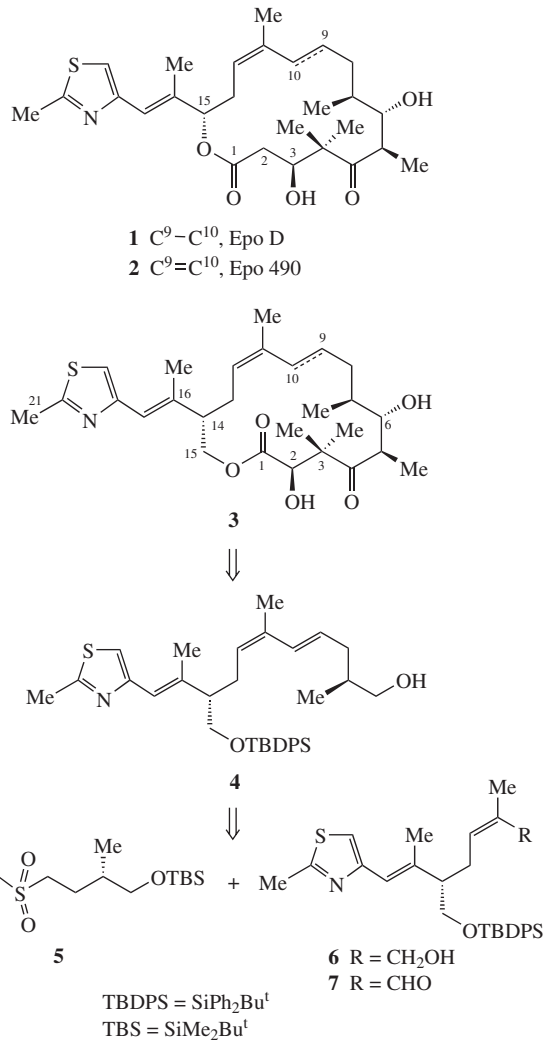

Scheme 1

4-Bromobutyryl chloride was used as a starting compound for the synthesis of compound **5** (Scheme 2).† To introduce the chiral center in the target molecule, the Evans asymmetric alkylation[13] was chosen. The chiral auxiliary **8** was prepared from L-valine as described.[14] 4-Bromobutyryl chloride reacted with lithium derivative of **8** giving bromo amide **9**. Subsequent substitution of bromine by the action of 1-phenyl-1*H*-tetrazole-5-thiol in the presence of Na_2CO_3 resulted in sulfide **10**. Methylation of the sodium enolate of **10** with MeI at –78 °C furnished a mixture of diastereomers in a ratio of 1:10 (according to ^{1}H NMR) with the predominance of the (*S*)-isomer **11**. Reduction of **11** with $LiAlH_4$ provided an inseparable mixture of products (by TLC analysis) which was subjected to oxidation with H_2O_2 in the

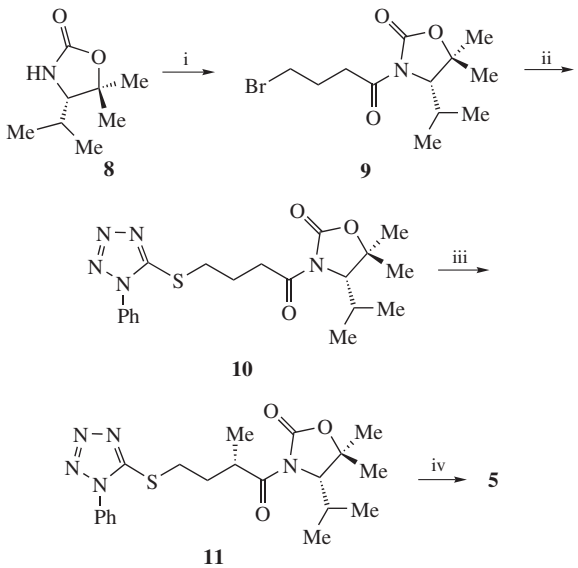

Scheme 2 *Reagents and conditions*: i, BuLi, –80 °C, 40 min, then $Br(CH_2)_3C(O)Cl$, –80 °C, 2 h, 84%; ii, 1-phenyl-1*H*-tetrazole-5-thiol, Na_2CO_3, acetone, room temperature, 12 h, 88%; iii, $NaN(SiMe_3)_2$ (NaHMDS), –78 °C, 1 h, then MeI, –70 °C for 2 h, 85%; iv, $LiAlH_4$, THF, 5 °C, 30 min, room temperature, 1 h, then $(NH_4)_6Mo_7O_{24}\cdot4H_2O$, 30% aqueous H_2O_2, EtOH, room temperature, 12 h, then Bu^tSiMe_2Cl (TBSCl), imidazole, DMAP, CH_2Cl_2, room temperature, 8 h (65% yield for 3 steps).

† For experimental details and characteristics of compounds obtained, see Online Supplementary Materials.

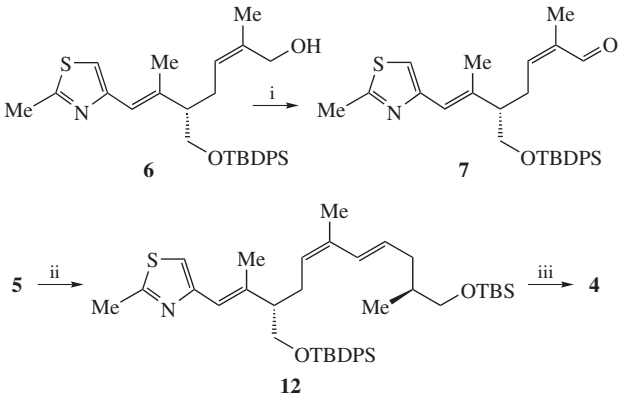

Scheme 3 *Reagents and conditions*: i, 2,2,6,6-tetramethylpiperidine-*N*-oxyl (TEMPO), $PhI(OAc)_2$, CH_2Cl_2, room temperature, 6 h, 93%; ii, KHMDS, –78 °C for 20 min, then **7**, –78 °C, 30 min, 86%; iii, *p*-TSA, MeOH–CH_2Cl_2 (1:1), 15 °C, 12 h, 95%.

presence of ammonium heptamolybdate in EtOH.[15] After standard workup the crude product was treated with TBSCl followed by the separation of the resulting sulfone **5** and recovered oxazolidinone **8** using column chromatography.

The careful oxidation of thiazole-containing alcohol **6** was achieved under mild conditions by the action of $PhI(OAc)_2$ under TEMPO catalysis (Scheme 3).† The coupling **5** + **7** was accomplished using the Julia–Kocienski method. The coupling proceeds rapidly affording *E*-isomer **12** exclusively (^{1}H NMR, $J_{C^9H–C^{10}H}$ 15.6 Hz). Upon analysis of the ^{1}H and ^{13}C NMR spectra of **12**,‡ none of the other isomers was detected.

Finally, the selective hydrolysis of the TBS-protecting group in **12** has been achieved in MeOH–CH_2Cl_2 solution under *p*-TSA catalysis. Thus, the synthesized C^6–C^{21} fragment as monoprotected diol **4** ‡ can be used for the further selective transformations.

Online Supplementary Materials

Supplementary data associated with this article can be found in the online version at doi:10.1016/j.mencom.2014.11.022.

References

1 D. G. I. Kingston, *Chem. Biol.*, 2004, **11**, 153.
2 F. Feyen, F. Cachoux, J. Gertsch, M. Wartmann and K.-H. Altmann, *Acc. Chem. Res.*, 2008, **41**, 21.
3 C. R. Harris and S. J. Danishefsky, *J. Org. Chem.*, 1999, **64**, 8434.
4 C. Monti, O. Sharon and C. Gennari, *Chem. Commun.*, 2007, 4271.
5 K. Gerth, N. Bedorf, G. Höfle, H. Irshik and H. Reichenbach, *J. Antibiotics*, 1996, **49**, 560.
6 J. Mulzer, K.-H. Altmann, G. Höfle, R. Müller and K. Prantz, *C. R. Chim.*, 2008, **11**, 1336.
7 A. Conlin, M. Fornier, C. Hudis, S. Kar and P. Kirkpatrick, *Nat. Rev. Drug Discov.*, 2007, **6**, 953.
8 F. Cachoux, T. Isarno, M. Wartmann and K. H. Altmann, *Angew. Chem. Int. Ed.*, 2005, **44**, 7469.
9 A. Rivkin, F. Yoshimura, A. E. Gabarda, T. C. Chou, H. J. Dong, W. P. Tong and S. J. Danishefsky, *J. Am. Chem. Soc.*, 2003, **125**, 2899.
10 R. F. Valeev, R. F. Bikzhanov, N. Z. Yagafarov and M. S. Miftakhov, *Tetrahedron*, 2012, **68**, 6868.
11 P. R. Blakemore, W. J. Cole, P. J. Kocienski and A. Morley, *Synlett.*, 1998, **1**, 26.
12 K. Biswas, H. Lin, J. T. Njardarson, M. D. Chappell, T.-C. Chou, Y. Guan, W. P. Tong, L. He, S. B. Horwitz and S. J. Danishefsky, *J. Am. Chem. Soc.*, 2002, **124**, 9825.
13 D. A. Evans, M. D. Ennis and D. J. Mathre, *J. Am. Chem. Soc.*, 1982, **104**, 1737.
14 S. D. Bull, S. G. Davies, S. Jones and H. J. Sanganee, *J. Chem. Soc., Perkin Trans. 1*, 1999, 387.
15 B. M. Trost, D. Amans, W. M. Seganish and C. K. Chung, *J. Am. Chem. Soc.*, 2009, **131**, 17087.

Received: 11th April 2014; Com. 14/4347

‡ *4-{(1*E*,3*S*,5*Z*,7*E*,10*S*)-11-[*tert*-Butyl(dimethyl)silyloxy]-3-[*tert*-butyl(diphenyl)silyloxymethyl]-2,6,10-trimethylundeca-1,5,7-trien-1-yl}-2-methyl-1,3-thiazole* **12**. 1.5 M solution of KHMDS in THF (1.1 ml, 1.65 mmol) was added to a stirred solution of sulfone **5** (0.34 g, 0.83 mmol) in dry THF (15 ml) under Ar at –78 °C. After stirring this mixture for 20 min, aldehyde **7** (0.32 g, 0.63 mmol) was added *via* cannula as a solution in THF (5 ml). The mixture was stirred for 30 min at –78 °C, then the cooling bath was removed, and the mixture was allowed to warm to room temperature. A saturated aqueous solution of NH_4Cl (20 ml) was added, the layers were separated, the aqueous one was extracted with ethyl acetate (3×20 ml), the combined organic phase was dried over $MgSO_4$, filtered and evaporated. Purification of the residue by column chromatography (9% ethyl acetate–light petroleum) afforded **12** (0.38 g, 86%) as a colourless liquid. R_f (20% ethyl acetate–light petroleum) 0.62; $[\alpha]_D^{20}$ –1.3 (*c* 1.53, CH_2Cl_2). IR (Nujol mull, ν_{max}/cm^{-1}): 3428, 2956, 2929, 2857, 1462, 1112, 837, 702, 505. ^{1}H NMR (300 MHz, $CDCl_3$) δ: 0.04 (s, 6H), 0.87 (d, 3H, *J* 7.0 Hz), 0.90 (s, 9H), 1.04 (s, 9H), 1.72–1.74 (m, 1H), 1.76 (s, 3H), 1.89–1.90 (m, 1H), 1.91 (s, 3H), 2.23–2.64 (m, 4H), 2.70 (s, 3H), 3.41–3.43 (m, 2H), 3.67–3.72 (m, 2H), 5.20 (t, 1H, *J* 7.0 Hz), 5.57–5.68 (m, 1H), 6.35 (s, 1H), 6.45 (d, 1H, *J* 15.6 Hz), 6.83 (s, 1H), 7.33–7.40 (m, 6H), 7.65 (d, 4H, *J* 6.7 Hz). ^{13}C NMR (75 MHz, $CDCl_3$) δ: –5.4, 14.2, 16.6, 18.3, 19.1, 19.2, 20.7, 26.0, 26.9, 27.5, 36.3, 37.0, 52.3, 66.1, 67.9, 114.5, 120.6, 126.3, 127.6, 128.5, 129.0, 129.5, 132.7, 133.8, 135.7, 141.0, 153.5, 164.1. MS (APCI), *m/z*: 721 (66), 704 (100), 689 (24, MH$^+$). Found (%): C, 71.28; H, 8.76; N, 1.89; S, 4.62. Calc. for $C_{41}H_{61}NO_2SSi_2$ (%): C, 71.56; H, 8.93; N, 2.04; S, 4.66.

*(2*S*,4*E*,6*Z*,9*S*,10*E*)-9-[*tert*-Butyl(diphenyl)silyloxymethyl]-2,6,10-trimethyl-11-(2-methyl-1,3-thiazol-4-yl)undeca-4,6,10-trien-1-ol* **4**. *p*-TSA (0.01 g, 0.08 mmol) was added to an ice-bath cooled solution of compound **12** (0.26 g, 0.38 mmol) in MeOH–CH_2Cl_2 (1:1, 20 ml). The mixture was stirred at 15 °C for 12 h, then it was quenched with solid $NaHCO_3$ and filtered. The filtrate was evaporated and the residue was purified by column chromatography (30% ethyl acetate–light petroleum) to provide **4** (0.21 g, 95%) as a light yellow oil. R_f (20% ethyl acetate–light petroleum) 0.21; $[\alpha]_D^{20}$ –0.7 (*c* 1.14, CH_2Cl_2). IR (Nujol mull, ν_{max}/cm^{-1}): 3374, 2956, 2929, 2857, 1428, 1112, 702, 505. ^{1}H NMR (300 MHz, $CDCl_3$) δ: 0.92 (d, 3H, *J* 7.0 Hz), 1.05 (s, 9H), 1.72–1.73 (m, 1H), 1.76 (s, 3H), 1.91 (s, 3H), 1.98–2.05 (m, 1H), 2.19–2.31 (m, 2H), 2.40–2.59 (m, 2H), 2.71 (s, 3H), 3.41–3.51 (m, 2H), 3.65–3.73 (m, 2H), 5.22 (t, 1H, *J* 7.0 Hz), 5.63–5.68 (m, 1H), 6.34 (s, 1H), 6.48 (d, 1H, *J* 15.6 Hz), 6.84 (s, 1H), 7.35–7.41 (m, 6H), 7.65 (d, 4H, *J* 6.7 Hz). ^{13}C NMR (75 MHz, $CDCl_3$) δ: 16.7, 16.9, 19.1, 19.3, 20.7, 26.9, 27.6, 36.1, 37.0, 52.4, 66.1, 67.7, 114.5, 120.5, 126.8, 127.6, 128.3, 128.9, 129.6, 132.6, 133.8, 135.7, 141.1, 153.4, 164.2. MS (APCI), *m/z*: 575 (31, MH$^+$), 557 (100). Found (%): C, 73.20; H, 8.05; N, 2.36; S, 5.54. Calc. for $C_{35}H_{47}NO_2SSi$ (%): C, 73.25; H, 8.25; N, 2.44; S, 5.59.

Available online at www.sciencedirect.com
ScienceDirect
Mendeleev Commun., 2014, **24**, 374–376
Mendeleev Communications

Bu^tMe_2SiOTf-promoted cyanosilylation of six-membered cyclic nitronates with trialkylsilyl cyanides or *tert*-butyl isocyanide†

Andrey A. Mikhaylov,*[a] Yuliya A. Khomutova,[a] Dmitry E. Arkhipov,[b] Alexander A. Korlyukov[b] and Sema L. Ioffe*[a]

[a] *N. D. Zelinsky Institute of Organic Chemistry, Russian Academy of Sciences, 119991 Moscow, Russian Federation. Fax: +7 499 135 5328; e-mail: iof@ioc.ac.ru*
[b] *A. N. Nesmeyanov Institute of Organoelement Compounds, Russian Academy of Sciences, 119991 Moscow, Russian Federation*

DOI: 10.1016/j.mencom.2014.11.023

Six-membered cyclic nitronates smoothly react with trialkylsilyl cyanide/Bu^tMe_2SiOTf or *tert*-butyl isocyanide/Bu^tMe_2SiOTf systems to afford 2-trialkylsilyloxy-3-cyanotetrahydro-[4*H*]-1,2-oxazines or δ-oxo-α-trialkylsilyloximinonitriles depending on the ring-substitution pattern.

The recently discovered nucleophile addition to nitronate function under silyl Lewis acid (LA) catalysis significantly extends synthetic potential of nitro compounds and their derivatives.[1] Thus, we previously reported C,C- and C,N-couplings for six-membered cyclic nitronates **1** with silyl ketene acetal or related species[2] and N–Si and N–H amines,[3] respectively, as well as silyl ketene acetal addition to five-membered cyclic nitronates **2**[4] and their acyclic analogues **3** (Scheme 1).[5] Noteworthy, six-membered nitronates **1** are usually considered as model compounds in such investigations due to their availability in diastereo- and entantiopure forms.[1]

previous works:[1–5]

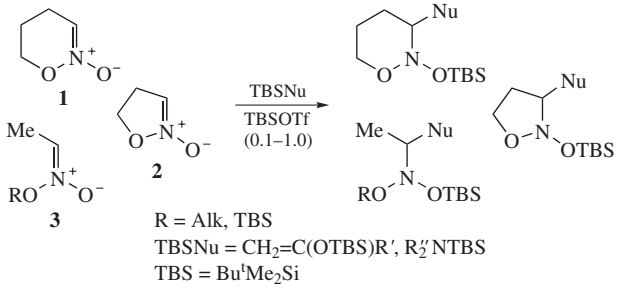

previous works:[7]

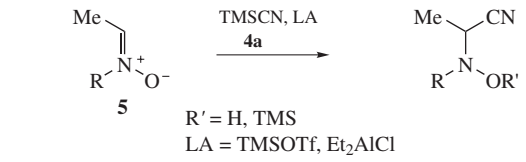

current work:

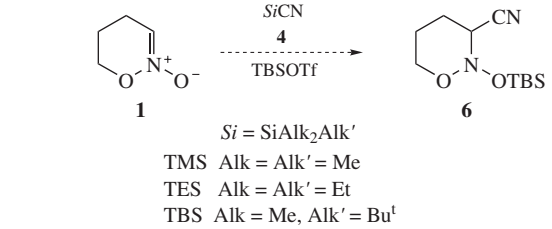

Scheme 1

The extension of the nucleophiles range is the priority task. In this context ability of silyl cyanides **4** to act as nucleophilic agents under LA catalysis is of special interest (for recent progress, see, *e.g.*, ref. 6). In particular, the reaction of structural analogues of nitronates – nitrones **5** – with these reagents is widely employed in synthesis either with or without electrophilic activation (Scheme 1).[7]

According to considered above, the detailed investigation of C,C-coupling of six-membered cyclic nitronates **1** with silyl cyanides **4** is the topic of this manuscript (Scheme 1).‡

Starting from general considerations, cyanosilylation of nitronates **1** could be analyzed with recently developed by H. Mayr and co-workers[9] scale nucleophilicity – electrophilicity.

For iminium cations $[\mathbf{1}\cdot Si]^+$ (Scheme 2) derived from C-3 unsubstituted nitronates **1**, electrophilicity parameter *E* belongs to –4 ... –6 interval.[2(b),§] According to these data, nitronates **1** are supposed to react at low temperature with nucleophiles with *N* parameter higher than 4.[2(b)] Unfortunately, there are no *N* parameters in literature given for silyl cyanides (as though for any other organic cyanides); however, from general considerations their nucleophilicities should be lower than those for cor-

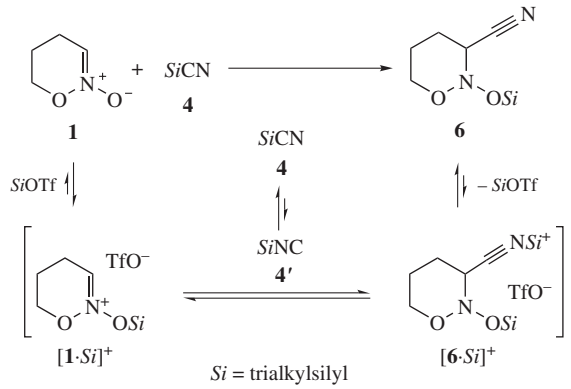

Scheme 2

† In memory of Dr. Ilya M. Lyapkalo.

‡ The only example of interaction **1** + **4** is reported in our recent paper,[8] though a detailed investigation of the process as well as the optimization of the synthesis are not discussed.

§ The C-3 substituted nitronates evidently have electrophilicity parameter *E* 5–6 points lower.[2(b)]

responding isocyanides. In fact, structurally similar to *Si*NC *tert*-butyl isocyanide has $N = 5.47$.[10]

With rather fast equilibrium

$$SiCN + SiOTf \rightleftharpoons [SiCNSi]^+TfO^- \rightleftharpoons SiOTf + SiNC$$

given,[11] one may suggest that the coupling partners in the reaction **1** + **4** are more nucleophilic silyl isocyanide **4′** species and the iminium cations [**1**·SiAlk$_2$Alk′]$^+$ (Scheme 2).

Nitronate **1a** was chosen as a model object for cyanosilylation in the current work.[2(a)] We started with investigation of interaction at –78 °C between its pregenerated *in situ* salt [**1a**·Bu^{t}Me$_2$Si]$^+$TfO$^-$ [2(b)] and available inexpensive Me$_3$SiCN **4a**. We took into account that earlier silyl group *Si* in products of the reactions of nitronates **1** with π-nucleophiles was introduced only by *Si*OTf promoter (taken in stoichiometric amount) but not from nucleophile.[2(b)] However, in our case only equimolar mixture of Bu^{t}Me$_2$Si- and Me$_3$Si-nitroso acetals (**6a** and **6a′**, respectively) was obtained in 89% yield (Scheme 3). Moreover, nitroso acetal **6a′** with trimethylsilyl group turned out to be unstable during isolation on silica. For this reason, in the next studies we focused on *tert*-butyldimethylsilyl-substituted nitroso acetals **6**.

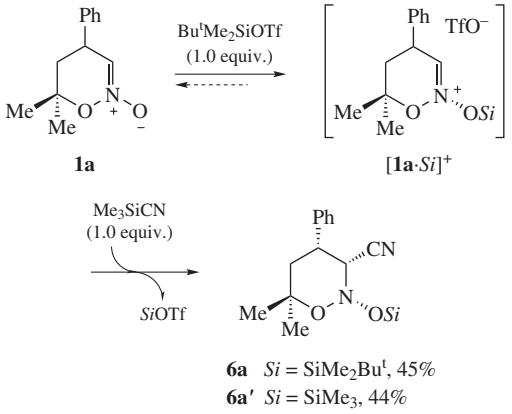

Scheme 3 *Conditions*: CH_2Cl_2, –78 °C, 3 h.

When nitronate **1a** was reacted with Bu^{t}Me$_2$SiCN **4b** under reduced to substechiometric amounts (20 mol%) of Bu^{t}Me$_2$SiOTf, its conversion into nitroso acetal **6a** reached only 19%. Only the use of full equivalent of Bu^{t}Me$_2$SiOTf succeeded in 88% yield of **6a**. Obviously, it could be associated with final nitroso acetal **6a** reversibly forming complex with Bu^{t}Me$_2$SiOTf and drawing out of the reaction a large amount of catalyst. However, the discussed procedure opened access for a presentative series of 3-cyano nitroso acetals **6** (procedure A in Table 1).¶

Table 1 Cyanosilylation of nitronate **1** series.

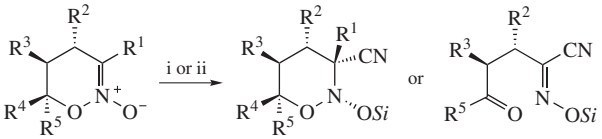

Reagents and conditions: i, Bu^{t}Me$_2$SiCN (1.2 equiv.), Bu^{t}Me$_2$SiOTf (1.0 equiv.), CH_2Cl_2, –78 °C, 24 h; ii, *Si*OTf (1.05 equiv.), CH_2Cl_2, –78 °C, then Bu^{t}NC (1.05 equiv.), –78 °C, 15 min, then Et$_3$N (1.2 equiv.).

Entry	Nitronate	R^1	R^2	R^3	R^4	R^5	*Si*	Product	Yield (%)	Procedure
1	**1a**	H	Ph	H	Me	Me	Bu^{t}Me$_2$Si	**6a**	88	A
2	**1a**	H	Ph	H	Me	Me	Bu^{t}Me$_2$Si	**6a**	56	B
3	**1a**	H	Ph	H	Me	Me	Et$_3$Si	**6a′**	55	B
4	**1b**	H	(CH$_2$)$_2$Ph	H	Me	Me	Bu^{t}Me$_2$Si	**6b**	91	A
5	**1c**	H	OBz	H	Me	Me	Bu^{t}Me$_2$Si	**6c**[a]	88	A
6	**1d**	H	Ph	–(CH$_2$)$_4$–		H	Bu^{t}Me$_2$Si	**6d**	84	A
7	**1e**	Me	Ph	H	Me	Me	Bu^{t}Me$_2$Si	**6e**	60	A[b]
8	**1f**	H	Ph	H	Me	OMe	Bu^{t}Me$_2$Si	**8a**	71	A
9	**1f**	H	Ph	H	Me	OMe	Bu^{t}Me$_2$Si	**8a**	54	B

[a] Mixture of four diastereomers, *dr* 1.0 : 4.8 : 0.2 : 2.1. [b] Reaction time 48 h.

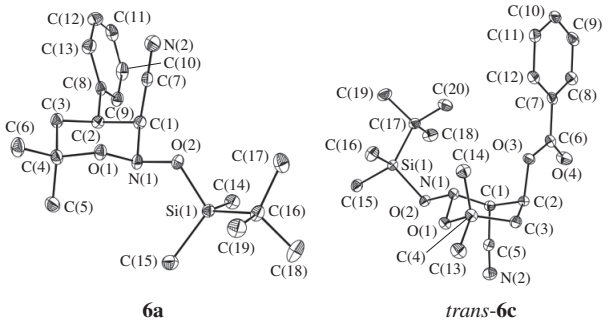

Figure 1 Molecular structures of **6a** and the major *trans*-**6c** diastereomer. Thermal ellipsoids are shown at 50% probability level. Hydrogen atoms are omitted for clarity.

The other method employed stable Bu^{t}NC **7** instead of **4** (procedure B, Table 1).¶ Compound **7** is known to react with acylnitronates giving rise to α-oximino amides,[12] as well to serve cyanide equivalent under basic conditions.[10]

¶ *Procedure A*: Bu^{t}Me$_2$SiOTf (23 μl, 264 mg, 1 mmol) was added at –78 °C to a stirred solution of nitronate **1** (1 mmol), 2,6-lutidine (30 μl, 27 mg, 0.25 mmol) and Bu^{t}Me$_2$SiCN (169 mg, 1.2 mmol) in CH_2Cl_2 (5 ml). The reaction mixture was kept for 24 h at –78 °C, then poured into mixture of hexane (12 ml) and saturated aqueous solution of $NaHCO_3$ (15 ml). The organic layer was separated and the aqueous one was extracted with hexane (2×4 ml). The combined organic layers were washed successively with H_2O (10 ml), brine (15 ml) and dried over Na_2SO_4. The solvents were evaporated *in vacuo*. The residue was subjected to column chromatography (hexane–EtOAc, 10 : 1 → 5 : 1) either recrystallized from hexane (1–3 ml) to give pure nitroso acetal **6** or γ-oxocyanoxime **8a**.

Procedure B: Bu^{t}Me$_2$SiOTf or Et$_3$SiOTf (277 mg, 1.05 mmol) was added at –78 °C to a stirred solution of nitronate **1** (1 mmol) in CH_2Cl_2 (5 ml). The resulting clear solution was kept for 5 min at –78 °C, and then Bu^{t}NC (119 μl, 87 mg, 1.05 mmol) was added. After additional 15 min Et$_3$N (170 μl, 121 mg, 1.2 mmol) was added. The resulting orange reaction mixture was stirred at –78 °C for 2 h and poured into mixture of hexane (12 ml)/H_2O (15 ml). The organic layer was separated and aqueous one was extracted with hexane (2×4 ml). The combined organic layers were washed successively with H_2O (10 ml), brine (15 ml) and dried over Na_2SO_4. The solvents were evaporated *in vacuo*. The residue was subjected to column chromatography (hexane–EtOAc, 10 : 1 → 5 : 1) to give nitroso acetal **6** or δ-oxo-α-oximino nitrile **8a**. Products **6** and **8** yields, their spectral and analytical data are described in Online Supplementary Materials.

†† *Crystal data for* **6a**: colorless crystals, $C_{19}H_{30}N_2O_2Si$ (M = 346.54), monoclinic, space group $C2/c$, at 100 K: a = 25.561(2), b = 6.1744(5) and c = 27.689(2) Å, β = 114.841(2)°, V = 3965.8(6) Å^3, Z = 8, d_{calc} = 1.161 g cm^{-3}, μ(MoKα) = 0.131 mm^{-1}, F(000) = 1504. Bruker Smart Apex II CCD diffractometer, 23501 reflections collected, 5777 independent reflections (R_{int} = 0.1014), 3448 observed reflections with $I > 2\sigma(I)$, R_1 = 0.0527 [$I > 2\sigma(I)$], wR_2 = 0.1222 (all reflections), 224 refined parameters, GOOF = 0.991 (all reflections).

Crystal data for trans-**6c**: colorless crystals, $C_{20}H_{30}N_2O_4Si$ (M = 390.55), monoclinic, space group $C2/c$, at 120 K: a = 32.602(2), b = 7.9334(5) and c = 21.8174(14) Å, β = 130.862(1)°, V = 4267.7(5) Å^3, Z = 8, d_{calc} = 1.216 g cm^{-3}, μ(MoKα) = 0.136 mm^{-1}, F(000) = 1680. Bruker Smart Apex II CCD diffractometer, 17805 reflections collected, 6291 independent reflections (R_{int} = 0.0475), 4808 observed reflections with $I > 2\sigma(I)$, R_1 = 0.0561 [$I > 2\sigma(I)$], wR_2 = 0.1260 (all reflections), 251 refined parameters, GOOF = = 1.077 (all reflections).

CCDC 973921 and 973922 contain the supplementary crystallographic data for this paper. These data can be obtained free of charge from The Cambridge Crystallographic Data Centre *via* http://www.ccdc.cam.ac.uk. For details, see 'Notice to Authors', *Mendeleev Commun.*, Issue 1, 2014.

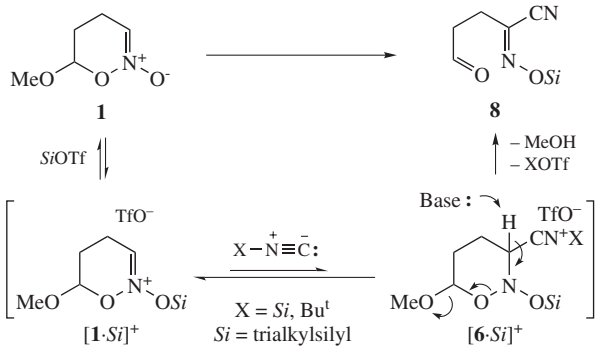

Scheme 4

Indeed, when pregenerated cation [**1a**·$SiMe_2Bu^t$]$^+$ was treated with **7** and Et_3N successively, nitroso acetal **6a** was obtained in 56% yield (Table 1, entry 2). This seemed to be a simple procedure for the preparation of nitroso acetals **6** with various silyl groups, for example, triethylsilyl derivative **6a′** (Table 1, entry 3), although providing lower yields compared to the procedure A.

Cyanosilylation of nitronates **1b–e** with various ring-substituents afforded cyanides **6b–e** in 60–84% yields (Table 1, entries 4–7), though long reaction time (~48 h) was necessary for full conversion of substituted at C^3 nitronate **1e**.

The stereochemistry of products **6** and substituents positions were assigned with NMR (based on spin-spin coupling constants and NOESY) and X-ray analysis (Figure 1).†† The nitroso acetals **6a**,**b**,**d**,**e** were obtained as single 3,4-*cis* diastereomers. Product **6c** was a mixture of four diastereomers (*dr* 1.0 : 4.8 : 0.2 : 2.1) with preferred formation of 3,4-*trans* diastereomers (*trans* : *cis* ~ 5.8 : 1).

These data are in a good agreement with mechanistic model, previously proposed for coupling of nitronates **1** with π-nucleophiles, which was also based on stereochemistry of final products.[2(*a*)]

Reaction between 6-methoxy substituted nitronate **1f** and silyl cyanide **4** either *tert*-butyl isocyanide **7** proceeded in a different way and gave cyanoxime *O*-silyl ether **8a** as the only product (Table 1, entries 8 and 9). Apparently, it could be associated with increased acidity of proton at C^3 position in cationic intermediate [**6**·*Si*]$^+$ which in case of methoxy group at C^6 can undergo methanol elimination (Scheme 4).

In summary, two procedures for cyanosilylation of six-membered cyclic nitronates **1** were developed to provide an access to new promising compounds. The cyanosilylations of 5-membered cyclic and acyclic nitronates are in near progress.

This work was supported by grants from the Council of the President of the Russian Federation for Young Scientists and Leading Scientific Schools (NSh-412.2012.3) and from the Russian Foundation for Basic Research (project no. 12-03-00278a).

Online Supplementary Materials

Supplementary data associated with this article can be found in the online version at doi:10.1016/j.mencom.2014.11.023.

References

1 S. L. Ioffe, in *Nitrile Oxides, Nitrones and Nitronates in Organic Synthesis*, 2nd edn., ed. H. Feuer, John Wiley & Sons, Chichester, 2008, pp. 435–748.
2 (*a*) V. O. Smirnov, S. L. Ioffe, A. A. Tishkov, Yu. A. Khomutova, I. D. Nesterov, M. Yu. Antipin, W. A. Smit and V. A. Tartakovsky, *J. Org. Chem.*, 2004, **69**, 8485; (*b*) Yu. A. Khomutova, V. O. Smirnov, H. Mayr and S. L. Ioffe, *J. Org. Chem*., 2007, **72**, 9134.
3 A. A. Mikhaylov, A. D. Dilman, Yu. A. Khomutova, D. E. Arkhipov, A. A. Korlyukov and S. L. Ioffe, *Eur. J. Org. Chem.*, 2013, 5670.
4 V. O. Smirnov, A. S. Sidorenkov, Yu. A. Khomutova, S. L. Ioffe and V. A. Tartakovsky, *Eur. J. Org. Chem*., 2009, 3066.
5 V. O. Smirnov, Yu. A. Khomutova, V. A. Tartakovsky and S. L. Ioffe, *Eur. J. Org. Chem*., 2012, 3377.
6 M. North, D. L. Usanov and C. Young, *Chem. Rev*., 2008, **108**, 5146.
7 (*a*) O. Tsuge, S. Urano and T. Iwasaki, *Bull. Chem. Soc. Jpn*., 1980, **53**, 485; (*b*) A. Hosomi, H. Shoji and H. Sakurai, *Chem. Lett*., 1985, 1049; (*c*) A. Padwa and K. F. Koehler, *J. Chem. Soc., Chem. Commun.*, 1986, 789; (*d*) F. L. Merchan, P. Merino and T. Tejero, *Tetrahedron Lett.*, 1995, **36**, 6949; (*e*) P. Merino, A. Lanaspa, F. L. Merchan and T. Tejero, *J. Org. Chem*., 1996, **61**, 9028; (*f*) A. Peer and A. Vasella, *Helv. Chim. Acta*, 1999, **82**, 1044; (*g*) P. Merino, T. Tejero, J. Revuelta, P. Romero, S. Cicchi, V. Mannucci, A. Brandi and A. Goti, *Tetrahedron: Asymmetry*, 2003, **14**, 367; (*h*) T. Okino, Y. Hoashi and Y. Takemoto, *Tetrahedron Lett*., 2003, **44**, 2817; (*i*) M. Marradi, S. Cicchi, J. I. Delso, L. Rosi, T. Tejero, P. Merino and A. Goti, *Tetrahedron Lett*., 2005, **46**, 1287; (*j*) O. G. Mancheño, P. Tangen, R. Rohlmann, R. Fröhlich and J. Alemán, *Chem. Eur. J*., 2011, **17**, 984.
8 A. S. Naumova, A. A. Mikhaylov, M. I. Struchkova, Yu. A. Khomutova, V. A. Tartakovsky and S. L. Ioffe, *Eur. J. Org. Chem*., 2012, 2219.
9 H. Mayr, B. Kempf and A. R. Ofial, *Acc. Chem. Res*., 2003, **36**, 66.
10 V. V. Tumanov, A. A. Tishkov and H. Mayr, *Angew. Chem. Int. Ed*., 2007, **46**, 3563.
11 J. A. Seckar and J. S. Thayer, *Inorg. Chem.*, 1976, **15**, 501.
12 P. Dumestre, L. El Kaim and A. Grégoire, *Chem. Commun*., 1999, 775.

Received: 19th February 2014; Com. 14/4310

Available online at www.sciencedirect.com
ScienceDirect
Mendeleev Commun., 2014, **24**, 377–379
Mendeleev Communications

Synthesis and conformations of cross-conjugated polyenes containing heterocyclic moieties with diverse structures

Zhanna A. Krasnaya,* Vadim V. Kachala and Sergei G. Zlotin

N. D. Zelinsky Institute of Organic Chemistry, Russian Academy of Sciences, 119991 Moscow, Russian Federation. Fax: +7 499 135 5328; e-mail: kra@ioc.ac.ru

DOI: 10.1016/j.mencom.2014.11.024

New non-linear cross-conjugated polyenes containing a central 4-ylidene-substituted pyran or *N*-methyldihydropyridine ring have been synthesized. Interaction of chromophores in these compounds occurs through the ylidene group linked to the heterocycles.

Previously, we performed the reaction of β-dimethylaminoacrolein aminal $Me_2NCH{=}CHCH(NMe_2)_2$ **1** with 2,6-dimethyl-4-pyrone or *N*-methyl-2,6-dimethylpyridin-4-one to give ketocyanine dyes **2** and **3** (cross-conjugated polyene ω,ω′-bisaminoketones with a central pyran or dihydropyridine moiety) containing two aminopolyene chromophores with equal lengths linked by a carbonyl group and a central bridge.[1,2]

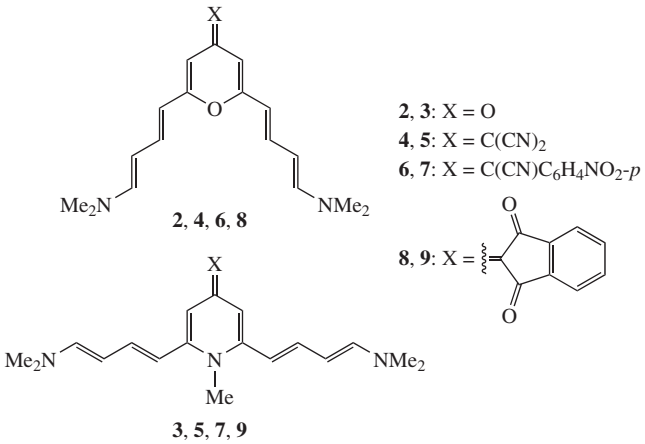

Replacement of the bridging O atom by an NMe group drastically changes the dye absorption spectrum, since in compound **2** the chromophores are arranged at a sharp angle to each other, whereas at an obtuse angle in compound **3**.[3–5]

The same phenomenon occurred in the case of cross-conjugates ω,ω′-dimethylaminopolyenes **4–9** containing a central pyran or *N*-methyldihydropyridine moiety. The aminopolyene chromophores in these compounds interact through 2,2-dicyano-, 2-cyano-2-(4-nitrophenyl)- or dioxoindan-2-ylidene groups located at 4-position of the heterocycle.[6]

Previously, interesting data were reported that new chromophores based on pyranone and functionalised conjugated aldehydes containing bridging moieties demonstrated nonlinear optical properties,[7] whereas pyran dyes with push-pull structures incorporating a CN group were found to be promising for solar energy cells.[8] Furthermore, a D-π-A-π-D dye containing a central acceptor core A similar to the core of polyene **3** and heterocyclic donor groups D was recently synthesized.[9]

In view of this, we decided to synthesize new cross-conjugated polyenes containing a pyran or dihydropyridine ring and a methylidene acceptor linked to carbonyl-containing polynitrogen or nitrogen-oxygen heterocycles with various structures. Of these,

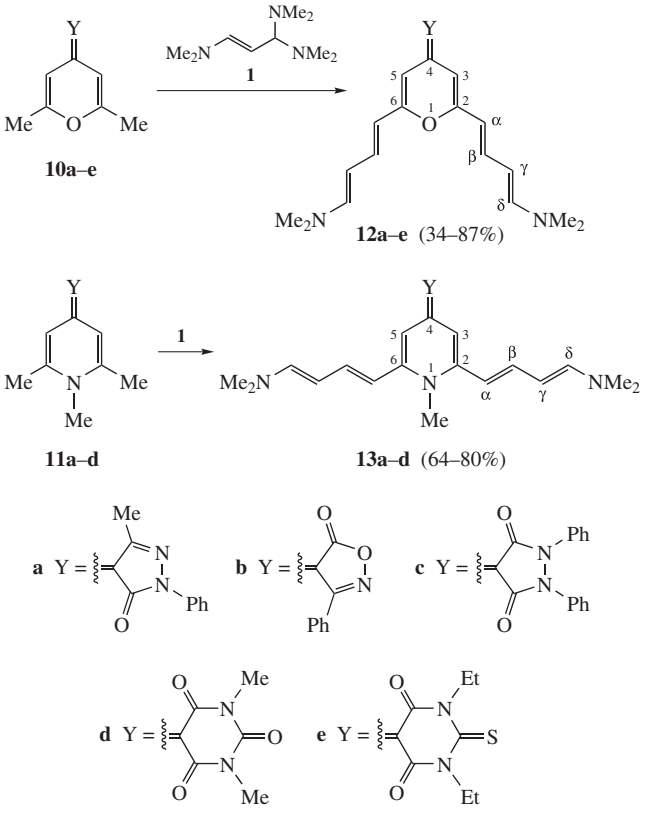

Scheme 1

ylidene derivatives of barbituric acids are promising not only as biologically active compounds[10] but also as potential dyes.[11]

To perform this task, we studied the reaction of aminal **1** with substituted 2,6-dimethyl-4*H*-pyrans **10a–e** and 1,2,6-trimethyl-1,4-dihydropyridines **11a–e** containing the corresponding heterocycles at 4-position (Schemes 1 and 2).

Compounds **10a–e** were obtained by heating 2,6-dimethyl-4*H*-pyran-4-one with heterocyclic compounds containing a reactive methylene group (the residue of the latter is denoted as Y in Scheme 1) in acetic anhydride. Substituted 1,2,6-trimethyl-1,4-dihydropyridines **11a–e** were synthesized from the corresponding pyrans **10a–e** by treatment with 40% $MeNH_2$ aqueous solution or 15% $MeNH_2$ solution in EtOH (see Online Supplementary Materials).

Dyes **12a–e** and **13a–d** were prepared by condensation of pyrans **10a–e** or dihydropyridines **11a–d** with excess aminal **1** (reactant ratio of 1:3) in the absence of a solvent, except for

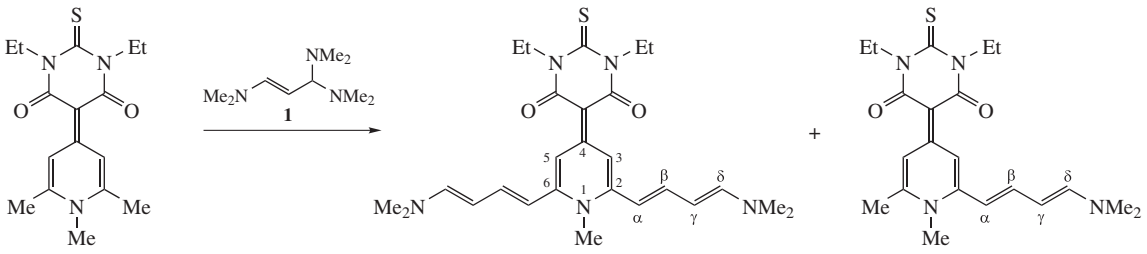

11e **13e** **14**

Scheme 2

polyenes **12b**,**e** which were obtained in dry benzene.† Note that, though the reaction conditions vary, in all cases (except for dihydropyridine **11e**), the reaction of aminal **1** involves both methyl groups to afford polyenes containing two polyene chromophores. The reaction of dihydropyridine **11e** with aminal **1** in dry benzene without heating gave a mixture of polyene **13e** and tetraene **14** in 2:3 ratio (Scheme 2).‡

Fractional crystallization of this mixture provided pure tetraene **14**. Heating of the mixture of compounds **13e** and **14** with excess aminal **1** finally led to polyene **13e**.

The structures and conformations of the obtained compounds **12a–e**, **13a–e** and **14** were proved from 1D and 2D ^{1}H and

† *4-{2,6-Bis[(1*E*,3*E*)-4-dimethylaminobuta-1,3-dienyl]-4*H*-pyran-4-ylidene}-3-methyl-1-phenyl-1*H*-pyrazol-5(4*H*)-one* **12a**. Aminal **1** (0.18 g, 1.08 mmol) was added to substituted pyran **10a** (0.1 g, 0.36 mmol). The reaction mixture was heated for 15 min at 65 °C, then evaporated *in vacuo*. Dry Et_2O was added to the residue; the precipitate that formed was filtered off and washed with Et_2O to give 0.12 g (76%) of polyene **12a** as dark violet crystals, mp 230–233 °C. UV [λ_{max}/nm (ε)]: 380 (44850), 520 (67600), 580 (sh., 39000) (EtOH); 360 (26000), 540 (46800) ($CHCl_3$). ^{1}H NMR (DMSO-d_6, 80 °C) δ: 5.87 (d, 2H, H$^\alpha$, *J* 14.7 Hz), 7.29–7.33 (m, 2H, H$^\beta$), 5.31 (t, 2H, H$^\gamma$, *J* 12.0 Hz), 7.12 (d, 2H, H$^\delta$, *J* 12.7 Hz), 8.04 (d, 2H, *o*-H$_{Ph}$, *J* 8.0 Hz), 7.29–7.33 (m, 2H, *m*-H$_{Ph}$), 7.04 (t, 1H, *p*-H$_{Ph}$, *J* 7.3 Hz), 2.95 (s, 12H, NMe_2), 7.33 (s, 1H, H^3), 6.50 (s, 1H, H^5), 2.39 (s, 3H, Me). ^{13}C NMR (DMSO-d_6, 80 °C) δ: 107.58 (C$^\alpha$), 140.29 (C$^\beta$), 97.66 (C$^\gamma$), 151.28 (C$^\delta$), 117.38 (*o*-C$_{Ph}$), 127.74 (*m*-C$_{Ph}$), 122.04 (*p*-C$_{Ph}$), 39.49 (NMe_2), 162.76 (C^2, C^6), 108.28 (C^3, C^5), 17.59 (Me). MS (ESI), *m*/*z*: 443.2433 [M+H]$^+$ (calc. for $C_{27}H_{30}N_4O_2$, *m*/*z*: 443.2442).

*4-{2,6-Bis[(1*E*,3*E*)-4-dimethylaminobuta-1,3-dienyl]-4*H*-pyran-4-ylidene}-3-phenylisoxazol-5(4*H*)-one* **12b**. Aminal **1** (0.33 g, 2 mmol) was added dropwise with stirring to a suspension of substituted pyran **10b** (0.2 g, 0.75 mmol) in 2 ml of dry benzene. The reaction mixture was stirred for 45 min at 20 °C and then concentrated *in vacuo*. The residue (a black viscous substance) was repeatedly triturated with anhydrous Et_2O which then was poured off. EtOH (1 ml) was added to the residue; the mixture was triturated and mixed with water (30 ml). After 1.5 h, the resulting extra-fine precipitate was filtered off and washed with water and diethyl ether to give 0.11 g (34%) of polyene **12b** as dark green crystals, mp 250 °C. UV [λ_{max}/nm (ε)]: 363 (26658), 400 (25177), 495 (54798), 595 (26658) (EtOH); 370 (31100), 518 (53317), 546 (sh., 44430) ($CHCl_3$). ^{1}H NMR (DMSO-d_6, 80 °C) δ: 5.55 (d, 2H, H$^\alpha$, *J* 12.0 Hz), 7.21 (t, 2H, H$^\beta$, *J* 12.0 Hz), 5.31 (t, 2H, H$^\gamma$, *J* 12.1 Hz), 6.71 (d, 2H, H$^\delta$, *J* 12.1 Hz), 7.44–7.55 (m, 5H, Ph), 7.37 (s, 2H, H^3, H^5), 2.91 (s, 12H, NMe_2). ^{13}C NMR (DMSO-d_6, 80 °C) δ: 109.39 (C$^\alpha$), 140.30 (C$^\beta$), 98.39 (C$^\gamma$), 150.32 (C$^\delta$), 129.00, 128.47, 132.74 (Ph), 162.71 (C^2, C^6), 104.19 (C^3, C^5), 46.37 (NMe_2), 149.82 (C^8), 97.69 (C^7), 105.61 (C^4). MS (ESI), *m*/*z*: 430.2136 [M+H]$^+$ (calc. for $C_{26}H_{27}N_3O_3$, *m*/*z*: 430.2125).

*4-{2,6-Bis[(1*E*,3*E*)-4-dimethylaminobuta-1,3-dienyl]-1-methylpyridin-4(1*H*)-ylidene}-3-methyl-1-phenyl-1*H*-pyrazol-5(4*H*)-one* **13a**. Aminal **1** (0.17 g, 1.02 mmol) was added to substituted dihydropyran **11a** (0.1 g, 0.34 mmol). The reaction mixture was stirred for 1 h at 60 °C and then concentrated *in vacuo*. Et_2O was added to the residue. The precipitate was separated and washed with diethyl ether to give 0.12 g (77%) of polyene **13a** as bright orange crystals, mp 227–229 °C. UV [λ_{max}/nm (ε)]: 485 (62840) (EtOH); 465 (54170) ($CHCl_3$). ^{1}H NMR (DMSO-d_6) δ: 3.62 (s, 3H, NMe), 8.12 (s, 2H, H^3, H^5), 2.41 (s, 3H, Me), 6.07 (d, 2H, H$^\alpha$, *J* 14.5 Hz), 7.05 (dd, 2H, H$^\beta$, *J* 14.5 Hz, *J* 11.1 Hz), 5.28 (t, 2H, H$^\gamma$, *J* 11.1 Hz, *J* 11.9 Hz), 7.00 (d, 2H, *J* 11.9 Hz), 8.15 (d, 2H, *o*-H$_{Ph}$, *J* 7.6 Hz), 7.30 (t, 2H, *m*-H$_{Ph}$, *J* 7.9 Hz), 6.98 (t, 1H, *p*-H$_{Ph}$, *J* 3.4 Hz), 2.88 (s, 12H, NMe_2). ^{13}C NMR (DMSO-d_6) δ: 38.11 (NMe), 105.22 (C^3, C^5), 18.02 (Me), 108.08 (C$^\alpha$), 141.05 (C$^\beta$), 98.15 (C$^\gamma$), 150.08 (C$^\delta$), 118.15 (*o*-C$_{Ph}$), 128.08 (*m*-C$_{Ph}$), 122.02 (*p*-C$_{Ph}$), 40.08 (NMe_2), 161.22 (C^2, C^6). MS (ESI), *m*/*z*: 456.2744 [M+H]$^+$ (calc. for $C_{28}H_{33}N_5O$, *m*/*z*: 456.2758).

*4-{2,6-Bis[(1*E*,3*E*)-4-dimethylaminobuta-1,3-dienyl]-1-methylpyridin-4(1*H*)-ylidene}-3-phenylisoxazol-5(4*H*)-one* **13b**. Aminal **1** (0.13 g, 0.76 mmol) was added to substituted dihydropyridine **11b** (0.07 g, 0.2 mmol) and the mixture was stirred for 35 min at 70–75 °C. The reaction mixture containing a cherry-coloured precipitate was concentrated *in vacuo*, then Et_2O was added. The precipitate was filtered off and washed with a small amount of EtOH to give 0.08 g (73%) of polyene **13b** as brick-red crystals, mp > 240 °C. UV [λ_{max}/nm (ε)]: 360 (22100), 430 (sh., 35360), 490 (61880) (EtOH); 470 (47883) ($CHCl_3$). ^{1}H NMR (DMSO-d_6) δ: 5.97 (d, 2H, H$^\alpha$, *J* 14.5 Hz), 6.54 (dd, 2H, H$^\beta$, *J* 13.5 Hz, *J* 12 Hz), 5.22 (t, 2H, H$^\gamma$, *J* 12 Hz), 6.76 (d, 2H, H$^\delta$, *J* 12.7 Hz), 7.45 (m, 2H, *m*-H$_{Ph}$, *J* 7.7 Hz), 7.59 (m, 3H, *p*-H$_{Ph}$, *o*-H$_{Ph}$, *J* 7.04 Hz), 7.28 (s, 2H, H^3, H^5), 2.89 (s, 12H, NMe_2), 3.56 (s, 3H, NMe). MS (ESI), *m*/*z*: 443.2403 [M+H]$^+$ (calc. for $C_{27}H_{30}N_4O_2$, *m*/*z*: 443.2442).

For synthesis and characteristics of compounds **12c–e** and **13c**,**d**, see Online Supplementary Materials.

‡ *5-{2,6-Bis[(1*E*,3*E*)-4-dimethylaminobuta-1,3-dienyl]-1-methylpyridin-4(1*H*)-ylidene}-1,3-diethyl-2-thioxodihydropyrimidine-4,6(1*H*,5*H*)-dione* **13e** and *1,3-diethyl-5-{2-[(1*E*,3*E*)-4-dimethylaminobuta-1,3-dienyl]-1,6-dimethylpyridin-4(1*H*)-ylidene}-2-thioxodihydropyrimidine-4,6(1*H*,5*H*)-dione* **14**. *Procedure A.* Aminal **1** (0.32 g, 1.88 mmol) was added dropwise to a suspension of dihydropyrimidine **11e** (0.2 g, 0.63 mmol) in 1.2 ml of dry benzene. The reaction mixture was stirred at 20–22 °C. After 2.5 h, a fine carrot-coloured precipitate formed. Stirring was continued for more 2 h, the precipitate was separated and washed with dry Et_2O to give a mixture of polyene **13e** and tetraene **14** in 2:3 ratio (according to ^{1}H NMR data in DMSO-d_6). After double recrystallization of the mixture of compounds **13e** and **14** from EtOH, the mother liquor was cooled to give tetraene **14** as bright-orange crystals, mp 175–178 °C. UV [λ_{max}/nm (ε)]: 285 (60149), 380 (46992), 440 (sh., 39473), 490 (54510) (EtOH); 325 (12530), 390 (26315), 480 (43232) ($CHCl_3$). ^{1}H NMR (DMSO-d_6) δ: 6.20 (d, 1H, H$^\alpha$, *J* 14.4 Hz), 7.18 (dd, 1H, H$^\beta$, *J* 11.8 Hz, *J* 14.2 Hz), 5.38 (t, 1H, H$^\gamma$, *J* 12.0 Hz), 7.16 (d, 1H, H$^\delta$, *J* 12.0 Hz), 2.95 (s, 6H, NMe_2), 3.75 (s, 3H, NMe), 2.54 (s, 3H, Me), 8.42 (s, 1H, H^3), 8.98 (s, 1H, H^5), 1.15 (t, 6H, $NCH_2\mathit{Me}$, *J* 6.8 Hz), 4.48 (q, 4H, $NC\mathit{H}_2$Me, *J* 6.8 Hz). ^{13}C NMR (DMSO-d_6) δ: 106.53 (C$^\alpha$), 143.25 (C$^\beta$), 98.08 (C$^\gamma$), 151.59 (C$^\delta$), 160.35 (C=O), 39.63 (NMe_2), 37.40 (NMe), 21.37 (Me), 119.08 (C^3), 115.19 (C^5), 175.45 (C=S), 12.56 ($NCH_2\mathit{Me}$), 41.86 ($NC\mathit{H}_2$Me). MS (ESI), *m*/*z*: 401.2009 [M+H]$^+$ (calc. for $C_{21}H_{28}N_4O_2S$, *m*/*z*: 401.2006).

Procedure B. Aminal **1** (0.035 g) was added to 0.04 g of the mixture of polyene **13e** and tetraene **14** obtained as described above and the mixture was stirred for 75 min at 60–70 °C. The crystalline mixture was concentrated *in vacuo*. The residue was repeatedly washed with dry Et_2O and boiled with EtOH to give 0.03 g of polyene **13e** as red crystals, mp > 240 °C. UV [λ_{max}/nm (ε)]: 285 (21690), 430 (15424), 500 (22172) (EtOH); 325 (7680), 370 (7680), 440 (plateau, 14880), 490 (19280). ^{1}H NMR (DMSO-d_6) δ: 6.11 (d, 2H, H$^\alpha$, *J* 14.4 Hz), 7.05 (dd, 2H, H$^\beta$, *J* 11.8 Hz, *J* 14.2 Hz), 5.30 (t, 2H, H$^\gamma$, *J* 12.0 Hz), 7.04 (d, 2H, H$^\delta$, *J* 12.0 Hz), 3.7 (s, 3H, NMe), 2.90 (s, 12H, NMe_2), 8.67 (s, 2H, H^3, H^5), 1.15 (t, 6H, $NCH_2\mathit{Me}$, *J* 6.8 Hz), 4.48 (q, 4H, $NC\mathit{H}_2$Me, *J* 6.8 Hz). ^{13}C NMR (DMSO-d_6) δ: 107.89 (C$^\alpha$), 141.67 (C$^\beta$), 97.86 (C$^\gamma$), 150.52 (C$^\delta$), 37.90 (NMe), 39.77 (NMe_2), 114.19 (C^3, C^5), 160.34 (C=O), 175.26 (C=S), 12.61 ($NCH_2\mathit{Me}$), 41.83 ($NC\mathit{H}_2$Me). MS (ESI), *m*/*z*: 482.2582 [M+H]$^+$ (calc. for $C_{26}H_{35}N_5O_2S$, *m*/*z*: 482.2584).

^{13}C NMR, UV and micrOTOF mass spectra. Assignment of signals in the ^{1}H and ^{13}C NMR spectra was based on COSY, NOESY, HSQC and HMBC 2D experiments. Dyes **12a–e** possess a conformation with a sharp angle between the chromophores since the NOESY and ROESY spectra demonstrate correlation between the H^3/H^5 and H^α protons but no correlation between the H^3/H^5 and H^β protons, whereas dyes **13a–e** and **14** have a conformation with an obtuse angle between the chromophores since the protons of the NMe group show coupling with H^α protons but not with H^β protons, which give correlation with the H^3/H^5 protons; there is no correlation between the H^α and H^3 protons.

The configuration of double bonds in all the dyes was determined from NOESY and ROESY NMR spectra and the vicinal coupling constants of methine protons (J 11.1–14.5 Hz). It follows from these data that the protons at the C^α=C^β and C^γ=C^δ double bonds are *trans*-arranged, while the diene moieties in polymethine chains C^α=C^β and C^γ=C^δ exist predominantly in the *S-trans*-conformation.

The spectrofluorescent and photochemical properties of cross-conjugated polyenes **12a–e**, **13a–e** and **14** will be described in detail in a subsequent paper.

This study was supported by the Russian Foundation for Basic Research (project no. 10-03-00647-a).

Online Supplementary Materials

Supplementary data associated with this article can be found in the online version at doi:10.1016/j.mencom.2014.11.024.

References

1 Zh. A. Krasnaya, Yu. V. Smirnova, A. S. Tatikolov and V. A. Kuz'min, *Russ. Chem. Bull.*, 1999, **48**, 1329 (*Izv. Akad. Nauk, Ser. Khim.*, 1999, 1340).
2 Zh. A. Krasnaya, Yu. V. Smirnova, L. A. Shvedova, A. S. Tatikolov and V. A. Kuz'min, *Russ. Chem. Bull., Int. Ed*., 2003, **52**, 2029 (*Izv. Akad. Nauk, Ser. Khim.*, 2003, 1920).
3 A. S. Davydov, *Teoriya molekulyarnykh eksitonov* (*Theory of Molecular Excitons*), Nauka, Moscow, 1968 (in Russian).
4 A. I. Kiprianov and G. G. Dyadyusha, *Ukr. Khim. Zh.*, 1969, **35**, 608 (in Russian).
5 L. A. Shvedova, A. S. Tatikolov, A. S. Shashkov, V. Ya. Artyukhov and Zh. A. Krasnaya, *Russ. Chem. Bull., Int. Ed*., 2007, **56**, 2021 (*Izv. Akad. Nauk, Ser. Khim.*, 2007, 1954).
6 Zh. A. Krasnaya, E. O. Dorofeeva, V. V. Kachala, A. S. Tatikolov and S. G. Zlotin, *Russ. Chem. Bull., Int. Ed.*, 2013, **62**, 2012 (*Izv. Akad. Nauk, Ser. Khim.*, 2013, 2012).
7 G. Koeckelberghs, L. D. Groof, J. Perez-Moreno, J. Asselberghs, K. Clays, Th. Verbiest and C. Samyn, *Tetrahedron*, 2008, **64**, 3772.
8 S. G. Awuah, J. Polreis, J. Prakash, Q. Qiao and Y. You, *J. Photochem. Photobiol. A*, 2011, **224**, 116.
9 C. Sissa, F. Terenziani, A. Painelli, R. B. K. Siram and S. Patil, *J. Phys. Chem. B*, 2012, **116**, 4959.
10 A. V. Moskvin, N. R. Reznikova and B. A. Ivin, *Russ. J. Org. Chem*., 2002, **38**, 463 (*Zh. Org. Khim*., 2002, **38**, 487).
11 I. Bolz, M. Bauer, A. Rollberg and S. Spange, *Macromol. Symp.*, 2010, **287**, 8.

Received: 17th February 2014; Com. 14/4307

Available online at www.sciencedirect.com
ScienceDirect
Mendeleev Commun., 2014, **24**, 380–382
Mendeleev Communications

New approaches to the synthesis of 2,5-dihydro-1,5-benzothiazepines containing nitro groups

Valentina M. Berestovitskaya,*[a] Ruslan I. Baichurin,[a] Nataliya I. Aboskalova[a] and Vladislav V. Gurzhiy[b]

[a] *A. I. Herzen State Pedagogical University of Russia, 191186 St. Petersburg, Russian Federation. Fax: +7 812 571 3800; e-mail: kohrgpu@yandex.ru*
[b] *Department of Crystallography, St. Petersburg State University, 199034 St. Petersburg, Russian Federation. E-mail: vladgeo17@mail.ru*

DOI: 10.1016/j.mencom.2014.11.025

Reaction between *o*-aminothiophenol and 4-(2-furyl)-3-nitrobut-3-en-2-one affords 4-methyl-3-nitro-2-(2-furyl)-2,5-dihydro-1,5-benzothiazepine whose structure was characterized by X-ray diffraction analysis.

Pharmaceuticals whose molecules contain the 1,5-benzothiazepine moiety are widely used in medical practice. For example, Diltiazem manifests antianginal, antihypertensive and antiarrhythmic properties, and Quetiapine belongs to neuroleptics.[1–4]

Previously, we reported a one-pot synthesis of 2-aryl-4-methyl-3-nitro-2,3-dihydro-1,5-benzothiazepines **A** by condensation of *gem*-acetylnitrostyrenes with *o*-aminothiophenol.[5,6]

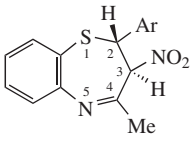

A

Ar = Ph, 4-MeOC$_6$H$_4$, 4-Me$_2$NC$_6$H$_4$

To expand the scope of similar dihydrobenzothiazepines, it is of interest to move to *gem*-acetylnitroethenes containing pharmacophoric heterocycles. In this work we studied the condensation of *o*-aminothiophenol with 4-(2-furyl)-3-nitrobut-3-en-2-one **1** (for its preparation see ref. 7). The reaction proceeds under the same conditions as that with *gem*-acetylnitrostyrenes (MeOH, 18–20 °C, 30 min). However, not a 2,3-dihydro- but 2,5-dihydro-1,5-benzothiazepine **2** is formed,† probably due to isomerization of the initial 2,3-dihydro-1,5-benzothiazepine to a more energetically favourable 2,5-dihydro one containing a nitroenamine moiety.

In the case of 2-(4-methoxyphenyl)-4-methyl-3-nitro-2,3-dihydro-1,5-benzothiazepine **3** obtained previously,[5,6] we succeeded to perform its prototropic conversion (by refluxing its

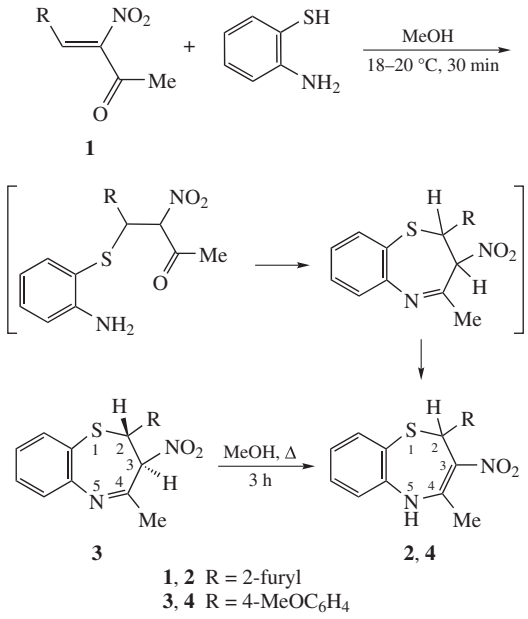

1

3 **2, 4**

1, **2** R = 2-furyl
3, **4** R = 4-MeOC$_6$H$_4$

Scheme 1

methanolic solution for 3 h) to the 2,5-dihydro compound **4**.‡ This confirms that benzothiazepine **2** is formed from the initially generated 2,3-dihydro form.

Note that sometimes,[8–15] the reactions of *gem*-substituted enones with *o*-aminothiophenol directly give 2,5-dihydro-1,5-benzothiazepines, in particular, those containing an alkoxycarbonyl or acetyl group at the C^3 atom.[8–13] In most cases, 2,5-dihydro deriva-

† *2-(2-Furyl)-4-methyl-3-nitro-2,5-dihydro-1,5-benzothiazepine* **2**. A solution of *o*-aminothiophenol (0.250 g, 2 mmol) in methanol (4 ml) was added to 4-(2-furyl)-3-nitrobut-3-en-2-one **1**[7] (0.362 g, 2 mmol). After 30 min, the reaction solution was poured into a Petri dish. The residue that remained after solvent evaporation was repeatedly treated with ethanol. Yield 0.394 g (68%), yellow crystals, mp 170–172 °C (ethanol). IR (ν/cm^{-1}): 1180–1290 (NOO$^-$), 1620 (C=C, C=N$^+$), 3410 (NH$^+$). ^{1}H NMR, δ: 2.75 (s, 3H, Me), 6.32 (s, 1H, C^{2}H), 6.65 (s, 1H, NH), 5.68 (d, 1H, H$^3_{Fur}$, ^3J 3.23 Hz), 5.94 (dd, 1H, H$^4_{Fur}$, ^3J 3.23, 1.86 Hz), 7.11 (d, 1H, H$^5_{Fur}$, ^3J 1.86 Hz), 6.90–7.00 (m), 7.14–7.22 (m, C$_6$H$_4$). ^{13}C{^{1}H} NMR, δ: 27.94 (Me), 44.98 (C^2), 128.24 (C^3), 150.78 (C^4), 108.44 (C$^3_{Fur}$), 109.87 (C$^4_{Fur}$), 142.27 (C$^5_{Fur}$), 151.36 (C$^2_{Fur}$), 122.10, 125.51, 125.71, 128.99, 134.83, 142.65 (C$_6$H$_4$). Found (%): C, 58.31; H, 4.31. Calc. for C$_{14}$H$_{12}$N$_2$O$_3$S (%): C, 58.33; H, 4.17.

‡ *2-(4-Methoxyphenyl)-4-methyl-3-nitro-2,5-dihydro-1,5-benzothiazepine* **4**. A suspension of 2-(4-methoxyphenyl)-4-methyl-3-nitro-2,3-dihydro-1,5-benzothiazepine **3**[6] (0.220 g, 0.67 mmol) in methanol (10 ml) was refluxed for 3 h. The precipitate gradually appeared in solution, while the colouring intensity increased. The reaction mixture was poured into a Petri dish and the residue after solvent evaporation was treated with ethanol. Yield 0.121 g (55%), yellow crystals, mp 146–148 °C (ethanol). IR (ν/cm^{-1}): 1180–1290 (NOO$^-$), 1605 (C=C, C=N$^+$), 3410 (NH$^+$). ^{1}H NMR, δ: 2.75 (s, 3H, Me), 3.65 (s, 3H, OMe), 6.23 (s, 1H, C^{2}H), 6.68 (s, 1H, NH), 6.56, 6.92 (2d, 4H, OC$_6$H$_4$, ^3J 8.54 Hz), 6.80–6.91 (m, 2H, C$_6$H$_4$), 6.96 (m, 1H, C$_6$H$_4$), 7.11 (m, 1H, C$_6$H$_4$). ^{13}C{^{1}H} NMR, δ: 27.68 (Me), 50.52 (C^2), 55.23 (OMe), 129.36 (C^3), 150.94 (C^4), 113.37, 122.10, 125.43, 125.89, 128.44, 128.88, 131.95, 135.13, 143.05, 158.29 (2C$_6$H$_4$). Found (%): N, 8.33. Calc. for C$_{17}$H$_{16}$N$_2$O$_3$S (%): N, 8.54.

tives are generated on heating.[8–12] In case of alkoxycarbonyl-containing benzothiazepines 2,5 ⇄ 2,3-dihydro tautomerism was discovered.[12] However, for compounds **2**, **4** such a tautomerism was not observed, which could be due to greater –M-effect of nitro group compared to an ester one.

The composition and structure of the new compounds **2** and **4** were confirmed by elemental analyses, IR, electronic and NMR (^{1}H, ^{13}C, HMQC, HMBC) spectroscopic data.[§] Their IR spectra do not contain characteristic bands of the covalent nitro group, but exhibit intense bands of ionized nitro group in the range of 1180–1290 cm^{-1} as well as a set of C=C and C=N$^+$ double bonds at 1605–1620 cm^{-1}. This indicates a high polarization of molecules involving vicinal nitro and amino groups and a considerable contribution of bipolar forms to their electronic structure. The electronic spectra of 2,5-dihydro-1,5-benzothiazepines **2**, **4** contain long-wave absorption bands at 386 nm (ε 12950) and 390 nm (ε 10550), respectively, that are typical of nitroenamine systems.[16]

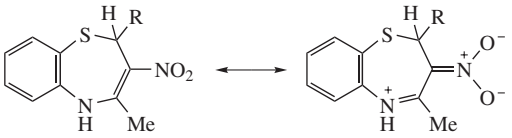

The methine protons of compounds **2**, **4** resonate in the ^{1}H NMR spectra ($CDCl_3$) as singlets at δ 6.32 and 6.23 ppm, while signals at δ 6.65 and 6.68 ppm belong to the protons of the NH groups.

The structure of product **2** was ultimately established by X-ray diffraction study (Figures 1, 2).[¶] Seven-membered heterocycle in a molecule had a slightly distorted boat conformation, with the S(1) and C(6) atoms deviating from the plane by 1.088(2) and 0.440(2) Å, respectively. The structure of the nitroenamine moiety is nearly planar, with deviation from the plane not exceeding

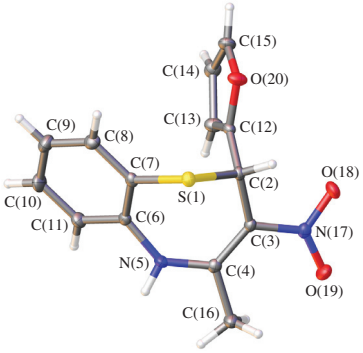

Figure 1 General view of molecule **2** with atoms represented as thermal vibration ellipsoids at 50% probability.

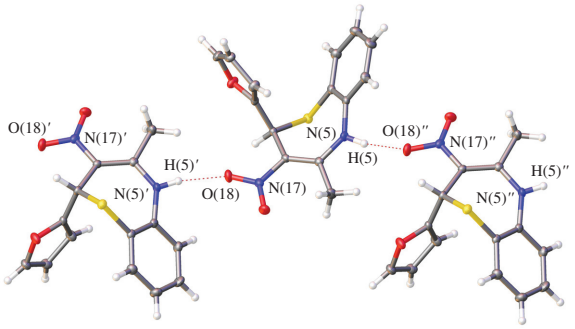

Figure 2 Coordination of compound **2** molecules by formation of intermolecular hydrogen bonds.

12° [torsion angles: N(17)–C(3)–C(4)–N(5) –167.98(15)°, H(5)–N(5)–C(4)–C(3) –172.88(15)°, C(4)–C(3)–N(17)–O(18) 172.47(14)°, C(4)–C(3)–N(17)–O(18) –6.4(2)°]. This geometry results in efficient conjugation, so the C(4)–N(5) [1.352(2) Å], C(3)–N(17) [1.416(2) Å] bonds become shorter and the C(3)–C(4) [1.391(2) Å] bond elongates. In contrast, the C=C and C–NO$_2$ bond lengths in the molecules of nitroethene[17] and 1-methoxycarbonyl-1-nitro-2-phenylethene[18] containing no amino groups are 1.337, 1.331 Å and 1.470, 1.475 Å, respectively. Note that in molecules of the model compound, *E*-2-methylamino-1-nitroethene,[22] the trend in the variation of the bond lengths examined is the same as in our sample, namely, C–NH [1.303(7) Å], C–NO$_2$ [1.378(6) Å], C=C [1.356(7) Å].

Analogous trends in the variation of these parameters are observed in the structures of open-chain compounds with *cis*-orientation of arylamino and nitro groups, namely, in the 1-bromo-1-nitro-2-piperidino-2-phenylethene[23] and 3-bromo-2-(4-bromoanilino)-3-nitroacrylate[24] molecules. Data of X-ray diffraction analysis for two other substituted 2,5-dihydro-1,5-benzothiazepines containing no nitro groups were reported.[10,25] In fact, the seven-membered heterocycle in 2,4-diphenyl-3-(1,2,4-triazol-1-yl)-2,5-dihydro-1,5-benzothiazepine[25] is turned in another direction [C(4)–N(5) 1.394(4) Å, C(3)–C(4) 1.339(4) Å], while the geometries of fluorine-substituted ethyl 4-methyl-2-(4-fluorophenyl)-2,5-dihydro-1,5-benzothiazepine-3-carboxylate [C(4)–N(5) 1.379(3) Å, C(3)–C(4) 1.367(4) Å][10] and compound **2** are similar.

The molecules of compound **2** in a crystal are associated to give chains arranged along axis *b* (Figure 2) due to a set of hydrogen bonds [N(5)–H(5)···O(18)″ 2.053(1) Å] between the adjacent molecules. The chains are held together in a three-dimensional structure (Figure 3) by van der Waals interactions directed along axis *a* [the shortest contacts between atoms of adjacent molecules are C(10)–H(10)···O(20) 2.539(1) Å, C(14)–H(14)···O(19) 2.616(1) Å and C(11)–H(11)···O(18) 2.706(1) Å].

In summary, a convenient access to 2-(2-furyl)-4-methyl-3-nitro-2,5-dihydro-1,5-benzothiazepine has been developed. Similar compounds can be of interest as potential biologically

§ Physico-chemical studies were performed in the Center for Collective Use at A. I. Herzen State Pedagogical University of Russia. ^{1}H, ^{13}C{^{1}H} NMR, ^{1}H–^{13}C HMQC, and ^{1}H–^{13}C HMBC spectra were recorded with a Jeol JNM ECX400A spectrometer operating at 399.78 (^{1}H) and 100.53 MHz (^{13}C) in $CDCl_3$ solution; the signals of the residual nondeuterated solvents were used as internal standard. IR spectra were recorded with a Shimadzu IR-Prestige-21 Fourier spectrometer in chloroform (c = 40 mg ml^{-1}). Electronic absorption spectra were recorded with a Shimadzu UV2401PC spectrophotometer in ethanol solution in quartz cuvettes (l = 1.01 mm) at 0.5–0.8 mM. Elemental analysis was performed with an Eurovector EA 3000 (CHN Dual mode) analyzer.

¶ For single crystal X-ray diffraction experiment, crystal of **2** was fixed on a micro mount, placed in an Agilent Technologies Excalibur diffractometer equipped with an EOS CCD detector and measured at a temperature of 100 K using monochromated MoKα radiation. The unit cell parameters [space group *C*2/*c*, a = 9.4605(3), b = 13.9936(3) and c = 20.2494(5) Å, β = 100.523(3)°, Z = 8] were refined by least square techniques using 6307 reflections in the 2θ range of 5.26–54.98°. The structure was solved by the direct methods and refined R_1 = 0.036 (wR_2 = 0.076) for 2501 unique reflections with $|F_0| \geqslant 4\sigma_F$ by means of the SHELXL–97 program[19] incorporated in the OLEX2 program package.[20] The carbon and nitrogen-bound H atoms were placed in calculated positions and were included in the refinement in the 'riding' model approximation, with U_{iso}(H) set to 1.5U_{eq}(C) and C–H 0.96 Å for Me groups, U_{iso}(H) set to 1.2U_{eq}(C) and C–H 0.93 Å for the CH groups, U_{iso}(H) set to 1.2U_{eq}(C) and C–H 0.98 Å for the tertiary CH groups and U_{iso}(H) set to 1.2U_{eq}(N) and N–H 0.86 Å for the NH groups. Empirical absorption correction was applied in CrysAlisPro[21] program complex using spherical harmonics, implemented in SCALE3 ABSPACK scaling algorithm.

CCDC 1001599 contains the supplementary crystallographic data for this paper. These data can be obtained free of charge from The Cambridge Crystallographic Data Centre *via* http://www.ccdc.cam.ac.uk. For details, see 'Notice to Authors', *Mendeleev Commun.*, Issue 1, 2014.

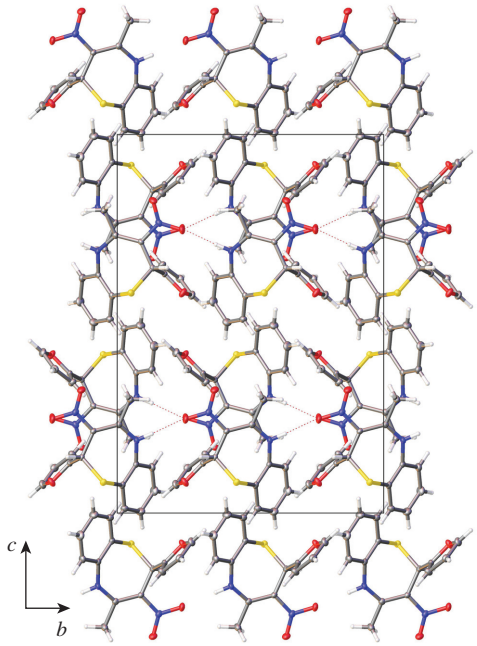

Figure 3 Packing of compound **2** molecules in a crystal.

active compounds and can be recommended for primary pharmacological tests.

This study was supported by the Ministry of Education and Science of the Russian Federation within the state assignment base part. X-ray diffraction analysis was carried out at the resource center 'X-ray Diffraction Research Methods' of St. Petersburg State University.

References

1 M. D. Mashkovskii, *Lekarstvennye sredstva (Drugs)*, Novaya Volna, Moscow, 2012 (in Russian).
2 M. Chaffman and R. N. Brogden, *Drugs*, 1985, **29**, 387.
3 V. G. Granik, *Lekarstva (Drugs)*, Vuzovskaya Kniga, Moscow, 2006 (in Russian).
4 M. D. Mashkovskii, *Lekarstva XXI veka (Drugs of XXI Century)*, Novaya Volna, Moscow, 1998 (in Russian).
5 R. I. Baichurin, N. I. Aboskalova and V. M. Berestovitskaya, *Russ. J. Org. Chem*., 2010, **46**, 1590 (*Zh. Org. Khim*., 2010, **46**, 1583).
6 V. M. Berestovitskaya, R. I. Baichurin, N. I. Aboskalova, K. A. Lysenko and I. V. Anan'ev, *Russ. J. Gen. Chem.*, 2011, **81**, 1163 (*Zh. Obshch. Khim*., 2011, **81**, 970).
7 V. M. Berestovitskaya, N. I. Aboskalova, E. A. Ishmaeva, S. V. Bakhareva, G. A. Berkova, Ya. A. Vereshchagina, A. V. Fel'gendler and G. R. Fattakhova, *Russ. J. Gen. Chem*., 2001, **71**, 1942 (*Zh. Obshch. Khim*., 2001, **71**, 2049).
8 K. S. Atwal, J. L. Bergey, A. Hedberg and S. Moreland, *J. Med. Chem.*, 1987, **30**, 635.
9 D. G. Schmidt and H. Zimmer, *J. Org. Chem*., 1983, **48**, 4367.
10 W. Li, J. Lan, C. Li, Y. Cao, H. Wang, L. Wang, P. Zhang, Y. Wang and Y. Li, *Acta Chimica Sinica (Huaxue Xuebao)*, 2009, **67**, 2732 (in Chinese) (*Chem. Abstr.*, 2010, **152**, 525825).
11 K. Tian, X. Liu, Z. Xue, T. Yang, X. Du and P. Zhang, *Chin. J. Org. Chem. (Youji Huaxue)*, 2013, **33**, 2237 (in Chinese) (*Chem. Abstr*., 2014, **161**, 55144).
12 Y. Wu, K. Tian, T. Yang, X. Du and P. Zhang, *Chin. J. Org. Chem. (Youji Huaxue)*, 2013, **33**, 1465 (in Chinese) (*Chem. Abstr*., 2013, **160**, 278894).
13 L. Wang, P. Zhang, X. Zhang, Y. Zhang, Y. Li and Y. Wang, *Eur. J. Med. Chem.*, 2009, **44**, 2815.
14 D.-B. Yang, F.-M. Liu, S.-Q. Shen and S.-W. Chen, *Chin. J. Org. Chem. (Youji Huaxue)*, 2010, **30**, 244 (in Chinese) (*Chem. Abstr*., 2010, **153**, 11631).
15 S.-Q. Chen, F. Ding and F.-M. Liu, *Phosphorus Sulfur Silicon Relat. Elem.*, 2011, **186**, 574.
16 S. Rajappa, *Tetrahedron*, 1999, **55**, 7065.
17 H. D. Hess, A. Bauder and H. H. Günthard, *J. Mol. Spectrom*., 1967, **22**, 208.
18 V. G. Andrianov, Yu. T. Struchkov and K. K. Babievsky, *Cryst. Struct. Commun.*, 1982, **11**, 31.
19 G. M. Sheldrick, *Acta Crystallogr., Sect. A*, 2008, **64**, 112.
20 O. V. Dolomanov, L. J. Bourhis, R. J. Gildea, J. A. K. Howard and H. Puschmann, *J. Appl. Crystallogr*., 2009, **42**, 339.
21 *CrysAlisPro*, Agilent Technologies, Version 1.171.36.32 (release 02-08-2013).
22 E. N. Gate, M. A. Meek, C. H. Schwalbe, M. F. G. Stevens and M. D. Threadgill, *J. Chem. Soc., Perkin Trans. 2*, 1985, 251.
23 E. A. Ishmaeva, V. M. Berestovitskaya, I. A. Litvinov, Ya. A. Vereshchagina, E. G. Yarkova, G. R. Fattakhova, D. B. Krivolapov, S. V. Makarenko, E. V. Trukhin and I. V. Pavlova, *Russ. J. Gen. Chem*., 2001, **71**, 429 (*Zh. Obshch. Khim*., 2001, **71**, 466).
24 V. M. Berestovitskaya, S. V. Makarenko, K. S. Kovalenko, I. A. Litvinov, D. B. Krivolapov and A. D. Shevchenko, *Russ. J. Gen. Chem.*, 2011, **81**, 376 (*Zh. Obshch. Khim*., 2011, **81**, 277).
25 S.-Q. Chen and F.-M. Liu, *J. Chem. Crystallogr*., 2011, **41**, 485.

Received: 15th May 2014; Com. 14/4374

Available online at www.sciencedirect.com
ScienceDirect
Mendeleev Commun., 2014, **24**, 383–385
Mendeleev Communications

Synthesis of benzo[*de*]isoquino[1,8-*gh*]quinolines and light-induced electron transfer in their composites with conductive polymer poly(3-hexylthiophene)

Denis S. Baranov,*[a,b] Aleksandr G. Popov,[a,b] Mikhail N. Uvarov[a] and Leonid V. Kulik[a,b]

[a] *V. V. Voevodsky Institute of Chemical Kinetics and Combustion, Siberian Branch of the Russian Academy of Sciences, 630090 Novosibirsk, Russian Federation. Fax: +7 383 330 7350; e-mail: baranov@kinetics.nsc.ru*
[b] *Novosibirsk State University, 630090 Novosibirsk, Russian Federation*

DOI: 10.1016/j.mencom.2014.11.026

Benzo[*de*]isoquino[1,8-*gh*]quinolines were prepared by the reaction between 1,5-diethynyl-9,10-anthraquinones and urea in DMF. Light-induced electron transfer from regioregular poly(3-hexylthiophene) to the synthesized molecules was detected by an EPR spectroscopy technique.

In most organic photovoltaic cells, fullerenes are used as an acceptor.[1] Meanwhile a search for simple and inexpensive acceptor materials with molecules of small size is progressing.[2] At present, the variety of approved substances is small and represented mostly by perylene (perylenediimide) derivatives.[3] Perylene derivatives are also used in other devices, such as organic field-effect transistors.[4] Here, we report on a new synthesis of benzo[*de*]-isoquino[1,8-*gh*]quinolines, perylene 1,7-diazo analogues, which are promising acceptor materials for organic photovoltaics. Note that the reported procedures for synthesizing these compounds are rather sparse and laborious.[5]

Compounds **1**[†] were obtained by heterocyclization of 1,5-dialkynyl-9,10-anthraquinones **2**[‡] with an excess of urea in DMF upon boiling (Scheme 1). The optimal reaction time was 2 h, the yields of target heterocycles **1** were from 35 to 47%.

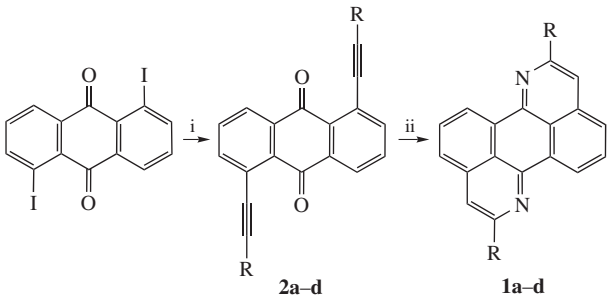

2a–d **1a–d**

a R = Bu **c** R = CH_2OCHMe_2
b R = C_6H_{13} **d** R = CH_2OBu

Scheme 1 *Reagents and conditions*: i, RC≡CCu, Py, 75 °C, 25 min; ii, $(NH_2)_2CO$, DMF, 153 °C, 2 h.

The temperature and the high excess of urea were the crucial reaction factors. Heating DMF provided sufficient urea dissolu-

[†] Combustion analysis was performed with a CHN-analyzer (Model 1106, Carlo Erba). The NMR spectra were recorded on a Bruker AV 400 spectrometer (400.13 MHz for ^{1}H, 100 MHz for ^{13}C) in $CDCl_3$. Melting points were determined with a Kofler apparatus. Mass spectra were obtained on a Thermo Electron Corporation DFS mass spectrometer (70 eV) using direct injection, the temperature of the ionization chamber was 220–270 °C. The IR spectra were recorded in KBr pellets on a Bruker Vector 22 instrument. Column chromatography was performed on 60 (Merck) and the Silufol UV-254 plates were used for TLC analysis.

*2,8-Di-R-benzo[*de*]isoquino[1,8-*gh*]quinolines* **1** *(general procedure)*. A mixture of 1,5-dialkynyl-9,10-anthraquinone **2** (0.4 mmol) and urea (4 g, 66.7 mmol) in 2.8 ml of DMF was boiled for 2 h. A mixture of toluene (50 ml) and water (50 ml) was then added, the organic layer was separated, dried over $MgSO_4$ and evaporated to dryness under reduced pressure. The crude product was purified by column chromatography on Al_2O_3 (elution with toluene). Subsequent recrystallization gave pure compounds.

*2,8-Dibutylbenzo[*de*]isoquino[1,8-*gh*]quinoline* **1a**. Yield 65 mg (45%), mp 166–167 °C (toluene). ^{1}H NMR, δ: 1.01 (t, 6H, 2Me, *J* 7.4 Hz), 1.50 (m, 4H, $2CH_2$), 1.90 (m, 4H, $2CH_2$), 2.99 (t, 2H, $2CH_2$Pr, *J* 7.7 Hz), 7.39 (s, 2H, $2H_{Py}$), 7.72 (m, 4H, $4H_{Ar}$), 8.88 (m, 2H, $2H_{Ar}$). ^{13}C NMR, δ: 14.2, 22.7, 32.1, 38.2 (2Bu), 118.2, 123.1, 123.5, 127.8, 130.8, 132.8, 137.5, 150.1, 156.8 (C_{Ar}). Found (%): C, 85.19; H, 7.03; N, 7.55. Calc. for $C_{26}H_{26}N_2$ (%): C, 85.21; H, 7.15; N, 7.64. HRMS, *m/z*: 366.2087 $[M]^+$ (calc. for $C_{26}H_{26}N_2$, *m/z*: 366.2091).

*2,8-Dihexylbenzo[*de*]isoquino[1,8-*gh*]quinoline* **1b**. Yield 60 mg (35%), mp 143–144 °C (toluene–light petroleum). ^{1}H NMR, δ: 0.91 (t, 6H, 2Me, *J* 7.3 Hz), 1.37 [m, 8H, $2(CH_2)_2$], 1.46 (m, 4H, $2CH_2$), 1.91 (m, 4H, $2CH_2$), 2.98 [t, 4H, $2CH_2(CH_2)_4$Me, *J* 7.8 Hz], 7.39 (s, 2H, H_{Py}), 7.73 (m, 4H, $4H_{Ar}$), 8.88 (m, 2H, $2H_{Ar}$). ^{13}C NMR, δ: 14.3, 22.8, 29.3, 29.9, 32.0, 38.5 (hexyl), 118.2, 123.1, 123.5, 127.8, 130.8, 132.8, 137.5, 150.1, 156.9 (C_{Ar}). Found (%): C, 85.70; H, 8.31; N, 6.65. Calc. for $C_{26}H_{26}N_2$ (%): C, 85.26; H, 8.11; N, 6.63. HRMS, *m/z*: 422.2724 $[M]^+$ (calc. for $C_{30}H_{34}N_2$, *m/z*: 422.2717).

*2,8-Bis(prop-2-yloxymethyl)benzo[*de*]isoquino[1,8-*gh*]quinoline* **1c**. Yield 70 mg (44%), mp 174–175 °C (light petroleum). ^{1}H NMR, δ: 1.35 (d, 12H, 4Me, *J* 6.0 Hz), 3.89 (m, 2H, $2CHMe_2$), 4.87 (s, 4H, $2CH_2$), 7.73 (s, 2H, H_{Py}), 7.76 (m, 2H, $2H_{Ar}$), 7.81 (m, 2H, $2H_{Ar}$), 8.86 (m, 2H, $2H_{Ar}$). ^{13}C NMR, δ: 22.4 (2Me), 71.3 ($2CH_2$), 72.1 ($CHMe_2$), 117.1, 123.7, 124.0, 128.6, 130.9, 132.6, 137.5, 150.0, 153.9 (C_{Ar}). Found (%): C, 78.29; H, 6.25; N, 7.14. Calc. for $C_{26}H_{26}N_2O_2$ (%): C, 78.36; H, 6.58; N, 7.03. HRMS, *m/z*: 398.1984 $[M]^+$ (calc. for $C_{26}H_{26}N_2O_2$, *m/z*: 398.1989).

*2,8-Bis(butoxymethyl)benzo[*de*]isoquino[1,8-*gh*]quinoline* **1d**. Yield 80 mg (47%), mp 122–123 °C (toluene–light petroleum). ^{1}H NMR, δ: 0.98 (t, 6H, 2Me, *J* 7.4 Hz), 1.50 (m, 4H, $2CH_2$), 1.73 (m, 4H, $2CH_2$), 3.70 (t, 4H, $2CH_2$Pr, *J* 6.7 Hz), 4.85 (s, 4H, $2CH_2$OBu), 7.70 (s, 2H, H_{Py}), 7.75 (m, 2H, $2H_{Ar}$), 7.81 (dd, 2H, $2H_{Ar}$, *J* 1.1 and 8.2 Hz), 8.87 (dd, 2H, $2H_{Ar}$, *J* 1.2 and 7.2 Hz). ^{13}C NMR, δ: 14.2, 19.6, 32.1 (Pr), 71.2 (OCH_2Pr), 74.0 (CH_2OBu), 117.2, 123.8, 124.1, 128.6, 130.9, 132.5, 137.4, 150.1, 153.4 (C_{Ar}). Found (%): C, 79.67; H, 7.25; N, 6.40. Calc. for $C_{28}H_{30}N_2O_2$ (%): C, 78.84; H, 7.09; N, 6.57. HRMS, *m/z*: 426.2304 $[M]^+$ (calc. for $C_{28}H_{30}N_2O_2$, *m/z*: 426.2302).

[‡] *1,5-Dialkynyl-9,10-anthraquinones* **2** *(general procedure)*. A mixture of 1,5-diiodo-9,10-anthraquinone (1.1 mmol) and copper acetylides (2.5 mmol) in 15 ml of pyridine was stirred under stream of argon at 75°C for 25 min. Then ethyl acetate (100 ml) was added, the organic layer was washed with 5% aqueous NH_3 (50 ml) and water (100 ml), dried over $MgSO_4$. The crude product was purified by column chromatography on SiO_2 (elution with toluene). Subsequent recrystallization gave pure compounds **2a–d**.

tion as compared with most of the organic solvents (alcohols, pyridine, *etc*.) tested. The technique used to perform reaction in liquid urea[6] failed to provide satisfactory yields of target products.

The choice of substituents R was determined mainly by the need to get products **1** with acceptable solubility and melting temperature which is of major importance for producing conducting films with optimal morphology and electric characteristics. The effect of substituents R on the yield and the time of reaction between bis-alkynes **2** and urea was minor. Compounds **2** are poorly examined[7] and represent polyfunctional electrophilic substrates that are sensitive to thermal and chemical action. Some of these compounds are even unstable upon chromatography on Al_2O_3 and long storage. Probably, these characteristics of bis-alkynes **2** are responsible for the undesired negative processes during their synthesis and transformation with urea which undergoes complex destruction upon heating.

Bis-alkynes **2** were synthesized by the Castro method[8] from 1,5-diiodo-9,10-anthraquinone[9] and the corresponding copper acetylides in pyridine at 75 °C (see Scheme 1). After 0.5 h, the yield of products **2** was 63–84%.

1,5-Di(hexyn-1-yl)-9,10-anthraquinone **2a**. Yield 254 mg (63%), mp 114–115 °C (light petroleum). ^{1}H NMR, δ: 0.99 (t, 6H, 2Me, *J* 7.2 Hz), 1.57 (m, 4H, 2CH_2), 1.71 (m, 4H, 2CH_2), 2.60 (t, 4H, 2CH_2Pr, *J* 7.1 Hz), 7.67 (t, 2H, 2H_{Ar}, *J* 7.8 Hz), 7.82 (dd, 2H, 2H_{Ar}, *J* 1.2 and 7.8 Hz), 8.28 (dd, 2H, 2H_{Ar}, *J* 1.2 and 7.8 Hz). ^{13}C NMR, δ: 13.9, 20.0, 22.3, 30.9 (2Bu), 80.2, 98.3 (2C≡C), 124.4, 127.1, 132.7, 133.0, 135.3, 140.4 (C_{Ar}), 182.1 (2C=O). IR (ν/cm^{-1}): 2953, 2928, 2868 (Bu), 2216 (C≡C), 1674 (C=O). Found (%): C, 85.20; H, 6.34. Calc. for $C_{26}H_{24}O_2$ (%): C, 84.75; H, 6.57.

1,5-Di(octyn-1-yl)-9,10-anthraquinone **2b**. Yield 300 mg (64%), mp 105–106 °C (light petroleum). ^{1}H NMR, δ: 0.92 (t, 6H, 2Me, *J* 7.1 Hz), 1.36 [m, 8H, 4$(CH_2)_2$], 1.55 (m, 4H, 2CH_2), 1.72 (m, 4H, 2CH_2), 2.59 [t, 4H, 2$CH_2(CH_2)_2$Me, *J* 7.1 Hz], 7.67 (t, 2H, 2H_{Ar}, *J* 7.8 Hz), 7.82 (dd, 2H, 2H_{Ar}, *J* 1.3 and 7.8 Hz), 8.28 (dd, 2H, 2H_{Ar}, *J* 1.3 and 7.8 Hz). ^{13}C NMR, δ: 14.2, 20.3, 22.7, 28.8, 28.9, 31.6 (2hexyl), 80.3, 98.4 (2C≡C), 124.4, 127.1, 132.72, 133.0, 135.3, 140.4 (C_{Ar}), 182.1 (2C=O). IR (ν/cm^{-1}): 2953, 2936, 2924, 2853 (hexyl), 2220 (C≡C), 1672 (C=O). Found (%): C, 85.84; H, 7.57. Calc. for $C_{30}H_{32}O_2$ (%): C, 84.87; H, 7.60.

1,5-Bis[3-(prop-2-yloxy)propyn-1-yl]-9,10-anthraquinone **2c**. Yield 370 mg (84%), mp 119–120 °C (light petroleum). ^{1}H NMR, δ: 1.29 (d, 12H, 4Me, *J* 6.2 Hz), 4.05 (m, 2H, 2C*H*Me$_2$), 4.55 (s, 4H, 2CH_2), 7.71 (t, 2H, 2H_{Ar}, *J* 7.8 Hz), 7.88 (dd, 2H, 2H_{Ar}, *J* 1.2 and 7.8 Hz), 8.31 (dd, 2H, 2H_{Ar}, *J* 1.3 and 7.8 Hz). ^{13}C NMR, δ: 22.1 (2Me), 56.5 (2*C*HMe$_2$), 71.0 (2CH_2), 84.8, 93.2 (2C≡C), 123.0, 127.8, 132.8, 133.2, 135.1, 140.3 (C_{Ar}), 181.7 (2C=O). IR (ν/cm^{-1}): 2970, 2936, 2903, 2872 (CH_2OCHMe$_2$), 2220 (C≡C), 1672 (C=O). Found (%): C, 78.72; H, 5.79. Calc. for $C_{26}H_{24}O_4$ (%): C, 77.98; H, 6.04.

1,5-Bis(3-butoxypropyn-1-yl)-9,10-anthraquinone **2d**. Yield 300 mg (64%), mp 120–121 °C (light petroleum). ^{1}H NMR, δ: 0.97 (t, 6H, 2Me, *J* 7.4 Hz), 1.46 (m, 4H, 2CH_2), 1.68 (m, 4H, 2CH_2), 3.73 (t, 4H, 2CH_2Pr, *J* 6.7 Hz), 4.54 (s, 4H, 2CH_2OBu), 7.72 (t, 2H, 2H_{Ar}, *J* 7.8 Hz), 7.88 (dd, 2H, 2H_{Ar}, *J* 1.3 and 7.8 Hz), 8.32 (dd, 2H, 2H_{Ar}, *J* 1.3 and 7.8 Hz). ^{13}C NMR, δ: 14.1, 19.5, 31.9, 59.2 (2Bu), 70.3 (2CH_2O), 85.3, 92.9 (2C≡C), 123.1, 127.8, 132.9, 133.2, 135.2, 140.3 (C_{Ar}), 181.7 (2C=O). Found (%): C, 78.72; H, 6.38. Calc. for $C_{28}H_{28}O_4$ (%): C, 78.48; H, 6.59.

§ UV-VIS spectra were obtained on an Ocean Optics USB-650UV spectrometer. Extinction coefficient was determined for chloroform solutions of compounds **1a**–**d** as 3.9×10^4, 3.1×10^4, 2.1×10^4 and 2.7×10^4 dm^3 mol^{-1} cm^{-1}, respectively. The spectra lineshapes coincide both for **1a**,**b** and for **1c**,**d** (data not showed).

¶ EPR spectra were obtained using an X-band ELEXSYS ESP-580 EPR spectrometer equipped with a dielectric cavity (Bruker ER 4118 X-MD-5) at room temperature, mw frequency 9.6033 GHz, mw power 6.3 mW, modulation amplitude 3 G. LiF standard was used to determine the *g*-value of EPR line. To prepare an EPR sample, chloroform solution of **1c** and regioregular poly(3-hexylthiophene), P3HT (Aldrich), was prepared at 3:1 weight ratio in the tube with 4.5 mm inner diameter, and chloroform was evaporated. The sample in an EPR cavity was illuminated by laser diode light with 660 nm wavelength, light power was about 1 mW.

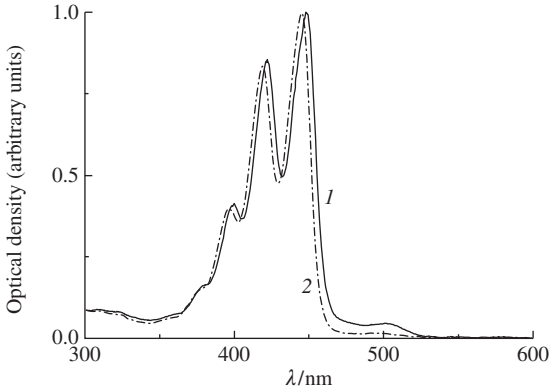

Figure 1 Optical absorption spectra of (*1*) **1a** and (*2*) **1c** in chloroform.

Figure 1 shows UV-VIS spectra of solutions of compounds **1a** and **1c** in chloroform.§ The lineshapes of the spectra coincide but with a slight shift in positions of the spectrum maxima: λ_{max} = 449 and 444 nm for **1a** and **1c**, respectively. The energy gap E_g = 2.4 eV between the HOMO and LUMO levels for **1** was determined from the absorption edge (525 nm).

Conducting polymer regioregular poly(3-hexylthiophene) (P3HT) is widely applied as p-type semiconductor in bulk heterojunction photovoltaic cells.[10] P3HT has small energy gap E_g = = 1.7 eV, which corresponds to a 760 nm optical absorption edge.[11] Figure 2 represents EPR spectra of the composite consisting of **1c** and P3HT.¶ When the sample is irradiated by continuous (660 nm) laser light, the intensity of EPR spectrum line is increased as compared with the dark line. Commonly light-induced EPR signal in the donor-acceptor composites appear from charge carriers, from cation radicals in donor and anion radicals in acceptor phase.[12] Appearance of these radicals may cause photocurrent generation in a photoelectric cell.[13] On absorption of 660 nm light by P3HT the light induced electron transfer occurs: EPR spectrum consists of two lines with homogeneous broadening. The most intensive line has width of about 3 G, *g*-factor of 2.0023±0.0001; on this basis it can be interpreted as the line of P3HT$^+$ radical cation.[14] The other light-induced EPR signal is weaker and slightly shifted to low-field and possibly originates from **1c**$^-$ radical anion. This line has a large linewidth (~10 G) due to hyperfine splitting on nitrogen and hydrogen nuclei of the π-conjugated acceptor part of the molecule.

In conclusion, heterocyclization of 1,5-dialkynyl-9,10-anthraquinones with excess of urea in boiling DMF affords 2,8-bis-R-benzo[*de*]isoquino[1,8-*gh*]quinolines. Light-induced electron transfer from P3HT to **1c** molecules was detected by EPR spectroscopy.

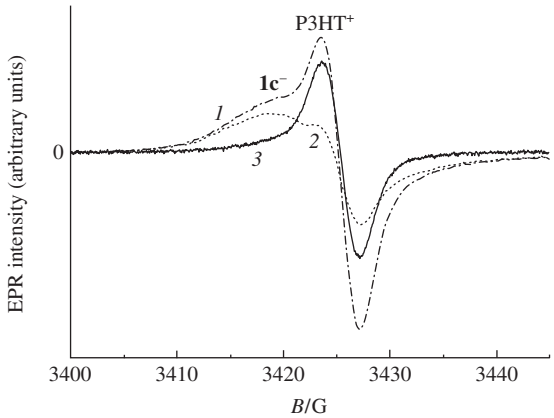

Figure 2 EPR spectra of composite **1c**:P3HT obtained from (*1*) irradiated sample and (*2*) in the dark, and (*3*) light-induced EPR signal.

This work was supported by the Russian Foundation for Basic Research (grant no. 14-03-31183), the Ministry of Education and Science of the Russian Federation and the Chemical Service Centre of Siberian Branch of the Russian Academy of Sciences.

References

1 *Organic Photovoltaics: Concepts and Realization*, eds. C. J. Brabec, V. Dyakonov, J. Parisi and N. S. Sariciftci, Springer, Berlin, 2010.
2 C. L. Chochos, N. Tagmatarchis and V. G. Gregoriou, *RSC Adv*., 2013, **3**, 7160.
3 E. Kozma and M. Catellani, *Dyes Pigm.*, 2013, **98**, 160.
4 A. V. Mumyatov, L. I. Leshanskaya, D. V. Anokhin, N. N. Dremova and P. A. Troshin, *Mendeleev Commun.*, 2014, **24**, 306.
5 (*a*) E. A. Braude and J. S. Fewcett, *J. Chem. Soc.*, 1951, 3117; (*b*) R. H. B. Galt, J. D. Loudon and A. D. B. Sloan, *J. Chem. Soc*., 1958, 1588; (*c*) C. Naumann and H. Langhals, *Chem. Ber*., 1990, **123**, 1881; (*d*) H. Langhals and C. Naumann, *German Patent 4005056*, 1991; (*e*) F. Bienewald, B. Schmidhalter, U. Berens, H. J. Kirner, *US Patent WO 2006/120143*, 2006; (*f*) F. Bienewald, B. Schmidhalter, U. Berens and H. J. Kirner, *US Patent US 2009/101890*, 2009.
6 D. S. Baranov, S. F. Vasilevsky, B. Gold and I. V. Alabugin, *RSC Adv*., 2011, **1**, 1745.
7 (*a*) A. A. Moroz, A. V. Piskunov and M. S. Shvartsberg, *Bull. Acad. Sci. USSR, Div. Chem. Sci*., 1981, **30**, 304 (*Izv. Akad. Nauk SSSR, Ser. Khim.*, 1981, 386); (*b*) M. Murata, M. Yamada, T. Fujita, K. Kojima, M. Kurihara, K. Kubo, Y. Kobayashi and H. Nishihara, *J. Am. Chem. Soc.*, 2001, **123**, 12903; (*c*) A. Gouloumis, D. Gonzalez-Rodriguez, P. Vazquez, T. Torres, S. Liu, L. Echegoyen, J. Ramey, G. L. Hug and D. M. Guldi, *J. Am. Chem. Soc*., 2006, **128**, 12674; (*d*) F. Li, J. Cheng, X. Chai, S. Jin, X. Wu, G.-A. Yu, S. H. Liu and G. Chen, *Organometallics*, 2011, **30**, 1830; (*e*) N. Seidel, T. Hahn, S. Liebing, W. Seichter, J. Kortus and E. Weber, *New J. Chem*., 2013, **37**, 601.
8 C. E. Castro and R. D. Stephens, *J. Org. Chem*., 1963, **28**, 2163.
9 H. Scholl, S. Hass and H. K. Meyer, *Chem. Ber*., 1929, **62**, 107.
10 A. Marrocchi, D. Lanari, A. Fachetti and L. Vaccaro, *Energy Environ. Sci*., 2012, **5**, 8457.
11 T. Chen, X. Wu and R. D. Rieke, *J. Am. Chem. Soc*., 1995, **117**, 233.
12 N. S. Sariciftci, L. Smolowitz, A. J. Heeger and F. Wudl, *Science*, 1992, **258**, 1474.
13 K. Marumoto, T. Fujimori, M. Ito and T. Mori, *Adv. Energy Mater*., 2012, **2**, 591.
14 K. Marumoto, Y. Muramatsu, Y. Nagano, T. Iwata, S. Ukai, H. Ito, S. Kuroda, Y. Shimoi and S. Abe, *J. Phys. Soc. Jpn*., 2005, **74**, 3066.

Received: 13th March 2014; Com. 14/4323

Available online at www.sciencedirect.com
ScienceDirect
Mendeleev Commun., 2014, **24**, 386–387
Mendeleev Communications

[4,5]-Bicyclic sydnone imines

Ilya A. Cherepanov, Alina S. Samarskaya, Roman G. Nosov, Ivan A. Godovikov, Yulia V. Nelyubina and Valery N. Kalinin*

A. N. Nesmeyanov Institute of Organoelement Compounds, Russian Academy of Sciences, 119991 Moscow, Russian Federation. Fax: +7 499 135 6549; e-mail: vkalin@ineos.ac.ru

DOI: 10.1016/j.mencom.2014.11.027

Lithiation of N^6-(α-haloacyl)-3-isopropylsydnone imines at 4-position followed by treatment with sulfur affords the 4-lithiosulfanyl derivatives whose intramolecular cyclization leads to [4,5]-bicyclic sydnone imines.

Sydnone imines[1,2] are the most well-studied representatives of mesoionic heterocyclic compounds. They show a broad spectrum of biological activity; sydnone imines were found to be effective exogenous donors of nitrogen oxide (NO).[1–3] However, only few polycyclic representatives condensed with a 3,4-edge of a ring were reported.[4–6]

The purpose of this study was working out a new synthetic way for bicyclic sydnone imines **1** condensed at 4,5-edge.

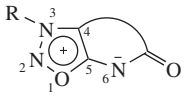

1

Earlier we showed that 4-lithiated sydnone imines easily reacted with sulfur to form the corresponding lithium thiolates **2**.[7] The *in situ* treatment of these thiolates with alkyl halides gives the corresponding sulfides **3** (Scheme 1).

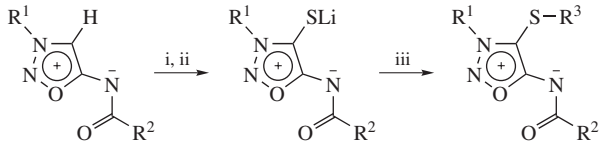

2 **3**

Scheme 1 *Reagents and conditions*: i, BuLi, THF, –90 °C, 30 min; ii, S_8, THF, –90 → +20 °C, 30 min; iii, R^3X, THF, 20 °C, 2–24 h.

We assumed that intramolecular nucleophilic substitution with the formation of a bicyclic product would be possible by using a sydnone imine with halogen atom at α-position of N^6-acyl group. The required N^6-α-halogenacyl derivatives **4a**,**b** were obtained by acylation of sydnone imine hydrochlorides with α-haloacyl chlorides (Scheme 2).

Lithiation of compounds **4a**,**b** having active halogen atom with BuLi to afford derivatives **5a**,**b** proceeded cleanly (Scheme 2). This was proved by treatment of organolithium compounds **5a**,**b** with 4-trifluoromethylbenzaldehyde, which gave the corresponding secondary alcohols in high yields.

Treatment of lithium derivatives **5a**,**b** with elementary sulfur led to lithium thiolates which spontaneously cyclized into bicyclic sydnone imines **7a**,**b**† at room temperature (see Scheme 2).

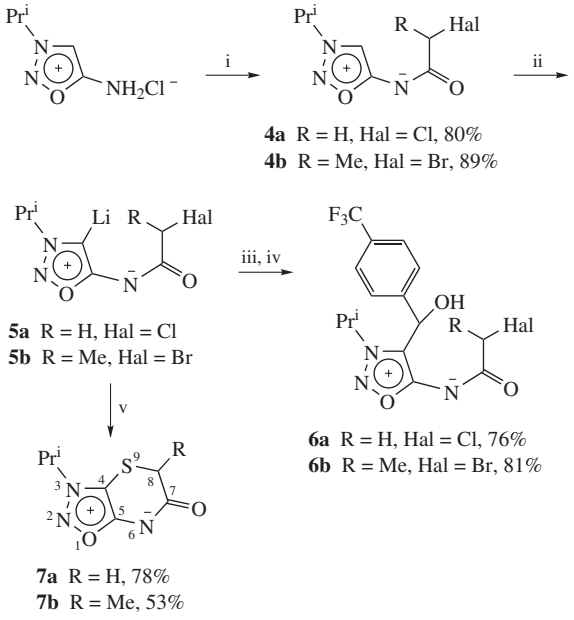

4a R = H, Hal = Cl, 80%
4b R = Me, Hal = Br, 89%

5a R = H, Hal = Cl
5b R = Me, Hal = Br

6a R = H, Hal = Cl, 76%
6b R = Me, Hal = Br, 81%

7a R = H, 78%
7b R = Me, 53%

Scheme 2 *Reagents and conditions*: i, RCH(Hal)C(O)Cl, Et_3N, CH_2Cl_2, –30 °C, 60 min; ii, BuLi, THF, –90 °C, 30 min; iii, 4-$CF_3C_6H_4CHO$, THF, –90 → +20 °C, 30 min; iv, H^+; v, S_8, THF, –90 → +20 °C, 30 min.

† *Standard procedure. n*-Butyllithium solution in hexane (2.1 mmol) was added to sydnone imine (2.0 mmol) in dry THF (50 ml) at –90 °C. The solution was stirred at –90 °C for 30 min, then 2.2 mmol of powdered sulfur was added. The resulting mixture was stirred at –90 °C for 15 min, heated up at a bath to room temperature. The mixture was stirred for additional 4 h to complete the reaction (TLC control) and quenched with water (1 ml). The solvent was evaporated under reduced pressure, the residue was dissolved in dichloromethane (50 ml) and the solution was filtered through a layer of Al_2O_3. The solvent was evaporated, the residue was purified by chromatography (column with SiO_2, eluent chloroform–ethyl acetate, 5:1). The product was crystallized from isopropyl alcohol–hexane mixture.

For **7a**: yield 78%, mp 125–127 °C. IR (KBr pellet, ν/cm^{-1}): 2922 (m), 2853 (m), 1653 (s), 1572 (vs), 1458 (vs), 1377 (m), 1343 (w), 1259 (w), 1188 (vw), 1172 (vw), 1128 (w), 1101 (vw), 1066 (vw), 1050 (vw). ^{1}H NMR ($CDCl_3$) δ: 1.44 (d, 3H, CH*Me*, J_{AB} 6.83 Hz), 1.64 (d, 6H, *Me*$_2$CH, J_{AB} 6.54 Hz), 3.56 (q, 1H, C*H*Me, J_{AB} 6.83 Hz), 4.75 (sp, 1H, Me$_2$C*H*, J_{AB} 6.54 Hz). ^{13}C NMR ($CDCl_3$) δ: 18.06, 20.47, 20.52, 36.59, 57.75, 102.56, 171.44, 172.10.

For **7b**: yield 53%, mp 115–117 °C. IR (KBr pellet, ν/cm^{-1}): 2928 (m), 2849 (m), 1650 (s), 1575 (vs), 1454 (s), 1375 (m), 1340 (w), 1255 (w), 1186 (w), 1170 (w), 1154 (vw), 1131 (w), 1105 (vw), 1083 (vw), 1068 (vw), 1048 (vw). ^{1}H NMR ($CDCl_3$) δ: 1.44 (d, 3H, CH*Me*, J_{AB} 6.83 Hz), 1.64 (d, 6H, *Me*$_2$CH, J_{AB} 6.54 Hz), 3.56 (q, 1H, C*H*Me, J_{AB} 6.83 Hz), 4.75 (sp, 1H, Me$_2$C*H*, J_{AB} 6.54 Hz). ^{13}C NMR ($CDCl_3$) δ: 18.06, 20.47, 20.52, 36.59, 57.75, 102.56, 171.44, 172.10.

For detailed synthetic procedures and characteristics of compounds **4a**,**b** and **6a**,**b**, see Online Supplementary Materials.

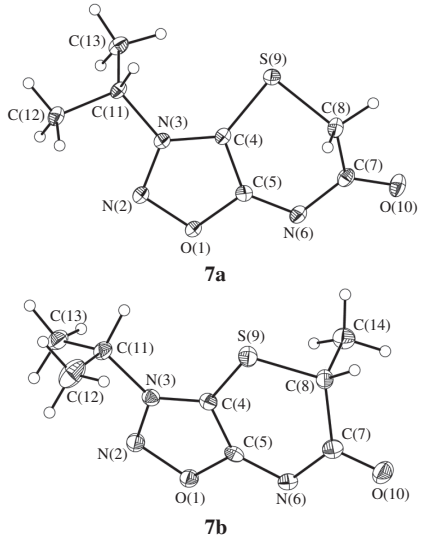

Figure 1 General view of sydnone imines **7a** and **7b** in representation of non-hydrogen atoms by thermal ellipsoids (p = 50%); the second independent molecule of product **7a** is not shown. Selected bond lengths (Å) for **7a** and **7b**, respectively, are: O(1)–N(2) 1.3975(13)/1.3918(15) and 1.3903(19), O(1)–C(5) 1.3674(14)/1.3668(16) and 1.366(2), N(2)–N(3) 1.3182(14)/1.3201(15) and 1.319(2), N(3)–C(4) 1.3397(14)/1.3403(15) and 1.331(2), C(4)–C(5) 1.3949(16)/1.3949(17) and 1.387(2), C(4)–S(9) 1.7230(12)/1.7231(13) and 1.7263(17), C(5)–N(6) 1.3053(15)/1.3055(17) and 1.305(2), N(6)–C(7) 1.3780(16)/1.3719(18) and 1.372(2), C(7)–O(10) 1.2201(15)/1.2253(15) and 1.217(2), C(7)–C(8) 1.5312(17)/1.5345(19) and 1.543(2), C(8)–S(9) 1.8271(12)/1.8282(13) and 1.8341(17).

The nomenclature of condensed cyclic compounds appears to be not quite convenient for such bicyclic sydnone imines because of the exocyclic nitrogen atom N^6, which is a part of the mesoionic fragment and the second cycle at the same time. We have suggested easier nomenclature (Scheme 2) by describing the second cycle as a linker between N^6 and C^4 positions of the mesoionic fragment. According to such nomenclature the mesoionic nature of these compounds is emphasized and usual numeration for sydnone imines is saved. So compound **7a** should be named as 3-isopropyl-7-oxo-9-thia[4,6-propano]sydnone imine, and **7b** as 3-isopropyl-8-methyl-7-oxo-9-thia[4,6-propano]sydnone imine.

The structures of these two bicyclic sydnone imines (**7a** and **7b**) were clarified by single-crystal X-ray diffraction analysis[‡] (Figure 1). According to it the molecular geometries of these compounds are very close: the largest difference in bond lengths between **7a** and **7b** is less than 0.01 Å. Geometrical parameters of mesoionic core are very similar to those of earlier described 3-isopropyl-4-methylsulfanyl-N^6-benzoylsydnone imine;[8] the largest difference of ~0.02 Å was observed for the bond C(4)–C(5) that belongs to only one (mesoionic) heterocyclic moiety. In all cases, mesoionic cycle is planar within 0.01 Å as expected. The second cycle adopts a distorted half chair conformation [the atom C(8) deviates by 0.60(1)–0.83(1) Å from the plane of the others having a mean deviation of 0.04(1)–0.06(1) Å]; note that the largest deviation of the atom C(8) was observed for the second independent molecule of the sydnone imine **7a**, which together with some minor discrepancies in positions of the methyl groups is the most pronounced difference between the two independent molecules in a crystal.

In conclusion, the study performed has extended the range of valuable and promising sydnone imines.

Online Supplementary Materials

Supplementary data associated with this article can be found in the online version at doi:10.1016/j.mencom.2014.11.027.

References

1 C. G. Newton and C. A. Ramsden, *Tetrahedron*, 1982, **38**, 2967.
2 V. G. Yashunskii and L. E. Holodov, *Russ. Chem. Rev*., 1980, **49**, 28 (*Usp. Khim*., 1980, **49**, 54).
3 K. Schonafinger, *Il Farmaco*, 1999, **54**, 316.
4 H. U. Daeniker and J. Druey, *Helv. Chim. Acta*, 1962, **45**, 2426.
5 J. M. Ruxer, J. Mauger, D. Benard and C. Lachoux, *J. Heterocycl. Chem*., 1995, **32**, 643.
6 J. M. Ruxer, J. Mauer, C. Lachoux, V. Richard, A. Bredeaux, P. Martorana and H. Bohn, *French Patent, FR 2693726*, A1 19940121, 1994.
7 I. A. Cherepanov, S. N. Lebedev, A. S. Samarskaya, I. A. Godovikov, Yu. V. Nelyubina and V. N. Kalinin, *Mendeleev Commun.*, 2009, **19**, 322.
8 Yu. V. Nelyubina, M. Yu. Antipin, I. A. Cherepanov and K. A. Lyssenko, *CrystEngComm*, 2010, **12**, 77.
9 G. M. Sheldrick, *Acta Crystallogr., Sect. A*, 2008, **64**, 112.

Received: 21st February 2014; Com. 14/4313

‡ *Crystallographic data*.

Crystals of **7a** ($C_7H_9N_3O_2S$, M = 199.23) are triclinic, space group $P\bar{1}$, at 100 K: a = 9.1443(6), b = 9.6390(6) and c = 10.4539(6) Å, α = 87.4420(10)°, β = 74.0010(10)°, γ = 77.7110(10)°, V = 865.34(9) Å^3, Z = 4 (Z' = 2), d_{calc} = 1.529 g cm^{-3}, μ(MoKα) = 3.43 cm^{-1}, F(000) = 416.

Crystals of **7b** ($C_8H_{11}N_3O_2S$, M = 213.26) are orthorhombic, space group $P2_12_12_1$, at 100 K: a = 6.1696(6), b = 8.1555(8) and c = 19.6390(19) Å, V = 988.16(17) Å^3, Z = 4 (Z' = 1), d_{calc} = 1.433 g cm^{-3}, μ(MoKα) = = 3.05 cm^{-1}, F(000) = 448.

Intensities of 11083 and 6469 reflections for **7a** and **7b**, respectively, were measured with a BrukerAPEX2 DUO CCD diffractometer [λ(MoKα) = = 0.71072 Å, ω-scans, $2\theta < 60°$ and 58°]; 5039 and 2628 independent reflections [R_{int} = 0.0217 and 0.0234] were used in further refinement for **7a** and **7b**, respectively. The structures were solved by direct method and refined by the full-matrix least-squares technique against F^2 in the anisotropic–isotropic approximation. The H(C) atom positions were calculated, and they were refined in the isotropic approximation using a riding model. For **7a**, the refinement converged to wR_2 = 0.0873 and GOF = 1.008 for all the independent reflections [R_1 = 0.0325 was calculated against F for 4300 observed reflections with $I > 2\sigma(I)$]. For **7b**, the refinement converged to wR_2 = 0.0686 and GOF = 1.002 for all the independent reflections [R_1 = 0.0339 was calculated against F for 2502 observed reflections with $I > 2\sigma(I)$]. All calculations were performed using SHELXTL PLUS 5.0.[9]

CCDC 985517 and 985518 contain the supplementary crystallographic data for this paper. These data can be obtained free of charge from The Cambridge Crystallographic Data Centre *via* http://www.ccdc.cam.ac.uk. For details, see 'Notice to Authors', *Mendeleev Commun.*, Issue 1, 2014.

Mendeleev Communications

Author Index

2014, Volume 24, Issues 1–6, pp. 1–388